



University
of Glasgow

Chan, Kee Han (2002) Transient analysis and modelling of multimachine systems with power electronics controllers for real-time application. PhD thesis.

<http://theses.gla.ac.uk/4840/>

Copyright and moral rights for this thesis are retained by the author

A copy can be downloaded for personal non-commercial research or study, without prior permission or charge

This thesis cannot be reproduced or quoted extensively from without first obtaining permission in writing from the Author

The content must not be changed in any way or sold commercially in any format or medium without the formal permission of the Author

When referring to this work, full bibliographic details including the author, title, awarding institution and date of the thesis must be given.

Transient Analysis and Modelling of Multimachine Systems with Power Electronics Controllers for Real-time Application

by

Kee Han Chan

A Thesis submitted to the
Department of Electronics and Electrical Engineering of
the University of Glasgow
for the degree of
Doctor of Philosophy (Ph.D.)

November 2002

Dedicated to my parents ...

For their unconditional love and support throughout my life, without which, all these would not have been possible.

And to my lovely Cindy for her love, encouragement and patience.

Abstract

Electricity usage has grown steadily ever since the first commercial generator came into operation more than one century ago. Power transmission networks too, have grown in size and in operational complexity to be able to handle the large blocks of electricity that travel from generator to consumers round-the-clock and with huge variations. At various stages of the development, state-of-the-art equipment, methods and techniques have been incorporated in the vast array of tools that power systems engineers have at their disposal to keep up with the demands imposed by the planning, management, operation and control of modern power systems.

Transient stability has always been an issue of paramount importance in power system planning and operation. Arguably, most of the ideas and concepts associated with power system stability analysis were conceived many years ago. Nonetheless, continuous expansion of the network and the emergence of a new generation of fast acting, multi-purpose power system controllers have called for renewed research efforts in this all-important application area of power systems.

In particular, there is growing concern that the power network is becoming more unbalanced, owing to higher operating voltages and a relentless drive for interconnection, and that unbalances may impair the effectiveness of power electronic-based loads and controllers. These are issues that may be difficult to address satisfactorily with conventional transient stability modelling approaches since they are based on the premise that the transmission network observes a perfect balance, even under faulted operating regimes. The study of a limited range of asymmetrical transient stability problems using conventional methods can be achieved, but only with great difficulty, which involves transforming the network into fictitious components (i.e. symmetrical components). This is significant since asymmetrical short-circuit faults constitute the largest percentage of faults that occur in the power network, and network designs based solely on the three-phase short-circuit-to-ground faults result in under-engineered networks. Equally important issues are the widespread commissioning of modern power electronics controllers and the lack of suitable models and methods for assessing the impact of such controllers in network-wide operation with particular reference to transient stability and unbalanced operation.

The research reported in this thesis addresses these issues and develops a direct time phase-domain model for conducting multimachine transient stability analysis where asymmetrical operating conditions and the impact of modern power electronics controllers are represented.

In this simulation environment, AC synchronous and asynchronous generators are represented together with asynchronous motors. The set of non-linear equations describing the machines are solved using discretisation and the trapezoidal rule of integration. The proposed model is compared against an industry standard power system package for cases of symmetrical operation. The generality and versatility of the model is demonstrated when applied to the analysis of symmetrical and asymmetrical power system operations.

An important aspect of this research is a drive towards the solution of transient stability in real-time, where the results produced are in actual world time. This is achieved by embedding the model into a commercially available multi-purpose real-time station. To this end, coherency-based synchronous generators equivalent has been developed to enable the solution of multimachine systems in real-time. The equivalent unit is obtained based on the aggregation of the coherent generators using phase-domain techniques.

Dynamic loads in the form of asynchronous motors are implemented within the multimachine network. The adverse influences of motor operation on voltage problems in the network under symmetrical and asymmetrical conditions are analysed. Transient analysis of dispersed generation is also considered where the asynchronous machine is operated as a generator alongside synchronous generators. The behaviours of the two type of generators under various networks and operating conditions are presented.

Models of power electronics controllers in the direct time phase-domain are also described in this thesis. The generalised models of the Static Var Compensator (SVC), Static Synchronous Compensator (STATCOM), Dynamic Voltage Restorer (DVR) and High Voltage Direct Current-Voltage Source Converter (HVDC-VSC) station are proposed. The SVC comprised of a fix capacitor and a thyristor controlled reactor (TCR) is developed. Here, switching functions are used to represent the operation of the thyristor. Models of STATCOM, DVR and HVDC-VSC station are developed based on the self-commutated voltage source converter (VSC) technology. The VSC is represented by the switching functions of its pulse width modulation (PWM) control, hence, providing a flexible model within the direct time phase-domain approach. The model of the VSC is implemented into the respective power electronics controllers enabling a convenient modular approach to be adopted. The power electronics controllers are incorporated into the multimachine environment for the analysis of transient and power quality related issues.

Acknowledgements

I wish to express my sincere gratitude to Professor Enrique Acha for his supervision, friendship and most importantly, his believe in me throughout the course of my research project.

I am sincerely thankful to Dr. Manuel Madrigal for his technical help and hot “salsa” tips, both are deeply cherished. Thanks to Dr. John Parle for his advice and support in real-time station related work, and of course not forgetting the many drunken night out that we had.

I am very grateful to my friend Cross Tan for always being there to offer help when I needed them most, and his patience in dealing with my constant complaints. Many thanks to Dr. Pichai Aree for his words of wisdom and encouragement during the first two years of my research project. Also like to thank Cesar Angeles and Olimpo Anaya for adding that little bit of flavour that never failed to lighten up my life.

Special thanks to my sisters for their moral support throughout the course of my research.

Thanks to my colleagues at the University of Glasgow for their friendship and assistance over the course of my research, especially my officemates from the Power System Group. I gratefully acknowledge the financial assistance given to me by CVCP UK and University of Glasgow. Also grateful to my current employer Power Technologies International (PTI) for their understanding in granting me time out to complete my thesis modifications.

Finally my time in Glasgow is up I shall leave this wonderful place with bags of fond memories, which will forever remain a pivotal part of my life. Cheers, Glasgow !!!

Contents

1. Introduction	1
1.1. Foreword	1
1.2. Background and Power System Modelling for Transient Analysis	2
1.3. Power System Transient Enhancement through Power Electronics	4
1.4. Real-Time Digital Power System Simulation	5
1.5. Motivation and Objectives of the Present Research Work	6
1.6. Contributions	8
1.7. Publications	9
1.7.1. Transaction-grade Papers	9
1.7.2. Conference Papers	9
1.8. Outline of thesis	10
2. Modelling of AC Machines for Transient Analysis	12
2.1. Introduction	12
2.2. Approach to AC Machine Modelling	14
2.3. Synchronous Generator Model	14
2.3.1. Direct Time Phase-Domain Model	15
2.3.2. The $d - q - 0$ Transformation Model	20
2.4. Simulations and Results of Synchronous Generator Model Performance	24
2.4.1. Validation Tests	24
2.4.2. Asymmetrical Fault Condition with Line Opening and Re-closure	26
2.5. Asynchronous Machine Model	28
2.5.1. Direct Time Phase-Domain Model	29

Contents

2.5.2.	The Two Axis Transformation Model	33
2.6.	Simulations and Results of Asynchronous Machine Model Performance . . .	35
2.6.1.	Asynchronous Machine Operational Tests	36
2.6.2.	Asymmetrical Operating Conditions	36
2.7.	Conclusions	38
3.	Multimachine Dynamic Model in the Phase-Domain for Real-Time Simulation	39
3.1.	Introduction	39
3.2.	Methodology and Approach	41
3.2.1.	Discrete Model of the Synchronous Generator	41
3.2.2.	Discrete Representation of the Network Linking the Generators . . .	43
3.3.	Solution Algorithms	44
3.4.	Model Validation	46
3.5.	Generator Controllers	46
3.5.1.	Generator Excitation Control	46
3.5.2.	Speed Turbine Governor	50
3.6.	Real-Time Simulation of the Multimachine Network Model	52
3.6.1.	The Real-Time Station (RTS)	54
3.6.2.	Real-Time Simulations	55
3.7.	Conclusions	59
4.	Further Consideration of the Direct Time Phase-Domain Multimachine Model	60
4.1.	Introduction	60
4.2.	Coherency-based Multimachine Transient Analysis	61
4.2.1.	Aggregation of Coherent Generators	62
4.2.2.	Results of Stability Analysis	66
4.2.3.	Real-Time Simulation	72
4.3.	Implementation of Dynamic Load into Power System Network	73
4.3.1.	Discrete Model of Induction Machine	74
4.4.	Analysis of Motor Dynamics in Power System Networks	76
4.4.1.	Induction Motor Run-up Characteristic	76

Contents

4.4.2. Influence of Motor Behaviour on Voltage Sags when Subjected to Network Disturbances	80
4.5. Conclusions	87
5. Dynamic Behaviour of a Network with Embedded Wind Driven Fixed Speed Induction Generator	89
5.1. Introduction	89
5.2. Transient Stability of a Network with Grid Connected Wind Driven Induction Generator	90
5.3. Transient Performance of an Islanded Wind Driven Induction Generator from the Network	96
5.4. Operation of the Wind-driven Induction Generator Under Unbalance Network Conditions	101
5.5. Effect of Wind Driven Induction Generator Oscillating Output on Network Stability Margin	104
5.6. Conclusions	104
6. Power Electronics Controllers in the Phase-Domain	106
6.1. Introduction	106
6.2. Static Var Compensator (SVC)	108
6.2.1. Mathematical Model of SVC	109
6.2.2. Time-Step Consideration When Modelling Thyristor Switching	110
6.2.3. SVC Control Scheme	111
6.2.4. Application of SVC to Voltage Sags Mitigation During Motor Start-Up	112
6.2.5. Generator Transient Stability Enhancement with SVC	114
6.3. Voltage Source Converter (VSC) Representation in the Phase-Domain	117
6.4. Static Synchronous Compensator (STATCOM)	120
6.4.1. Mathematical Model of STATCOM	121
6.4.2. STATCOM's AVR Control	122
6.4.3. Application of STATCOM to Voltage Sags Mitigation During Motor Start-Up	123
6.4.4. STATCOM Control and Operation for Asymmetrical Operation	123

Contents

6.4.5. Application of STATCOM to a network with fixed speed wind driven induction generator	130
6.5. The Dynamic Voltage Restorer (DVR)	132
6.5.1. Mathematical Model of DVR	133
6.5.2. Dynamic Voltage Restorer Control Scheme	134
6.5.3. DVR Simulations and Results	135
6.6. HVDC-VSC Station	138
6.6.1. Phase Domain HVDC-VSC Model	138
6.6.2. Operations and Control of the HVDC-VSC	140
6.6.3. Real-time Implementation of the HVDC-VSC Model for Application in a Scaled-Down WECS	141
6.7. Conclusions	145
7. General Conclusions and Suggestions for Future Research Work	148
7.1. General Conclusions	148
7.2. Suggestions for Future Research Work	150
A. Generator Data and PSCAD/EMTDCTM Schematic Diagrams	164
A.1. Synchronous Generator Data Used for Validation with PSCAD/EMTDC TM	164
A.2. Synchronous Generator and Asynchronous Machine Data for Other Simulation Studies	165
A.3. Schematic Diagrams in PSCAD/EMTDC TM	166
B. Trapezoidal Rule of Integration and Discretisation of Network and Generator Controllers Equations	170
B.1. Trapezoidal Rule	170
B.2. Discretisation of the Network Equations	171
B.3. Discretisation of Generator Controllers Equations	172
B.3.1. Generator Excitation Control	172
B.3.2. Turbine Governor	173
C. Network Reduction of Coherent Generators Bus	174

Contents

D. Computer Program Code Listing	177
D.1. General Transient Stability Program Listing	177
D.2. Power Electronics Controllers Subroutines	195

List of Figures

2.1. Schematic diagram of a synchronous generator	15
2.2. Stator and field currents of the generator connected to an infinite bus following a three-phase-to-ground fault at its terminal	25
2.3. Experimental results from [28] for similar studies as those shown in Figure 2.2	26
2.4. Test network with load	26
2.5. Stator and field currents for a three-phase-to-ground fault at the terminal of a loaded generator	27
2.6. Generator current under single-phase-to-ground fault with line opening and re-closure	27
2.7. Generator dynamic response and electrical torque under single-phase-to-ground fault with line opening and re-closure	28
2.8. Schematic circuit of asynchronous machine	29
2.9. Asynchronous machine response under two modes of operation	36
2.10. Asynchronous machine stator current under single-phase opening and re-closure	37
2.11. Asynchronous machine rotor current under single-phase opening and re-closure	37
2.12. Asynchronous machine electrical torque under single-phase opening and re-closure	38
3.1. Flowchart of direct time phase-domain multimachine solution algorithm	45
3.2. Three nodes test network	46
3.3. Stator and field currents for a three-phase-to-ground fault at <i>Node 2</i> of the three nodes test network	47

List of Figures

3.4. Block model of an excitation system	48
3.5. Six nodes network for study of excitation control on system stability	49
3.6. Terminal voltage and load angle of <i>Gen 1</i> following a three-phase-to-ground fault at its terminal	50
3.7. Speed and electrical torque response of <i>Gen 1</i> following a three-phase-to-ground fault at its terminal	50
3.8. Block model of a speed turbine governor	51
3.9. Response of <i>Gen 1</i> when subjected to a load increase with turbine governor control	52
3.10. RTS configuration	55
3.11. Five nodes network used in real-time simulations	56
3.12. Stator voltages and currents for a three-phase-to-ground fault at <i>Node 2</i> of the five nodes network	56
3.13. Stator voltages and currents for a single-phase-to-ground fault at <i>Node 2</i> of the five nodes network	57
3.14. Comparison of AFT between simulations with no line couplings and with line couplings	58
3.15. Comparison of different time steps on the accuracy of the response on stator current of <i>Gen 1</i>	58
3.16. Test network to obtain data overhead of the RTS	58
3.17. AFT versus number of generator nodes	59
4.1. Test network	67
4.2. Load angle of generators using detailed model during a three-phase-to-ground fault at <i>Node 7</i>	67
4.3. Load angle of <i>Gen 2</i> using an equivalent model for <i>Gen 4</i> and <i>5</i> during a three-phase-to-ground fault at <i>Node 7</i>	68
4.4. Load angle of <i>Gen 3</i> using an equivalent model for <i>Gen 4</i> and <i>5</i> during a three-phase-to-ground fault at <i>Node 7</i>	68
4.5. Load angle of equivalent generator representing <i>Gen 4</i> , <i>5</i> and <i>6</i> during a three-phase-to-ground fault at <i>Node 7</i>	68
4.6. Load angle of <i>Gen 2</i> using an equivalent model for <i>Gen 4</i> and <i>5</i> during a single-phase-to-ground fault at <i>Node 7</i>	69

List of Figures

4.7. Field current of <i>Gen 2</i> using an equivalent model for <i>Gen 4</i> and <i>5</i> during a single-phase-to-ground fault at <i>Node 7</i>	69
4.8. Load angles of generators detailed models during a three-phase-to-ground fault at <i>Node 7</i> with additional generators	70
4.9. Load angle of <i>Gen 2</i> using an equivalent model for <i>Gen 4, 5</i> and <i>6</i> during a three-phase-to-ground fault at <i>Node 7</i>	70
4.10. Load angle of <i>Gen 3</i> using an equivalent model for <i>Gen 4, 5</i> and <i>6</i> during a three-phase-to-ground fault at <i>Node 7</i>	71
4.11. Load angle of equivalent generator representing <i>Gen 4, 5</i> and <i>6</i> during a three-phase-to-ground fault at <i>Node 7</i>	71
4.12. 39 nodes and 9 generators test network	72
4.13. Load angle of <i>Gen 1,2 and 3</i> using an equivalent model for the coherent units during a three-phase-to-ground fault at <i>Node 31</i>	72
4.14. Load angle of the group of coherent generators with the equivalent during a three-phase-to-ground fault at <i>Node 31</i>	73
4.15. AFT of the real-time simulations	73
4.16. Test network with dynamic load	77
4.17. Feeder bus voltage and motor speed in event of direct online motor starting in the test network	77
4.18. Test network in Figure 4.1 with dynamic load connected at <i>Node 8</i>	78
4.19. Motor speed and electrical torque following direct online start-up	80
4.20. Busbar voltage magnitude and motor inrush current following direct on-line start-up	81
4.21. Active and reactive power of motor following direct on-line start-up	81
4.22. Phase angle and initial stator loss due to high inrush current following motor direct on-line start-up	82
4.23. Voltage and reactive power at different loading conditions	82
4.24. Speed and electrical torque of <i>Gen 3</i> and <i>4</i> in event of direct online motor starting	83
4.25. Mechanical torque and field current of <i>Gen 3</i> and <i>4</i> in event of direct online motor starting	83
4.26. Bus voltage and phase angle of <i>Node 8</i> subjected to a three-phase-to-ground fault	84

List of Figures

4.27. Unloaded motor speed and electrical torque subjected to a three-phase-to-ground fault at <i>Node 8</i>	85
4.28. 0.5 <i>p.u.</i> loaded motor speed and electrical torque subjected to various faults at <i>Node 8</i>	85
4.29. Motor active and reactive power demand subjected to a three-phase-to-ground fault at <i>Node 8</i>	86
4.30. Bus voltage and phase angle at <i>Node 8</i> without motor subjected to a single-phase-to-ground fault	86
4.31. Bus voltage and phase angle at <i>Node 8</i> with motor subjected to a single-phase-to-ground fault	87
4.32. Bus voltage and phase angle at <i>Node 8</i> without motor subjected to a phase-to-phase fault	87
4.33. Bus voltage and phase angle at <i>Node 8</i> with motor subjected to a phase-to-phase fault	88
5.1. Test system of a dispersed generation distribution network	91
5.2. Induction generator speed and terminal voltage following a three-phase-to-ground fault with synchronous generators' AVR and turbine governor control	92
5.3. Synchronous generator load angle and terminal voltage following a three-phase-to-ground fault with synchronous generator's AVR and turbine governor control	92
5.4. Induction generator speed and terminal voltage following a three-phase-to-ground fault without synchronous generators' AVR and turbine governor control	94
5.5. Synchronous generator load angle and terminal voltage following a three-phase-to-ground fault without AVR and turbine governor control	94
5.6. Induction generator speed and terminal voltage cleared at $CT = 0.216s$ with different X/R ratios	95
5.7. Induction generator speed under different network strength	96
5.8. Islanded induction generator speed and terminal voltage with no isolated load under different excitations	97
5.9. Islanded induction generator torque and reactive power demand with no isolated load under different excitations	98
5.10. Islanded induction generator terminal voltage with no isolated load under unbalanced excitation due to capacitor bank phases disconnection	99

List of Figures

5.11. Islanded induction generator speed with no isolated load under unbalanced excitation due to capacitor bank phases disconnection	99
5.12. Islanded induction generator speed and terminal voltage with isolated load under different excitation	100
5.13. Islanded induction generator speed and terminal voltage with isolated load under different loading condition with excitation $C = 0.585 p.u.$	100
5.14. Induction generator speed and electrical torque under a single-phase-to-ground fault in phase a with different network conditions	102
5.15. Induction generator speed and electrical torque under a single-phase-to-ground fault on phase a with different network conditions with mechanical input torque of $P_m = 0.9 p.u.$	102
5.16. Induction generator terminal voltage under : a) Single-phase-to-ground fault, b) Phase-to-phase fault	102
5.17. Induction generator speed and electrical torque under a single-phase-to-ground fault on Phase a with different network conditions	103
6.1. FC/TCR configuration of SVC	108
6.2. Thyristor switching at current zero crossing	110
6.3. TCR current and voltage waveforms	111
6.4. SVC control blocks	111
6.5. Bus voltage at <i>Node 8</i> and the thyristor firing angle following a direct online motor starting with $t_r = 0.05 s$	113
6.6. Bus voltage at <i>Node 8</i> and the thyristor firing angle following a direct online motor starting with $t_r = 0.1 s$	113
6.7. Motor speed and electrical torque following a direct online start-up	114
6.8. Active and reactive power of motor following a direct online start-up with SVC	114
6.9. Motor current and phase angle following a direct online start-up with SVC	115
6.10. <i>Gen 3</i> terminal voltage and electrical torque following a three-phase-to-ground fault without AVR and turbine governor control	116
6.11. <i>Gen 3</i> speed and load angle following a three-phase-to-ground fault without AVR and turbine governor control	116
6.12. <i>Gen 3</i> terminal voltage and electrical torque following a three-phase-to-ground fault with AVR and turbine governor control	116

List of Figures

6.13. <i>Gen 3</i> speed and load angle following a three-phase-to-ground fault with AVR and turbine governor control	117
6.14. Three phase VSC	118
6.15. PWM with unipolar switching	118
6.16. One-line representation of a Voltage Source Converter	119
6.17. Basic STATCOM configuration	121
6.18. Simplified STATCOM's AVR control blocks	122
6.19. Bus voltage at <i>Node 8</i> and converter modulation index following direct on-line motor starting with $K_r = 10$ and $t_r = 0.1s$	124
6.20. Motor speed and electrical torque following direct on-line motor start-up with $K_r = 10$ and $t_r = 0.1s$	124
6.21. Active and reactive power following direct on-line motor start-up with STATCOM	125
6.22. Motor current and phase angle following direct on-line motor start-up with STATCOM	125
6.23. Segregation of instantaneous variables into positive and negative sequence	127
6.24. Block diagram of the dynamic control scheme for the STATCOM	128
6.25. Bus voltage at <i>Node 8</i> : a) without overcurrent control; and b) with overcurrent control	128
6.26. Motor speed and electrical torque with and without overcurrent control	129
6.27. a) Magnitude of positive and negative sequence bus voltage at <i>Node 8</i> ; and b) Magnitude of negative sequence STATCOM compensating current	129
6.28. STATCOM compensating current: a) Without overcurrent control; and b) With overcurrent control	130
6.29. Induction generator speed and terminal voltage cleared at $CT = 0.247s$ with STATCOM in the network	131
6.30. Islanded induction generator speed and terminal voltage with no isolated load with STATCOM	132
6.31. Islanded induction generator torque and reactive power with no isolated load with STATCOM	132
6.32. Basic DVR configuration and connection to the network	133
6.33. DVR control scheme	135

List of Figures

6.34. Section of test network as in Figure 4.18 with DVR installed between the induction motor and common coupling point	135
6.35. a) Common coupling point voltage and motor terminal voltage; and b) Motor current when subjected to a three-phase-to-ground fault with DVR	136
6.36. Single-phase-to-ground fault with DVR; a) Common coupling point voltage at <i>Node 8</i> ; and b) Motor terminal voltage	136
6.37. Phase-to-phase fault with DVR; a) Common coupling point voltage at <i>Node 8</i> ; and b) Motor terminal voltage	137
6.38. Loaded motor speed and electrical torque subjected to various fault conditions with DVR	137
6.39. HVDC-VSC configuration	140
6.40. Power dispatch control	141
6.41. DC voltage regulation control	141
6.42. Schematic diagram of the scaled-down WECS	142
6.43. Scaled-down WECS power characteristics	142
6.44. Test setup	143
6.45. HVDC-VSC response during WECS run-up to rated power	145
6.46. HVDC-VSC response when carrying oscillating power	146
6.47. AFT of simulations	146
A.1. Generator connected to an infinite bus for short circuit fault analysis using PSCAD/EMTDC TM ; corresponding results in Figure 2.2	166
A.2. Generator connected to a load for short circuit fault analysis in PSCAD/EMTDC TM ; corresponding results in Figure 2.5	167
A.3. Multimachine network for short circuit fault analysis using PSCAD/EMTDC TM ; corresponding results in Figure 3.3	168
A.4. Asynchronous machine connected to a source for operational analysis using PSCAD/EMTDC TM ; corresponding results in Figure 2.9	169
B.1. The trapezoidal rule	171
B.2. Connection of simple network to node	171
C.1. Actual power system network	174
C.2. Reduced equivalent power system network	175

List of Tables

3.1. steady state values of generators' variables in Figure 3.5	49
4.1. steady state values of generators' variables in Figure 4.1	66
5.1. Induction generator and capacitor loading at steady state	91
5.2. Induction generator parameters	92
5.3. CCT of the wind driven induction and synchronous generator with different oscillating magnitudes of the WECS power output	104

Abbreviations

DC	direct current
AC	alternating current
EMTP	electromagnetic transient program
PSCAD/EMTDC	Power System Computer Aided /Electromagnetic Transient Direct Current
AVR	automatic voltage regulator
PSS	power system stabiliser
FACTS	flexible AC transmission systems
GTO	gate turn – off thyristor
VSC	voltage source converter
IGBT	insulated gate bipolar transistor
PWM	pulse – width modulation
TNA	transient network analyser
HIL	hardware – in – the – loop
RTS	real – time station
STATCOM	static synchronous compensator
DVR	dynamic voltage restorer
HVDC	high voltage DC transmission
HVDC – VSC	HVDC station based on voltage source converters
SVC	static var compensator
WECS	wind energy conversion system
<i>p.u.</i>	per – unit
<i>d – axis</i>	direct axis
<i>q – axis</i>	quadrature axis
L_d	transformed <i>d – axis</i> inductance
L_q	transformed <i>q – axis</i> inductance
L_{ad}	transformed axis mutual inductance between stator and rotor

L_l	leakage inductance
L_{a0}, L_{a2}, M_{s0}	inductance coefficients of the stator
L_{ff}, L_{kd}, L_{kq}	inductances coefficients of the rotor
M_{ad}, M_{aq}, M_{af}	mutual inductance coefficients of stator and rotor windings
M_{fkd}	mutual inductance between field and d – axis winding
R_s	stator resistance
R_f	field winding resistance
R_{kd}	d – axis damper winding resistance
R_{kq}	q – axis damper winding resistance
$\delta\delta$	generator load angle
H	inertia constant
L_{ss}, L_{rr}	self – inductances of three – phase induction machine stator and rotor circuits
L_{sm}	mutual inductance between stator phases
L_{rm}	mutual inductance between rotor phases
M_{sr}	mutual inductance between three – phase stator and rotor circuits
E_{fd}	apparent synchronous generator field excitation voltage
$[v_{his}]$	vector representation of preceding time – step variables of the discretised generator terminal voltage equation
$[R_T(t)]$	coefficient matrix of the discretised generator terminal voltage equation
$[e_s(t)]$	vector of instantaneous generator stator voltages
$[e_r(t)]$	vector of instantaneous generator rotor voltages
$[i_s(t)]$	vector of instantaneous generator stator currents
$[i_r(t)]$	vector of instantaneous generator rotor currents
$[R_{T_{ss}}(t)]$	stator coefficient matrix of the of the discretised generator terminal voltage equation
$[R_{T_{rr}}(t)]$	rotor coefficient matrix of the discretised generator terminal voltage equation
$[R_{T_{rs}}(t)], [R_{T_{sr}}(t)]$	mutual stator and rotor coefficient matrix of the discretised generator terminal voltage equation
$[v_{his_s}]$	vector of stator preceding time – step variables of the discretised generator terminal voltage equation
$[v_{his_r}]$	vector of rotor preceding time – step variables of the discretised generator terminal voltage equation
$[R_{equ}(t)]$	coefficient matrix of the discretised generator stator voltage equation
$[E_s(t)]$	vector of known input variables of the discretised generator stator voltage equation
$[R_{mT}(t)]$	coefficient matrix of the discretised induction machine terminal voltage equation

$[e_{ms}(t)]$	vector of instantaneous induction machine stator voltages
$[e_{mr}(t)]$	vector of instantaneous induction machine rotor voltages
$[i_{ms}(t)]$	vector of instantaneous induction machine stator currents
$[i_{mr}(t)]$	vector of instantaneous induction machine rotor currents
$[R_{mT_{ss}}(t)]$	stator coefficient matrix of the of the discretised induction machine terminal voltage equation
$[R_{mT_{rr}}(t)]$	rotor coefficient matrix of the discretised induction machine terminal voltage equation
$[R_{mT_{rs}}(t)], [R_{mT_{sr}}(t)]$	mutual stator and rotor coefficient matrix of the discretised induction machine terminal voltage equation
$[v_{mhis_s}]$	vector of stator preceding time – step variables of the discretised induction machine terminal voltage equation
$[v_{mhis_r}]$	vector of rotor preceding time – step variables of the discretised induction machine terminal voltage equation
$[R_{mequ}(t)]$	coefficient matrix of the discretised induction machine stator voltage equation
$[E_{ms}(t)]$	vector of known input variables of the discretised induction machine stator voltage equation
$[G_{abc}]$	matrix of three – phase network conductance
$[v_{n_{abc}}(t)]$	vector of three – phase instantaneous n – node network nodal voltage
$[i_{n_{abc}}(t)]$	vector of three – phase instantaneous n – node network nodal current injection
$[hist_{abc}]$	vector of three – phase preceding n – node network variables in the instantaneous three – phase network equation
$[i_{ng_{abc}}(t)]$	vector of three – phase instantaneous n – node network generator node current injection
$[i_{nl_{abc}}(t)]$	vector of three – phase instantaneous n – node network load node current injection
$[v_{ng_{abc}}(t)]$	vector of three – phase instantaneous n – node network generator node voltage
$[v_{nl_{abc}}(t)]$	vector of three – phase instantaneous n – node network load node voltage
$[G_{gg_{abc}}]$	coefficient matrix consisting of network conductances between generator nodes
$[G_{ll_{abc}}]$	coefficient matrix of network conductances between load nodes
$[G_{lg_{abc}}], [G_{gl_{abc}}]$	coefficient matrix of network conductances between generator and load nodes
$[G_T]$	coefficient matrix of the network generator node current injection

$[H_{isr}]$	vector of known input variables of the network generator node current injection equation
I/O	input/output
ADI	Applied Dynamic International
SP	simulation processor
CE	compute engine
GUI	graphical user interface
AFT	actual frame time
DFT	desired frame time
CT	clearing time
CCT	critical clearing time
TCR	thyristor controlled reactor
FC	fixed capacitor
TSC	thyristor controlled capacitor
PI	propotional plus integral
secs	second
<i>ms</i>	millisecond
μs	microsecond
W	watt

1. Introduction

1.1. Foreword

The operation of electrical power systems began in 1882 when Edison first built his *direct current (DC)* generation station to supply a load of 400 lamps, each consuming 83W [1]. However, engineers at that time were very determined to find an alternative method of generation, which could be transmit electricity effectively over long distances. In 1883, Tesla made inroad with the discovery of the rotating magnetic flux machine, which forms the principle of the *alternating current (AC)* generator. The more beneficial concepts of AC generation and transmission were transformed into a practical scheme, which was successfully demonstrated in 1896 by Westinghouse to be viable for power transmission over long distance. This lead to the rapid development of interconnected power system transmission and distribution network, which the renowned electrical engineer, Charles P. Steinmetz, called it, the largest and most complex machine ever devised by man. Ever since, the challenge for power engineers worldwide has been to maintain the safe and reliable operation of the power system network. To this end, many great developments in power system engineering have had to be created continuously.

The analysis of power systems can be generally thought as intended for two different conditions of operation, i.e. the steady state and dynamic analysis [1]-[3]. The steady state analysis involves studying the operation of the power system independently of time variation. In general, steady state analyses in power systems covers the area of load flow, optimal power flow, fault analysis, economic optimisation and state estimation. The dynamic analysis mainly involves stability studies of the power system over time, subjected to disturbances. Different types of power system stability studies are identified and can be categorised into two main areas, i.e. transient stability and small-signal stability [4]-[9].

Power system stability may be defined broadly as the property of a power system that enables it to remain in a stable equilibrium state under normal operating conditions and to regain an acceptable equilibrium state after being subjected to a disturbance [4]-[9]. Typical examples of events causing disturbances are sudden faults on the network, switching on of heavy loads or loss of a generation unit. Arguably, of all the complex issues surrounding power system

1. Introduction

operations, stability is the most intricate to understand and handle. Power system stability analysis has, in the past, created many opportunities for in-depth research. At present, increase demand for electricity, interconnected networks that are intrinsically linked to highly volatile economic signals and widespread dissemination of non-linear loads are a few of the factors that have exacerbated and created renewed interest in power system stability.

1.2. Background and Power System Modelling for Transient Analysis

Power system stability entails the evaluation of a power system's ability to withstand large disturbances, and to survive transition to a normal and acceptable operating condition. At the occurrence of such disturbances, the system's responses involve large excursion of the interconnected generators' load angles. Classically, power system stability denotes a condition in which various synchronous generators of a power system network are connected together to remain in *synchronism* with each other [4]-[9]. Conversely, *loss of synchronism* of the generators denotes instability. Hence, with an intuitive definition, the synchronism of interconnected synchronous generators constitutes one of the most important components for the study of power system stability. Under normal operating conditions, all the system generators run at synchronous speed, if a large disturbance occurs, the generators start swinging with respect to each other and their motion being governed by non-linear differential equations.

There are two main approaches aimed at power system transient stability assessment, the conventional time-step solutions and the direct method of Lyapunov type formulation [9]. The most practical and popular method for transient stability is the time-step method based on a step-by-step numerical integration technique. This method has the ability to solve large scale power systems very reliably and has no difficulty in including complex plant component models. In its simplest form, the power system stability phenomena is governed by a set of non-linear ordinary differential equations representing all the generating units as in (1.1), and a set of algebraic equations representing the networks and loads as in (1.2). Upon inception of a disturbance, the non-linear sets of differential and algebraic equations are solved numerically, both during-fault and post-fault configurations of the power system. The time-step method has prevailed as the universal way of assessing the stability of a general interconnected multimachine system owing to its intrinsically attractive features.

$$\dot{x} = f(x, y) \tag{1.1}$$

$$0 = g(x, y) \tag{1.2}$$

1. Introduction

The non-linear equations are solved numerically using a step-by-step integration technique. The simulation process of interest are normally in the range of 10^{th} to 100^{th} of a second for cases of unstable systems to be identified. For cases where the interest is to observe stable systems reaching stability following the post fault period, the simulation could take up to a few seconds.

The direct method assessed system stability without having to solve the system of differential equations. This method resorts to a transient energy function for assessing the system stability characteristic [4]-[8]. The energy based method is a special case of the general Lyapunov's second method, with the energy function being the Lyapunov function. The application of direct methods to practical power systems presents a number of difficulties and many simplifying assumptions are necessary to form the energy function. This has discouraged its adoption by power engineers worldwide.

The solution of stability problems using the time-step method is rather straightforward, it involves the solution of two sets of equations. However, in practice it is almost impossible to effectively solve the set of non-linear differential equations, which represent the generator, without the help of computers. This is more so if the system is an interconnected system with more than one generator. Hence, the area of modelling of the synchronous generator has been an area of constant interest ever since the first model was proposed by R.H. Park [10][11] in 1921, and subsequently published in several classic literatures on electrical machines [12]-[15]. In his work, the non-linear coefficients in the differential equations of the synchronous generator is simplified using mathematical transformations to obtain a set of time independent coefficients. This allows the computation of the power system stability problem to be carried out easily, a fact, which was highly beneficial in light of the limited computing facilities available at that time [6][16]-[24]. However, the use of such transformations introduces assumptions on the generator model, which impair the study of certain aspects of stability analysis [25]-[33].

In classic stability analysis, which involves this model [1]-[6][16]-[24], the network is normally represented in steady state by its equivalent impedances. This quasi steady state representation for stability analysis is based on the assumptions that the electrical time-constants of the network is much smaller than the mechanical time-constants of the generators, which determine the stability of the system. Hence, the steady state network representation does not affect the overall accuracy of the stability analysis [16]. This statement does not apply to other components in the network, which might be affected by changes in network variables under faulted conditions.

A more accurate modelling of the network was introduced by Dommel [34], where the network components are represented by their actual active components and solved in the time domain. Some of the most widely used industrial programs available today for the calculation of transients in power systems, such as EMTP and EMTDC [34][35], are based on such

1. Introduction

a modelling approach when solving the network equations. In these packages, the simplified transformed model of the synchronous generator is interfaced to the rest of the network in the direct time phase-domain by constant transformation at every time-step. Thus, a complete direct time phase-domain stability model of power system components remains to be realised, and the development and application of such a model provides the focus of this research project.

1.3. Power System Transient Enhancement through Power Electronics

Maintaining synchronism of the interconnected synchronous generator plays an important role in ensuring the stable and uninterrupted operation of the whole power system network. This synchronism can be easily affected by various switching events in the network, which among others include faults, change of loading conditions and loss of generation are among others. The main cause for losing synchronism is due to the electrical changes at the terminals of the generators during the above mentioned events. For example, during a fault, the voltage at the terminal of a generator can drop substantially resulting in the power generation to be disrupted, which then causes the generator to accelerate out of synchronism. Sometimes upon clearance of faults, high oscillations in generator power can result in loss of synchronism [4]-[8]. Traditionally, these problems were often resolved by implementation of complex control systems for the generator such as the automatic voltage regulator (AVR), power system stabiliser (PSS) and speed turbine governor [36]-[40]. However, with the expansion of power system networks through non-conventional generating sources and increasing loads, the response at the terminal of the generators can be very erratic when faced with a disturbance due to a weak link in the network. Engineers have sought alternative solutions to improve the stability of the network in light of the restricted capability of the generator's controllers due to their limited rating and flexibility [4][36].

The advent of high rating fast control power electronics technology has given rise to the possibility of enhancing the stability of a power system network, externally of the generators. At transmission level, these new power electronics controllers are termed Flexible AC Transmission System (FACTS) devices [41]-[44], while at low rating, they are known as custom power devices [45]. The main objectives of introducing these controllers into power systems are to increase the power transfer capability and to provide control of power flow over a designated transmission or distribution network [44]. These controllers achieve their objective by providing continuous control over a wide range of power system parameters, which include voltage magnitude, phase angle, active and reactive power flow, and the network impedance. The first generation of these controllers, which were based on thyristor's operations have

1. Introduction

been extensively used in industries to mitigate power oscillations, stabilise power system's transient conditions and to improve the overall power system dynamics [44][48]-[55]. They are normally connected as a shunt device in high voltage transmission system for voltage control. More recently, a newer generation of devices based on the self-commutated voltage source converter (VSC) using gate turn-off thyristor (GTO) and integrated gate bipolar transistor (IGBT) have been developed [56]-[62]. The detailed explanation of these controllers will be presented in later chapters.

The research into the effects that power electronics controllers have on enhancing power system stability has become a topic of great interest in the last decade. Hence, several dynamic models of these controllers are available in the open literature. The most common models are based on the study of their series impedance, power and reactive power flow characteristic in quasi steady state conditions [50][52]-[55][57]. These models are useful in describing some aspects of the controllers, which influence the generator's dynamic characteristic. However, the models exhibit serious short comings as detailed representation are often omitted, and analysis through the use of equal area criteria technique only apply to very simple network [50][54][56]. The more detailed models involve transformation into the time independent representation to coincide with the transformed axis generator models [58][59], which are mathematically complex. For the VSC based controllers, which functions on the critically time-dependent PWM technique, it is important to represent the model in the original time-domain without transformations. Another major drawback of existing models is that the dynamic interaction between the controllers, generators and the power system network has not been fully implemented. Hence, further research activity is required to develop more accurate and reliable models for power electronics controllers in network-wide applications.

1.4. Real-Time Digital Power System Simulation

Manufacturers, large utilities and research organisations use powerful and reliable digital simulation tools to analyse the various aspects of power networks. Such analyses are necessary in order to obtain useful information to achieve effective power system network design and operations. From the power system stability point of view, the analysis will aid in the design of the generator controllers, network interconnection and power electronics devices that are necessary to prevent outages in times of disturbances. Simulation packages such as the EMTP [34] and EMTDC [35] are widely used for analysing power system stability problems.

The simulation tools are normally software packages where analysis is conducted based on the mathematical model of the power system components within the same package. The time taken by the simulation is the function of the complexity of the analysis and the computational efficiency with which the packages operates. In most circumstances, for a given period of analysis defined in real-world time, the simulation packages will require much longer

1. Introduction

computation time to produce the solution [64]-[69]. Hence, these packages do not provide a platform suitable for real-time test environments, where external equipment can be directly interfaced to the simulation tools. The mismatch between the computation time taken by the simulation tools and the actual physical systems response makes this a difficult task.

In order to fulfil the aspect of simulations, which include the interfacing of physical devices, analogue simulators have been used excessively in the past [67]-[69]. In these simulators, the results from off-line simulations, or actual data are fed, in real-time, to the device under test. However, this approach is restricted to open-loop testing and there can be no dynamic interaction between the device under test and the simulator [63][64]. For closed-loop testing of the physical devices, a specially designed AC Transient Network Analyser (TNAs) can be used [65]-[67]. The TNAs is essentially a scaled-down power system network, which is expensive to build and maintain [65]-[67].

In recent years, the development of modern real-time digital power system simulators with hardware-in-the-loop (HIL) capabilities [66][67][69], have provided a cost-effective and flexible alternative. The real-time simulator (RTS) executes the mathematical model of power system components and continuously produces output signals in real-time that accurately represent the real system under investigation. This permits physical electric devices to be mixed with mathematical models in simulation to replicate an actual power system network. The closed-loop operation afforded by these simulators provides a powerful test bed for evaluating and accurately testing new and existing physical electric devices under any operating conditions desired by the user.

The importance and advantages of performing HIL testing of physical devices has provided new research opportunities in the area of power system modelling that are suitable for real-time applications. This issue will be reported in the thesis in later chapters.

1.5. Motivation and Objectives of the Present Research Work

This research is primarily concerned with the direct time phase-domain modelling of power system components for both non-real-time and real-time stability analyses. Despite the fact that interest in phase-domain modelling has been shown over the years [25]-[31], there is to date no phase-domain model available in the open-literature in which a complete analysis of a complex system is undertaken in the phase co-ordinates. The lack of computing capability may have been responsible for this, but the lack of efficient solution techniques for dealing with large sets of non-linear differential equations may have also played a part.

The formulation of power system models, namely the synchronous generator, for stability analysis has always involved the need for tedious mathematical transformation and, hence,

1. Introduction

restricting the model to various assumptions. The restrictions imposed on the model have resulted in the inability to study certain power system conditions. It is known that transformed models of power system components into two axis ($d - q$) representations are not suitable for studies of ground related asymmetrical operating conditions [25][27][30][31]. In order to overcome the difficulties, a third or zero sequence component must be defined so that the three phase quantities can be accurately represented by the transformed axis variables. This more flexible transformed model, termed the $d - q - 0$ axis model, allows the asymmetrical condition to be analysed. However, the model could still be unsuitable under severe asymmetrical operating conditions, such as open or short circuit of the machine windings. Under these conditions, the balance of the machine's actual windings arrangements could be affected. This will affect the accuracy of the transformed axis model as the transformation is based on the notion that the machine windings have a balance three phase arrangement [12][13].

Hence, the present work is motivated by the need to improve on the models of power system components, which power engineers use to assess potential stability problems. Also the need to study power electronic devices to enhance the stability of existing and new networks in view of load growth. The inclusion of power electronic devices in the direct time phase-domain for stability analysis, in the current work, is a contribution in that direction.

The objectives of the research carried out in this thesis are as follow:

- To develop comprehensive synchronous generator models in the direct time phase-domain for stability analysis. Develop an integral approach to employ this model for solving a multimachine network with time-domain representation of the interconnecting network. Perform analysis concerning operating conditions of the network and the generators.
- To develop a comprehensive asynchronous machine model in the direct time phase-domain. To study the interaction of this machine with the synchronous generator in an interconnected network as a dynamic load. Application of this machine as a generator to represent a renewable source and study its effect on the interconnected network stability.
- To develop power electronics model and their control in the direct time phase-domain. The model must be represented by its actual operating condition with its controllers.
- To integrate the various power electronic controller into the multimachine model. To gain physical insight into the dynamic interactions between the generators and the controllers. To investigate the capabilities of these controllers to improve the overall network stability.

1. Introduction

- To implement the complete multimachine system phase-domain model in the real-time environment for hardware-in-the-loop (HIL) application.

1.6. Contributions

The main original contributions of the research work are summarised below:

- Developed a new method for efficient solution of a multimachine power system network in the direct time phase-domain enabling a unified approach to study both symmetrical and asymmetrical fault conditions.
- The model of the AC machines and the multimachine network are carefully evaluated for different operating conditions. The responses of the model is compared to existing models available in all EMTP-type industry packages, i.e. PSCAD/EMTDCTM. Conclusions are reached to justify the benefit of the novel model in the direct time phase-domain.
- Implemented the multimachine model into a real-time station to perform a real-time simulation of the model. Demonstrated that the new multimachine model is capable of producing real-time response.
- Developed a new method of coherency-based multimachine approach based on the direct time phase-domain model. The benefit of this approach is demonstrated to reduce computing time when applied in a real-time environment.
- Performed analysis on the impact of dynamic loads in a power system network using the new multimachine model. The influence of the load can be assessed with greater effect using the new multimachine model.
- Analysis on the transient behaviour of an asynchronous generator with respect to conventional generator in a dispersed generation environment. Dynamic scenarios related to a wind driven asynchronous generator is studied in greater detail .
- Development of new power electronics controllers models in the direct time phase-domain for transient analysis with actual representation of their time dependent switching operations. The models of controllers developed are:
 - SVC
 - STATCOM
 - DVR
 - HVDC-VSC

1. Introduction

- Implemented detail control scheme for the above mentioned controllers.
- Integrated the power electronics controllers model for the SVC, STATCOM and DVR into the new multimachine model. Performed analysis on the effectiveness of these controllers for compensation of various network dynamic conditions as well as to improve stability limits.
- Implemented the HVDC-VSC model into a real-time station to perform a real-time simulation. Demonstrated the ability to interface the model in the real-time station to a physical device in the form of a scaled down laboratory model of a WECS.

1.7. Publications

The following publications were generated during the course of the present research:

1.7.1. Transaction-grade Papers

- K.H. Chan, E. Acha, M. Madrigal and J. Parle, “The Use of Direct Time Phase-Domain Synchronous Generator Model in Standard EMTP-Type Industrial Packages”, *IEEE Power Engineering Review*, June 2001, pp. 63–65.
- K.H. Chan, J.A. Parle and E. Acha, “Real-time Transient Simulation of Multi-Machine Power System Networks in the Phase-Domain”, Revised paper submitted to *IEE Proceedings - Gen, Trans. and Distr. Part C*, March 2002.
- K.H. Chan, E. Acha and A. Ekwue, “Direct Time Phase-Domain Coherency-based Multimachine Transient Analysis for Real-Time Application”, Paper submitted to *IEEE Trans. on Power System*, 2002.

1.7.2. Conference Papers

- K.H. Chan and M. Madrigal, “Phase Domain Dynamic Analysis of Conventional and Advanced Static Var Compensator in Voltage Sag due to Motor Start-Up”, *Conf. Proceedings of IASTED EuroPES 2001*, Rhodes, Greece, July 2001, pp. 394–400.
- K.H. Chan and E.Acha, “Transient Stability Behaviour of a Distribution Network with Embedded Wind-driven Induction Generator”, *Conf. Proceedings of IASTED EuroPES 2001*, Rhodes, Greece, July 2001, pp. 663–668.

1. Introduction

- K.H. Chan, J.A. Parle, N. Johnson and E. Acha, “Real-Time Implementation of a HVDC-VSC Model for Application in a scaled-down Wind Energy Conversion System (WECS)”, *Proceedings of the 7th International Conference on AC-DC Power Transmission 2001*, London, November 2001, pp. 169-174.

1.8. Outline of thesis

This thesis is organised as follow:

Chapter 2 presents the mathematical modelling of AC machines for transient analysis. The direct time phase-domain model and the conventional transformed model of the synchronous and asynchronous machines are presented in detail. Validation tests of the direct time phase-domain model with an industrial power system package, using the transformed model, are performed. Versatility of the direct time phase-domain model to deal with non-conventional studies are demonstrated through simulations.

Chapter 3 applies the direct time phase-domain model of the synchronous machines to a practical multimachine network. A new mathematical model for the multimachine network, based on a discretisation technique, is presented in detail. Validation tests are performed to verify the new multimachine model by making comparisons with an industrial power system package. The general synchronous generator controllers are also presented where it can be implemented into the multimachine network with no complications. The real-time capability of the multimachine model is demonstrated by simulation using a real-time station. The frame time of simulation will be presented as a proof of actual simulation in the real-time environment.

Chapter 4 presents a novel method to aggregate a group of coherent generators in the direct time phase-domain. The coherency-based approach can reduce computing time by reducing the number of generators nodes involved in a simulation by representing the coherent generators as a single unit. The benefit of this approach is applied in a practical real-time simulation enabling larger networks to be simulated. The implementation of dynamic load into the multimachine network is also presented in this chapter. The voltage disruption caused by the direct online start-up of induction motor is investigated. The effect of motor's post fault re-acceleration on the voltage recovery period of network is explained.

Chapter 5 deals with the implementation of the asynchronous machine in a wind energy conversion system (WECS). The effect of having a co-generation multimachine network is studied for various conditions including transient stability and power quality issues.

Chapter 6 presents the novel model of power electronics controllers in the direct time phase-domain. The model of the conventional static var compensator (SVC), advanced static var

1. Introduction

compensator (STATCOM), dynamic voltage restorer (DVR) and HVDC-VSC system are described in detail. A comparison is made between the effectiveness of the SVC and STATCOM in the mitigation of voltage sags caused by motor start-up. The SVC is studied with emphasis on transient stability of the network. A detailed control scheme for the STATCOM is also presented in order to control its operation under severe unbalances. The application of the STATCOM to enhance the performance of an asynchronous generator in a dispersed generation network is presented in this chapter. The implementation of the HVDC-VSC station in the real-time environment, and its application into the study of power transfer between a scaled down WECS model and a network will be discussed in full detail.

Chapter 7 covers the general conclusions emphasising on the original contributions of the thesis. Several suggestions for future research work will also be outlined.

This manuscript has been prepared using LyX (version 1.1.4) document processor for L^AT_EX, using times pslatex font size 12. The figures were drawn using Xfig (version 3.2). Both packages run under the Solaris SunOS release 5.7 (UNIX system release 4.0) in an Ultra10 SunSparc work station. The simulations were conducted using MatlabTM (version 5.3) code. The plots were produced using MatlabTM plot command.

2. Modelling of AC Machines for Transient Analysis

For many decades, the modelling of AC machines for transient analysis has been the subject of much interest in the development of power system's electromagnetic transient programs, such as EMTP and PSCAD/EMTDCTM. This chapter provides a summary of the models and techniques involved in the modelling of the AC machines. The model of the machines in the direct time phase-domain is presented in detail, and the traditional approach to transform this model into time-independent reference frame is also described. Results are presented to show the flexibility of the direct time phase-domain model for analyses of symmetrical and asymmetrical network conditions.

2.1. Introduction

The transient stability of a power system network depends largely on the AC machines systems that are interconnected to the network. Loss of stability signifies the loss of synchronism between the machines in the network [4][6]. Hence, the accurate and flexible modelling of AC machines has been the subject of much effort even in the beginning of the last century. The evolution of analytical methods for determining the response on the interconnected machines systems has led to the development of efficient analytical tools that are well received by power engineers worldwide.

Perhaps the main contributor to the theory of machine modelling is R.H. Park [10][11]. In his approach, the time-varying coefficients associated with the physical machine, due to certain machine inductances, which are a function of the machine rotor displacement, are transformed into a different axis of representation by eliminating the time-dependency of these coefficients. This involves the reference frame transformation theory, which leads to a set of more easily solved machine equations, but, in essence, not representing the actual physical machine as it is intended to operate [25][27].

This transformation technique, otherwise known as the two axis ($d - q$) model, relies on rig-

2. Modelling of AC Machines for Transient Analysis

orous mathematical transformation, which only apply if certain fundamental restrictions are assumed to exist in the machine. Notable among them is the fact that the electrical quantities and windings of the machine are balanced. In order to represent unbalance conditions in the machine electrical quantities, a third or zero sequence component must be defined in the transformed model so that the three phase electrical quantities can be accurately represented by the transformed variables. This more complete and flexible model is termed the $d - q - 0$ axis model.

However, the validity of the $d - q - 0$ axis model depends on the balance three phase winding arrangements of the machine [12]. Under severe asymmetrical operating conditions, such as open or short circuit winding, the balance winding arrangement will be affected, thus hampering its representation in the $d - q - 0$ axis. This is not to say that the $d - q - 0$ axis model has not served engineers well for almost half a century in light of limited computing resources. With the severe constraints imposed by analogue computers and past generations of digital computers, it made sense to use the $d - q - 0$ axis model at the expense of network study flexibility.

One possible solution to relax this constraint in current machine models is to represent the generator in the direct time phase-domain frame of reference. The direct time phase-domain model is, in fact derived from the most fundamental law in electrical systems, i.e. Faraday's Law, which is used to characterise the operation of an AC machine with respect to the voltage at its terminal. In principle, the model is a matrix model relating instantaneous primary variables such as the three-phase voltages and currents through a set of differential equations involving the non-linear linkage inductances of the machine. The use of this model for transient analysis purposes is well documented in open literature [25]-[31]. However, this model has yet to gain recognition from power systems software developers and from the industry. For instance, the machine models adopted in all EMTP-type packages [34][35] are based on the classic $d - q - 0$ axis approach.

In the past, one of the hindrances to the wide acceptance of this model was the extensive computing requirements needed to solve the non-linear equations of the machine. However, with the current hardware and software computer capabilities, the solution of the direct time phase-domain model can be conducted almost as efficiently as the transformed $d - q - 0$ axis model. This, together with the fact that the direct time phase-domain model retains the physical picture of the actual machine, leads to a more versatile model, capable of solving symmetrical, asymmetrical, and non-sinusoidal operating conditions with a unified approach within the same frame-of-reference.

This chapter outlines the main steps involved in AC machines modelling for transient analysis. The AC machine models in the direct time phase-domain and $d - q - 0$ axis are presented. The effects of AC machine magnetic saturation are not considered in this thesis. The main objective of this thesis is to develop a new method for multimachine model solution in the

2. Modelling of AC Machines for Transient Analysis

direct time phase-domain. It is justifiable to first develop and test this new model using the most fundamental of the AC machine models without the effect of saturation.

2.2. Approach to AC Machine Modelling

In general, the two types of AC machines associated with power system transient analysis are the synchronous machine and the asynchronous machine. In this thesis, the synchronous machine is considered to be a generating unit, hence from here on with, it will be termed the synchronous generator. The asynchronous machine more popularly known as the induction machine, because of the nature of its operation, normally operates as a motor to provide mechanical torque. However, for specific operations, the asynchronous machine can be used as a generator. For example in the case of non-conventional generation, such as wind generation.

The effort is directed towards deriving the mathematical formulation of the machines in order to develop a generalised modelling approach. The general representation may be considered to be a set of closed-form differential equations as in (2.1),

$$[\dot{x}] = [A][x] + [B][u] \quad (2.1)$$

where $[A]$ contains the inductance coefficients of the machine, $[\dot{x}]$ is the derivative of time dependent variables, the so called state variables, i.e. machine currents, and $[u]$ is the input to the machine which is related to the terminal voltage of the machine. Finally, $[B]$ relates the input to the rest of the system.

2.3. Synchronous Generator Model

Synchronous generators form the main source of electric energy in power systems. As mentioned earlier, the power system stability problem is largely one of keeping interconnected synchronous generators in synchronism throughout the network. Therefore, an understanding of their characteristics and accurate modelling of their dynamic performance are of fundamental importance to the study of power system stability.

For the purpose of transient stability analysis, the basic approach to generator modelling is to consider the generator as an arrangement of three stator windings with a 120° electrical degrees separation between them, and a rotating structure with a field excitation winding and one or more damper windings [12][15][24][30][70]. The schematic representation of the generator is as shown in Figure 2.1.

In Figure 2.1, the rotor circuit comprises one field and, one or two damper windings. The field winding is connected to a source of direct current. The damper windings may be assumed

2. Modelling of AC Machines for Transient Analysis

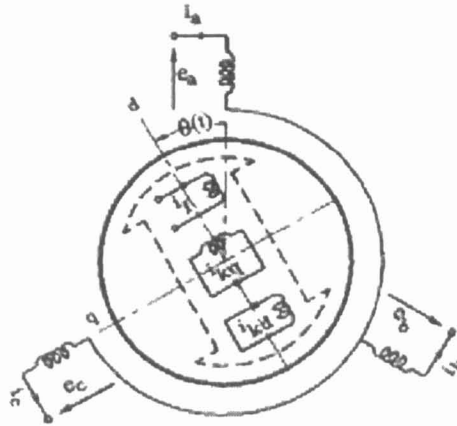


Figure 2.1.: Schematic diagram of a synchronous generator

to exist in two sets of circuits. One on the d -axis where the flux is in line with the field winding and another set where flux is perpendicular to the field winding on the q -axis. From the modelling viewpoint, the number of damper windings used determines the order of the generator. The criteria for selecting the number of damper windings depend on the purpose of the analysis. Even though for some specialised studies the rotor may be represented with a large number of damper windings, in transient studies one or two windings on each axis has been found sufficient to represent the generator accurately [12][24][30][70].

2.3.1. Direct Time Phase-Domain Model

In this part of the thesis, the mathematical model of a salient pole synchronous generator for transient analysis is developed. The generator under consideration consists of a three-phase stator winding, a field winding and two damper windings on the d and q – axis, as depicted in Figure 2.1. The model is based on the actual physical operation of the generator involving several inductively coupled circuits, where the self and mutual inductances vary periodically with the angular position of the rotor [4][6].

From Faraday's law, the instantaneous terminal voltage equations of the windings can be generally represented by,

$$e_a = \frac{d\Psi_a}{dt} - R_s i_a \quad (2.2)$$

$$e_b = \frac{d\Psi_b}{dt} - R_s i_b \quad (2.3)$$

$$e_c = \frac{d\Psi_c}{dt} - R_s i_c \quad (2.4)$$

2. Modelling of AC Machines for Transient Analysis

$$e_f = \frac{d\Psi_f}{dt} + R_f i_f \quad (2.5)$$

$$0 = \frac{d\Psi_{kd}}{dt} + R_{kd} i_{kd} \quad (2.6)$$

$$0 = \frac{d\Psi_{kq}}{dt} + R_{kq} i_{kq} \quad (2.7)$$

The negative sign convention associated with the stator windings' currents is based on the perceived direction of flow. In generation, the current will be assumed to flow from the generator into any connection out with the terminal. The field and damper windings are closed *DC* circuit, hence, the loop current flows in the direction of the voltage. The zero voltages at the terminal of the damper windings are due to their close circuited construction.

The set of equations (2.2)-(2.7) can be better represented as a matrix of differential equations,

$$\begin{bmatrix} e_a \\ e_b \\ e_c \\ e_f \\ e_{kd} \\ e_{kq} \end{bmatrix} = \frac{d}{dt} \begin{bmatrix} \Psi_a \\ \Psi_b \\ \Psi_c \\ \Psi_f \\ \Psi_{kd} \\ \Psi_{kq} \end{bmatrix} - \begin{bmatrix} R_s & & & & & \\ & R_s & & & & \\ & & R_s & & & \\ & & & -R_f & & \\ & & & & -R_{kd} & \\ & & & & & -R_{kq} \end{bmatrix} \begin{bmatrix} i_a \\ i_b \\ i_c \\ i_f \\ i_{kd} \\ i_{kq} \end{bmatrix} \quad (2.8)$$

The negative terms of the field and damper windings resistances are only an indication of the current flow in the direction of the voltage. Please refer to earlier paragraph for the explanation of the perceived direction of current flow.

In concise form,

$$[e] = \frac{d[\Psi]}{dt} - [R][i] \quad (2.9)$$

where $[e]$ contains the stator and rotor windings voltages, $[i]$ the currents in the windings and $[R]$ the resistances in the windings.

The flux linkages, $[\Psi]$, associated with the self-inductance of a winding and the mutual inductances between any two windings, and the currents in the windings,

$$[\Psi] = [L][i] \quad (2.10)$$

Sub-dividing the flux linkages in (2.10) into the stator and rotor self and mutual inductances yield the following,

$$\begin{bmatrix} \Psi_{(abc)} \\ \Psi_{(fkd kq)} \end{bmatrix} = \begin{bmatrix} L_{(abc, abc)} & L_{(abc, fkd kq)} \\ L_{(fkd kq, abc)} & L_{(fkd kq, fkd kq)} \end{bmatrix} \begin{bmatrix} i_{(abc)} \\ i_{(fkd kq)} \end{bmatrix} \quad (2.11)$$

2. Modelling of AC Machines for Transient Analysis

The inductances elements are based on the flux rotation of the generator during operation. The general elements of the inductances are explained as follow.

Stator Inductances

The stator inductances are represented by (2.12). They consist of self and mutual inductances of the stator windings. The self-inductances are the elements in the diagonal and the mutual inductances are the off-diagonal elements. The inductances are a function of the rotor displacement, θ , with respect to phase a of the stator, and therefore a function of rotor speed as depicted in Figure 2.1. The maximum self-inductance is obtained when the field axis is in line with the phase axis, and the opposite occurs when the quadrature axis goes in line with phase axis [4][6]. The inductances vary periodically due to the winding arrangement and the three-phase symmetry of the stator structure, taking into consideration that the common design for synchronous machines is a sinusoidally distributed stator windings. The existence of negative inductance like quantities is due to the direction of current flow that is seen as flowing from the windings to the external connection. This is in opposite direction to a general magnetic circuit, which the model of the generator windings are based on. The mutual inductances between the stator windings consist of two parts, one is the component of mutual inductance that does not link the rotor and is therefore independent of rotor displacement while the other varies with the rotor displacement.

$$[L_{(abc,abc)}] = \begin{bmatrix} -L_{a0} - L_{a2}\cos(2\theta) & M_{s0} - L_{a2}\cos(2\theta - 2\pi/3) & M_{s0} - L_{a2}\cos(2\theta + 2\pi/3) \\ M_{s0} - L_{a2}\cos(2\theta - 2\pi/3) & -L_{a0} - L_{a2}\cos(2\theta + 2\pi/3) & M_{s0} - L_{a2}\cos(2\theta) \\ M_{s0} - L_{a2}\cos(2\theta + 2\pi/3) & M_{s0} - L_{a2}\cos(2\theta) & -L_{a0} - L_{a2}\cos(2\theta - 2\pi/3) \end{bmatrix} \quad (2.12)$$

The negative terms on the self-inductances are to indicate the direction of current flows out of the windings. The negative terms on the second part of the mutual-inductances are due to the winding arrangement of the generator at 120° apart. This negative term can be omitted by adding a 90° shift in the cosine term.

Rotor Inductances

The rotor inductances have constant values for both the self and mutual element,

$$[L_{(fkdq, fkdq)}] = \begin{bmatrix} L_{ff} & M_{fkd} & 0 \\ M_{fkd} & L_{kkd} & 0 \\ 0 & 0 & L_{kkq} \end{bmatrix} \quad (2.13)$$

It is apparent that the mutual inductances between the direct and quadrature axis are zero

2. Modelling of AC Machines for Transient Analysis

since the two axis are 90° apart from each other, resulting in a natural decoupling of these quantities.

Stator and Rotor Mutual Inductances

The mutual inductances between the stator and rotor vary sinusoidally with the rotor position. This is a reasonable assumption since the stator windings are sinusoidally distributed around the rotating rotor.

$$[L_{(abc, fkdq)}] = \begin{bmatrix} M_{af}\cos(\theta) & M_{ad}\cos(\theta) & -M_{aq}\sin(\theta) \\ M_{af}\cos(\theta - 2\pi/3) & M_{ad}\cos(\theta - 2\pi/3) & -M_{aq}\sin(\theta - 2\pi/3) \\ M_{af}\cos(\theta + 2\pi/3) & M_{ad}\cos(\theta + 2\pi/3) & -M_{aq}\sin(\theta + 2\pi/3) \end{bmatrix} \quad (2.14)$$

Since the d and q -axis winding are 90° apart, their mutual inductances with the stator winding will also be shifted by the same degree. This explained the negative term on the mutual inductance between the stator and the q -axis winding, where the varying term should be $\cos(\theta + \pi/2)$, which is equal to $-\sin(\theta)$.

The matrix of mutual inductances between the rotor and stator is the transpose of $[L_{(abc, fkdq)}]$.

$$[L_{(fkdq, abc)}] = - [L_{(abc, fkdq)}]^t \quad (2.15)$$

Generator's Mechanical Dynamic and Electrical Torque

In order to maintain synchronous speed throughout its operation, the generator's input mechanical torque of the prime mover, T_m , should be equal to that of the output electrical torque, T_e . Any difference will result in the acceleration or deceleration of the generator's rotor, which in turn results in speed variations. Hence, the equation of motion, for a rotor system of inertia H , can be expressed as a set of differential equations,

$$\frac{d\delta}{dt} = \omega_r - \omega_s \quad (2.16)$$

$$\frac{d\delta^2}{dt} = \frac{d\omega_r}{dt} = \frac{\omega_s}{2H} (T_m - T_e) \quad (2.17)$$

where the electrical torque is given by [25][26][32],

$$T_e = \frac{2\omega_s}{3\sqrt{3}} (\Psi_a (i_b - i_c) + \Psi_b (i_c - i_a) + \Psi_c (i_a - i_b)) \quad (2.18)$$

2. Modelling of AC Machines for Transient Analysis

The above equation for phase-domain electrical torque can be obtained from the torque equation of the transformed axis model that are widely available in the open literature. A good example of the approach is presented in [25]. The above torque equation can also be obtained from the electromechanical energy relationships.

In the above equations [25][26][32], ω_r , is the instantaneous speed of the machine; δ is the load angle and ω_s is the rated synchronous speed. The rotor position, θ , can be expressed as,

$$\theta = \omega_s t + \delta \quad (2.19)$$

General Solution of the Direct Time Phase-Domain Generator Model

In order to solve the model of the generator, we need to obtain a generalised closed-form representation of the model. Equation (2.9) is not in closed-form because both the flux linkages and currents are variables. From these two sets of variables, one would have to be selected to be the output variables, which serve the purpose of interfacing the synchronous generator to the network. From (2.9) and (2.10) the following is obtained,

$$[e] = \frac{d[L][i]}{dt} - [R][i] \quad (2.20)$$

Since both the inductances and currents are time dependent,

$$[e] = L \frac{d[i]}{dt} + \frac{d[L]}{dt} [i] - [R][i] \quad (2.21)$$

where

$$\begin{aligned} \frac{d[L]}{dt} &= \frac{d\theta}{dt} \frac{d[L]}{d\theta} \\ &= \omega_r \frac{d[L]}{d\theta} \end{aligned} \quad (2.22)$$

Hence, by suitable algebraic manipulation (2.21) becomes,

$$\frac{d[i]}{dt} = [L]^{-1} [e] - [L]^{-1} \left(\omega_r \frac{d[L]}{d\theta} + [R] \right) [i] \quad (2.23)$$

The complete model of the generator in the phase-domain is represented electrically by (2.23) and the mechanical dynamic by (2.16)-(2.19). The inductances matrix of the generator is dependent on the rotor position, which varies with time as indicated by (2.19). Hence, the performance equations of the generator are differential equations with variable coefficients.

2. Modelling of AC Machines for Transient Analysis

If the speed of the generator is varying under transient conditions, variations of the rotor position will cause these equations to become non-linear. Standard numerical techniques such as the Runge-Kutta can be applied to solve these differential equations in the time-domain. Various fault conditions can be simulated at the terminal of the generator model by suitable modifications to $[e]$ and $[R]$, depending on the type of fault simulated. This is well illustrated in [25] and [28].

2.3.2. The $d - q - 0$ Transformation Model

As seen from the inductances matrix in (2.12)-(2.15), where the majority of the coefficients are a function of the time varying rotor position, θ , are difficult to handle directly. This is especially the case when computer capabilities are limited. A simpler approach may be obtained by appropriate transformation of the stator variables. There are several transformation techniques that may be used to this end, but the most popular was recommended by R.H. Park, where the three-phase stator variables are transformed to a new set of variables. In this new frame-of-reference, a set of fictitious currents, voltages and flux linkages are defined as functions of actual currents, voltages and flux linkages [10][12]. This transformation technique is termed '*Park's Transformation*'.

The purpose of the transformation is to obtain a simplified set of equations for the generator, independent of rotor position, θ . With reference to flux equations (2.10), where each of the elements relates a rotor flux to the stator and rotor currents,

$$\Psi_f = -M_{af} \left(i_a \cos\theta + i_b \cos \left(\theta - \frac{2\pi}{3} \right) + i_c \cos \left(\theta + \frac{2\pi}{3} \right) \right) + L_{ff} i_f + M_{fkd} i_{kd} \quad (2.24)$$

$$\Psi_{kd} = -M_{ad} \left(i_a \cos\theta + i_b \cos \left(\theta - \frac{2\pi}{3} \right) + i_c \cos \left(\theta + \frac{2\pi}{3} \right) \right) + M_{fkd} i_f + L_{kkd} i_{kd} \quad (2.25)$$

$$\Psi_{kq} = M_{aq} \left(i_a \cos\theta + i_b \cos \left(\theta - \frac{2\pi}{3} \right) + i_c \cos \left(\theta + \frac{2\pi}{3} \right) \right) + L_{kkq} i_{kq} \quad (2.26)$$

By inspection of (2.24)-(2.26), it can be observed that the flux linkages of the rotor is dependent on the rotor position with respect to the currents in the stator windings. In order for the analysis to be performed independently of the rotor position, the stator currents will need to be transformed into a new set of variables, which can be described generally as follow [4][10]-[13],

$$i_d = k_d \left(i_a \cos\theta + i_b \cos \left(\theta - \frac{2\pi}{3} \right) + i_c \cos \left(\theta + \frac{2\pi}{3} \right) \right) \quad (2.27)$$

$$i_q = -k_q \left(i_a \sin\theta + i_b \sin \left(\theta - \frac{2\pi}{3} \right) + i_c \sin \left(\theta + \frac{2\pi}{3} \right) \right) \quad (2.28)$$

2. Modelling of AC Machines for Transient Analysis

These new variables are divided into two axis, namely the direct d – axis and quadrature q – axis. The direct current i_d is defined as the current in the fictitious winding that is located on the same axis and rotates at the same speed as the field winding on the rotor. The quadrature current i_q is the current in a fictitious winding located perpendicular to the field winding. The current in the fictitious winding will setup the same magnetic force as the actual currents in the three-phase stator.

The constant, k_d and k_q , are of arbitrary values chosen as $\frac{2}{3}$ for numerical purposes in order for the maximum value of the transform axis current i_d and i_q , to be equal to the peak value of the stator current [4][10]-[13]. Since a three-phase stator is replaced by a system of two axis, a degree of freedom needs to be allowed in the form of a zero sequence component. The zero sequence current may be visualised physically as the magnitude of each set of equal currents flowing in all the three-phases and therefore producing no resultant air-gap flux. The current is given as,

$$i_0 = \frac{1}{3}(i_a + i_b + i_c) \quad (2.29)$$

The current transformation equations giving the new currents i_d , i_q and i_0 in terms of the three-phase stator currents, can be expressed in the following matrix form,

$$\begin{bmatrix} i_d \\ i_q \\ i_0 \end{bmatrix} = \frac{2}{3} \begin{bmatrix} \cos\theta & \cos(\theta - \frac{2\pi}{3}) & \cos(\theta + \frac{2\pi}{3}) \\ -\sin\theta & -\sin(\theta - \frac{2\pi}{3}) & \sin(\theta + \frac{2\pi}{3}) \\ \frac{1}{2} & \frac{1}{2} & \frac{1}{2} \end{bmatrix} \begin{bmatrix} i_a \\ i_b \\ i_c \end{bmatrix} \quad (2.30)$$

The transformation technique applies also to the stator three-phase voltages and flux linkages. The three-phase quantities can be obtained from the transformed variables by inverse transformation.

From the stator three-phase flux linkages obtained by expanding (2.11) and carrying out a transformation of the stator current into the $d - q - 0$ frame-of-reference, and with proper trigonometric manipulation and reduction, the transformed inductances for the stator and rotor are obtained as [4][6],

$$\begin{bmatrix} \Psi_d \\ \Psi_q \\ \Psi_0 \\ \Psi_f \\ \Psi_{kd} \\ \Psi_{kq} \end{bmatrix} = \begin{bmatrix} -L_d & & & M_{af} & M_{ad} & \\ & -L_q & & & & M_{aq} \\ & & -L_0 & & & \\ -\frac{3}{2}M_{af} & & & L_{ff} & M_{fkd} & \\ -\frac{3}{2}M_{ad} & & & M_{fkd} & L_{kkd} & \\ & -\frac{3}{2}M_{aq} & & & & L_{kkq} \end{bmatrix} \begin{bmatrix} i_d \\ i_q \\ i_0 \\ i_f \\ i_{kd} \\ i_{kq} \end{bmatrix} \quad (2.31)$$

The negative sign on the inductances are the effect of the transformation.

2. Modelling of AC Machines for Transient Analysis

where

$$L_d = L_{a0} + M_{s0} + \frac{3}{2}L_{a2} \quad (2.32)$$

$$L_q = L_{a0} + M_{s0} - \frac{3}{2}L_{a2} \quad (2.33)$$

$$L_0 = L_{a0} - 2L_{a2} \quad (2.34)$$

The resulting inductance matrix is simpler than the phase-domain inductance matrix since all the coefficients are constants, independent of the rotor position, θ . The inductance matrix displays a linear characteristic, which is less demanding to solve in terms of computing time.

By applying the transformation technique (2.30) to the three-phase terminal voltages in (2.2)-(2.4), the following expressions are obtained in terms of the transformed variables,

$$e_d = \frac{d\Psi_d}{dt} - R_a i_d - \Psi_d \omega_r \quad (2.35)$$

$$e_q = \frac{d\Psi_q}{dt} - R_a i_q + \Psi_q \omega_r \quad (2.36)$$

$$e_0 = \frac{d\Psi_0}{dt} - R_a i_0 \quad (2.37)$$

The term ω_r in the above equations represents the angular velocity of the rotor in electrical degrees, rad/s. Under steady state condition the speed is fixed based on the frequency of the system. The terms $\Psi_d \omega_r$ and $\Psi_q \omega_r$ are the speed voltages due to flux change in space as a result of the rotor rotation. The terms, $\frac{d\Psi_d}{dt}$ and $\frac{d\Psi_q}{dt}$, are referred to as the transformer voltage due to the flux change with respect to time.

The flux linkage matrix equation (2.31) associated with the stator and rotor, and the voltage equations (2.35)-(2.37) for the stator in the transformed variables constitute the major difference between the direct time phase-domain and the transformed axis model. The voltage equations for the rotor are the same as (2.5)-(2.7) for both models.

These equations for the transformed model can be written concisely as,

2. Modelling of AC Machines for Transient Analysis

$$\begin{bmatrix} e_d \\ e_q \\ e_0 \\ e_f \\ e_{kd} \\ e_{kq} \end{bmatrix} = \frac{d}{dt} \begin{bmatrix} \Psi_d \\ \Psi_q \\ \Psi_0 \\ \Psi_f \\ \Psi_{kd} \\ \Psi_{kq} \end{bmatrix} + \begin{bmatrix} R_s & & & & & \\ & R_s & & & & \\ & & R_s & & & \\ & & & -R_f & & \\ & & & & -R_{kd} & \\ & & & & & -R_{kq} \end{bmatrix} \begin{bmatrix} i_d \\ i_q \\ i_0 \\ i_f \\ i_{kd} \\ i_{kq} \end{bmatrix} - \begin{bmatrix} \Psi_d \omega_r \\ \Psi_q \omega_r \\ 0 \\ 0 \\ 0 \\ 0 \end{bmatrix} \quad (2.38)$$

Equation (2.38) contains the flux linkages and current as the variables. We can eliminate the flux linkages by substituting (2.31) into the above equations. An ideal, closed-form differential equations will then be obtained where the solution method discussed for the phase-domain model can be applied to solve the transformed model. Even though a computer based solution is still necessary, computing time for solution of this model is greatly reduced due to the constant nature of the inductances [25]. However, the benefit of the reduced computing time is only justified if a balance condition exist in the stator windings of the generator. The accuracy of the transformed model will be compromised when unbalance or non-sinusoidal conditions occur in the windings, since most of the transformation perform in equations (2.27)-(2.38) are based on balance sinusoidal behaviour of the stator.

Electrical Torque in the transformed variables

The electrical torque in the transformed variables can be obtained by directly substituting the three-phase flux linkages and currents in (2.18) with the transformed equivalent. After mathematical reduction, the electrical torque is obtained as follow,

$$T_e = \frac{\omega_s}{2} (\Psi_d i_q - \Psi_q i_d) \quad (2.39)$$

The generator's mechanical dynamic equations remain the same as the direct time phase-domain model as in (2.16) and (2.17).

The equations presented for the synchronous generator models in both the direct time phase-domain and the transformed axis are correct if the effects of magnetic saturation are neglected. In this thesis, the effects of saturation are ignored, as noted in Section 2.1, to make development of the new multimachine solution method more manageable at this stage. Due to time constraints, this interesting aspect of machine modelling was not explore further in this thesis.

The magnetic saturation of electrical machine is important if the main aim is the detail study of the machine itself or its impact on neighbouring plant components, like a transformer, when fault currents become very large. However, it is less important if the purpose of analysis is network wide transient stability issues, where the presence of transformers are ignored. The

2. Modelling of AC Machines for Transient Analysis

impact of saturation on the machine closest to the point of fault would not have an impact on other machines in the network. One area of transient study that might be hindered by saturation is the response of the generator excitation controller. The effectiveness of the excitation controller can be affected by machine saturation. But again, this saturation is important only in detail design of the excitation controller is to be considered.

The major difference if magnetic saturation is to be included will be in the inductances matrix of (2.11) and (2.31). The inclusion on magnetic saturation can be achieved in both models using a semi-heuristic reasoning and approximations based on the magnetizing curves of the generator. The general assumptions made for the representation of magnetic saturation in stability studies are well documented in [4]. It is assumed that the inductances that will saturate are the mutual inductances between the stator and rotor. The effects of saturation may then be represented by multiplying the inductances by the saturation factors. The saturation factors are obtained using the magnetic saturation characteristic curves as presented in [4][31]. If the saturation effects are considered, the inductances in the $d - q - 0$ axis model are no longer constant and will be changed according to the saturation factors.

2.4. Simulations and Results of Synchronous Generator Model Performance

The generator model that has already been developed is applicable to the actual unit of their respective quantities. The per-unit (*p.u.*) equivalent is obtained by the same approach dividing the actual value with the selected base of the quantity. This general approach to obtain the *p.u.* representation is openly available in published literature [2][4][6][14] and will be left out of this thesis. The *p.u.* is used in most part of this thesis as it provides a more uniform information for the quantities obtained in the process of power system simulations. The actual unit can be easily obtained from the *p.u.* value by simple conversion.

2.4.1. Validation Tests

Validation and justification of mathematical models are important to establish confidence in the analysis conducted. In such a validation test, the objective is to justify the use of the direct time phase-domain model, which will be used throughout this thesis. This section aims to demonstrate the advantage of the model over the conventional transformed axis model.

Two simple test networks are used to test the response of the direct time phase-domain and the transformed $d - q - 0$ axis model under symmetrical conditions. In the first test case, the unloaded generator is connected to an infinite source through a short line. A three-phase-to-ground fault at the terminal of the generator is investigated. The results are compared

2. Modelling of AC Machines for Transient Analysis

with those obtained from available measurements, and simulations using an industry standard power system package, PSCAD/EMTDCTM. The model for the synchronous generator available in PSCAD/EMTDCTM is in the standard $d - q - 0$ axis frame of reference. The synchronous generator data, in standard $d - q - 0$ form and in phase quantities are given in Appendix A.1, and the experimental results were obtained from [28]. The schematic diagram of the equivalent network in PSCAD/EMTDCTM for the studies conducted in this section is given in Appendix A.3.

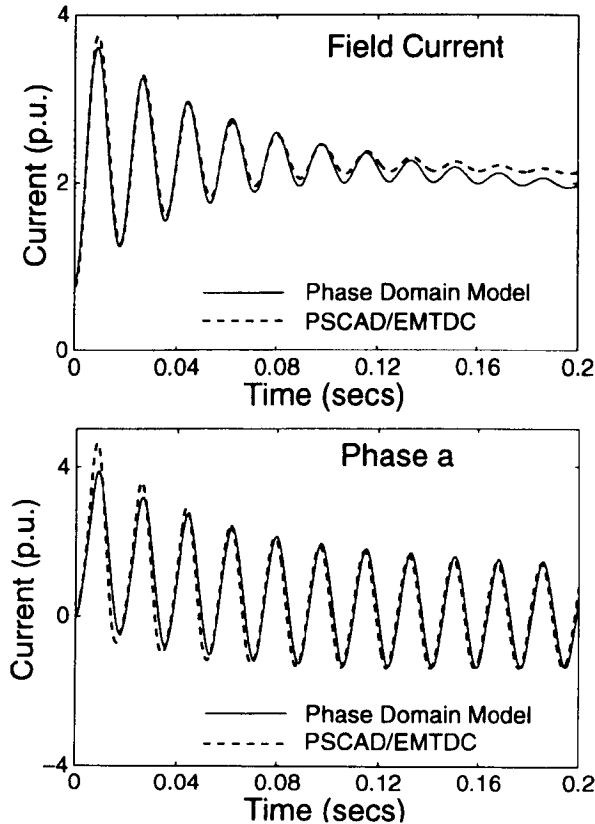


Figure 2.2.: Stator and field currents of the generator connected to an infinite bus following a three-phase-to-ground fault at its terminal

Figure 2.2 compares the result given by the direct time phase-domain model and PSCAD/EMTDCTM. The experimental results are shown in Figure 2.3, where they compare well with the results provided by the direct time phase domain model for both types of fault. For symmetrical faults, the direct time phase-domain model and PSCAD/EMTDCTM compare satisfactorily. The minor discrepancies observed, particularly in the field current results, may be due to the inaccuracies in the relationship between the $d - q - 0$ and phase parameters [12][28][29].

In order to ensure that the use of an infinite bus does not affect the conclusions reached by the study, it is removed from the test network. Further simulations conducted for the case when the synchronous generator is connected to a resistive load via a line are as shown in Figure 2.4. Again it is observed from Figure 2.5 that under a symmetrical three-phase-to-ground

2. Modelling of AC Machines for Transient Analysis

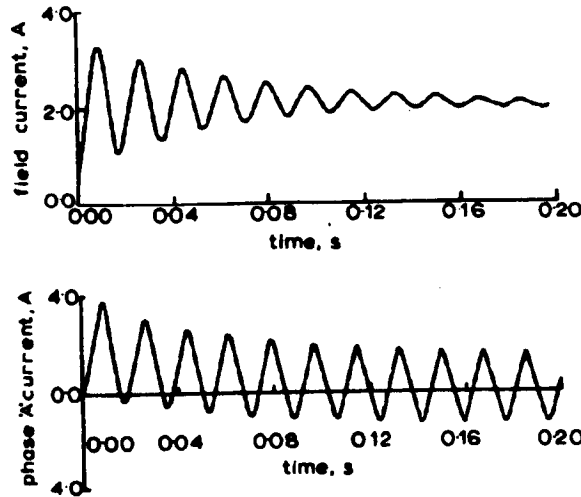


Figure 2.3.: Experimental results from [28] for similar studies as those shown in Figure 2.2

fault, the phase and field current of the direct time phase-domain and the $d - q - 0$ axis model agrees in unison.

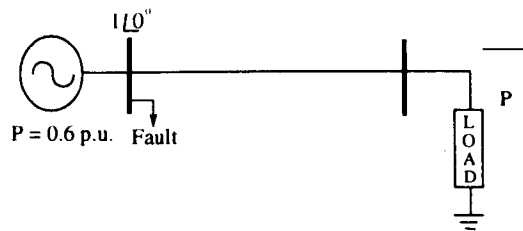


Figure 2.4.: Test network with load

2.4.2. Asymmetrical Fault Condition with Line Opening and Re-closure

The main advantage of the direct time phase-domain model of the synchronous generator is the ability to adopt a unified approach in simulating both symmetrical and asymmetrical faults. There are many situations where asymmetrical faults can occur, namely, the single-phase-to-ground, phase-to-phase and phase-to-phase-to-ground faults. One common instance of asymmetrical condition is when electrical networks are protected by single phase fuses or breakers. In this situation, one or two phases of the circuit may be open on a fault while other phases are still closed. This situation is similar to having an open or broken conductor in a particular phase.

With the transformed $d - q - 0$ model, it is not possible for such situations to be simulated without a great deal of effort and modification [12][13], while the direct time phase-domain model can be applied with ease. In this section, two instances of asymmetrical faulted conditions are simulated, namely, a single-phase-to-ground fault and the opening of a line conduc-

2. Modelling of AC Machines for Transient Analysis

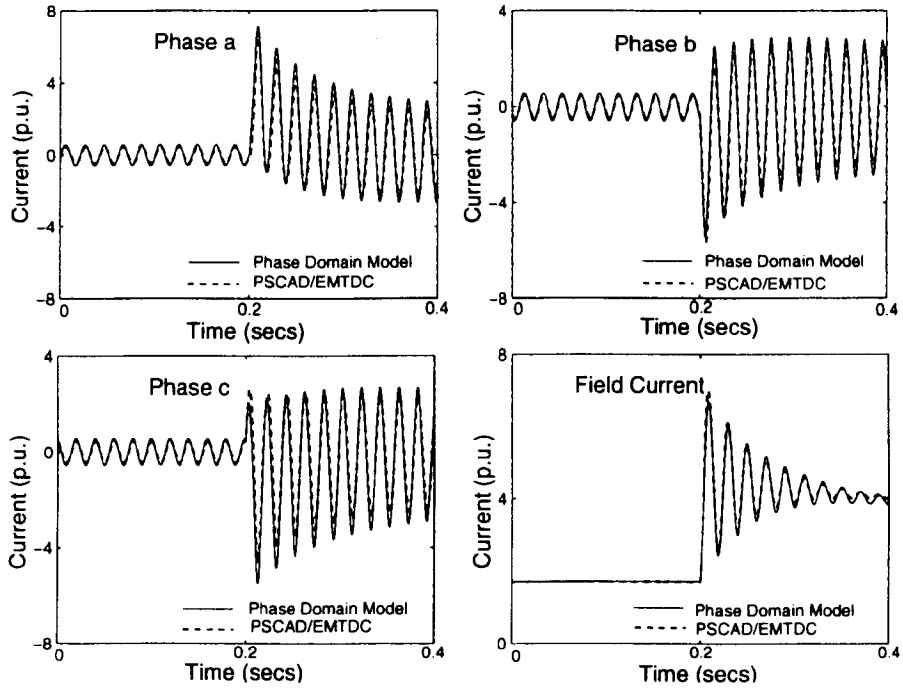


Figure 2.5.: Stator and field currents for a three-phase-to-ground fault at the terminal of a loaded generator

tor. The test network is a simple generator to infinite busbar arrangement. The main aim of this simulation is to demonstrate the versatility of the phase-domain model.

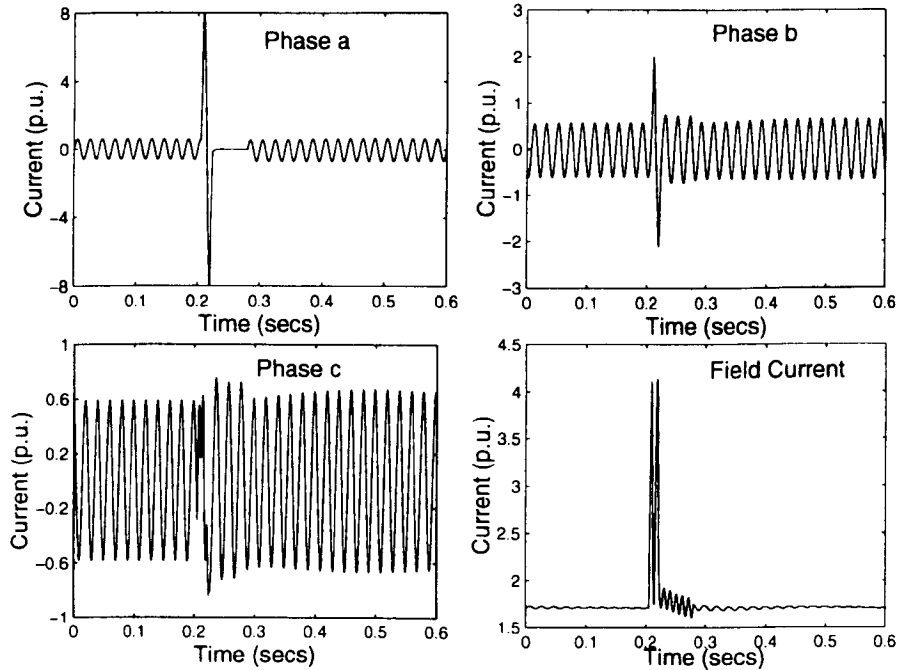


Figure 2.6.: Generator current under single-phase-to-ground fault with line opening and reclosure

The results of the generator response are as shown in Figure 2.6 and 2.7. The fault was

2. Modelling of AC Machines for Transient Analysis

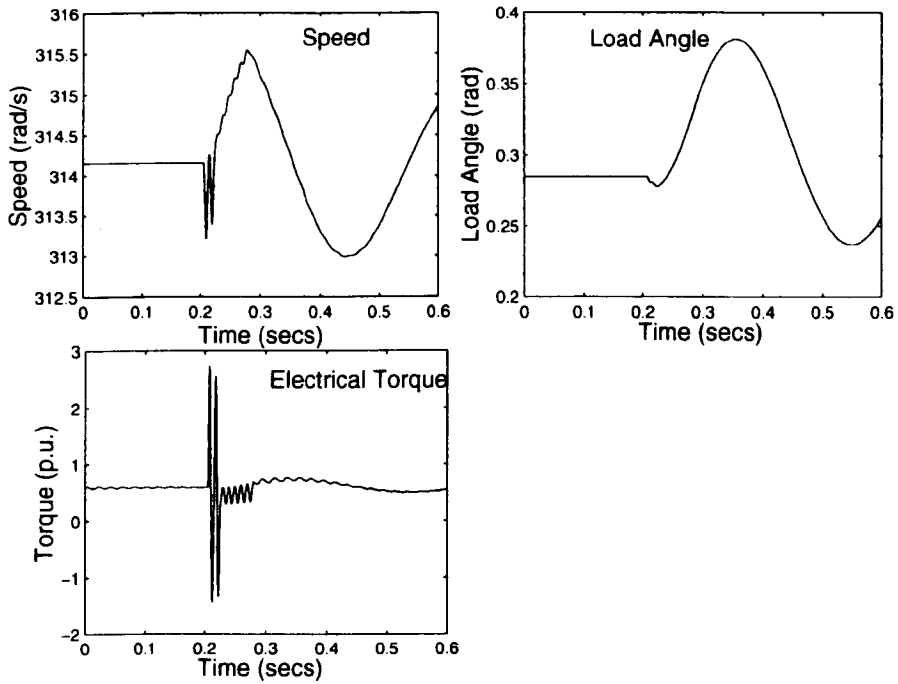


Figure 2.7.: Generator dynamic response and electrical torque under single-phase-to-ground fault with line opening and re-closure

applied on phase a at $t = 0.2s$. It is observed that the current of the faulted phase is very high compared to the other phases. If a sensitive circuit breaker is considered to be used as protection it will be tripped by the high current. Normally, the circuit breaker is designed to open at zero current crossing in order to reduce the electric arc across its connector [26]. The quick response of the circuit breaker operation was simulated by removing the faulted phase at zero current crossing after $30ms$ creating an open conductor. The current of the open phase goes to zero resulting in the reduction of the total fault current, which can be seen, from other phases and the electrical torque oscillations. The line was re-closed at $t = 0.285s$ upon which the generator resumes its pre-fault operating conditions.

2.5. Asynchronous Machine Model

Asynchronous machines, or more popularly known as induction machines, form a major portion of power system loads and to a certain extent also generators. The asynchronous machine is popular in industrial drive systems because of its robustness and low manufacturing cost. Under special conditions, it is preferred over the synchronous machine as a generator. This is true when the mechanical input to the generator is random and the generator is subjected to changes in its operating speed, for example in wind generators. The generating and motoring action of the machine does not significantly affect the modelling of the machine, the differences being a change of sign in its mechanical input to indicate direction of power flow.

2. Modelling of AC Machines for Transient Analysis

The direct time phase-domain model of the induction machine is similar in principle to that of the synchronous generator. However, in the induction motor, the rotor equations differ from the synchronous generator as the rotor windings are also considered as a three-phase distributed winding similar to that of the stator windings. The schematic representation of the induction machine is shown in Figure 2.8.

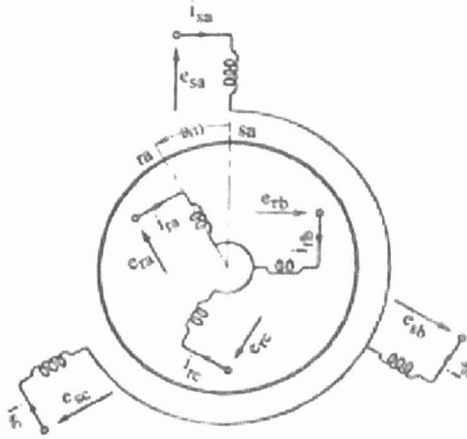


Figure 2.8.: Schematic circuit of asynchronous machine

2.5.1. Direct Time Phase-Domain Model

In a similar manner to that of the synchronous machine, the voltage equations for the phase-domain asynchronous or induction machine can be obtained for the individual phase of the stator and rotor. Since both are windings in three-phases, subscripts s and r are used to describe them individually. The saturation of the machine is neglected at this stage of development. Applying Faraday's law, the terminal voltage equations is given by,

$$e_{sa} = \frac{d\Psi_{sa}}{dt} + R_{sa}i_{sa} \quad (2.40)$$

$$e_{sb} = \frac{d\Psi_{sb}}{dt} + R_{sb}i_{sb} \quad (2.41)$$

$$e_{sc} = \frac{d\Psi_{sc}}{dt} + R_{sc}i_{sc} \quad (2.42)$$

$$e_{ra} = \frac{d\Psi_{ra}}{dt} + R_{ra}i_{ra} \quad (2.43)$$

$$e_{rb} = \frac{d\Psi_{rb}}{dt} + R_{rb}i_{rb} \quad (2.44)$$

$$e_{rc} = \frac{d\Psi_{rc}}{dt} + R_{rc}i_{rc} \quad (2.45)$$

2. Modelling of AC Machines for Transient Analysis

Since the asynchronous machine is more commonly used as a motor, the sign convention of the stator currents is based on the flow of current into the machine, hence, it is positive. This is true for the rotor windings as well.

The set of equations (2.40)-(2.45) can be better represented as a matrix of differential equations,

$$\begin{bmatrix} e_{sa} \\ e_{sb} \\ e_{sc} \\ e_{ra} \\ e_{rb} \\ e_{rc} \end{bmatrix} = \frac{d}{dt} \begin{bmatrix} \Psi_{sa} \\ \Psi_{sb} \\ \Psi_{sc} \\ \Psi_{ra} \\ \Psi_{rb} \\ \Psi_{rc} \end{bmatrix} + \begin{bmatrix} R_{sa} & & & & & \\ & R_{sb} & & & & \\ & & R_{sc} & & & \\ & & & R_{ra} & & \\ & & & & R_{rb} & \\ & & & & & R_{rc} \end{bmatrix} \begin{bmatrix} i_{sa} \\ i_{sb} \\ i_{sc} \\ i_{ra} \\ i_{rb} \\ i_{rc} \end{bmatrix} \quad (2.46)$$

In concise form where the subscript m , stands for the asynchronous machine,

$$[e_m] = \frac{d[\Psi_m]}{dt} + [R_m][i_m] \quad (2.47)$$

where $[e_m]$ are the stator and rotor windings voltages, $[i_m]$ the currents in the windings and $[R_m]$ the resistances in the windings. The flux linkages associated with the interaction between the the stator and rotor coupled windings can be represented by,

$$[\Psi_m] = [L_m][i_m] \quad (2.48)$$

$$\begin{bmatrix} \Psi_{m(sa sb sc)} \\ \Psi_{m(ra rb rc)} \end{bmatrix} = \begin{bmatrix} L_{m(sa sb sc, sa sb sc)} & L_{m(sa sb sc, ra rb rc)} \\ L_{m(ra rb rc, sa sb sc)} & L_{m(ra rb rc, ra rb rc)} \end{bmatrix} \begin{bmatrix} i_{m(sa sb sc)} \\ i_{m(ra rb rc)} \end{bmatrix} \quad (2.49)$$

The general elements of the inductances are explained as follow.

Stator Inductances

Due to the assumption that the air gap of an induction machine is uniform, and its stator and rotor windings are sinusoidally distributed, it will not have the 2θ , second harmonics, terms in its self and mutual inductances as opposed to the synchronous generator. The self-inductance of each phase, which is the summation of the stator leakage and magnetizing inductances is identical and independent of the rotor position. The mutual inductances between any two stator windings is of similar value due to the symmetrical arrangement.

2. Modelling of AC Machines for Transient Analysis

$$\left[L_{m_{(sa\ sb\ sc, sa\ sb\ sc)}} \right] = \begin{bmatrix} L_{ss} & L_{sm} & L_{sm} \\ L_{sm} & L_{ss} & L_{sm} \\ L_{sm} & L_{sm} & L_{ss} \end{bmatrix} \quad (2.50)$$

Rotor Inductances

With the same explanation as the stator inductances, the rotor self-inductances are independent of the rotor position, and is given by the sum of the rotor leakage and magnetizing inductances,

$$\left[L_{m_{(ra\ rb\ rc, ra\ rb\ rc)}} \right] = \begin{bmatrix} L_{rr} & L_{rm} & L_{rm} \\ L_{rm} & L_{rr} & L_{rm} \\ L_{rm} & L_{rm} & L_{rr} \end{bmatrix} \quad (2.51)$$

Stator and Rotor Mutual Inductances

The mutual inductances between a stator winding and any rotor winding varies sinusoidally with the rotor angular position, θ ,

$$\left[L_{m_{(sa\ sb\ sc, ra\ rb\ rc)}} \right] = \begin{bmatrix} M_{sr}\cos(\theta) & M_{sr}\cos(\theta + 2\pi/3) & M_{sr}\cos(\theta - 2\pi/3) \\ M_{sr}\cos(\theta - 2\pi/3) & M_{sr}\cos(\theta) & M_{sr}\cos(\theta + 2\pi/3) \\ M_{sr}\cos(\theta + 2\pi/3) & M_{sr}\cos(\theta - 2\pi/3) & M_{sr}\cos(\theta) \end{bmatrix} \quad (2.52)$$

$$\left[L_{m_{(ra\ rb\ rc, sa\ sb\ sc)}} \right] = \left[L_{m_{(sa\ sb\ sc, ra\ rb\ rc)}} \right]^t \quad (2.53)$$

Asynchronous Machine Mechanical Dynamic and Electrical Torque

In the dynamic term of the asynchronous machine, θ , is defined as the electrical angle by which the axis of phase a rotor winding leads the axis of phase a of the stator winding in the direction of rotation. If the machine is rotating at an electrical angular velocity corresponding to ω_r in rad/s,

$$\theta = \omega_r t \quad (2.54)$$

The electrical and mechanical angles can be related by the number of pole, p , as,

$$\theta = \frac{p}{2} \theta_m \quad (2.55)$$

2. Modelling of AC Machines for Transient Analysis

The dynamic equation representing changes in the motor mechanical speed is given by,

$$\frac{d\theta}{dt} = \omega_r \quad (2.56)$$

$$\frac{d^2\theta}{dt^2} = \frac{d\omega_r}{dt} = \frac{p}{2} \frac{d\omega_m}{dt} = \frac{p}{2} \frac{\omega_s}{2H_m} (T_e - T_m) \quad (2.57)$$

where ω_m is the mechanical speed of the machine and H_m is the inertia constant. The acceleration equations for the machine are based on motoring action of the machine. The speed increases when the electrical torque supply by the source is higher than that of the mechanical torque requirement of the load. However, this representation is also true for the asynchronous generator since a decreased in speed represents a generating action in this type of machine. For a motoring action the speed of the machine is higher than the rated synchronous speed, ω_s , and for generating action the machine speed is lower than ω_s .

The electrical torque of the machine can be obtained as [27],

$$T_e = -M_{sr} \left[(i_{sa}i_{ra} + i_{sb}i_{rb} + i_{sc}i_{rc}) \sin\theta + (i_{sa}i_{rb} + i_{sb}i_{rc} + i_{sc}i_{ra}) \sin\left(\theta + \frac{2\pi}{3}\right) + (i_{sa}i_{rc} + i_{sb}i_{ra} + i_{sc}i_{rb}) \sin\left(\theta - \frac{2\pi}{3}\right) \right] \quad (2.58)$$

The sign on the electrical torque will change according to the operation of the machine from motoring to generating. This is due to the rotor angle and the flow of the current. Hence, this torque equation is general for both modes of machine operation.

General Solution of the Asynchronous Machine Model

The requirement for a closed-form solution of the asynchronous machine model is identical to that of the synchronous generator. By a similar approach, the ready to solve closed-form equations can be obtained from (2.47) as follow,

$$\frac{d[i_m]}{dt} = [L_m]^{-1} [e_m] - [L_m]^{-1} \left(\omega_r \frac{d[L_m]}{d\theta} + [R_m] \right) [i_m] \quad (2.59)$$

The detailed electrical model of the asynchronous machine is by (2.59) and mechanically by (2.54)-(2.57). Like the synchronous generator, the asynchronous machine differential equations with variable coefficients cannot be solved without the help of a computer. Numerical solutions such as those discussed for the synchronous generator can be used to solve these equations in the time-domain.

2.5.2. The Two Axis Transformation Model

The use of asynchronous machine in industry took place at around the same period as the synchronous generator. There is no surprise that a similar transformation method was applied in the analysis of asynchronous machines to overcome computing shortcomings at that time. Similarly, the purpose of the transformation is to find a representation of the actual physical model where the machine's inductances can be represented independently of the variable's electrical angle, θ .

Unlike the synchronous generator, both the stator and rotor of the synchronous machine are modelled as a three phase windings. The stator and rotor windings are related by mutual inductances, which are dependent on the machines' rotating electrical angle. The decoupling of the phase domain into a new set of transformed variables need to be performed for both sets of windings individually.

There is no obvious feature of the machine that dictates a specific choice of reference but generally the preferred reference frame is one with an axis rotating at synchronous speed [4][14]. The transformed q -axis is assumed to be 90° ahead of the d -axis in the direction of rotation at synchronous speed, ω_s , as determined by the stator voltages. If the d -axis is placed to coincide with phase a of the stator at time $t = 0s$, its displacement from phase a at any time is $\omega_s t$. The transformed stator currents are then given as,

$$i_{ds} = \frac{2}{3} \left[i_{sa} \cos(\omega_s t) + i_{sb} \cos\left(\omega_s t - \frac{2\pi}{3}\right) + i_{sc} \cos\left(\omega_s t + \frac{2\pi}{3}\right) \right] \quad (2.60)$$

$$i_{qs} = -\frac{2}{3} \left[i_{sa} \sin(\omega_s t) + i_{sb} \sin\left(\omega_s t - \frac{2\pi}{3}\right) + i_{sc} \sin\left(\omega_s t + \frac{2\pi}{3}\right) \right] \quad (2.61)$$

The inverse transformation can be obtained by simultaneous solution of (2.60) and (2.61) under balanced condition where $i_{sa} + i_{sb} + i_{sc} = 0$. This is given by,

$$i_{sa} = i_{ds} \cos(\omega_s t) - i_{qs} \sin(\omega_s t) \quad (2.62)$$

$$i_{sb} = i_{ds} \cos\left(\omega_s t - \frac{2\pi}{3}\right) - i_{qs} \sin\left(\omega_s t - \frac{2\pi}{3}\right) \quad (2.63)$$

$$i_{sc} = i_{ds} \cos\left(\omega_s t + \frac{2\pi}{3}\right) - i_{qs} \sin\left(\omega_s t + \frac{2\pi}{3}\right) \quad (2.64)$$

It is now necessary to identify the corresponding transformation for the three-phase rotor quantities in relation to the synchronously rotating $d-q$ axis. Let θ_r be the angle by which d -axis leads phase a of the rotor. If the rotor is rotating at a fixed speed, the d -axis is advancing

2. Modelling of AC Machines for Transient Analysis

continuously with respect to a point on the rotor at the same speed. The transformation of the rotor currents into the $d - q$ variables is thus given as,

$$i_{dr} = \frac{2}{3} \left[i_{ra} \cos \theta_r + i_{sb} \cos \left(\theta_r - \frac{2\pi}{3} \right) + i_{sc} \cos \left(\theta_r + \frac{2\pi}{3} \right) \right] \quad (2.65)$$

$$i_{qr} = -\frac{2}{3} \left[i_{ra} \sin \theta_r + i_{rb} \sin \left(\theta_r - \frac{2\pi}{3} \right) + i_{rc} \sin \left(\theta_r + \frac{2\pi}{3} \right) \right] \quad (2.66)$$

where

$$\theta = \omega_s t - \theta_r \quad (2.67)$$

and the inverse transformation relations are,

$$i_{ra} = i_{dr} \cos \theta_r - i_{qr} \sin \theta_r \quad (2.68)$$

$$i_{rb} = i_{dr} \cos \left(\theta_r - \frac{2\pi}{3} \right) - i_{qr} \sin \left(\theta_r - \frac{2\pi}{3} \right) \quad (2.69)$$

$$i_{rc} = i_{dr} \cos \left(\theta_r + \frac{2\pi}{3} \right) - i_{qr} \sin \left(\theta_r + \frac{2\pi}{3} \right) \quad (2.70)$$

A transformation and inverse transformation techniques also apply to the stator and rotor flux linkages and voltages.

The inductances in the transformed variables can be obtained by substituting (2.60), (2.61) and (2.67) into the stator flux linkages as represented by equation (2.49), and followed by further trigonometric manipulations. The final simplified inductances are given as,

$$\begin{bmatrix} \Psi_{ds} \\ \Psi_{qs} \\ \Psi_{dr} \\ \Psi_{qr} \end{bmatrix} = \begin{bmatrix} L_{ss} & & L_m & \\ & L_{ss} & & L_m \\ L_m & & L_{rr} & \\ & L_m & & L_{rr} \end{bmatrix} \begin{bmatrix} i_{ds} \\ i_{qs} \\ i_{dr} \\ i_{qr} \end{bmatrix} \quad (2.71)$$

where $L_m = \frac{3}{2} M_{sr}$.

Notice that the coefficients of the inductances matrix are constant and independent of any time varying functions. Like the synchronous generator, there is a complete separation of the variables in the inductance matrix.

By applying the transformation in the flux linkages and voltages, the following expression is obtained for the stator and rotor voltages in $d - q$ variables,

2. Modelling of AC Machines for Transient Analysis

$$e_{ds} = \frac{d\Psi_{ds}}{dt} + R_s i_{ds} - \omega_s \Psi_{qs} \quad (2.72)$$

$$e_{qs} = \frac{d\Psi_{qs}}{dt} + R_s i_{qs} + \omega_s \Psi_{ds} \quad (2.73)$$

$$e_{dr} = \frac{d\Psi_{dr}}{dt} + R_r i_{dr} - \omega_r \Psi_{qr} \quad (2.74)$$

$$e_{qr} = \frac{d\Psi_{qr}}{dt} + R_r i_{qr} + \omega_r \Psi_{dr} \quad (2.75)$$

In matrix form,

$$\begin{bmatrix} e_{ds} \\ e_{qs} \\ e_{dr} \\ e_{qr} \end{bmatrix} = \frac{d}{dt} \begin{bmatrix} \Psi_{ds} \\ \Psi_{qs} \\ \Psi_{dr} \\ \Psi_{qr} \end{bmatrix} + \begin{bmatrix} R_s & & & \\ & R_s & & \\ & & R_r & \\ & & & R_r \end{bmatrix} \begin{bmatrix} i_{ds} \\ i_{qs} \\ i_{dr} \\ i_{qr} \end{bmatrix} + \begin{bmatrix} -\omega_s \Psi_{qs} \\ \omega_s \Psi_{ds} \\ -\omega_r \Psi_{qr} \\ \omega_r \Psi_{dr} \end{bmatrix} \quad (2.76)$$

A similar approach is used to eliminate the flux linkages in (2.76), leaving the currents as the only variables. By doing so, the above equation will be in a closed-form ready to be solved by numerical techniques discussed earlier.

Electrical Torque in the transformed variables

The electrical torque of the asynchronous machine can be obtained by direct substitution of the transformed stator and rotor currents into (2.58). The torque can then be obtained as,

$$T_e = \frac{3}{2} (\Psi_{qr} i_{dr} - \Psi_{dr} i_{qr}) \frac{p}{2} \quad (2.77)$$

The asynchronous machine dynamic equations remain the same as the earlier derived equations in (2.54)-(2.57).

2.6. Simulations and Results of Asynchronous Machine Model Performance

Similarly, the presented model is for the actual quantities of the machine parameters. Straight-forward approach can be used to convert the actual quantities into their *p.u.* equivalent for simpler computations [4][6][14]. Conversion of the *p.u.* to the actual quantities can be done with equal ease.

2. Modelling of AC Machines for Transient Analysis

2.6.1. Asynchronous Machine Operational Tests

The main objective of this test is to demonstrate the applicability of this phase-domain model in different operational modes. A simple test system consisting of a machine connected directly to an infinite source is used.

The motor is subjected to a direct connection start-up under no-load. At $t = 0.4s$, a mechanical load is applied to the machine so that it function as a motor. Subsequently, at $t = 0.7s$, the mechanical torque of the machine is reversed to create a generating action. The speed of the machine is at rated value under no-load; below the rated value at motoring; and above the rated value at generating. This is the expected operation of an asynchronous machine [4][12]-[14]. The electrical torque also changes from a positive value for motoring to negative for generating mode. Since the general use of the asynchronous machine is for motoring, it is not uncommon to treat the motoring action as positive. Results obtained from the phase-domain model were in good agreement with those obtained in the transformed axis domain provided in PSCAD/ EMTDCTM, where the schematic diagrams is given in Appendix A.3.

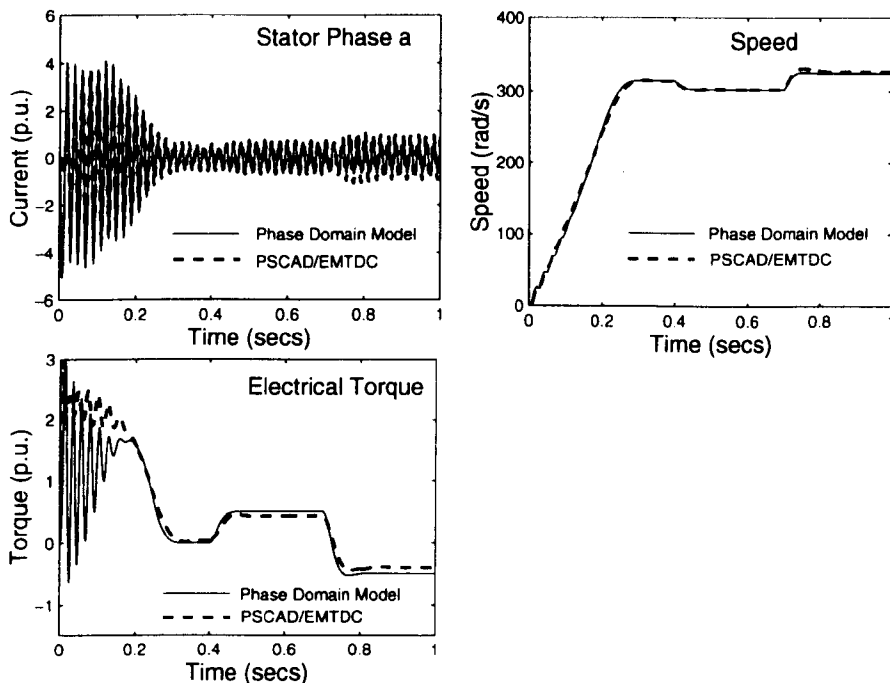


Figure 2.9.: Asynchronous machine response under two modes of operation

2.6.2. Asymmetrical Operating Conditions

The versatility of the direct time phase-domain induction machine model is used to study a typical asymmetrical condition involving the unbalanced stator voltages. The similar connection of the motor to an infinite source is used as the setup of the analysis. Upon the start-up

2. Modelling of AC Machines for Transient Analysis

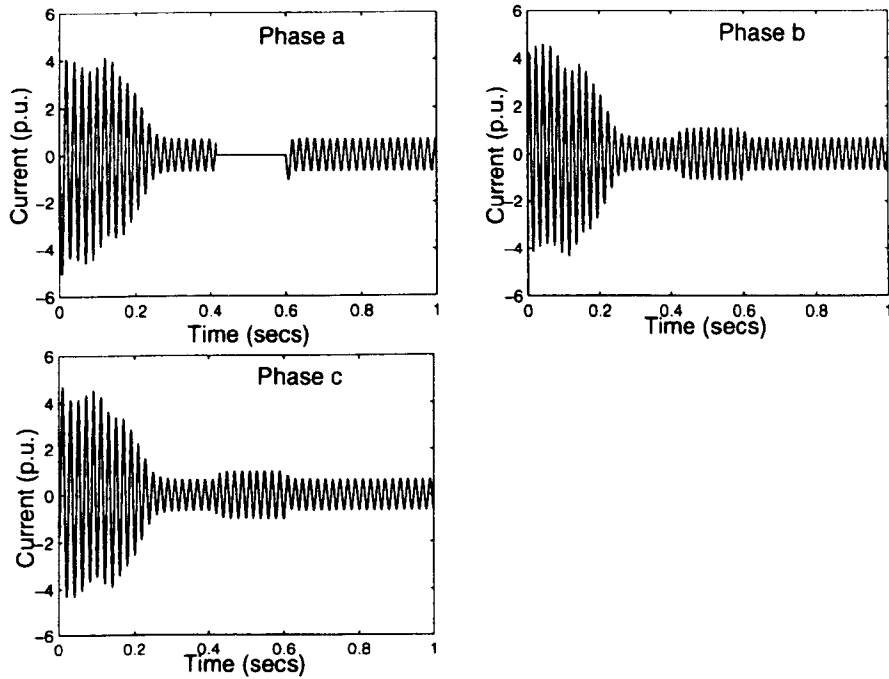


Figure 2.10.: Asynchronous machine stator current under single-phase opening and re-closure

of the motor reaching steady state, the line connecting phase *a* of the stator to the source is disconnected at current zero crossing, which occurs at time of $t = 0.4$ s.

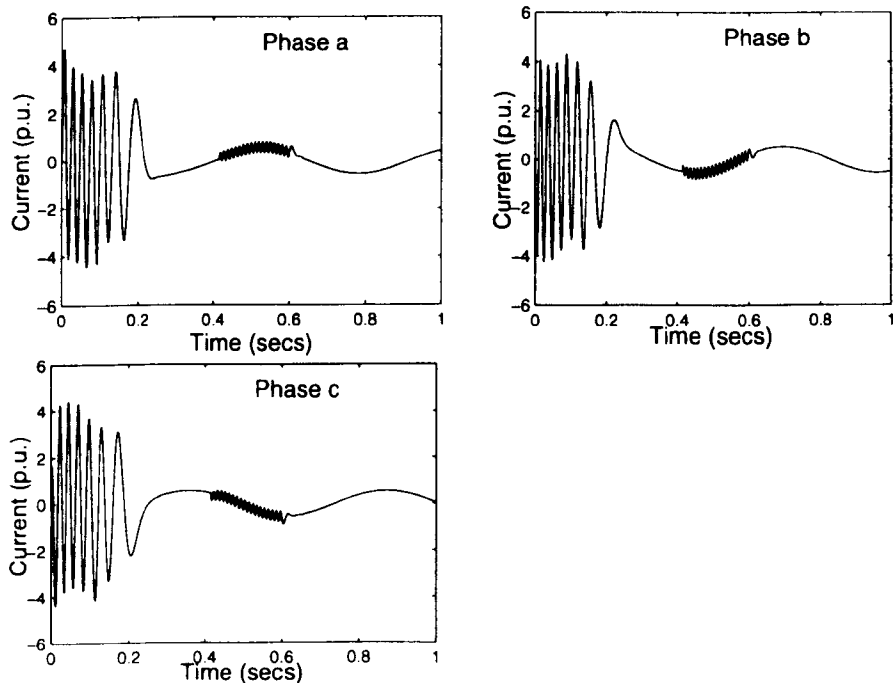


Figure 2.11.: Asynchronous machine rotor current under single-phase opening and re-closure

The responses of the machine's stator and rotor current are shown in Figure 2.10 and 2.11

2. Modelling of AC Machines for Transient Analysis

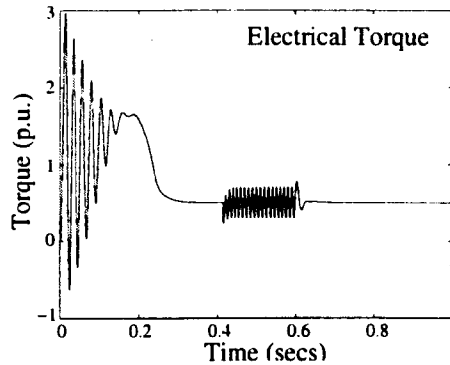


Figure 2.12.: Asynchronous machine electrical torque under single-phase opening and re-closure

respectively. The unbalanced voltage at the terminal causes a pulsating component, with two times the fundamental frequency [13], at the rotor current. The torque shown in Figure 2.12 is essentially constant varying only slightly due to the double frequency pulsating component. The line is re-connected after a period of 0.2s. With the source voltage resuming to balance supply, the response of the machine quickly returns to the pre-disturbance conditions. The results are satisfactory in comparison with those obtained using the approach reported in [13] where it involved complicated transformation of the machine model from one frame-of-reference to another.

2.7. Conclusions

This chapter has touched on the general aspects of AC machine modelling with emphasis on transient analysis. The basic theory used to obtain the model of synchronous and asynchronous machine equations in the direct time phase-domain has been addressed in detail. Their equivalent conventional transformed axis models were also presented. Results show that the phase-domain model is reliable and capable of efficiently simulating network symmetrical and asymmetrical operating conditions in a unified approach, without the need for complex mathematical transformation.

3. Multimachine Dynamic Model in the Phase-Domain for Real-Time Simulation

This chapter is concerned with developing a new approach to model a multimachine network with comprehensive representation of the synchronous generator in the direct time phase-domain. There has been little work reported in open literature on multimachine modelling and programming in the direct time phase-domain, and certainly none involving real-time simulation. The more involved and challenging state equations governing the phase-domain model have in the past mostly been applied to very simple networks. In this chapter, the implementation of this novel approach to multimachine modelling will be presented in detail. This model is general for networks of any size, and basic generator controllers can be incorporated without any change to the controllers' structure. The proposed model and solution method is validated against an industrial standard power system package, PSCAD/EMTDCTM for symmetrical conditions. The models of basic controllers namely the Automatic Voltage Regulator (AVR) and turbine governor will also be presented where they are incorporated into the multimachine environment. A full multimachine network, where transmission unbalances are fully take into account, has been implemented on a multi-purpose Real Time Station (RTS). A thorough investigation is conducted to evaluate the model performance in real-time where the frame time of simulation is a subject of study.

3.1. Introduction

In the previous chapter, a comprehensive phase-domain model of the synchronous and asynchronous machines was developed for transient analysis. The time honoured infinite-bus single loaded machine concept, which was the system under study in the previous chapter, served well as a first approach in investigating the transient behaviour of the machine models

3. *Multimachine Dynamic Model in the Phase-Domain for Real-Time Simulation*

developed. As reported, the performance of the model compares very well with the industrial power system software package, PSCAD/EMTDCTM, for symmetrical conditions, and with the results reported in open literature. It is realised, however, that modern power systems are more complicated and seldom can be seen as connected to an infinite source. The power networks are well connected with many generators, load points and other compensating components. Hence, there is a need to develop a power systems network model, suitable for a multimachine plant, with the potential to study detailed behaviour of the interconnected machines of practical power systems.

The challenge of multimachine modelling mainly involves the development of a fast and accurate solution method for the generators and the network. This is especially important when apply to real-time simulation. There are many techniques that had been proposed over the years to speed up power system dynamic simulations which have paved the way for real-time application [5][6][16][71]-[75]. In these reported techniques, the power system components are modelled following a classical approach where the network is represented by its positive sequence interconnected admittance, and the generator in the transformed $d - q - 0$ axis frame-of-reference. The general solution algorithm normally includes solving the generator dynamic equations by a numerical integration technique followed by a load flow solution to solve for the network variables at any given time step [73][75]. An iterative process is carried out until the generators and network variables are within a small specified tolerance before proceeding to the next time step. This iterative simultaneous solution approach is reliable and efficient especially when the trapezoidal rule is used as the numerical integration technique for the generator equations. In [71], a partitioned solution is used for the iterative simultaneous solution, enabling accurate simulations even at large time step, significantly speeding up the computation process.

However, the benefit of the reduced computing time in this approach is only possible if a symmetrical condition exist in the generator and network. The speed of simulation will be compromised if asymmetrical conditions are considered since additional transformation would be necessary for the generator and the network [4][5][12].

The direct time phase-domain method is uniquely placed to address such a modelling problem by providing a unified approach to simulate any operating conditions. While the direct time phase-domain model of the synchronous generator is not new, using the model to solve the multimachine, interconnected network is of considerable interest. The more involved and challenging state equations representing the generator have, in the past, mostly been used to study network of a node connected to an infinite bus via a tie-line reactance. The solution of larger multimachine network [29][30] was carried out using explicit integration methods resulting in excessive computing time, hampering the possibility of real-time simulations. The lack of adequate computing capability may have been responsible for this but also the lack of efficient solution techniques for dealing with the large set of state equations of the

3. *Multimachine Dynamic Model in the Phase-Domain for Real-Time Simulation*

generators and network involved in a multimachine environment, may have played a part. Such difficulties may have result in the scarcity of published work in the area of multimachine modelling in the direct time phase-domain especially for real-time application.

The aim of this chapter is to report on a solution technique that enables the direct time phase-domain multimachine model to be simulated efficiently for real-time application. This approach involves detailed representation of the generators and the network, which may contain unbalances, using a dynamic state equations and an implicit method of integration [34][31] to form a final set of algebraic equations. The algebraic nature of both the generators and the network equations allow a direct simultaneous solution without the need for any iterative process. The incorporation of basic generator controllers into the model can be easily achieved by similarly discretising the controllers' dynamic equations and solving then simultaneously, with the generators and network algebraic equations.

The added advantage of this model in real-time application is that its responses correspond to the actual instantaneous quantities of a physical network instead of fictitious transformed axis quantities. This makes the real-time model applicable to the testing of actual physical control and protective devices. In the case of a multimachine network, the most obvious applications is that of a test bed for prototype generator controllers, power electronic compensators and their control schemes. This has an important industrial applications where new products can be tested at the prototype stage and operator training can be conducted before full scale development is to take place [76]. The performance of the model for real-time application is evaluated where the frame time of simulation is investigated for different network configuration.

3.2. Methodology and Approach

In many applications for transient analysis [16][34], a synchronous generator is often modelled as a current source. In this proposed solution method, the generator is modelled as a voltage source. Thus, in the procedure adopted it is not only the current flow that is of interest but also the voltage characteristics of the machine.

3.2.1. Discrete Model of the Synchronous Generator

The generator terminal voltage and armature current are represented as a nodal voltage and current injection by discretising (2.9) using the trapezoidal rule of integration presented in Appendix B.1 [31]. When writing the equations of the discretised model it is clearer to proceed the variable's name with a function of time. This is to differentiate the current variable with the preceded known value. The following expression is obtained taking into account that $[\Psi(t)] = [L(t)][i(t)]$,

3. Multimachine Dynamic Model in the Phase-Domain for Real-Time Simulation

$$\begin{aligned}
 [e(t)] &= \frac{2}{\Delta t} [L(t)][i(t)] - [R][i(t)] - [v_{his}] \\
 &= \frac{2}{\Delta t} ([L(t)] - \frac{\Delta t}{2} [R]) [i(t)] - [v_{his}] \\
 &= [R_T][i(t)] - [v_{his}]
 \end{aligned} \tag{3.1}$$

where $[v_{his}]$ is the preceding time step variables defined by,

$$[v_{his}] = [e(t - \Delta t)] + \frac{2}{\Delta t} \left([L(t - \Delta t)] + \frac{\Delta t}{2} [R] \right) [i(t - \Delta t)] \tag{3.2}$$

and

$$[R_T(t)] = \frac{2}{\Delta t} \left([L(t)] - \frac{\Delta t}{2} [R] \right) \tag{3.3}$$

Separating the stator and rotor quantities from (3.1) result in the following,

$$\begin{aligned}
 \begin{bmatrix} [e_s(t)] \\ [e_r(t)] \end{bmatrix} &= \begin{bmatrix} [R_{T_{ss}}(t)] & [R_{T_{sr}}(t)] \\ [R_{T_{rs}}(t)] & [R_{T_{rr}}(t)] \end{bmatrix} \begin{bmatrix} [i_s(t)] \\ [i_r(t)] \end{bmatrix} \\
 &\quad - \begin{bmatrix} [v_{his_s}] \\ [v_{his_r}] \end{bmatrix}
 \end{aligned} \tag{3.4}$$

where subscript s refers to the stator windings, 'abc', and r the rotor windings, 'fkd kq'. Expansion of (3.4) gives,

$$[e_s(t)] = [R_{T_{ss}}(t)][i_s(t)] + [R_{T_{sr}}(t)][i_r(t)] - [v_{his_s}] \tag{3.5}$$

$$[e_r(t)] = [R_{T_{rs}}(t)][i_s(t)] + [R_{T_{rr}}(t)][i_r(t)] - [v_{his_r}] \tag{3.6}$$

By representing the stator quantities in terms of the rotor quantities, the following expression is obtained

$$[e_s(t)] = [R_{equ}(t)][i_s(t)] + [E_s(t)] \tag{3.7}$$

where

$$[R_{equ}(t)] = [R_{T_{ss}}(t)] - [R_{T_{sr}}(t)][R_{T_{rr}}(t)]^{-1}[R_{T_{rs}}(t)] \tag{3.8}$$

and

$$[E_s(t)] = [R_{T_{sr}}(t)][R_{T_{rr}}(t)]^{-1}([e_r(t)] + [v_{his_r}]) - [v_{his_s}] \tag{3.9}$$

3. Multimachine Dynamic Model in the Phase-Domain for Real-Time Simulation

The mechanical equations of motion are also discretised using trapezoidal rule. From (2.16) and (2.17) the following is obtained,

$$\delta(t) = \frac{\Delta t}{2} \omega_r(t) + \frac{\Delta t}{2} \left(\omega_r(t - \Delta t) + \frac{2}{\Delta t} \delta(t - \Delta t) - 2\omega_s \right) \quad (3.10)$$

$$\omega_r(t) = -\frac{\omega_s \Delta t}{4H} (T_e(t)) + \frac{\omega_s \Delta t}{4H} (2T_m - T_e(t - \Delta t)) + \omega_r(t - \Delta t) \quad (3.11)$$

3.2.2. Discrete Representation of the Network Linking the Generators

The most common representation of the power system network connecting the generators, for transient analysis, can be described by,

$$I_n = YV_n \quad (3.12)$$

Where I_n is the nodal injection currents, Y the admittance matrix and V_n the nodal voltages. This steady state positive sequence representation of the network works well when the interconnecting machines are modelled in the transformed $d - q - 0$ or $\alpha - \beta - 0$ axis. This is true owing to the fact that in the transformed model, the time dependent nature of the machines electrical quantities are eliminated, thus leaving only the mechanical dynamic as time dependent. The significant time constant difference between the mechanical and electrical quantities allows this to be done without any loss of accuracy. The electrical quantities in this case will appear as a steady state complex number.

This representation of the network, however, will not be suitable if the interconnected machines are modelled in the direct time phase-domain. A similar modelling approach will be required for the network. Representation of the network in direct time will create many more state equations thereby increasing the complexity of the whole system. A sensible approach is to discretise the state equations of the network into linear algebraic equations.

The discretisation of the connecting network is quite straightforward, where the elements connecting the generators and loads are resistors, inductors and capacitors. Full details of the approach are available in Appendix B.2 [34] and, therefore, only the final stage of derivation is presented in this chapter.

For a given n -node network, the network equation in three-phase quantities takes the following form,

$$[G_{abc}] [v_{nabc}(t)] = [i_{nabc}(t)] - [hist_{abc}] \quad (3.13)$$

where

3. Multimachine Dynamic Model in the Phase-Domain for Real-Time Simulation

$[v_{n_{abc}}(t)]$	vector of $3n$ node voltages
$[i_{n_{abc}}(t)]$	vector of $3n$ current injections
$[G_{abc}]$	$3n \times 3n$ matrix of network elements
$[hist_{abc}]$	vector of $3n$ known preceding terms

The matrix $[G_{abc}]$ is a conductance matrix representing the way various branches of the network are connected together with their numeric values. The matrix for each individual branch is a full 3×3 matrix due to the line couplings between phases.

At the generator bus, the nodal voltage corresponds to the stator voltage of the generator. Similarly, the injected current at the node is the stator current of the generator. At the bus connecting a passive load, the current injection is zero since the load is represented by a fixed impedance. If a non-passive load, like an induction motor, is connected to the bus, then the nodal voltage will correspond to the stator voltage of the motor. Taking these considerations into account, (3.13) can be further reduced to express the nodal voltage and current injections at the generator nodes as follow,

$$\begin{bmatrix} [i_{ng_{abc}}(t)] \\ [i_{nl_{abc}}(t)] \end{bmatrix} = \begin{bmatrix} [G_{gg_{abc}}] & [G_{gl_{abc}}] \\ [G_{lg_{abc}}] & [G_{ll_{abc}}] \end{bmatrix} \begin{bmatrix} [v_{ng_{abc}}(t)] \\ [v_{nl_{abc}}(t)] \end{bmatrix} + \begin{bmatrix} [hist_{g_{abc}}] \\ [hist_{l_{abc}}] \end{bmatrix} \quad (3.14)$$

Since $[i_{nl_{abc}}(t)]$ is zero then,

$$[i_{ng_{abc}}(t)] = [G_T][v_{ng_{abc}}(t)] - [H_{ist}] \quad (3.15)$$

where

$$[G_T] = [G_{gg_{abc}}] - [G_{gl_{abc}}] [G_{ll_{abc}}]^{-1} [G_{lg_{abc}}] \quad (3.16)$$

$$[H_{ist}] = - [G_{gl_{abc}}] [G_{ll_{abc}}]^{-1} [hist_{l_{abc}}] - [hist_{g_{abc}}] \quad (3.17)$$

3.3. Solution Algorithms

As mentioned earlier, the nodal voltage and current injection at a node connected to a generator is, in fact, the generator stator voltage and current. For example, if a given generator is connected to *Node m*, then the generator stator voltage $[e_{ms}(t)]$ is equal to $[v_{mg_{abc}}(t)]$, and similarly $[i_{ms}(t)]$ is equal to $[i_{mg_{abc}}(t)]$. Hence, if there are ng generator nodes, there will be ng

3. Multimachine Dynamic Model in the Phase-Domain for Real-Time Simulation

equations similar to (3.7). Together with (3.15), we have an equal number of known equations and variables. The algebraic nature of these equations allows us to perform a straightforward simultaneous solution to obtain the nodal voltages and currents injected at every time step. The solution algorithm for the new multimachine model in the direct time phase-domain can be summarised in a flowchart as shown in Figure 3.1. This approach is a new method, which is unique to this thesis. The program listing of the general multimachine transient stability program in Appendix D.1 is developed based on this flowchart.

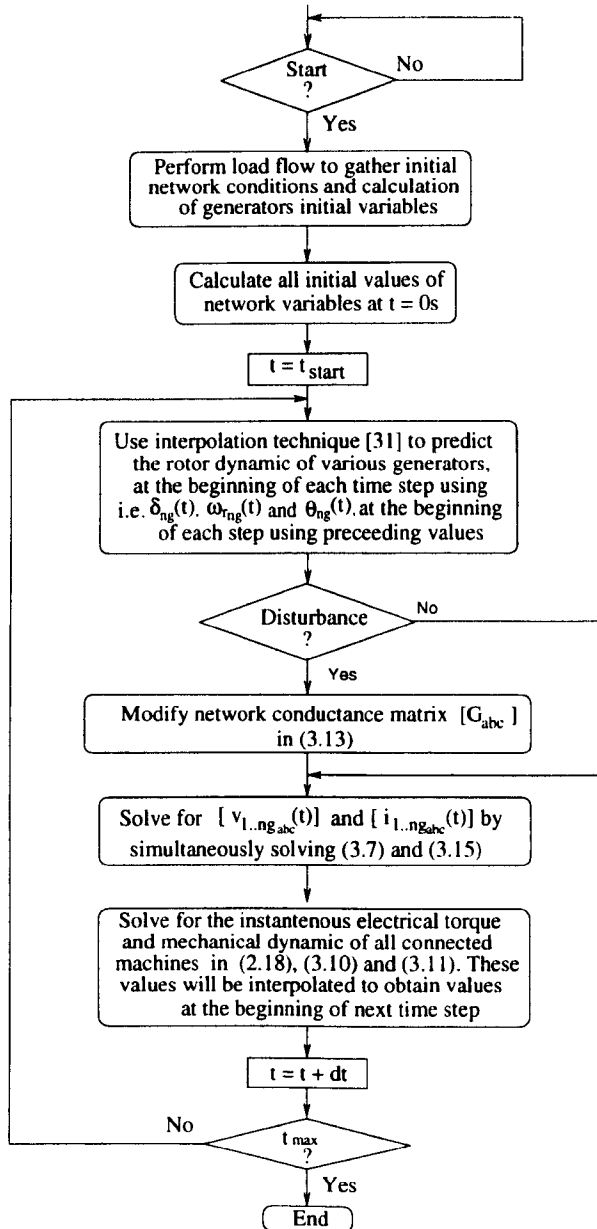


Figure 3.1.: Flowchart of direct time phase-domain multimachine solution algorithm

3.4. Model Validation

The proposed model of the synchronous generator and the multimachine network was validated against PSCAD/EMTDCTM for symmetric conditions. A simple multimachine test system, as shown in Figure 3.2, was used in performing the validation test. The details of the synchronous generator data in both the standard form and phase quantities were obtained from Appendix A.1. The network parameters provided are in *p.u.* of the generator base in the steady state positive sequence. The schematic diagram used in PSCAD/EMTDCTM is given in Appendix A.3.

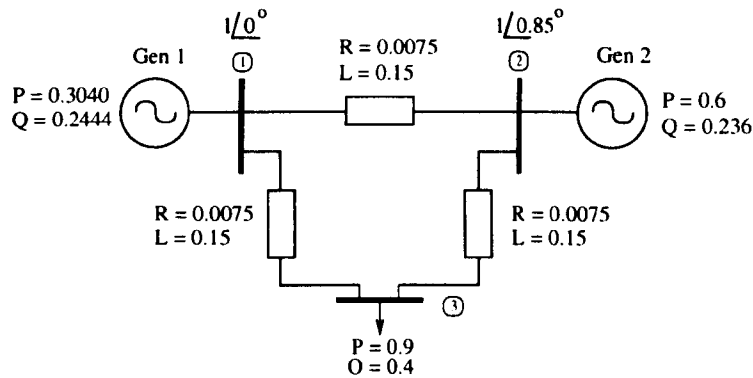


Figure 3.2.: Three nodes test network

Figure 3.3 shows the results where a three-phase-to-ground fault was applied at the terminal of *Node 2*. The results for both the generators compare well between the direct time phase-domain model and PSCAD/EMTDCTM.

3.5. Generator Controllers

There are various control systems associated with the synchronous generator as mentioned earlier. Two common most control systems for the generator are the excitation control and the speed turbine governor [36]-[38]. The excitation control regulates the terminal voltage of the generator by providing appropriate magnetic field through DC excitation. The speed turbine governors maintain constant turbine speed by limiting the difference between the input and output power. These two controllers play an important role in maintaining the stability of the generator when subjected to disturbances.

3.5.1. Generator Excitation Control

A three-phase synchronous generator is able to provide constant electrical torque due to the interaction between the armature stator AC currents with the rotating DC field current on the

3. Multimachine Dynamic Model in the Phase-Domain for Real-Time Simulation

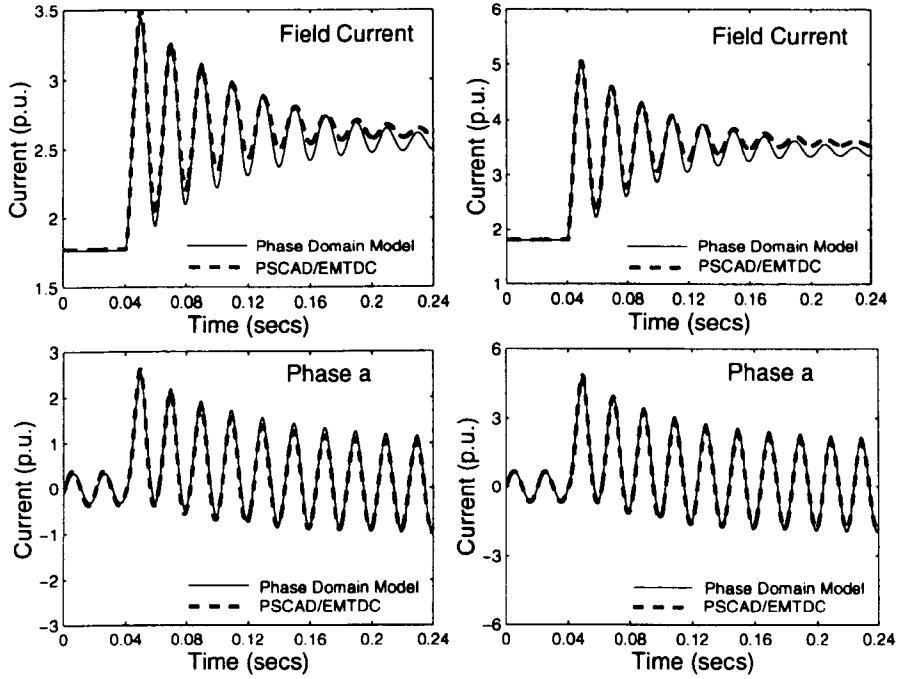


Figure 3.3.: Stator and field currents for a three-phase-to-ground fault at *Node 2* of the three nodes test network

rotor. The basic function of an excitation system is to provide DC current to the rotating DC field winding. Therefore, the excitation system plays a major role in control and protective functions to maintain the satisfactory voltage magnitude at the terminal of the generator by controlling the field voltage, e_f and hence, the field current, i_f . Many forms of excitation control that have been developed over the years [36][38], which are basically categorised into the DC, A.C and Static excitations systems.

The general block diagram representing the excitation control is depicted in Figure 3.4. The excitation control consists of an automatic voltage regulator (AVR), exciter and the stabilising loop. The AVR regulates the generator's terminal voltage by controlling the amount of current supplied to the generator field winding by the exciter. The measured generator's terminal voltage and the desired reference voltage are compared to produce a voltage error, which is used to alter the exciter output. The limiter is a device that prevents the exciter field voltage to go beyond the rated heating limit permitted in the field winding.

The excitation system adopted throughout this report is similar to the approved block model in Figure 3.4 [36][38] where the dynamic state equations representing the block model are given by,

$$\frac{dE_{fd}}{dt} = \frac{1}{\tau_{ex}} (V_r - E_{fd}) \quad (3.18)$$

$$\frac{dV_r}{dt} = \frac{1}{\tau_a} (K_a V_{ef} - V_r) \quad (3.19)$$

3. Multimachine Dynamic Model in the Phase-Domain for Real-Time Simulation

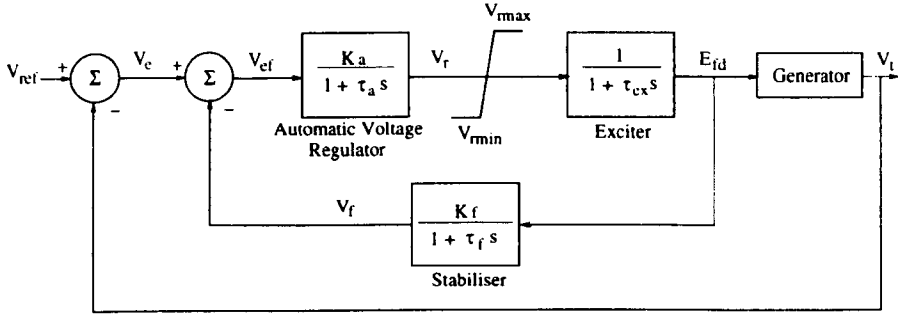


Figure 3.4.: Block model of an excitation system

$$\frac{dV_f}{dt} = \frac{1}{\tau_f} (K_f E_{fd} - V_f) \quad (3.20)$$

$$V_e = V_{ref} - V_t \quad (3.21)$$

$$V_{ef} = V_e - V_f \quad (3.22)$$

$$V_{rmin} \leq V_r \leq V_{rmax} \quad (3.23)$$

The above differential equations need to be integrated simultaneously with the generator equations to collectively solve the complete dynamic model. This can be achieved by employing the same trapezoidal rule of integration to discretise the control block. The detail process of the discretisation is presented in Appendix B.3.

Bearing in mind that E_{fd} is known from the initial operating condition of the generator where the subscript '0' here denotes the initial condition. The initial conditions and the desired value of V_{ref} can be obtained as follow ,

$$V_{r0} = E_{fd0} \quad (3.24)$$

$$V_{ef0} = \frac{V_{r0}}{K_a} \quad (3.25)$$

$$V_{f0} = K_f E_{fd0} \quad (3.26)$$

$$V_{ref} = \left(\frac{1}{K_a} + K_f \right) E_{fd0} + V_{t0} \quad (3.27)$$

3. Multimachine Dynamic Model in the Phase-Domain for Real-Time Simulation

Effect of Excitation Control on System Stability

The excitation control model described in Figure 3.4 is implemented to study the effect it has on maintaining the transient stability of a power system network. Figure 3.5 shows the simple network where two machines are connected in a six nodes network and an infinite bus. The generator data used are given in Appendix A.2 where the network power and reactances are in *p.u.* of the generator base. The parameters of the automatic voltage regulator are $K_a = 100$ and $\tau_a = 0.05s$, and $\tau_{ex} = 0.1s$. In this simulation the stabiliser loop is omitted from the control block.

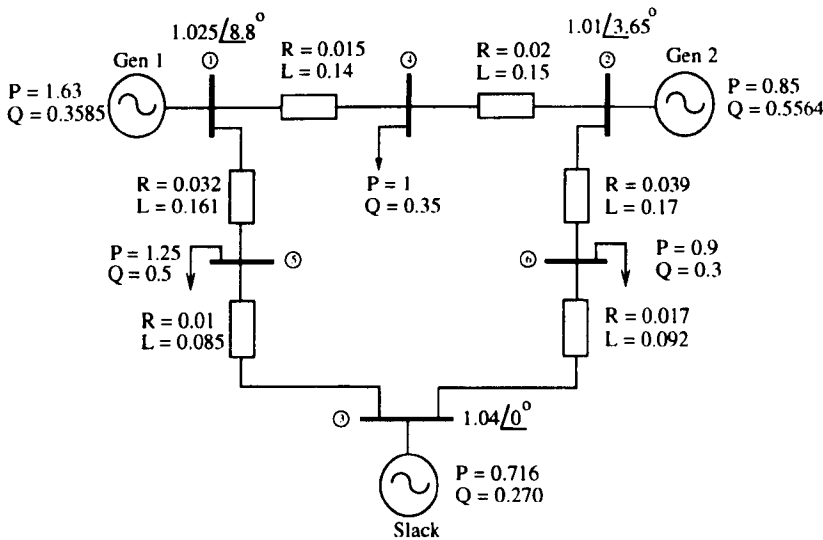


Figure 3.5.: Six nodes network for study of excitation control on system stability

	Slack	Gen 1	Gen 2
V (p.u.)	1	1.025	1.011
θ (degree)	0	8.799	3.645
Load angle, δ (rad)	-	0.730	0.455
Efd	-	2.637	1.754

Table 3.1.: steady state values of generators' variables in Figure 3.5

A transient condition is initiated by applying a three-phase-to-ground fault at *Node 1*. The fault is cleared after 0.209s. The generator *Gen 1* will suffer the greatest extent of the fault as it is closely located to the point-of-fault. The results of time responses of *Gen 1* are shown in Figure 3.6-3.7 under two different excitation conditions where a fixed and control excitation are used. It is observed from Figure 3.6a that with the fixed E_{fd} , the system is transiently unstable after the fault is cleared. The post-fault voltage at the generator's terminal continue to collapse resulting in the loss of electrical torque. With a constant input torque driving the rotor, its speed will continue to accelerate allowing the load angle to swing out of synchronism which make the system unstable and highly oscillatory.

3. Multimachine Dynamic Model in the Phase-Domain for Real-Time Simulation

The presence of excitation control through the AVR provides additional voltage support, which helps regulate the post-fault voltage to its initial condition. The generator resumes its electrical torque output matching the input torque driving the rotor, which in turn maintains the speed of the rotor.

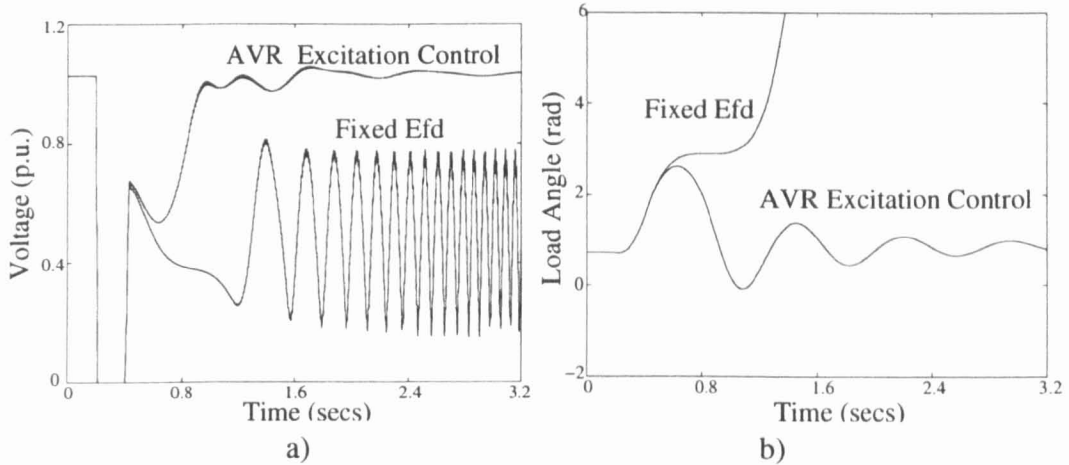


Figure 3.6.: Terminal voltage and load angle of *Gen 1* following a three-phase-to-ground fault at its terminal

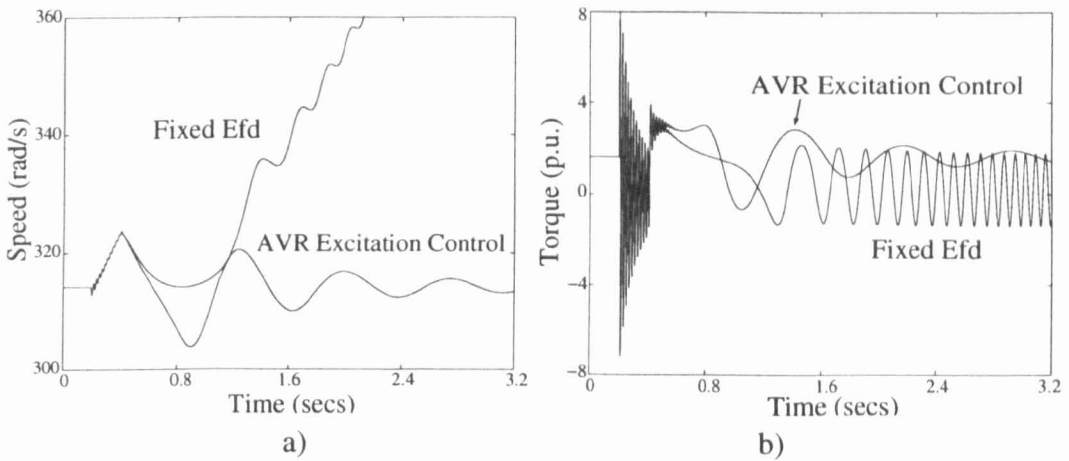


Figure 3.7.: Speed and electrical torque response of *Gen 1* following a three-phase-to-ground fault at its terminal

3.5.2. Speed Turbine Governor

For a magnetic field to form in the synchronous generator, the rotating flux interaction between the field voltage and the stator core must exist. The field voltage is produced by a DC source connected to the field winding located on the rotor of the generator. The rotation of the rotor at synchronous speed produces a flux linkage between the field and the voltage of the stator core to form the electromagnetic force at the terminal of the stator.

3. Multimachine Dynamic Model in the Phase-Domain for Real-Time Simulation

In most synchronous generators, the rotor is normally driven by turbines powered by conventional energy sources such as the steam and hydro power [4][37]. The role of the speed turbine governor is to maintain the generator speed by adjusting a valve to control the input power to the turbine. There are different types of speed governor models and configurations for different type of generation plant and energy sources [4][37].

The general model block diagram representing the speed turbine governor is depicted in Figure 3.8. This model consists of a speed regulator, a turbine and a governor block. The speed regulator monitors the change in the generator's speed due to the difference in the input and output power as given in (2.17). The governor block picks up the error and regulates its output, which in turn change the output of the turbine. By doing so the speed of the generator will maintain at near constant even when subjected to a change in network conditions.

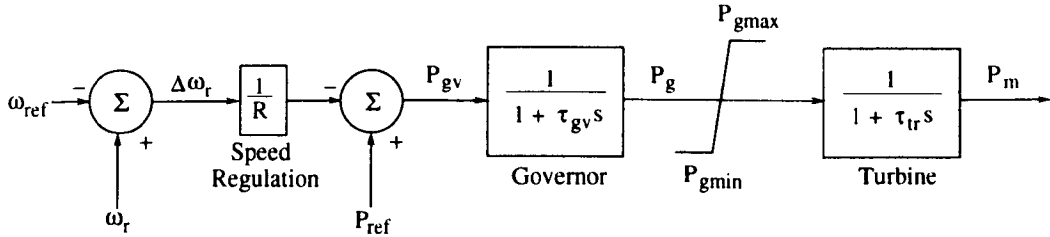


Figure 3.8.: Block model of a speed turbine governor

The equations representing the block model can be obtained as follow,

$$\frac{dP_m}{dt} = \frac{1}{\tau_r} (P_g - P_m) \quad (3.28)$$

$$\frac{dP_g}{dt} = \frac{1}{\tau_{gv}} (P_{gv} - P_g) \quad (3.29)$$

$$P_{gv} = P_{ref} - \frac{(\omega_r - \omega_{ref})}{R} \quad (3.30)$$

$$P_{gmin} \leq P_g \leq P_{gmax} \quad (3.31)$$

Similarly, the integration of the turbine governor equations into the multimachine network requires it to be discretised by the trapezoidal rule as in Appendix B.3. The reference point can be calculated by obtaining the initial conditions of all the variables of the control block. From the control block, the value of the variables and the reference value are obtained from the known initial value of P_{m0} as follow,

$$P_{g0} = P_{m0} \quad (3.32)$$

$$P_{gv0} = P_{g0} \quad (3.33)$$

$$P_{ref} = P_{m0} \quad (3.34)$$

3. Multimachine Dynamic Model in the Phase-Domain for Real-Time Simulation

Figure 3.9 shows the response of *Gen 1* when subjected to a slight increase in load. The parameters for the control blocks are $R = 0.05$, $\tau_{gv} = 0.2s$ and $\tau_{tr} = 0.5s$. These parameters are not of an actual system, but arbitrarily selected to demonstrate the operation of the turbine governor. In an actual system, the time constant of the turbine is normally in a factor of a few seconds to represent its slow operation.

The effect of an increase in load, which causes the speed of the machine to decrease, is governed by the dynamic equation of the generator. As the speed drops, the mechanical output from the turbine governor begins to increase. This will result in a reduced rate of speed decrease, and when the mechanical power is in excess of the load power, the speed will begin to increase. The speed will settle at the preset synchronous speed reference value and the steady state mechanical power increase by an amount to match the load demand.

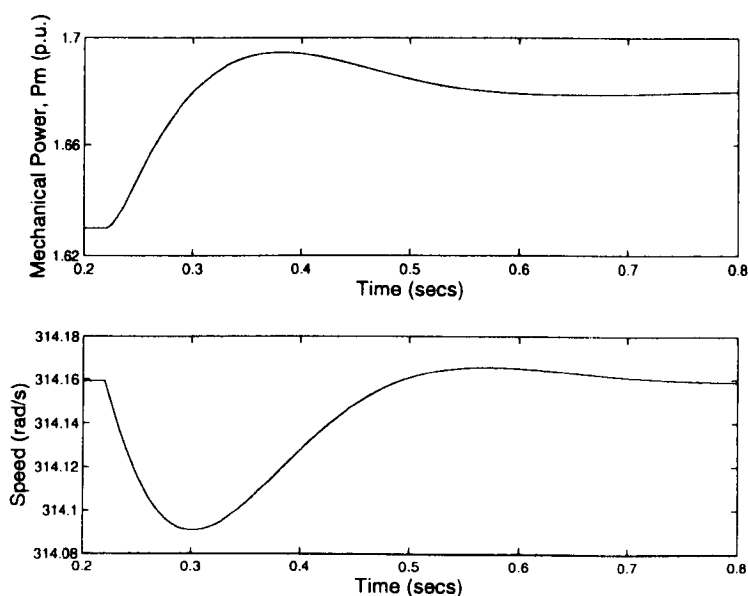


Figure 3.9.: Response of *Gen 1* when subjected to a load increase with turbine governor control

3.6. Real-Time Simulation of the Multimachine Network Model

Digital computer based simulation packages have been extensively used to observe the response of power system networks under particular operating conditions. The limitation of such digital simulators is the difficulty of interfacing the simulator to physical devices [63][69]. Such limitation is down to the inherent mismatch between the CPU time taken by the simulation tool and the actual system's response; thereby severely impairing their application in the area of physical equipment testing [63]. Hence, real-time simulation, where the

3. *Multimachine Dynamic Model in the Phase-Domain for Real-Time Simulation*

mathematical model is solved by the computer and outputted in actual world time, is seen as the way forward for a physical device to be interfaced to the simulator.

In the past, analogue HVDC simulators and AC Transient Network Analyzers (TNAs) have been widely used in this respect throughout the power industry. In recent years, a more flexible and cost effective alternative has been to use fully digital dynamic simulators with real-time capabilities [76][77][69]. The computing engines of these simulators mainly consist of flexible multiprocessor system with parallel computing capability. A very good example of this technology is the simulator developed in [76] which is based on closely coupled microprocessors enabling very efficient solutions when applied to large-scale applications such as power system dynamic analysis. The technique of construction in these simulators is well established. However, simulators, which are developed as a combination of special purpose computer architectures and a customised operating systems, can suffer from lack of generality. The implementation of new components or network structures might involve cumbersome modification to the operating system, hence, limiting the end user to study only the network that is permissible and already implemented in the simulator. In most available simulators, the model of the generators and network for dynamic analysis are in the $d - q - 0$ frame-of-reference limiting the possibility of a wider study area.

The solution to this problem is to use a general multi-purpose real-time simulator or a real-time station (RTS) where the simulator can be treated as a black box. The user can have the flexibility to implement any power system model or network configuration, as long as the workload stays within the computational limit of the RTS. No attention needs to be paid to the operating system and hardware construction of the RTS throughout the process.

The research reported in this chapter follow this approach where a commercially available RTS is used for the real time simulation of a power system multimachine network. The RTS is developed by Applied Dynamics International (ADI), and is designed for real-time hardware-in-the-loop dynamic simulations. Unlike other simulators that have been reported in open literature, the RTS is a multi-application real-time simulator suitable for a wide variety of dynamic systems, without confining the analysis to power systems alone. Bearing in mind that the cost associated with this state-of-the-art technology, the ability to analyse a wide variety of dynamical systems, over a variety of application areas, makes the facility a very cost effective technology.

One of the main points mentioned in Chapter 1 is the importance of having power system component's model capable for real-time simulation. This provides a useful approach where simulations that include interfacing of physical devices in a closed-loop are of interest. It is often too expensive to build a whole system just for testing of one or two devices of interest. For example, it is impossible to construct a test system if a physical protection or control device need to be tested with generators connected to a multimachine transmission network. Hence, real-time testing of devices under actual operating condition is of great importance to

3. *Multimachine Dynamic Model in the Phase-Domain for Real-Time Simulation*

device manufacturers. Under this condition a real-time mathematical multimachine network model will be handy where the physical device can be interface with the model's real-time responses in a hardware-in-the-loop situation.

Most modern RTS operates digitally to achieve better flexibility at a cheaper cost. Hence, the mathematical model to be use with these RTS needs to be represented digitally as well. The discretised direct time phase-domain modelling of power system components is one of the possible approach as the model is readily represented in discrete form and its responses are all instantaneous value with respect to actual time. The following subsections will see the simulation of the novel multimachine model in the real-time environment.

3.6.1. The Real-Time Station (RTS)

The RTS used in this thesis is a commercially available simulator, developed by Applied Dynamic International (ADI), and designed specifically for real-time, hardware-in-the-loop dynamic simulations. Unlike other simulators that have been reported in the open literature, this RTS is a multi-application real-time station suitable for simulating a wide variety of dynamic systems, without confining the analysis to power systems alone. Bearing in mind the costs associated with this state-of-the-art technology, the ability to analyse a wide variety of application areas, makes the facility a very cost effective technology.

Hardware Configuration

The RTS is a multiprocessor system capable of parallel processing and I/O interactions in real-time. The user interacts with the RTS through a host workstation that serves as the driver for the GUI based simulation package in which the multimachine model was developed. The RTS system architecture consists of several different processors types, the Simulation Processor (SP) and Compute Engine (CE) processors, coupled to a common VMEbus backplane, with each processor designed for a specific task. A block configuration of the RTS is given in Figure 3.10 [68][69].

Software Simulation Language

The two GUI based packages that allow the interaction between the user and the RTS are EASY5 developed by Boeing Inc. and the Integrated development Environment (IDE) by ADI [69]. EASY5 is a GUI based software used to model, analyse and design dynamic systems. Models can be constructed using a large set of pre-defined functional blocks, or by directly inputting user-defined FORTRAN codes. The complete dynamic model in EASY5 is loaded into IDE for real-time execution of the model. IDE oversees the allocation of I/O

3. Multimachine Dynamic Model in the Phase-Domain for Real-Time Simulation

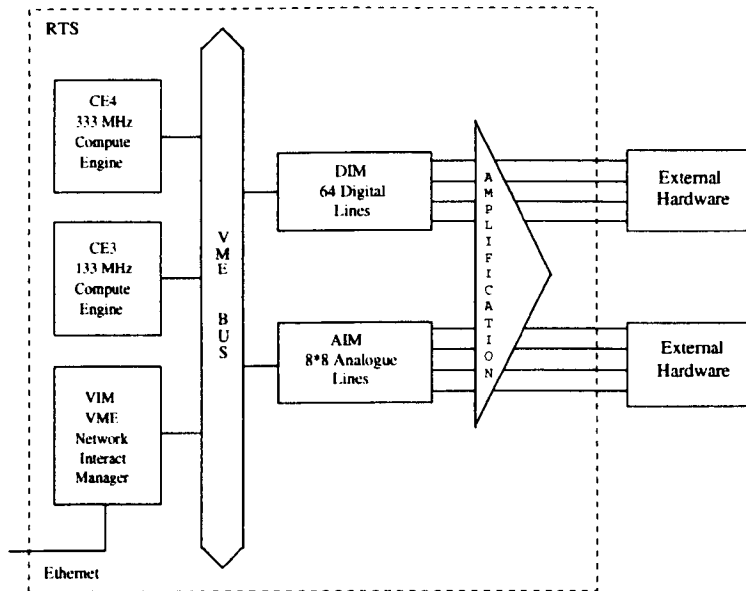


Figure 3.10.: RTS configuration

channels and scaling of the real-time I/O signals. The real-time simulation data can be viewed or collected within EASY5 at the end of each simulation or in real-time using the ADI's real-time data acquisition tool.

3.6.2. Real-Time Simulations

The main parameter that needs monitoring when performing real-time simulations is the Actual Frame Time (AFT) of the RTS. The AFT allows the user to observe the time taken by the RTS to compute each time step of the simulation. If the AFT exceeds the Desired Frame Time (DFT) at any point in the simulation then real-time simulation has failed to be maintained. The DFT is always given by the simulation time step. In order to test the limitations of the RTS, a larger and more realistic study network with reasonable complexity was used in the real-time simulation. The network under study is a five-node and two-generator network as shown in Figure 3.11. The network parameters provided are in *p.u.* of the generator base. The generator data are given in Appendix A.2.

The real-time simulations were conducted by considering two network cases, with line couplings and when line couplings are not considered. Figure 3.12 shows the generators phase *a* stator voltages and current for the case of a symmetrical three-phase-to-ground fault at the terminal of *Node 2*. The results are plotted using the real-time data output from the RTS. Figure 3.13 presents similar results for the case of an asymmetrical single-phase-to-ground fault at the same node, where phase *a* of *Node 2* is faulted to ground. The effect of line couplings can be observed from Figure 3.12 and Figure 3.13. It is realised that for symmetrical disturbances the effect of line couplings is not significant since the system network matrix is perfectly symmetrical prior to and after the disturbance. For the case of asymmetrical

3. Multimachine Dynamic Model in the Phase-Domain for Real-Time Simulation

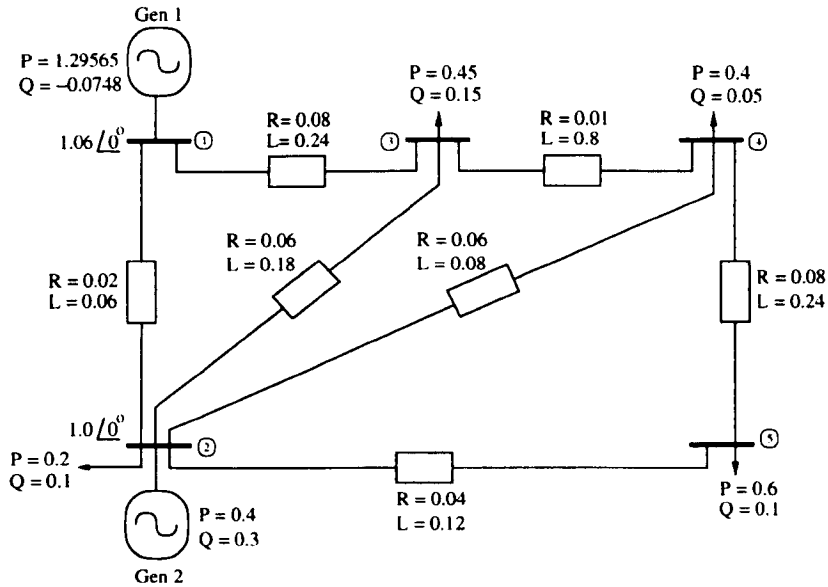


Figure 3.11.: Five nodes network used in real-time simulations

disturbances, there is a significant difference in the behaviour of *Gen 1*. This is due to the interaction of other phases with the faulted phase via the coupling impedances. For *Gen 2*, the behaviour of the faulted phase *a* is similar with and without line couplings because the fault occurs at its terminal, hence, the network elements related to the phase in fault during that period are the same for symmetrical and asymmetrical conditions.

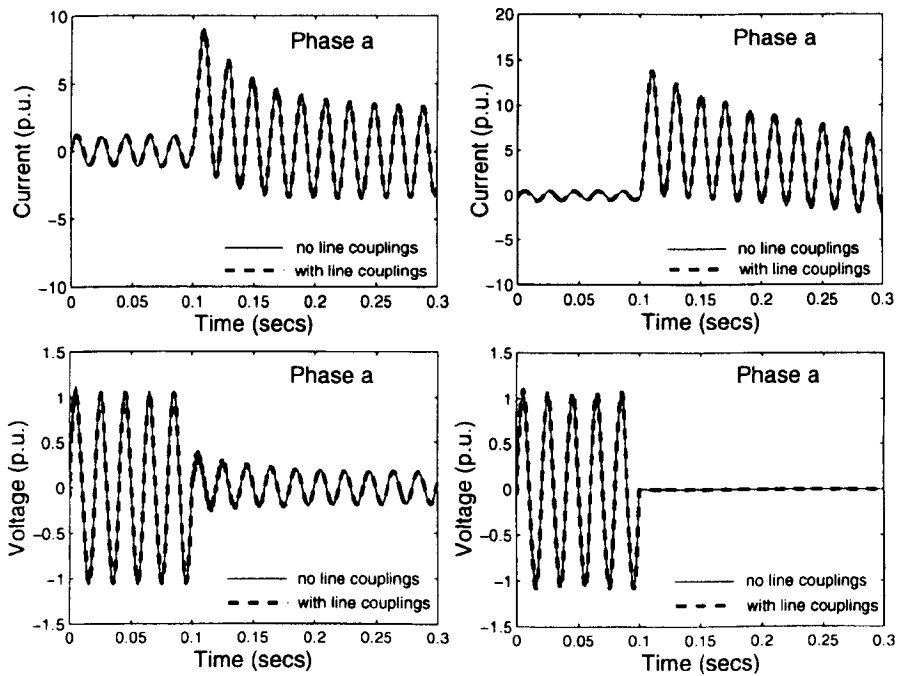


Figure 3.12.: Stator voltages and currents for a three-phase-to-ground fault at *Node 2* of the five nodes network

The simulations were undertaken with a time step of $300 \mu\text{s}$. It is acknowledged from Figure

3. Multimachine Dynamic Model in the Phase-Domain for Real-Time Simulation

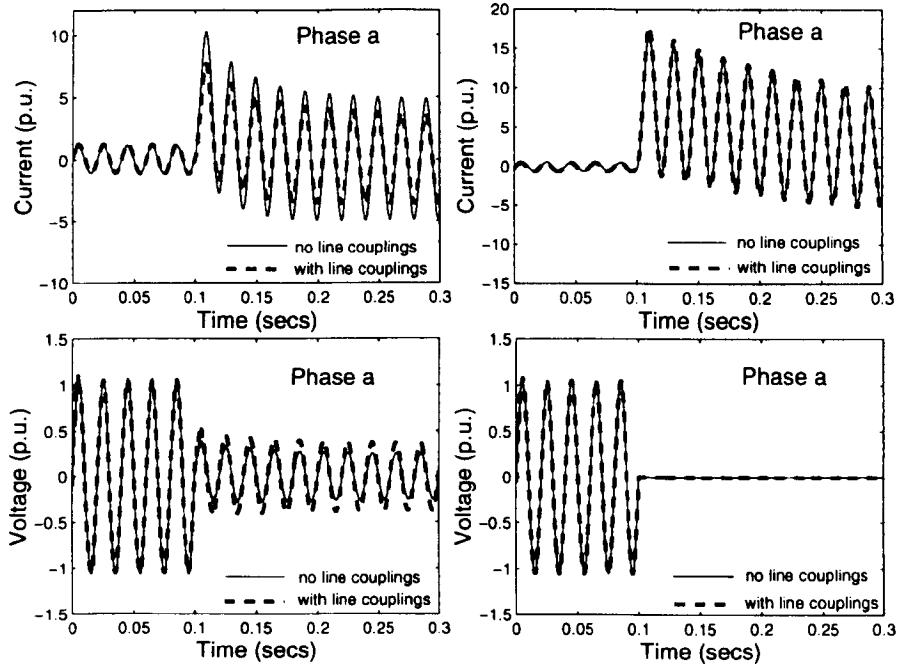


Figure 3.13.: Stator voltages and currents for a single-phase-to-ground fault at *Node 2* of the five nodes network

3.14 that the AFT of the simulation, when no network couplings are taken into consideration, is well below the DFT, with an average of $264 \mu s$. For the simulation when network couplings are considered the AFT is much closer to the DFT, with an average of $294 \mu s$, which means that real-time simulation can easily be upset at this stage by any occurrence of additional operations in the computation process. The reason for the increase in simulation time required is due to the increased complexity in the network conductance matrix $[G_{abc}]$ introduced by the line coupling elements. The initial rise in frame time in Figure 3.14 is caused by the internal initialization process undertaken by the processors in the RTS, and it has no prolonged effect on the simulation.

It should be remarked that in practice, the use of the trapezoidal rule of integration in the solution method of the multimachine model has enabled a larger time step to be used while maintaining stability and accuracy of the simulation. This is shown in Figure 3.15, where a comparison of different time steps on the effect of accuracy is studied. The comparison is based on the first peak of the faulted phase *a* current of *Gen 1*. It can be seen that the accuracy is acceptable up to a time step of $500 \mu s$ [33]. With the more relaxed selection of time steps that can be used, reasonably larger and more complicated network operations can also be simulated in real-time.

Even though larger time step may be used in the simulation, it is preferable to keep it small in order to achieve better accuracy. Hence, the selection of an appropriate time step is of concern prior to implementing a model in the real-time environment. This can be explained with relation to the overhead of data processing in the RTS. Since access to the information

3. Multimachine Dynamic Model in the Phase-Domain for Real-Time Simulation

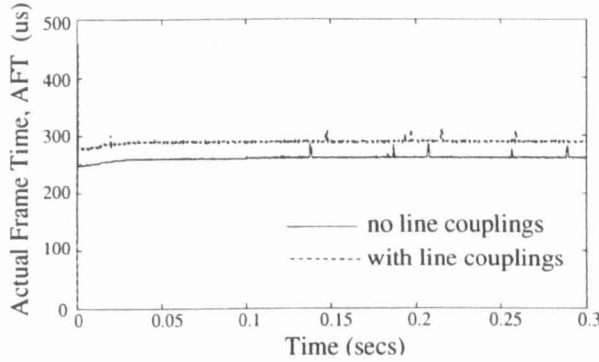


Figure 3.14.: Comparison of AFT between simulations with no line couplings and with line couplings

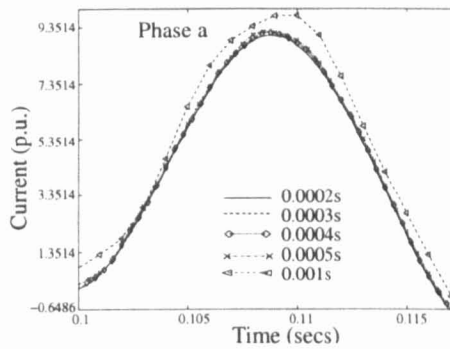


Figure 3.15.: Comparison of different time steps on the accuracy of the response on stator current of *Gen 1*

inside the RTS microprocessors is not permitted to the end user, an experimental approach needs to be adopted to study the data overhead in the simulator. The simple network shown in Figure 3.16 is used, where the number of generator nodes is increased in step from one to four. The required AFT of simulation is plotted against the number of generator nodes in Figure 3.17. It is observed that there exists an almost linear relationship when the number of generator nodes is small. However, as the number of node increases the step increment of the frame time becomes sharper. The additional data is needed to be process and outputted by the compute engine will build up a traffic in the VMEbus, which carries the information, resulting in the non-linear increment of frame time.

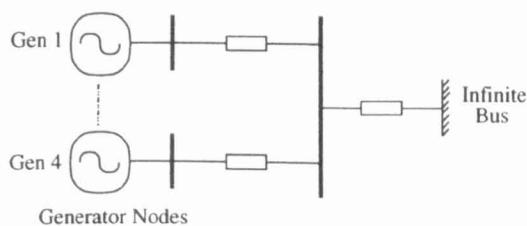


Figure 3.16.: Test network to obtain data overhead of the RTS

3. Multimachine Dynamic Model in the Phase-Domain for Real-Time Simulation

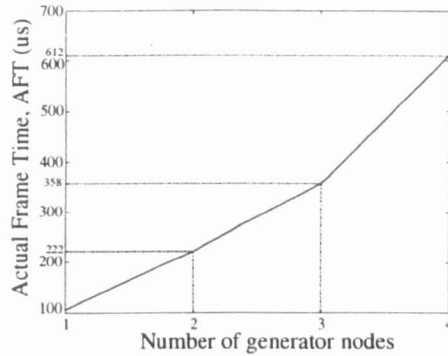


Figure 3.17.: AFT versus number of generator nodes

3.7. Conclusions

This chapter has presented a new algorithm for modelling of a multimachine network in the direct time phase-domain with similar full representation of the generators. This method is able to solve large volume of differential equations, representing the phase-domain generators and network model, by first discretising them to straightforward algebraic equations. It is a more efficient method than any published approach, which involves tedious solution of the differential equations using explicit integration method. The results obtained using the newly developed model are compared with those given by an industry standard power system package, PSCAD/EMTDCTM. The comparisons were found to be satisfactory under a symmetrical condition. A key feature in this chapter is the realization of the capability of this multimachine model for real-time simulations. The solution algorithm proposed for the multimachine model enable a larger time step to be utilised while maintaining accuracy and stability. Hence, it is possible to simulate larger and more complicated networks, involving more operations in real-time. Lastly, the general controllers for a generator is described, and simulations shows that classical controller can be implemented in a similar manner into the new multimachine model proposed here.

4. Further Consideration of the Direct Time Phase-Domain Multimachine Model

Generality and versatility are items of paramount importance when developing mathematical models of power system components. The generality of the model indicates that it can be applied to perform studies based on existing power system concepts while versatility points to the amount of flexibility afforded by the model to perform analysis that have been hampered by existing models. This chapter explores further these two aspects with relation to the direct time phase-domain multimachine model. The model is applied in a transient stability analysis where a group of coherent generators are represented by a single equivalent. The realisation of this equivalent model allows transient stability analysis of power systems in the phase-domain to be performed with unrivalled flexibility and less computation time, which is of great importance in real-time applications. These claims will be supported with results that demonstrate the versatility of the model when dealing with asymmetrical faults and real-time studies. This chapter also addresses the effect of dynamic load operation in the multimachine network. The dynamic load, represented by a detailed induction motor model, has an important role to play in the network responses, especially when one is interested in the study of power quality issues. The aim here is to study and understand the behaviour of the network voltage profile when subjected to direct online motor starting and network disturbances. Results will be presented to study the various attributes governing the operations of the induction motor that can affect the voltage profile of the network.

4.1. Introduction

Modelling in the direct time phase-domain is a modelling approach used to analyse the power system networks aiming at achieving a wide range of study flexibility and comprehensiveness. Up to a point, this was shown in the previous chapter when symmetrical and asym-

4. Further Consideration of the Direct Time Phase-Domain Multimachine Model

metrical operations were considered with respect to transient simulation of phase-domain multimachine model in real-time. The model is particularly useful for the analysis of complex dynamic situations that include a wide range of non-conventional network disturbances. The objectives of this chapter, which build on the merits of the model, are two fold, to develop an equivalent model of the generator and the consideration of dynamic loads in the phase-domain multimachine network. These are two timely contributions to power systems engineering where limited amount of work has been reported in the open literature.

While the use of this versatile model is a luxury afforded by current computing capability, there is always a need to reduce computational time when the study of large networks is of interest. The traditional approach to reduce computation time is to determine an equivalent model to represent the portion of network that is of no immediate concern [79][80]. There is a great deal of published literature in this area but the models of the generator used are either too simple or expressed in the transformed axis domain, thus rendering the equivalent generator models to complex mathematical transformations. Hence, similar equivalent model needs to be develop for the direct time phase-domain approach. By making possible the determination of the equivalent generator parameters through mathematical analysis, an accurate equivalent can be obtained for such a system in the phase-domain.

A major contribution to non-conventional network stability problems is the presence of dynamic loads, typically assumed to be induction motors. This is justifiable since induction motors consume 60 – 70% of the total energy supplied by a power system [4]. The operation of induction motors and their effect in a multimachine network can be complicated if a good model and sound approach is not available to interface the motors to the existing network and generator models. The focus in this chapter is on applying the discretised multimachine model to study the impact of the motor on overall network stability. In particular, the direct online starting of induction motor receives great attention.

4.2. Coherency-based Multimachine Transient Analysis

Power systems have experienced rapid growth in terms of size and operational complexity throughout the world due to increasing electricity demand. This has intensified the need for accurate and comprehensive analytical tools capable of dealing with the efficient numeric solution of large-scale power networks. One area that has required a great deal of research effort is the prediction of network transient stability, where detailed models of synchronous generators and their controls are required in order to carry out realistic studies of the transient response of the power network following a major disturbance. However, if the network is very large, excessive computational times may be incurred, denting the effectiveness of the simulation. This is particularly the case if comprehensive direct time phase-domain models

4. Further Consideration of the Direct Time Phase-Domain Multimachine Model

are used to represent both the synchronous generators and the transmission network, which, nowadays, may include several power electronics controllers.

In order to reduce the extra burden incurred by the use of the more realistic, though more time consuming, direct time phase-domain models, generator equivalents may be used to group together those generators that share similar operational attributes. Such an approach may be based on the observation of coherency between generators. If following a disturbance the variations of velocity and acceleration between generators remain fairly constant with respect to each other then the generators in the group are said to be coherent [79][81]. Upon identification of the coherent group of generators, they can be represented as one equivalent generator, hence, reducing the total number of non-linear differential equations required to represent the power system under study.

Over the years, a large volume of work has been published on different approaches to represent the group of coherent generators [79]–[88]. Most of the published work has focused mainly on network reduction techniques that would enable the connection of the equivalent generator to the common bus of the network but with the generator represented simply as a voltage source behind an equivalent reactance [79][87]. In such a representation the equivalent reactance is obtained as the parallel combination of the reactances of all the coherent generators. In [81], a more detailed model of the generators was used where frequency domain parameters for the equivalent model were obtained using transfer functions error adjustments. This is a time consuming and complex exercise and the analysis was restricted to cases of symmetrical operating conditions. More efficient models based on axis transformations were introduced in [82] and [83], however, such models are only suitable for the study of balanced operating conditions.

In this section, a novel equivalent model based on the aggregation of the coherent generators is put forward. This method ensures that the equivalent generator preserves the model of one of the generators in the group. In fact, the inductances of the chosen generator are suitably modified to incorporate the dynamic effects of the other generators in the group. The resulting model is solved, in discretised form, at each time step of the simulation with no need to resort to iterations. The solution method is quite a general one, in the sense that it can be applied to solve networks of any size in the direct time phase-domain. The model may be used to carry out symmetrical and asymmetrical analysis and it is well suited for real-time simulations. A test network is implemented in a real-time environment using an RTS system.

4.2.1. Aggregation of Coherent Generators

The equivalent generator of a coherent group of generating units is in essence a single generating unit that exhibits the same speed, voltage and total mechanical and electrical power as the group during a given perturbation period [79]. The aggregation technique is based on

4. Further Consideration of the Direct Time Phase-Domain Multimachine Model

these characteristics of the coherent group of generator.

Mechanical Dynamic

The swing equations representing the dynamic of a single generator is given by [4][25],

$$\begin{aligned} 2H \frac{d\omega}{dt} &= \omega_s (T_m - T_e) \\ &= P_m - P_e \end{aligned} \quad (4.1)$$

where H is the inertia constant, T_m and P_m are the mechanical torque and power, and, T_e and P_e are the electrical torque and power, respectively. If the rated speed, ω_s is 1 p.u., the torque and power will have equal values in per-unit. Using this key premise, the acceleration for the group of coherent generators is the same. Hence, summing up (4.1) for the group of n coherent generators,

$$\sum_{i=1 \dots n} 2H_i \frac{d\omega}{dt} = \sum_{i=1 \dots n} P_{m_i} - \sum_{i=1 \dots n} P_{e_i} \quad (4.2)$$

Equation (4.2) possesses the same structure as (4.1) and can be used to represent the mechanical dynamics of the equivalent generator if the following conditions hold,

$$H_g = \sum_{i=1 \dots n} H_i \quad P_{e_g} = \sum_{i=1 \dots n} P_{e_i} \quad P_{m_g} = \sum_{i=1 \dots n} P_{m_i} \quad (4.3)$$

where subscript g denotes the equivalent generator.

Coefficients of Stator Inductances

From the discretised equation (3.5) of the generator and making $[i_s(t)]$ the subject,

$$\begin{aligned} [i_s(t)] &= [R_{T_{ss}}(t)]^{-1} [e_s(t)] - [R_{T_{ss}}(t)]^{-1} ([R_{T_{sr}}(t)] [i_r(t)] - [v_{his_s}]) \\ &= [R_{T_{ss}}(t)]^{-1} [e_s(t)] - [E_q(t)] \end{aligned} \quad (4.4)$$

where

$$[E_q(t)] = [R_{T_{ss}}(t)]^{-1} ([R_{T_{sr}}(t)] [i_r(t)] - [v_{his_s}]) \quad (4.5)$$

Aiming at preserving the model structure of the equivalent generator the same as that of the individual generator, we assume that equation (4.4) holds for the equivalent generator. Summing of (4.4) for the group of coherent generators leads to the following equation,

$$\sum_{i=1 \dots n} [i_s(t)]_i = \sum_{i=1 \dots n} [R_{T_{ss}}(t)]_i^{-1} [e_s(t)]_i - \sum_{i=1 \dots n} [E_q(t)]_i \quad (4.6)$$

4. Further Consideration of the Direct Time Phase-Domain Multimachine Model

Since the power generated by the equivalent generator must be equal to the total power of the coherent group of generators and the stator voltages of all the units are equal, it can be concluded that the stator current of the equivalent generator must equal the total current of the coherent group. Hence from (4.6),

$$[i_s(t)]_g = \sum_{i=1\dots n} [R_{T_{ss}}(t)]_i^{-1} [e_s(t)]_g - \sum_{i=1\dots n} [E_q(t)]_i \quad (4.7)$$

It is assumed that the equivalent generator has the same structure as in (4.4), hence, by comparing coefficients with (4.7) leads to the following result,

$$[R_{T_{ss}}(t)]_g^{-1} = \sum_{i=1\dots n} [R_{T_{ss}}(t)]_i^{-1} \quad (4.8)$$

It should be remarked that the term $\sum_{i=1\dots n} [R_{T_{ss}}(t)]_i$ consist of the sum of the generator's inductances $[L(t)]$ and resistances $[R]$, respectively, which in turn are a function of time, t . Sufficient number of equations are generated from (4.8), for different values of t , in order to solve for the unknown coefficients in $[R_{T_{ss}}(t)]_g^{-1}$. By inverting the known values of $\sum_{i=1\dots n} [R_{T_{ss}}(t)]_i^{-1}$ and denoting the result as A , we have,

$$[R_{T_{ss}}(t)]_g = A \quad (4.9)$$

By expanding the first diagonal element of this matrix it is possible to obtain the coefficients of the equivalent generator's stator inductances [25][28],

$$-\frac{2}{\Delta t} L_{a0_g} - \frac{2}{\Delta t} L_{a2_g} \cos 2\theta_g - R_{s_g} = A(1, 1) \quad (4.10)$$

where $\theta_g = \omega_s t + \delta_g$ and the value of R_{s_g} is obtained by paralleling the stator resistance of the coherent group of generators [79][83]. Hence, from (4.10),

$$-\frac{2}{\Delta t} L_{a0_g} - \frac{2}{\Delta t} L_{a2_g} \cos 2\omega_s t \cos 2\delta_g + \frac{2}{\Delta t} L_{a2_g} \sin 2\omega_s t \sin 2\delta_g = A(1, 1) + R_{s_g} \quad (4.11)$$

There are three unknowns in (4.11), namely, L_{a0_g} , L_{a2_g} and δ_g , hence, the same number of equations can be generated for different values of t . With the value of L_{a2_g} known, the coefficient M_{s0_g} is found by equating the off-diagonal elements in (4.9),

$$M_{s0_g} = -L_{a2_g} \cos \left(2\theta_g - \frac{2\pi}{3} \right) - \frac{\Delta t}{2} A(1, 2) \quad (4.12)$$

The coefficients for the mutual inductances between the stator and rotor of the equivalent generator can be found by direct calculation using the general inductance equations of the generator [4][13][28]. Where the leakage inductance of the equivalent generator can be ob-

4. Further Consideration of the Direct Time Phase-Domain Multimachine Model

tained as,

$$L_{l_g} = L_{a0_g} - 2M_{s0_g} \quad (4.13)$$

Using the inductance equations from the transformed $d - q - 0$ axis, the mutual inductance between the stator and rotor windings can be obtained as [4][28],

$$\begin{aligned} L_{ad_g} &= L_{d_g} - L_{l_g} \\ &= L_{a0_g} + M_{s0_g} + \frac{3}{2}L_{a2_g} - L_{a0_g} + 2M_{s0_g} \\ &= 3M_{s0_g} + \frac{3}{2}L_{a2_g} \end{aligned} \quad (4.14)$$

The mutual inductance between the stator and rotor in the transformed variables is related to the phase-domain quantities in *p.u.* value as [4][13],

$$M_{af_g} = \frac{2}{3}L_{ad_g} \quad (4.15)$$

An assumption, which holds well in practice [28], is made,

$$M_{ad_g} = M_{af_g} \quad (4.16)$$

and using the ratio of saliency on the magnetizing inductance relations [28],

$$M_{aq_g} = \frac{L_{q_g}}{L_{d_g}}M_{ad_g} \quad (4.17)$$

From (4.13)-(4.17), the coefficients of the stator self-inductances and the mutual inductances between the stator and rotor are obtained for the equivalent generator.

Coefficients of Rotor Inductances

Performing a similar summation process as in (4.6)–(4.7) on the discretised equation given in (3.7) for the coherent generators, we obtain the following,

$$[R_{equ}(t)]_g^{-1} = \sum_{i=1 \dots n} [R_{equ}(t)]_i^{-1} \quad (4.18)$$

Similarly, the known value of $\sum_{i=1 \dots n} [R_{equ}(t)]_i^{-1}$ at any particular t can be inverted and denoted as B ,

$$[R_{equ}(t)]_g = B \quad (4.19)$$

Further expansion can be obtained by substituting (3.8) into (4.19),

$$[R_{T_{ss}}(t)]_g - [R_{T_{sr}}(t)]_g [R_{T_{rr}}(t)]_g^{-1} [R_{T_{rs}}(t)]_g = B \quad (4.20)$$

4. Further Consideration of the Direct Time Phase-Domain Multimachine Model

With the previously obtained coefficients for the stator and mutual inductances, between the stator and rotor, the following parameters of $[R_{T_{ss}}(t)]_g$, $[R_{T_{sr}}(t)]_g$ and $[R_{T_{rs}}(t)]_g$ are known at any particular t . Hence, by mathematical manipulation we can obtain the resultant value of $[R_{T_{rr}}(t)]_g$ with the help of the rotor inductance equations.

With the values of the stator self and mutual inductances already determined, the coefficients of the rotor self-inductances can then be obtained where it is assumed that the mutual inductance between the field and d – axis rotor windings is ,

$$M_{fkd} = M_{af} \quad (4.21)$$

The remaining elements of $[R_{T_{rr}}(t)]_g$ in (4.20) can be similarly obtained paying due consideration to the ratio of saliency, which also applies to the rotor self-inductances,

$$L_{kqg} = \frac{L_{qg}}{L_{dg}} L_{kdg} \quad (4.22)$$

Information on these constant coefficients for the rotor, which already include the rotor winding resistances, is sufficient to solve the equivalent generator model while preserving the model structure.

4.2.2. Results of Stability Analysis

The key step to obtain the dynamic equivalent is to carry out the network reduction of the coherent generators' busbars with reference to an equivalent busbar. Network reduction techniques are well established, and the technique employed in this paper is based on [82] where the approach is given in Appendix C. Even though the network reduction is carried out during steady state, the result obtained for the network impedances are equal to the actual resistances and inductances in the direct time phase-domain if the rated speed is taken as 1 p.u. .

	<i>Gen 1 (Slack)</i>	<i>Gen 2</i>	<i>Gen 3</i>	<i>Gen 4</i>	<i>Gen 5</i>
V (p.u.)	1	0.9880	0.9985	0.9950	0.9950
θ (degree)	0	-2.7173	-4.4455	-3.7630	-3.7737
Load angle, δ (rad)	-	0.566	0.441	0.166	0.280

Table 4.1.: steady state values of generators' variables in Figure 4.1

The thrust of this approach is the aggregation of the coherent generators on the common busbar. The proposed aggregation method is tested in a non-real time environment, using a power network consisting of five generators and nine nodes, as shown in the one-line diagram in Figure 4.1. *Gen 1* is the slack bus, assumed to be connected to an infinite source. The data for *Gen 2*, *3* and *4* are as given in Appendix A.3 and *Gen 5* in Appendix C.2. The controllers for the generators are omitted in the analysis of this section.

4. Further Consideration of the Direct Time Phase-Domain Multimachine Model

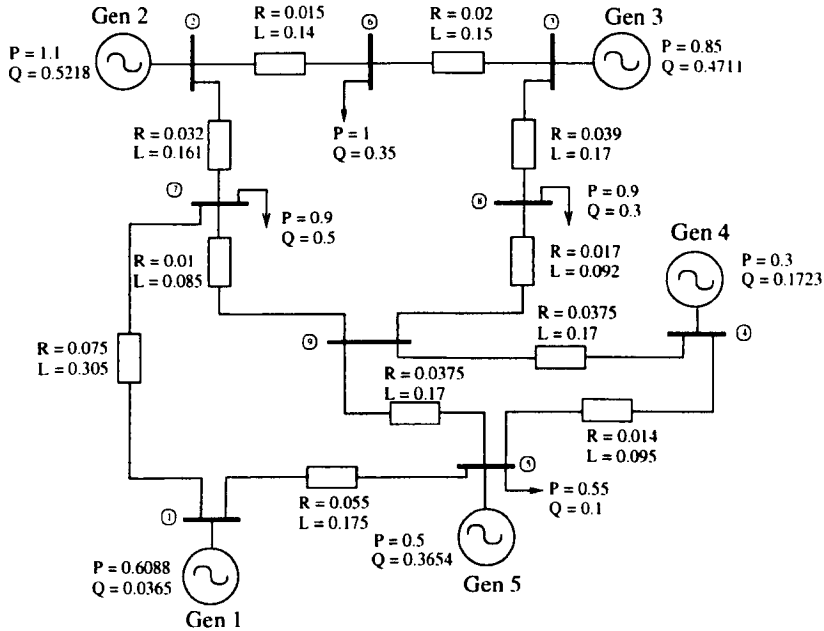


Figure 4.1.: Test network

A three-phase-to-ground fault is applied at *Node 7* of the network. The load angle responses of the generators are presented in Figure 4.2. It is clear that *Gen 2* and *3* have a larger load angle swing due to their closer location to the point in fault and loading condition. By observation of the curves in this result, it is clear that a level of coherency occurs between *Gen 4* and *5*. This suggests that *Gen 4* and *5* may be represented by an equivalent generator as their load angles swings are also less significant. The accuracy of the proposed aggregating approach is justified by looking at the load angle swing curve of *Gen 2*, which is nearest to the point in fault. One of the results correspond to the detailed generator models and the other to the equivalent model combining *Gen 4* and *5*, as shown in Figure 4.3. Similarly, accurate results are observed in Figure 4.4 for *Gen 3*. Figure 4.5 shows the load angle of *Gen 4* and *5* as compared to their equivalent.

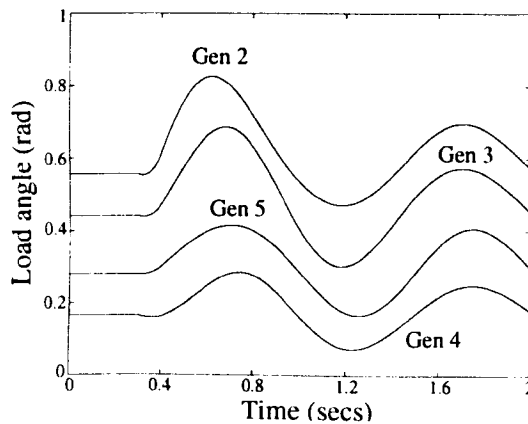


Figure 4.2.: Load angle of generators using detailed model during a three-phase-to-ground fault at *Node 7*

4. Further Consideration of the Direct Time Phase-Domain Multimachine Model

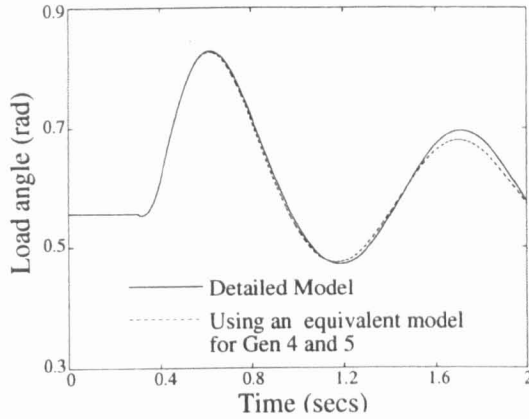


Figure 4.3.: Load angle of *Gen 2* using an equivalent model for *Gen 4* and *5* during a three-phase-to-ground fault at *Node 7*

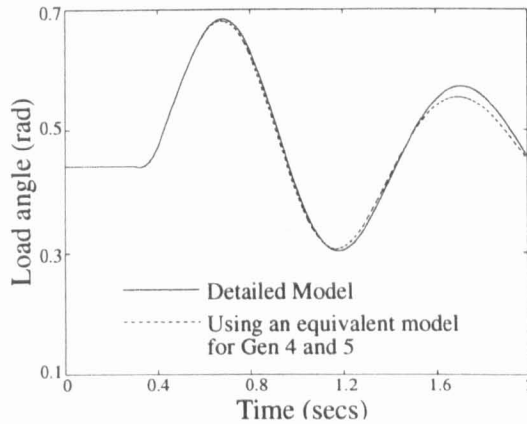


Figure 4.4.: Load angle of *Gen 3* using an equivalent model for *Gen 4* and *5* during a three-phase-to-ground fault at *Node 7*

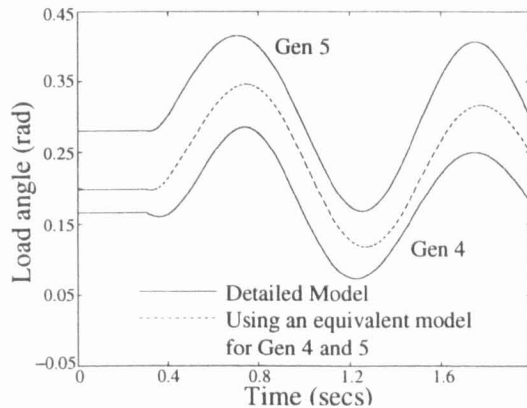


Figure 4.5.: Load angle of equivalent generator representing *Gen 4*, *5* and *6* during a three-phase-to-ground fault at *Node 7*

One significant advantage of direct time phase-domain modelling is the ability to simulate asymmetrical operating conditions. This is important as asymmetrical faults contribute the largest percentage of transient stability problems. In order to demonstrate the versatility of the model, a single-phase-to-ground fault is applied at *Node 7* of the network. It is observed

4. Further Consideration of the Direct Time Phase-Domain Multimachine Model

from Figure 4.6, that the load angle of *Gen 2*, undergoing an asymmetrical fault, compares quite well when represented in detail and when using the equivalent model of *Gen 4* and *5*. This is further highlighted by the response of its field current as shown in Figure 4.7.

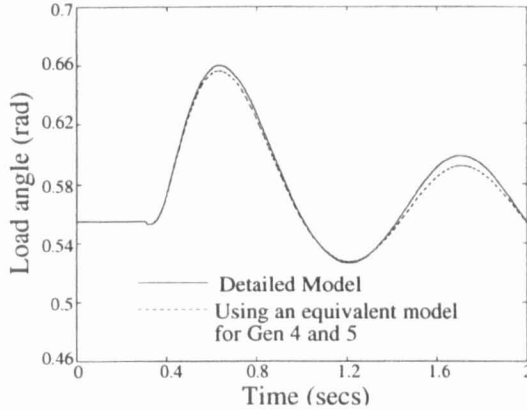


Figure 4.6.: Load angle of *Gen 2* using an equivalent model for *Gen 4* and *5* during a single-phase-to-ground fault at *Node 7*

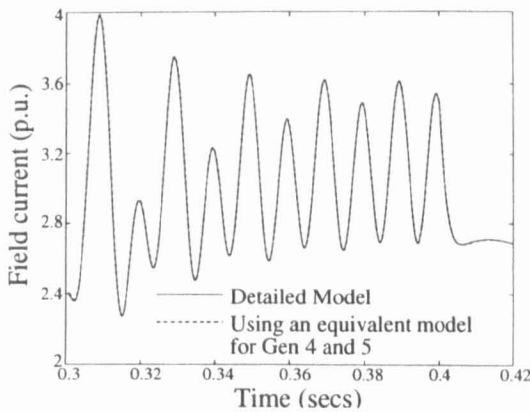


Figure 4.7.: Field current of *Gen 2* using an equivalent model for *Gen 4* and *5* during a single-phase-to-ground fault at *Node 7*

Three generators equivalent

The proposed aggregation method is further tested for limitations by increasing the number of coherent generators in the network. A sixth generator, *Gen 6*, is connected via a cable to *Node 8* of the network in Figure 4.1. The new generator is situated further away from the two already coherent generators in order to create a situation where the coherent generators are not clustered in a close parallel connection. The similar three-phase-to-ground fault is applied to *Node 7* in the network where the load angle responses of the generators are shown in Figure 4.8. It is observed that the load angle swing of *Gen 2* and *3* are still larger than the rest of the generators while coherency does exist between *Gen 4*, *5* and *6*.

4. Further Consideration of the Direct Time Phase-Domain Multimachine Model

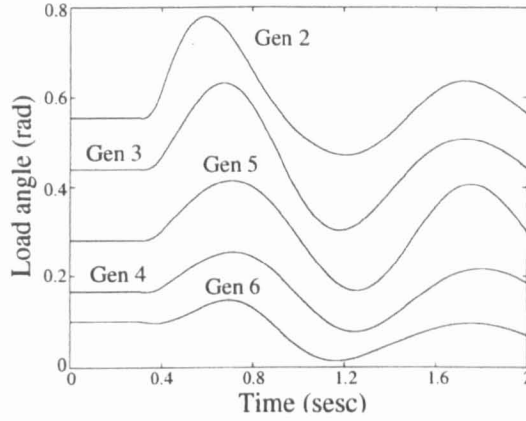


Figure 4.8.: Load angles of generators detailed models during a three-phase-to-ground fault at *Node 7* with additional generators

From Figure 4.9, it is observed that the use of the equivalent model for the coherent units provide a good first swing accuracy for the load angle of *Gen 2* which is the most critically affected unit in the network. However, slight discrepancy occurs when the load angle approaches the second swing. Similar observations are made from the load angle of *Gen 3* as shown in Figure 4.10. The equivalent technique is developed based on the notion that the coherent units have a similar terminal voltage, which is the case between *Gen 4*, *5* and *6* prior to the occurrence of fault. However, due to the distance of *Gen 6* from the other coherent units in the full network, the voltage might have taken different value when approaching steady state after the fault is cleared. In the reduced network simulation using the equivalent model technique, the voltage is considered to be the same throughout the process. This could be the reason for the slight discrepancy that occurs. The effect on the overall analysis is not significant as the discrepancy is small and the importance in stability analysis lies in the first swing of the load angle. Which in this case compares well between the full and the equivalent model. Figure 4.11 shows the load angle of *Gen 4*, *5* and *6* as compared to their equivalent.

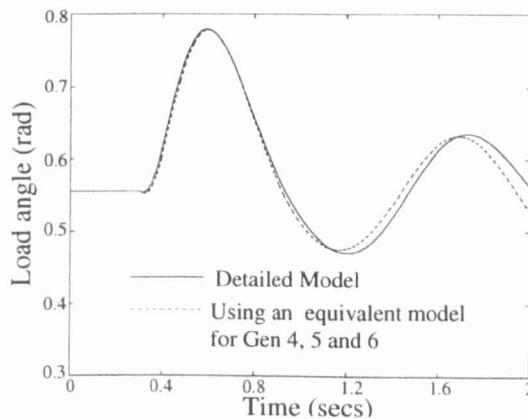


Figure 4.9.: Load angle of *Gen 2* using an equivalent model for *Gen 4*, *5* and *6* during a three-phase-to-ground fault at *Node 7*

4. Further Consideration of the Direct Time Phase-Domain Multimachine Model

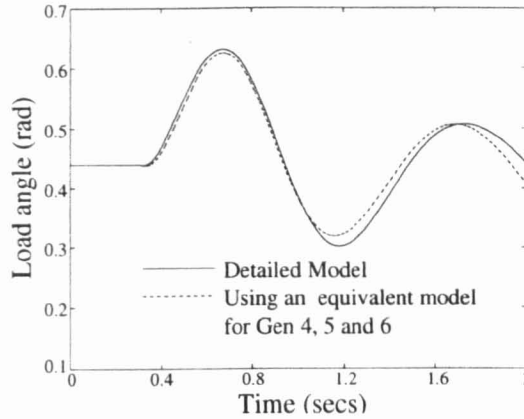


Figure 4.10.: Load angle of *Gen 3* using an equivalent model for *Gen 4, 5* and *6* during a three-phase-to-ground fault at *Node 7*

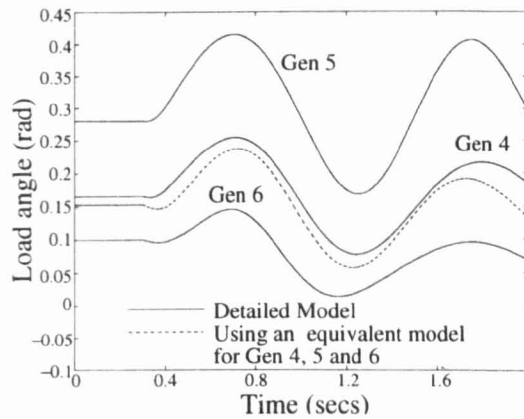


Figure 4.11.: Load angle of equivalent generator representing *Gen 4, 5* and *6* during a three-phase-to-ground fault at *Node 7*

Test on 39 Nodes System

The detailed equivalent model is further tested on a simple 39 nodes and 9 generators system based on the New England test network configuration shown by the Figure 4.12. The data regarding the network can be readily obtained from reference [85] and [88]. A three-phase-to-ground fault is simulated at *Node 31*. The coherent group of generators is determined by observing their load angle swing. The method for network reduction is similar to that already discussed and presented in Appendix C. The load angle responses of the generators are shown in Figure 4.13 and 4.14 where it is observed that *Gen 2* and *3* are more critically affected by the fault. While the swing of *Gen 1* load angle is not significant due to its close location to the strong slack bus. The remaining generator *Gen 4, 5, 6, 7, 8* and *9* are observed to swing in coherent with each other.

An equivalent unit replaces the coherent generators using the process described in previous section. It is observed that the first swing of the load angle between the detailed and the equivalent representation are comparable. However, greater discrepancies can be observed

4. Further Consideration of the Direct Time Phase-Domain Multimachine Model

from subsequent behaviour of the load angle especially in *Gen 2*. This could be explained as described previously where changes in voltage after the post-fault period would have affected the accuracy of using the equivalent representation.

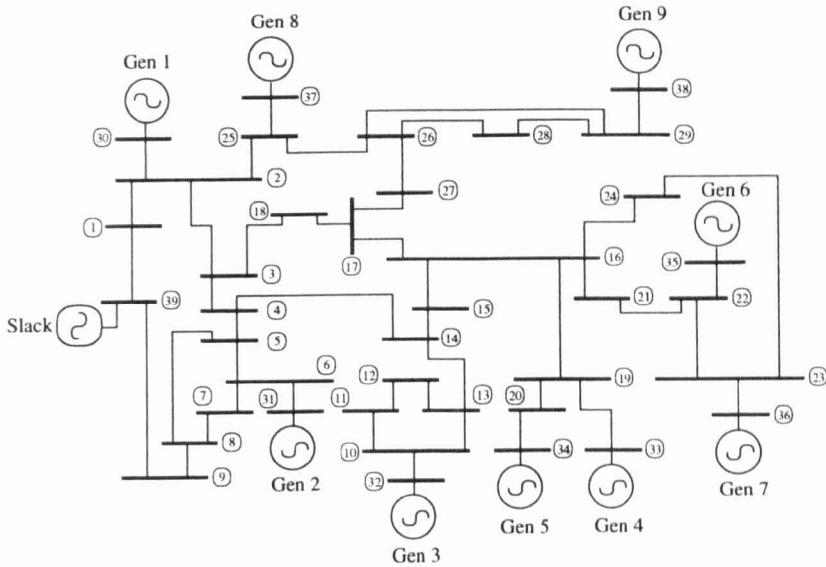


Figure 4.12.: 39 nodes and 9 generators test network

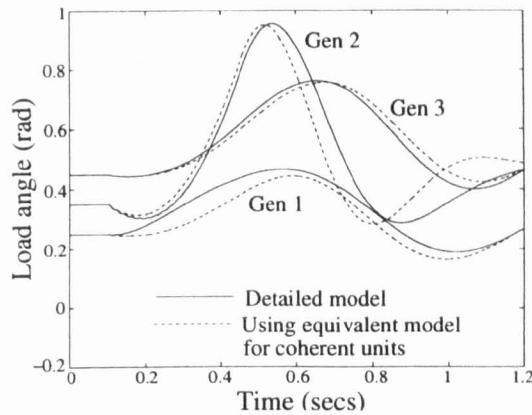


Figure 4.13.: Load angle of *Gen 1, 2 and 3* using an equivalent model for the coherent units during a three-phase-to-ground fault at *Node 31*

4.2.3. Real-Time Simulation

The main parameter that needs monitoring when performing real-time simulations is the AFT of the RTS [69]. The AFT shows the time required by the RTS to compute each time step of the simulation. The AFT must not exceed the desired time step of the simulation at any point in order to fulfil the objective of a real-time simulation.

It is observed in Figure 4.15, that the AFT for the detailed representation of the network, in Figure 4.1, is $710\mu\text{s}$ and the AFT reduces to $475\mu\text{s}$ if the equivalent model is used for *Gen*

4. Further Consideration of the Direct Time Phase-Domain Multimachine Model

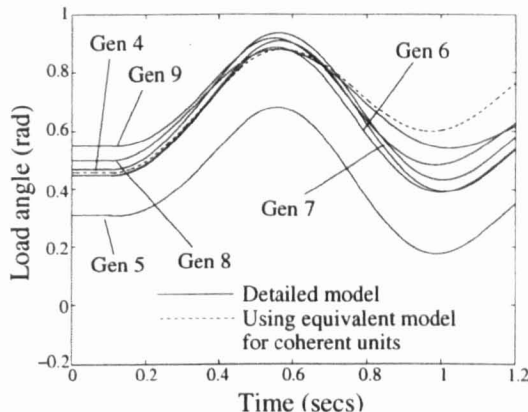


Figure 4.14.: Load angle of the group of coherent generators with the equivalent during a three-phase-to-ground fault at *Node 31*

4 and 5. For the detailed network representation to be simulated in real-time, a large time step of $710\mu s$ or above will be required. However, the use of a large time step can upset the accuracy of the simulation. It is thus important to ensure that accuracy is observed while making sure that the time step used is capable of achieving real-time simulation.

A significantly smaller time step, say $475\mu s$, can be used for the network using the equivalent model to achieve a similar real-time simulation. It has been reported elsewhere [33], that the use of the trapezoidal rule is well suited to solve power network with good accuracy using time step of up to $500\mu s$. Hence, the equivalent model allows a suitable time step to be used which complies with real-time simulation requirements.

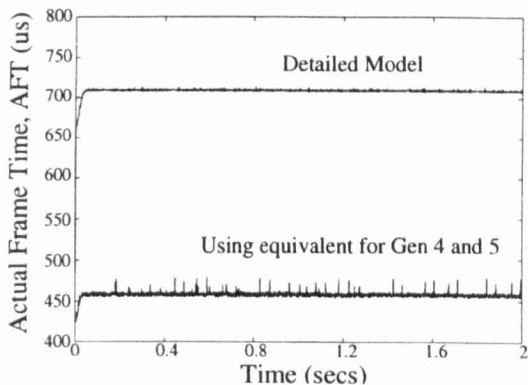


Figure 4.15.: AFT of the real-time simulations

4.3. Implementation of Dynamic Load into Power System Network

A realistic assessment of power system operation depends largely on the accurate prediction of power flow between the generating units and the electrical loads in the system. This makes

4. Further Consideration of the Direct Time Phase-Domain Multimachine Model

the modelling of electrical loads an important aspect of power system analysis especially for stability and power quality studies. There are various ways to represent a load, with the simplest being the bulk representation of electricity demand at a specific delivery bus. Under this circumstance, a constant quantity model such as power, current or impedance is normally used to represent the electrical load. The constant impedance representation is used throughout this thesis to model bulk demand points.

The bulk representation is particularly appropriate for loads that have low electrical time constants and enable the steady state to be achieved at a faster rate by disregarding the dynamic effects of the load [4]. However, it is appreciated that not all loads are free of dynamic components. For instance, in the study of electrical systems involving rotating motors it is necessary to represent the dynamics of the motors in good detail. In a typical power system, motors consumed up to two third of the total energy generated.

Asynchronous or induction motors in particular form the majority of rotating loads. The popularity of the induction motor, termed as the workhorse of industries, can be attributed to its versatility and economical factors. Hence, the inclusion of motor modelling in the analysis of a multimachine network stability is of great importance.

For the induction motor to be solved together with the discretised generator model in the multimachine environment, it is essential to represent the motor in the same discretised fashion as the generators. The general dynamic model of an induction machine has been presented in Chapter 2. In this section the state equations of the motor model are discretised using the trapezoidal rules along the same lines as for the synchronous generator model. It should be remarked that the term induction machine is used here because the discretised model is applicable to both motoring and generating modes of the machine.

4.3.1. Discrete Model of Induction Machine

The discretised expression of the machine's terminal voltage, equation (2.47), is obtained below, where subscript m stands for induction machine,

$$\begin{aligned} [e_m(t)] &= \frac{2}{\Delta t} [L_m(t)] [i_m(t)] + [R_m] [i_m(t)] - [v_{m_{his}}] \\ &= \frac{2}{\Delta t} \left([L_m(t)] + \frac{\Delta t}{2} [R_m] \right) [i_m(t)] - [v_{m_{his}}] \\ &= [R_{mT}] [i_m(t)] - [v_{m_{his}}] \end{aligned} \quad (4.23)$$

where

$$[v_{m_{his}}] = [e_m(t - \Delta t)] + \frac{2}{\Delta t} \left([L_m(t - \Delta t)] - \frac{\Delta t}{2} [R_m] \right) [i_m(t - \Delta t)] \quad (4.24)$$

and

$$[R_{mT}(t)] = \frac{2}{\Delta t} \left([L_m(t)] + \frac{\Delta t}{2} [R_m] \right) \quad (4.25)$$

4. Further Consideration of the Direct Time Phase-Domain Multimachine Model

Separating the stator and rotor quantities in (4.23) results in the following,

$$\begin{bmatrix} [e_{ms}(t)] \\ [e_{mr}(t)] \end{bmatrix} = \begin{bmatrix} [R_{mT_{ss}}(t)] & [R_{mT_{sr}}(t)] \\ [R_{mT_{rs}}(t)] & [R_{mT_{rr}}(t)] \end{bmatrix} \begin{bmatrix} [i_{ms}(t)] \\ [i_{mr}(t)] \end{bmatrix} - \begin{bmatrix} [v_{m_{his_s}}] \\ [v_{m_{his_r}}] \end{bmatrix} \quad (4.26)$$

Expansion of (4.26) gives,

$$[e_{ms}(t)] = [R_{mT_{ss}}(t)][i_{ms}(t)] + [R_{mT_{sr}}(t)][i_{mr}(t)] - [v_{m_{his_s}}] \quad (4.27)$$

$$[e_{mr}(t)] = [R_{mT_{rs}}(t)][i_{ms}(t)] + [R_{mT_{rr}}(t)][i_{mr}(t)] - [v_{m_{his_r}}] \quad (4.28)$$

By representing the stator quantities in terms of the rotor quantities, the following expression is obtained

$$[e_{ms}(t)] = [R_{mequ}(t)][i_{ms}(t)] + [E_{ms}(t)] \quad (4.29)$$

where

$$[R_{mequ}(t)] = [R_{mT_{ss}}(t)] - [R_{mT_{sr}}(t)][R_{mT_{rr}}(t)]^{-1}[R_{mT_{rs}}(t)] \quad (4.30)$$

and

$$[E_{ms}(t)] = [R_{mT_{sr}}(t)][R_{mT_{rr}}(t)]^{-1}([e_{mr}(t)] - [v_{m_{his_r}}] - [v_{m_{his_s}}]) \quad (4.31)$$

Notice that the discretised model of the induction machine is quite similar to that of the synchronous generator except in (4.23)–(4.25) where there is a change of sign in the matrix of the resistances. With such a representation, the induction machine is readily interfaced to the mutlimachine network just like a generator but with the direction of power flow reversed to take account for the change in sign. The procedure for the solution of the induction machine in the network is described in Chapter 3.

The discretised mechanical equations for the machine are also obtained in a similar fashion as for the synchronous generator,

$$\theta(t) = \frac{\Delta t}{2}\omega_r(t) + \frac{\Delta t}{2}\left(\omega_r(t - \Delta t) + \frac{2}{\Delta t}\theta(t - \Delta t)\right) \quad (4.32)$$

$$\omega_r(t) = \frac{\omega_s \Delta t}{4H}(T_e(t)) + \frac{\omega_s \Delta t}{4H}(T_e(t - \Delta t) - 2T_m) + \omega_r(t - \Delta t) \quad (4.33)$$

4.4. Analysis of Motor Dynamics in Power System Networks

Large induction motors has long been recognised as a burden to the transmission and distribution system, where some of the well identified problems are voltage sags, high inrush currents and slow voltage recovery of network after disturbances. A major contribution to these problems lies with the operational characteristics of induction motors. The induction motor requires a sustainable rotating magnetic field to be induced on its stator [13]. The rotating magnetic field is created by reactive power supplied from the network or from a compensator. When a sudden switching event occurs, the motor requires a large amount of reactive power in order to re-establish the rotating magnetic field, which can result in a sudden deficit of reactive power in the network. This can have a serious effect throughout the network with voltage magnitude dropping to unacceptable low levels in parts of the network if there is insufficient reactive power [91].

In the past, the adverse effects caused by the induction motor on power system network were studied under the umbrella of either transient stability studies or power quality studies. But in essence, both of these problems are caused by the same source, which is the operational characteristic of the motor. Several models have been developed over the years to study transient [89][90] and power quality [93][94] issues separately. However, the generality of the motor and network in the direct time phase-domain enables both studies to be performed easily at the same time.

Numerous case studies could be made to illustrate the effect of induction motor undergoing different fault conditions in a multimachine network. However, only studies relating to motor start-up, and the effect of the motor operations on symmetrical and asymmetrical short circuit faults in the network will be considered in this chapter.

4.4.1. Induction Motor Run-up Characteristic

Motor start-up is a classical example of a phenomenon where the induction motor could cause power system stability or power quality problems. The requirement for high reactive power at start-up very often leads to voltage sags in the network. The installation of a reasonably sized induction motors often include a capacitor banks to supply part of the required reactive power to limit the effect of voltage sags in the network during start-up. There are various switching methods that can be used for induction motor start-up to reduce this effect, but with the increasing number and rating of motor installations in the power network it is not uncommon to start the motor directly connected to the network.

In order to establish confidence in the multimachine model, including the induction motor as load, a contrived study is carried out and the results compared with those given by a more

4. Further Consideration of the Direct Time Phase-Domain Multimachine Model

conventional approach using PSCAD/EMTDCTM. Since direct motor start-up is a balanced condition it is valid to use the conventional $d - q - 0$ axis model as a basis for comparison.

The test network resembles a simple distribution network where a synchronous generator is connected to a feeder bus via a cable as in Figure 4.16. The static load and the induction motor are connected to the feeder bus. The capacitor bank is rated at $0.5 p.u.$. The generator excitation is controlled by the AVR, described in Chapter 3, and the generator speed is assumed constant for ease of comparison with PSCAD/EMTDCTM. The schematic diagram used in PSCAD/EMTDCTM is given in Appendix A.3.

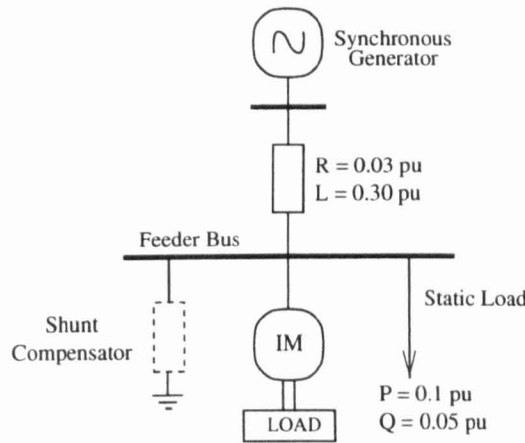


Figure 4.16.: Test network with dynamic load

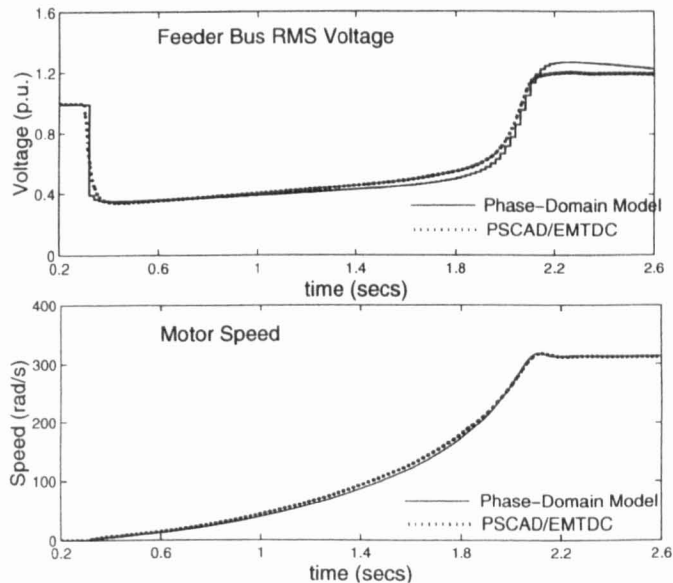


Figure 4.17.: Feeder bus voltage and motor speed in event of direct online motor starting in the test network

The motor is started by direct online connection at a time of $t = 0.3 s$. The feeder bus voltage and the motor speed are as shown in Figure 4.17a and b. The results generated using the direct time phase-domain method and PSCAD/EMTDCTM are in good agreement.

4. Further Consideration of the Direct Time Phase-Domain Multimachine Model

A further study is carried out using a larger interconnected network in order to study the behaviour of those generators located near the motor. The network in Figure 4.1 is used in modified form with the induction motor and capacitor bank connected at *Node 8*. The new modified network is depicted in Figure 4.18. The generators in the network are with AVRs and the turbine-governor controls with the structure and parameters given in Chapter 3. A fixed capacitor of $0.5 p.u.$ is connected at *Node 8* as a source of reactive power compensation for the motor.

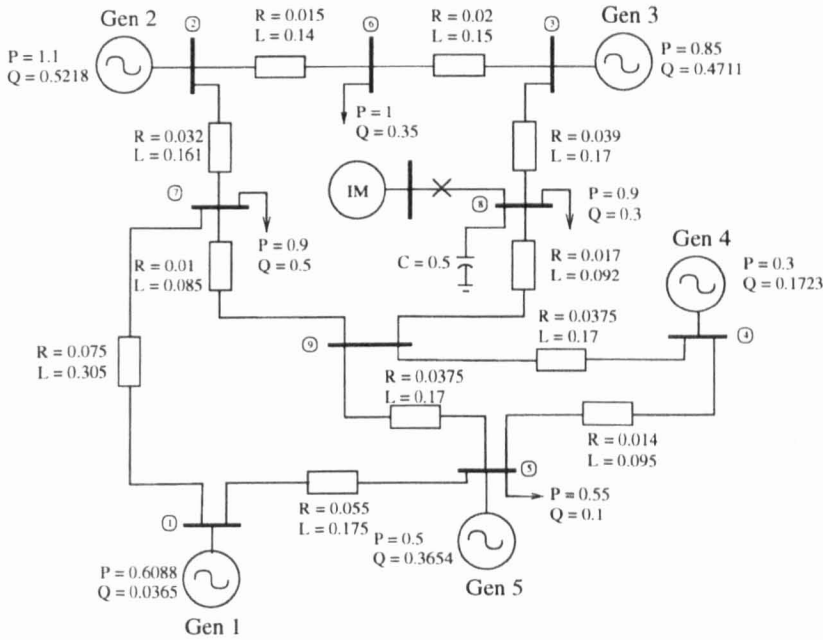


Figure 4.18.: Test network in Figure 4.1 with dynamic load connected at *Node 8*

The unloaded induction motor is directly connected to the feeder bus of *Node 8* at a time of $t = 0.3s$. The motor speed and electrical torque are shown in Figure 4.19a and b, where it is observed that the motor start-up time takes place at a faster rate than in the previous example. This is due to the stronger network used in this example where the combined reactive resources of the various generators are better able to make up for the deficit of reactive power due to motor start-up. This is also reflected in the bus voltage at *Node 8* shown in Figure 4.20a, where the magnitude and duration of voltage sag is not as pronounced as in the case of one generator in the previous example. Nevertheless, voltage sags of even 30% may have a significant detrimental effect on neighbouring power-electronics based loads.

There is an instantaneous rise in the motor stator current, as depicted in Figure 4.20b once the motor is switched on to supply. This is followed by a series of oscillations that may be due to the oscillatory torque resulting from increasing speed. The magnitude of the inrush current is high, as it needs to provide the reactive power needed to sustain the magnetic linkage as well as to meet the high starting torque of the motor.

This point is appreciated in Figure 4.21a and b, where both the active and reactive power

4. Further Consideration of the Direct Time Phase-Domain Multimachine Model

needed by the motor increases sharply upon start-up. The high active power needed is supplied by the various generating units in the network via the connecting lines. It is observed that the active power demanded by the motor is slightly higher than the actual electrical torque. This is especially the case when the magnitude of the current is high resulting in higher motor stator losses which is shown in Figure 4.22b. As the torque and current reaches their respective steady value, the active power reduces to a small value where the only demand is from the insignificant amount of losses in the unloaded motor. The power factor change of the motor current and voltage in Figure 4.22a further indicates this point. Initially the power factor is in the region of active and reactive power supply, but as steady state is achieved it settles to a value at around 1.571 rad or 90° . This indicates that only a small amount of active power flow exist between the busbar and the motor, hence the steady state current are mainly supplying the reactive power needed for continuous magnetisation of the motor.

The reactive power needed during the start-up is a few times higher (about 5 to 7 times) than the rated value. It is observed that the required amount is supplied by both the capacitor bank as well as the generating units through the connecting lines. This is the reason why deficit of reactive power occurs around the network resulting in voltage sags. The reactive power supplied by the capacitor bank is low during the most critical period at low voltage level, which occurs in the beginning. The ability of the capacitor, which depends on the voltage level is a major disadvantage in term of voltage sags mitigation. This is further highlighted in Figure 4.23, where after the motor has started up, an increase in load is simulated. It is observed that the reactive power needed by the motor increases at higher loading condition. As a result the voltage level at its terminal drops and the capacitor bank is not be able to provide the rated output. The slow response and dependency on the voltage level of the capacitor bank make it ineffective in helping to overcome voltage sags. A higher rating capacitor bank can be use to improve the response during the start-up process, but it is normally not preferred as overvoltages will be experienced at steady state. This can be suppressed to a certain extend by a switchable capacitor bank where the amount of reactive power supply can be increase or decrease depending on the demand. However, the switching which is normally perform mechanically is slow thereby making the capacitor bank ineffective in serious sags conditions.

The responses of *Gen 3* and *4*, which are electrically close to the induction motor busbar, are presented in Figure 4.24 and 4.25. The generators' responds to the increase in active power demand, due to motor starting torque, by increasing their respective output shown in 4.24a. The increase in electrical torques inevitably causes a decrease in the speed of the generators as shown in Figure 4.24b. The turbine governor control regulates the change in the generators' speed by closely meeting the need of the electrical torque by increasing the mechanical torque. The less drastic response of *Gen 4* compared to *Gen 3*, is due to its closer electrical position to the infinite bus which helps to regulate its response. The generators'

4. Further Consideration of the Direct Time Phase-Domain Multimachine Model

mechanical dynamic will eventually settle to the pre-motor starting conditions.

As a result of the deficit in the reactive power, the voltage magnitude at the terminal of the generators will also be reduced prompting the AVR to respond by increasing the excitation level of the generators in order to sustain the voltage at motor pre-starting level. This is done by increasing the DC voltage across the field winding, thus increasing the field current in the process. The action of the generators' AVR control is evident from the response of the field current in Figure 4.25b where the higher field current indicates an increase in the excitation level. The generators' voltage and field responses will be assumed a new steady state condition when the motor start-up is complete.

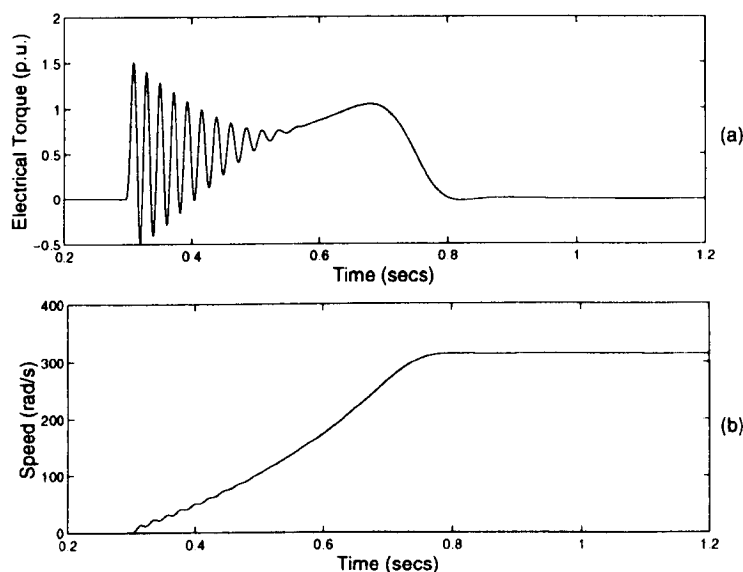


Figure 4.19.: Motor speed and electrical torque following direct online start-up

4.4.2. Influence of Motor Behaviour on Voltage Sags when Subjected to Network Disturbances

Voltage sags due to today's network disturbances are recognised as an important power quality problem faced by the industries. It has already been pointed out that induction motors have a big part in the occurrence of voltage sags when they are started by direct online connection. This is due to the high reactive power required to provide magnetic linkage in order to accelerate the stand-still motor to its rated speed. However, the acceleration of the motor is not only required during start-up but also on other occasions when the continuity of the motor is disrupted. It is known that the operation of a motor after a disturbance can have an undesired effect in terms of duration and shape of the voltage sags [93][95][96]. In an event of network disturbances, the voltage in the terminal of the motor can suffer voltage sags, which reduce the electrical torque. As a result, the speed of the motor starts to decrease. Depending on the initial speed loss and the magnitude of the voltage sags, the motor will re-accelerate to

4. Further Consideration of the Direct Time Phase-Domain Multimachine Model

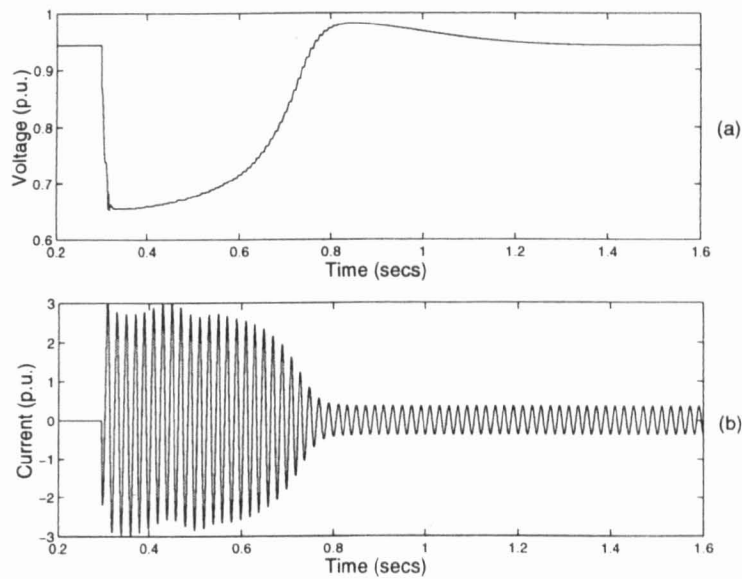


Figure 4.20.: Busbar voltage magnitude and motor inrush current following direct on-line start-up

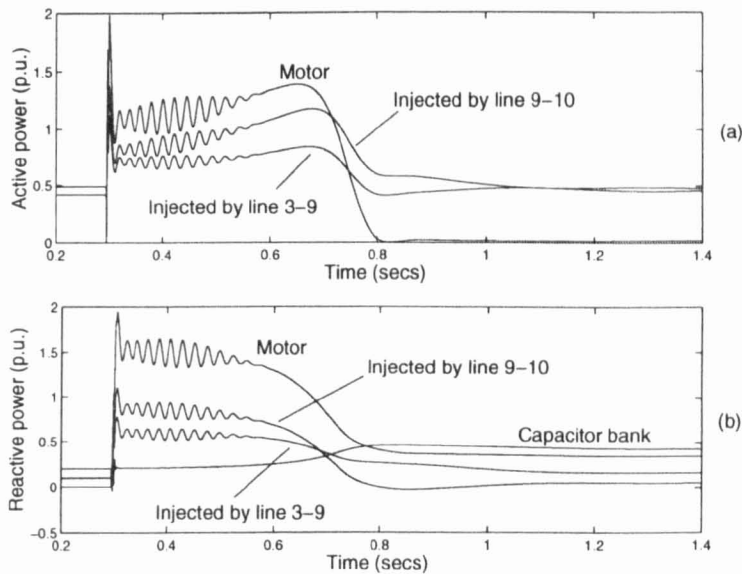


Figure 4.21.: Active and reactive power of motor following direct on-line start-up

recover its initial operating condition after the fault is removed. The re-acceleration of the motor again requires considerable amount of reactive power and in its course slows down the voltage recovery period at its terminal and throughout the network.

There are many attributes that govern the prolonged sag periods associated with the effect of motor re-acceleration. The types of fault, motor loading conditions and location of fault are some of the key factors. It is necessary to study the effect of such attributes when determining the options for compensation and protection in the network. The following results are directed towards developing an understanding of such attributes with respect to voltage sags problems.

4. Further Consideration of the Direct Time Phase-Domain Multimachine Model

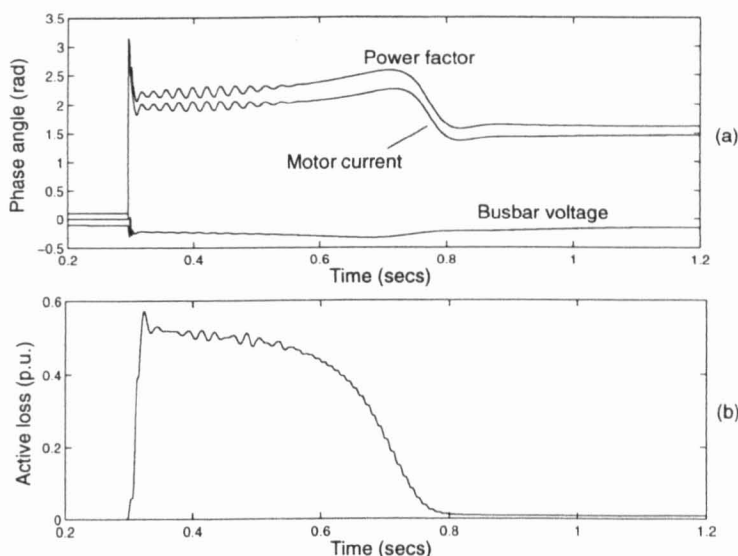


Figure 4.22.: Phase angle and initial stator loss due to high inrush current following motor direct on-line start-up

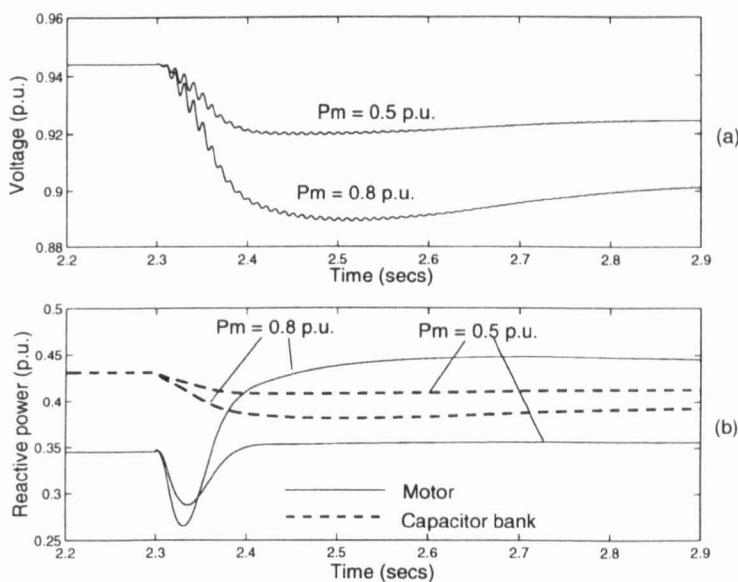


Figure 4.23.: Voltage and reactive power at different loading conditions

The similar study network, where the induction motor is connected to *Node 8* of Figure 4.1, is used to perform the studies. The faults are applied at time $t = 0.3s$ and cleared after $200ms$. The motor is operating at its steady state condition prior to the application of any faults.

a) Balanced Three-phase-to-ground fault

A three-phase-to-ground fault is applied to *Node 9*, which is close to the terminal of the motor. Figure 4.26 shows the voltage level at the *Node 8* where different network and loading conditions are considered. Neglecting the effect of the induction motor, the voltage magnitude drops to a level close to $0.2 p.u.$ upon fault, and recovering acutely to 90% of the pre-fault

4. Further Consideration of the Direct Time Phase-Domain Multimachine Model

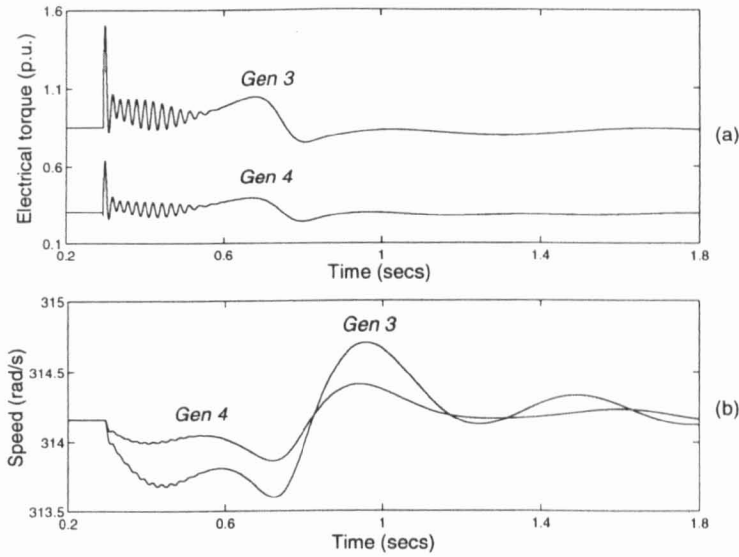


Figure 4.24.: Speed and electrical torque of *Gen 3* and *4* in event of direct online motor starting

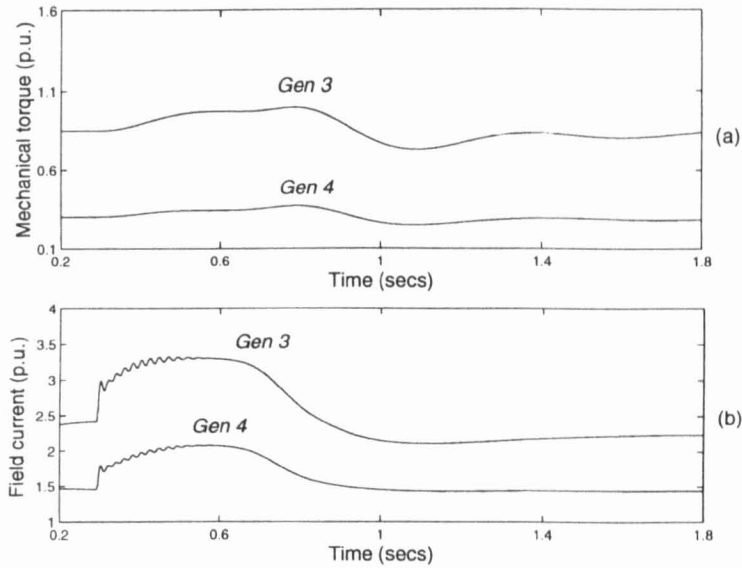


Figure 4.25.: Mechanical torque and field current of *Gen 3* and *4* in event of direct online motor starting

level after clearance. Due to the presence of the induction motor, the voltage briefly maintains a higher level immediately after the occurrence of fault. This voltage magnitude continues to decrease throughout the period of fault especially when a loaded motor is connected to the bus. The more important observation is that the presence of the motor delays the recovery of the voltage to its pre-fault level upon clearance of fault. Depending on the loading of the motor, these prolonged sags can be significant.

The reason for the slower duration of voltage recovery is due to the re-acceleration of the motor after the fault is cleared. In steady state conditions, the motor electrical torque is

4. Further Consideration of the Direct Time Phase-Domain Multimachine Model

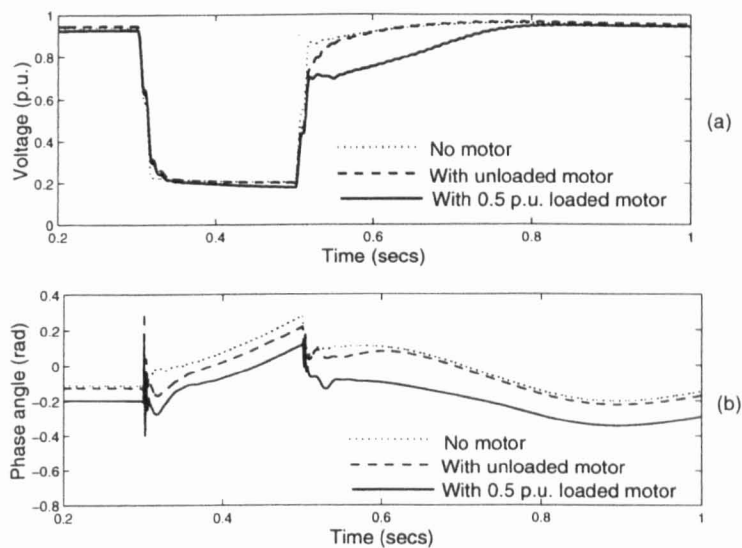


Figure 4.26.: Bus voltage and phase angle of *Node 8* subjected to a three-phase-to-ground fault

related to the square of the motor's terminal voltage. If voltage sags occur, the torque will be reduced resulting in decreasing speed of the motor. Depending on the initial speed loss and the magnitude of the recovery voltage after fault clearance, the motor will re-accelerate, taking reactive current that it needs from the network to achieve its steady state speed. For the unloaded motor in Figure 4.27, it is observed that the decrement in motor speed is small owing to the fact that the motor is running at low torque. Under unloaded condition the electrical torque of the motor is very close to zero except for the low amount of power needed for the losses, hence, the reduction in motor torque is not so severe as a result of the fault.

In the case of a loaded motor in Figure 4.28, the reduction in electrical torque will be of significant amount compared to the pre-fault condition. As a result, the motor suffers a rapid deceleration to a much lower level than the unloaded motor. This leads to a longer time period required by the loaded motor to re-accelerate in order to achieve the pre-fault speed upon clearance. The location of the fault from the motor also affects the changes in the motor torque and speed. During the period of motor re-acceleration, the reactive power required by the motor increases sharply in order to sustain a sizeable amount of magnetic field as shown in Figure 4.29. The demand for power reduces to pre-fault level when the motor is fully re-accelerated.

b) Asymmetrical single-phase-to-ground fault

Phase *a* on *Node 9* is faulted in the network to simulate the case of a single-phase-to-ground fault. The voltage response of the common busbar is presented in Figure 4.30 when no motor is connected in the network. It is observed that the voltage sags in the busbar is only concentrated on the faulted phase. The fault has relatively little effect on the two healthy phases, as it is still connected to the network. When the presence of the motor is considered, it is observed

4. Further Consideration of the Direct Time Phase-Domain Multimachine Model

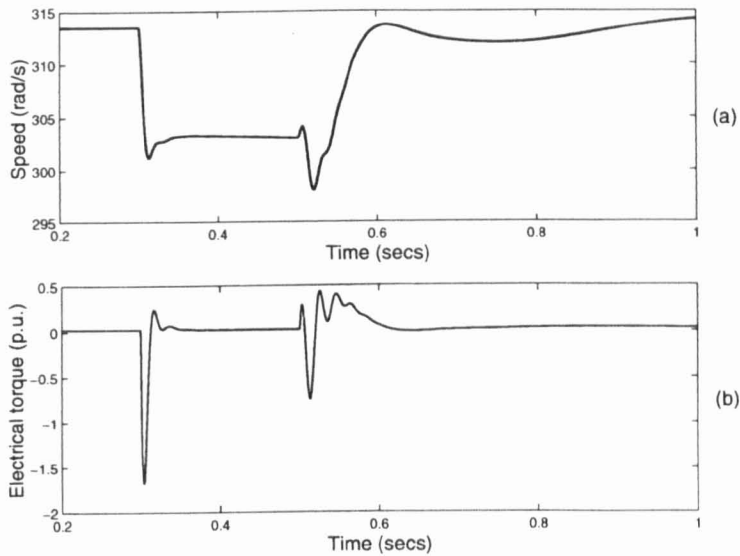


Figure 4.27.: Unloaded motor speed and electrical torque subjected to a three-phase-to-ground fault at *Node 8*

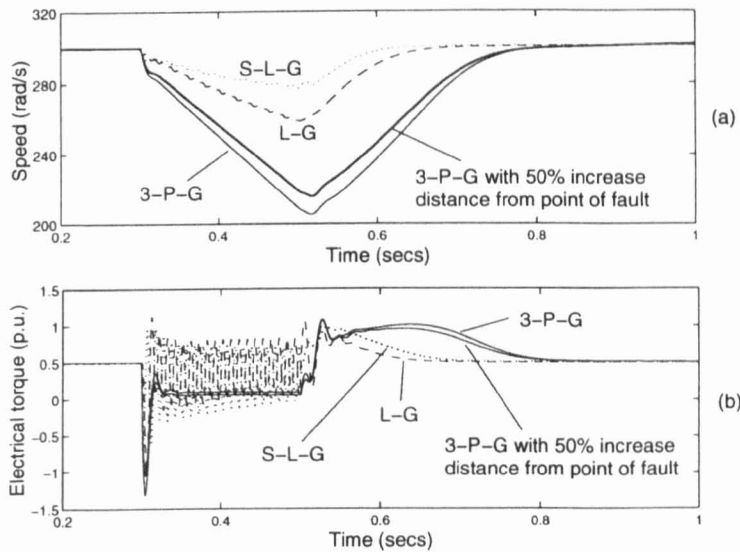


Figure 4.28.: $0.5 p.u.$ loaded motor speed and electrical torque subjected to various faults at *Node 8*

from Figure 4.31 that the voltage level on the two healthy phases can be significantly affected by the fault. This is due to the couplings between phases within the motor that can be affected by the fault in any one of the phases. The slow deceleration of motor speed in Figure 4.28a shows the extent of the fault is not as severe as the case of the three-phase-to-ground fault. The electrical torque of the motor contains an oscillating negative sequence component as a result of the unbalance that occurs between its phases.

4. Further Consideration of the Direct Time Phase-Domain Multimachine Model

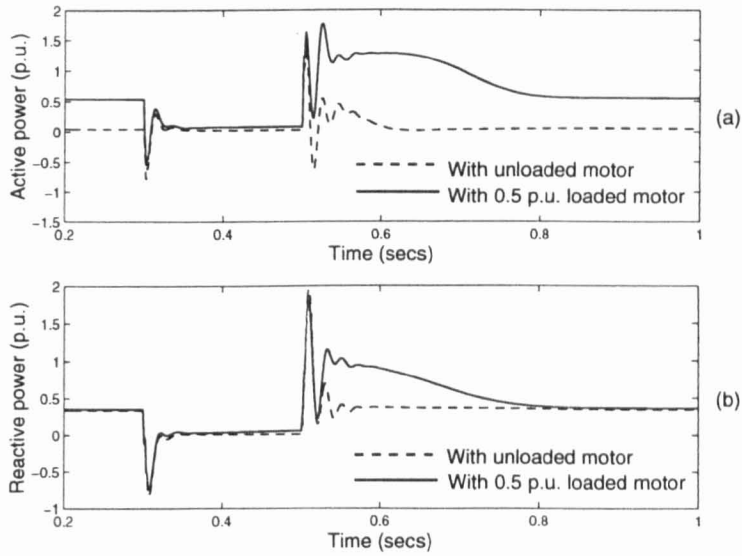


Figure 4.29.: Motor active and reactive power demand subjected to a three-phase-to-ground fault at *Node 8*

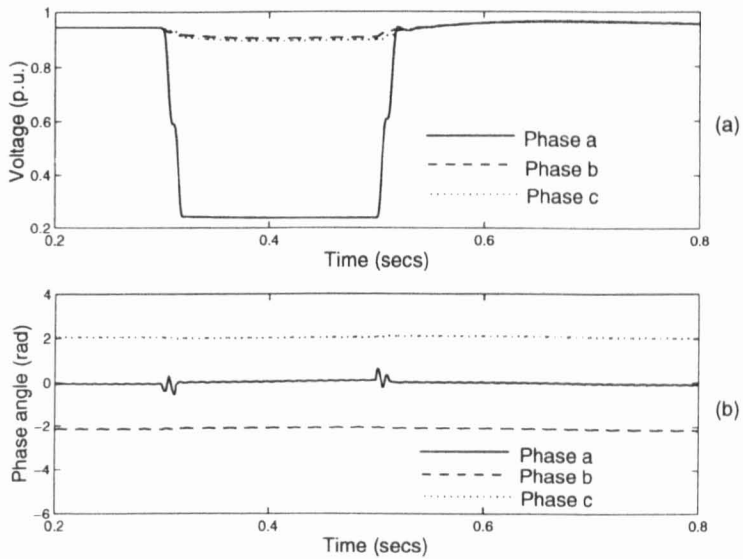


Figure 4.30.: Bus voltage and phase angle at *Node 8* without motor subjected to a single-phase-to-ground fault

c) Asymmetrical phase-to-phase fault

The phase-to-phase fault is simulated by short-circuiting phase *b* and *c* on *Node 9*. In the case without the motor, the healthy phase voltage is not significantly affected by the fault. The difference of response in the voltage magnitude is again observed in the presence of the motor. Where the voltage level of phase *a* decreases continuously when the fault is applied. The prolonged voltage sags period of all the phases are also evident due to the time required by the motor to re-accelerate. A phase angle change occurs in the faulted phases but the presence of motor has little effect on the change.

4. Further Consideration of the Direct Time Phase-Domain Multimachine Model

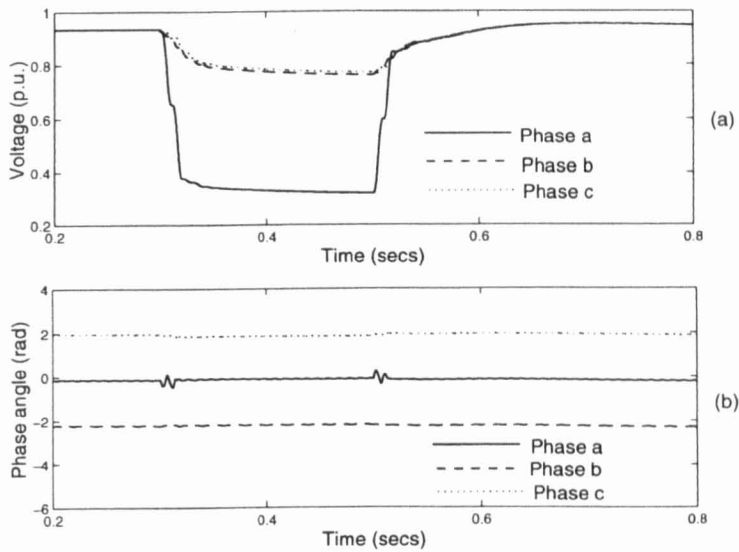


Figure 4.31.: Bus voltage and phase angle at *Node 8* with motor subjected to a single-phase-to-ground fault

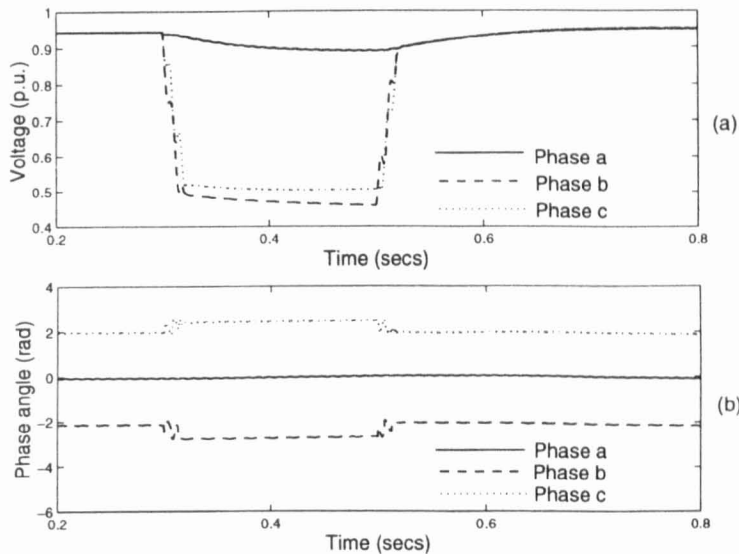


Figure 4.32.: Bus voltage and phase angle at *Node 8* without motor subjected to a phase-to-phase fault

4.5. Conclusions

This chapter has presented two very useful considerations that have further demonstrated the generality and versatility of the direct time phase-domain multimachine model. In the first section, the model is applied in a conventional transient stability study to reduce computing time based on the coherency approach. A novel aggregation technique is devised using the phase-domain multimachine model to obtain an equivalent generator to replace a group of coherent generators. The aggregation method for the equivalent generator model is straightforward to implement and applies with no need for iterations or error adjustment

4. Further Consideration of the Direct Time Phase-Domain Multimachine Model

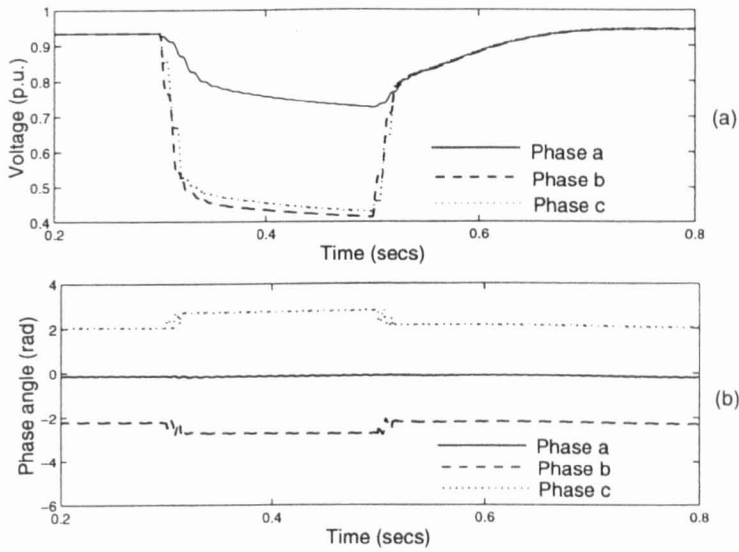


Figure 4.33.: Bus voltage and phase angle at *Node 8* with motor subjected to a phase-to-phase fault

methods. Results presented have shown that the model is capable of simulating both symmetrical and asymmetrical transient conditions with good comparable accuracy to that obtained using detailed models of generators. The importance of this phase-domain equivalent model is demonstrated in a situation involving real-time simulations. The benefit of using the equivalent model is shown by the AFT of the simulations, where it is observed that the time step required can be significantly reduced to achieve the real-time simulation while ensuring accuracy.

In the second consideration, the phase-domain multimachine model is used to perform analysis on a very practical power quality problem that is affecting current power system operations. Voltage sags as a result of dynamic load operations were considered with detail modelling of the load in the form of an induction motor. A similar discretisation approach was applied to the induction motor in order for its successful integration into the multimachine environment. The versatility of the overall network with dynamic load is demonstrated by the studies of various motor operating conditions. It is observed that the motor has a significant effect on the network voltage sags when subjected to direct online starting. The re-acceleration of such motor after a network fault is also an important issue affecting voltage sags. The attributes of the motor operations and fault conditions were observed to have an influence on the level and period of sags. These are important contributions to the development of compensating devices, which will be presented in the later chapters.

5. Dynamic Behaviour of a Network with Embedded Wind Driven Fixed Speed Induction Generator

Analysis on the application of induction generators in power systems, with particular reference to wind energy conversion system, WECS, is presented in this chapter. Direct time phase-domain modelling of the power system components is used to investigate the behaviour of the grid connected induction generator and its effect on the transient stability of a distribution network. It is observed that the parameters of the line connecting the induction generator to the grid can have a significant impact on the stability of the generator in event of a fault. One other transient phenomenon that often occurs is the disconnection of the induction generator from the grid during a network disturbance. Under this condition the balance of reactive and active power flow between the generator and the power system can be interrupted, and generator self-excitation will occur. The behaviour of the generator under this condition is investigated. Typical characteristics of a WECS that can affect the transient conditions of the induction generator are also investigated. It is observed that the oscillating input torque driving the wind driven induction generator has an adverse effect on the network stability margin.

5.1. Introduction

Renewable energy has come to the forefront of international interest as a plausible source to meet today's increasing power demand while ensuring environmental friendliness. This has led to inevitable growth in the connection of renewable energy sources into low voltage distribution systems. So far, wind generation has been dominant since the technology is well understood and there is general agreement that this primary resource is environmentally sound, abundant and free; it is sustainable [99]. Wind turbines coupled with induction generators have been extensively used in wind farms to convert wind energy into electricity. Induction

5. Dynamic Behaviour of a Network with Embedded Wind Driven Fixed Speed Induction Generator

generators outperform synchronous generators in terms of manufacturing cost and maintenance requirements; characteristics that have made them popular in wind power generation. Moreover, their ability to operate asynchronously is a technical strength in this application, since the induction generator does not suffer from pole angle stability. The flexibility of the induction generator allows it to be driven in various modes. The most straightforward and economical is the fixed speed wind turbines driven mode of operation. With the continuous growth of wind farms installations, it is not uncommon to find this mode of operation generally preferred.

Wind driven induction generators may be operated as autonomous systems or they may be connected to a distribution network. Autonomous systems are less reliable in terms of power generation due to the random nature of the wind. Hence, connection to the network is preferred to ensure a better continuity of supply. Connection to the grid may be carried out directly or using power electronics converters [99]. However, direct integration may result in several adverse effects that demand scrutiny at the planning stage to ensure a smooth operation of the network [100][101][103].

There are still many unresolved issues in the area of direct integration of a fixed speed wind driven induction generators, which require research work. One of such aspects is transient stability assessment of distribution networks with embedded wind driven induction generators and “conventional” synchronous generators [103][104][105]. This chapter looks into this timely issue and reports on the main findings of hybrid, multimachine transient stability studies. The analysis is also conducted on the isolated operation of the induction generator as a result of disconnection from the main network. The additional area of study presented here is the direct effect of the possible oscillating characteristics of the WECS output on the stability of the generators.

5.2. Transient Stability of a Network with Grid Connected Wind Driven Induction Generator

The analysis of the dispersed generation scheme is performed on the test network of Figure 4.18 where the position of the induction motor in *Node 8* is substituted by an induction generator. The network is a good representation of a closely knitted network where embedded generation can be implemented as an additional source of energy. The induction generator is connected to the main network via a transmission line, which is often the case given that a wind powered generator is normally located faraway from the main distribution network. The cut-out section of the network in Chapter 4, where the connection of the induction generator and a closely located synchronous generator is shown in Figure 5.1.

The capacitor bank is normally connected at the terminal of an induction generator to provide

5. Dynamic Behaviour of a Network with Embedded Wind Driven Fixed Speed Induction Generator

reactive power compensation. In steady state operation both, the capacitor bank and the network provide the reactive power needed by the induction generator for its magnetisation flux. The capacitor bank is of fixed capacity. If the reactive power demand of the induction generator increases, as a result of a load increment, the deficit will be obtained from the network. Vice-versa if the requirement of the generator reduces, the additional reactive power of the capacitor will flow into the utility. The parameters of the system under study are in *p.u.* on a base of 30 MVA. The initial loadings of the induction generators and the capacitor are given in Table 5.1. The initial conditions of the remaining network are unchanged as given in Chapter 4.

	P (p.u.)	Q (p.u.)
Induction generator	0.450	-0.395
Capacitor bank	-	0.585

Table 5.1.: Induction generator and capacitor loading at steady state

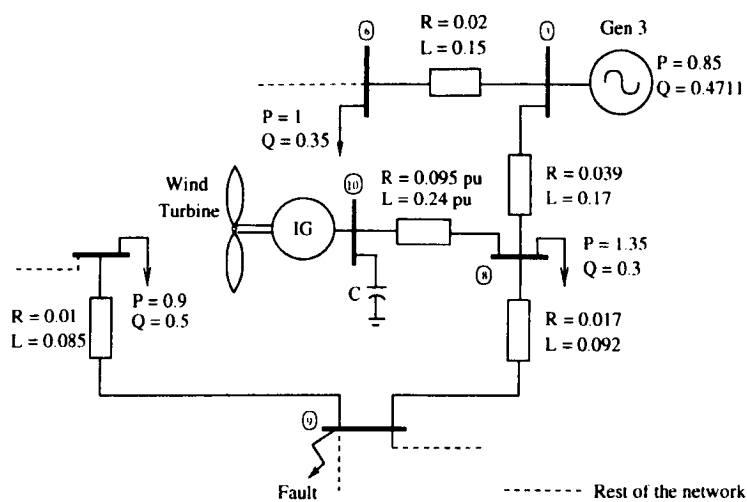


Figure 5.1.: Test system of a dispersed generation distribution network

The parameters of the discussed induction generator is given in Table 5.2. The reactances and resistances are in *p.u.* referred to the base of the synchronous generator at 30 MVA. The parameters of the synchronous generator are given in Appendix A.2. The inertia constant of the synchronous generator is $H = 4.6$ s.

A transient stability analysis is conducted by applying a three-phase-to-ground fault at *Node 9* of the network at time $t = 0.3$ s. In this study, the induction generator is assumed to be driven by a fixed input torque, which corresponds to a steady wind-turbine output profile. Since the size of the induction generator is smaller than that of the generators in the network, its direct effect will most likely affect only the closest located synchronous generator. Hence, the study of the induction and the synchronous generator, connected at *Node 3*, will be the focus of the analysis.

5. Dynamic Behaviour of a Network with Embedded Wind Driven Fixed Speed Induction Generator

Induction generator parameters :	
Rating	2.8 MW, 3.355 MVA
Inertia constant, H	0.5 s
L_{ss}	1.745 p.u.
L_{rr}	1.745 p.u.
r_s	0.0642 p.u.
r_r	0.0637 p.u.
M_{sr}	0.825 p.u.

Table 5.2.: Induction generator parameters

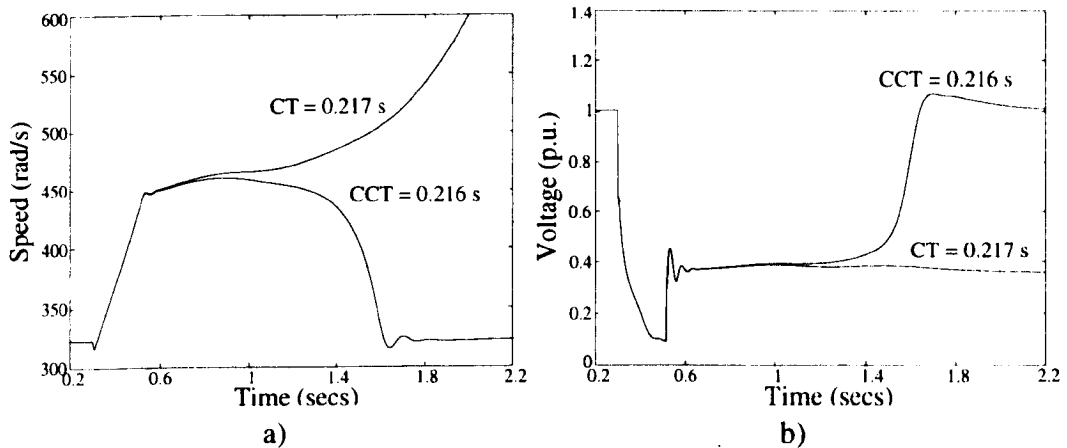


Figure 5.2.: Induction generator speed and terminal voltage following a three-phase-to-ground fault with synchronous generators' AVR and turbine governor control

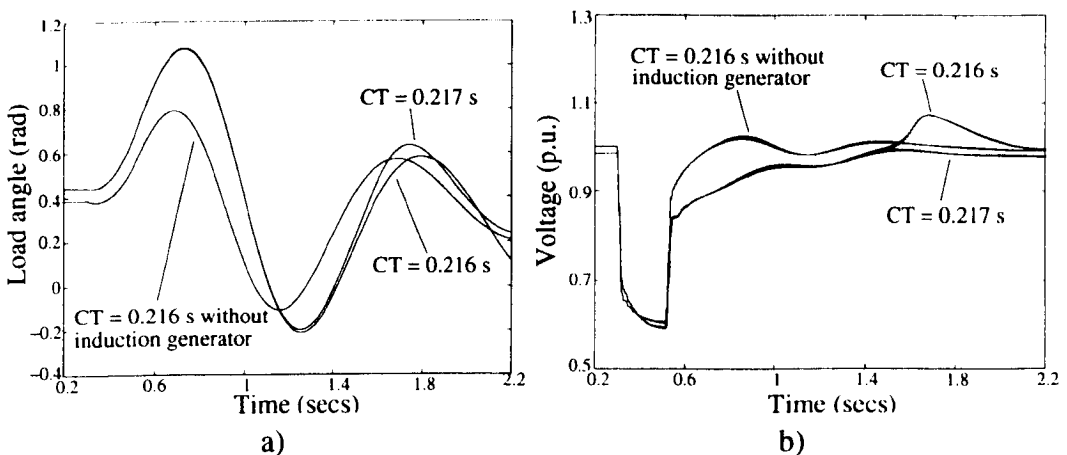


Figure 5.3.: Synchronous generator load angle and terminal voltage following a three-phase-to-ground fault with synchronous generator's AVR and turbine governor control

Figure 5.2 shows the speed and terminal voltage of the induction generator under different fault clearing time (CT). The critical clearing time (CCT) of the induction generator is approximately 0.216 s as shown by the response of its speed in Figure 5.2a. If the fault fails

5. Dynamic Behaviour of a Network with Embedded Wind Driven Fixed Speed Induction Generator

to be removed the speed of the induction generator will rise continuously. This is due to the discharge of the capacitor during the fault period, causing the voltage at the induction generator terminal to collapse, as shown in Figure 5.2b. The lack of voltage support causes the magnetisation flux of the induction generator to decay [104], preventing its operation even after the fault has been cleared.

The response of the synchronous generator's load angle and terminal voltage is shown in Figure 5.3. It is observed that its response is stable for the CT experimented on. This is due to the relatively larger size of the synchronous generator and the voltage support provided by its controllers. However, it is observed that the presence of the induction generator has a negative impact on the stability of the synchronous generator. The first swing of the generator's load angle shown in Figure 5.3a is considerably higher with the presence of the induction generator for a similar CT.

The similar studies are conducted but this time with the AVR of the synchronous generator deactivated. The absence of the AVR control result in the reduction of voltage support available in the network. The stability margin of the induction generator is further constrained where it is observed from Figure 5.4 that the CCT of the induction generator is reduced to 0.194s. The first swing stability of the synchronous generator also increases as a result of the lack of voltage support as in Figure 5.5.

In the study case provided, it is observed that the stability margin of the induction generator is more critical than that of the synchronous generator. This could be due to the induction generator being considerably smaller in size and also it is located closer to the point of fault. The stability of the induction generator are highly dependent of the voltage condition at its terminal. Hence, the results provided here is not conclusive to say that the induction generator will be less stable than a synchronous generator in a co-generation scheme. Further work needs to be conducted to determine this issue where a similar size and short-circuit ratio generators are to be used. However, it has been shown that the presence of the induction generator have a negative impact on the first swing stability of the synchronous generator.

Induction generator stability with various network parameters

Another important aspect that affects the stability of the wind-driven induction generator is the tie-line connecting the generator to the distribution network. Even slight changes of the inductance to resistance ratio of the cable connecting the generator can have a significant effect. The extend of this ratio on the stability of the induction generator is analysed here in greater detail. It is worth pointing out that this analysis can be performed in the direct time phase-domain approach by considering the steady state impedance X/R ratio of the line to be the same as the inductance to resistance ratio. This is possible because the value of the parameters used in the phase-domain is in *p.u.* and the rated speed is taken as 1 *p.u.*. As

5. Dynamic Behaviour of a Network with Embedded Wind Driven Fixed Speed Induction Generator

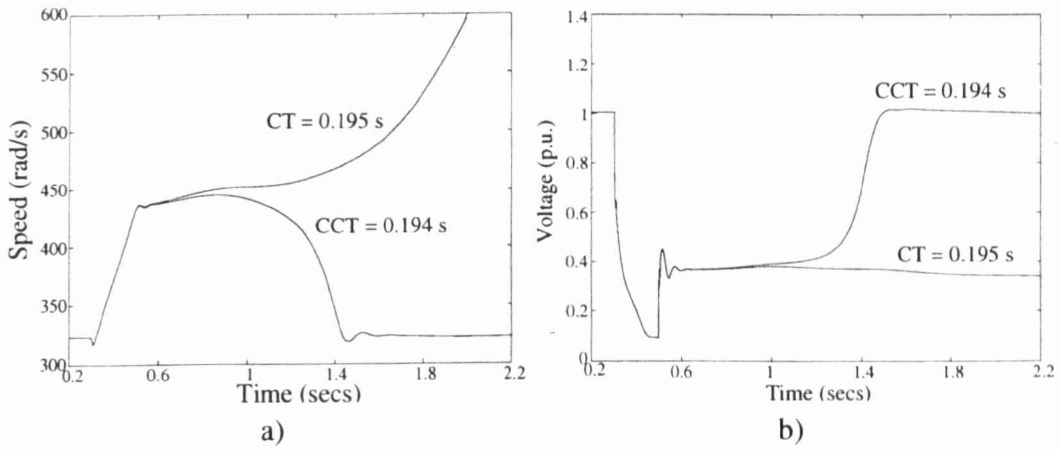


Figure 5.4.: Induction generator speed and terminal voltage following a three-phase-to-ground fault without synchronous generators' AVR and turbine governor control

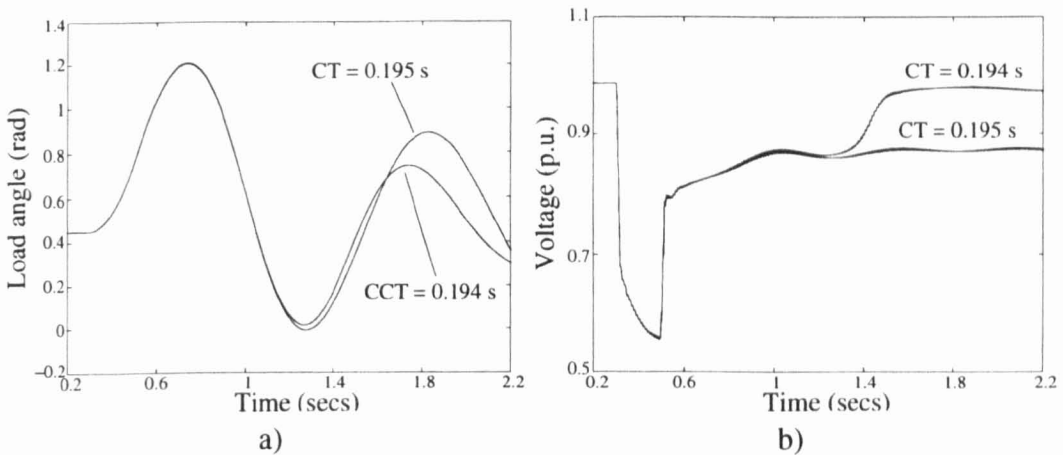


Figure 5.5.: Synchronous generator load angle and terminal voltage following a three-phase-to-ground fault without AVR and turbine governor control

such the value of a steady state reactance is the same as the value of an inductance use in the phase-domain, and similar observation applies to the resistance.

Typical transmission lines characteristically have an X/R ratio of 10 or higher [4][5][34], however in WECS installation this can be as close as a ratio of 2 [106]. This is especially the case when off-shore WECS are considered where connections are through submarine cables. In the sample network under study the line connecting the induction generator to the network, between *Node* 8 and 10 has an X/R ratio of 2.5. A similar fault condition is simulated for three different X/R ratio of 2, 3 and 10.

The induction generator speed responses and terminal voltage for the different X/R characteristic are presented in Figure 5.6 where the fault is cleared at $t = 0.216s$. It is observed that the generator has failed to maintain stability with the large value of X/R ratio, while lower ratio provides a better and quicker recovery of the generator terminal voltage and speed responses as compared to the default ratio of 2.5. This observation is generally agreed upon

5. Dynamic Behaviour of a Network with Embedded Wind Driven Fixed Speed Induction Generator

since network parameters play a significant role in determining the system dynamic performance. Increasing the resistive part of the line parameters introduces extra damping stability due to the increase of time constant, as shown by the induction generator speed swing, but this is at the expense of network losses.

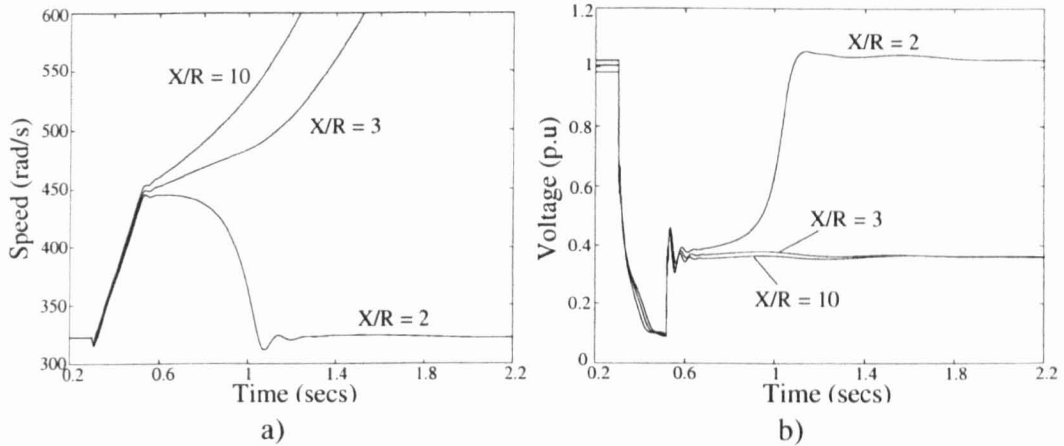


Figure 5.6.: Induction generator speed and terminal voltage cleared at CT = 0.216s with different X/R ratios

The total impedance along the line determines the electrical divide between the two points that it connects. If the impedance is high, the points are electrically far from each other making them weakly connected. Conversely, if the impedance is low they are strongly connected to each other. Hence, the strength of a line is dependent on its total impedance which is directly related to the total length and construction material of the line.

In the following analysis, the strength of the tie-line connecting the induction generator to the network between *Node 8* and *10* is experimented on. The short-circuit current is obtained by observing the current magnitude flowing into *Node 9* where it is given as $|I_{sc}| = 3.87 p.u.$. The Thevenin's equivalent circuit can be used to obtain the magnitude of the short-circuit impedance, which is the Thevenin's impedance, by taking nominal voltage of $1 p.u.$ as the source to the Thevenin's circuit where,

$$|Z_{th}| = \frac{1}{|I_{sc}|} \quad (5.1)$$

The default magnitude of the short-circuit impedance is $|Z_{th}| = 0.258 p.u.$. The parameters of the tie-line between *Node 8* and *10*, is modified in progression to reduce the overall short-circuit impedance. Three different values of the $|Z_{th}|$ used are 0.2516, 0.2454 and 0.2395 $p.u.$. Similarly, the $p.u.$ value of the impedance can be use based on data conversion between the impedances and actual quantities if the rated speed is given as $1 p.u.$, as explained earlier.

In Figure 5.7, the effects of reducing the total short-circuit impedance by changing the parameter of tie-line between *Node 8* and *10* is analysed with two different X/R ratios. It is

5. Dynamic Behaviour of a Network with Embedded Wind Driven Fixed Speed Induction Generator

observed that as the short-circuit impedance reduces, stability is observed in the induction generator for $X/R = 3$ with the same clearing time as those presented in Figure 5.6. For the strongest line considered here, the stability of the generator will be maintained even for a high $X/R = 10$. This indicates that if a strong line is used, the significance of the X/R ratio on the generator stability diminishes. This is a very important conclusion based on this limited set of results. However, the upgrading of line parameters needs to be justified by taking proper account of economic and technical factors.

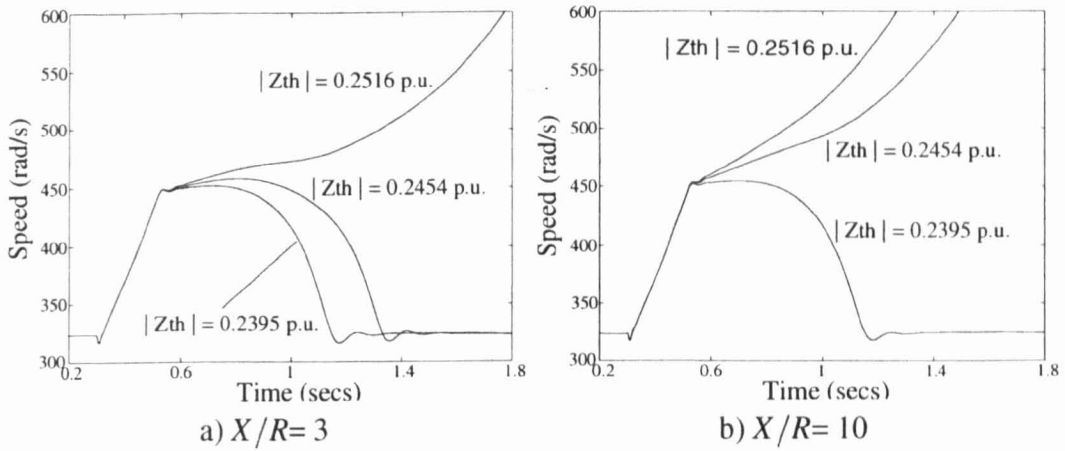


Figure 5.7.: Induction generator speed under different network strength

5.3. Transient Performance of an Islanded Wind Driven Induction Generator from the Network

When an induction generator is connected to a grid or network system, its operating features are governed by the connecting network [107]. The reactive power required for the induction generator excitation is supplied in part by the network and in part by the capacitor bank. As the output of the induction generator and loading of the network fluctuate, the amount of reactive power required is automatically adjusted to fit the new demand of the generator and the dynamic balance of the generator and the network is maintained.

In event of a fault, it is common that the wind driven induction generator of the WECS can be isolated from the grid [99][100], with such an action known as the ‘islanding’ phenomena. This is often necessary to prevent the fast increase in the speed of the induction generator in cases when the fault is not cleared in time to maintain stability. If grid disconnection should occur, the dynamic active and reactive power balance between the induction generator and the network will be disturbed. The generator will seek a new operating point where a new power flow balance can be achieved. Since the generator does not contain an independent controller, both the terminal voltage and speed of the generator will vary in accordance to the isolated network conditions.

5. Dynamic Behaviour of a Network with Embedded Wind Driven Fixed Speed Induction Generator

The main attributes that determine the new operating point are the excitation and loading level of the generator. When islanded, the generator will be in self-excitation where the required reactive power to produce flux linkages is supplied entirely by the capacitor bank. The load that remains after the islanding is also very important to the self-excitation of the generator as the load current changes the reactive power demand of the generator. Overvoltages can appear during this period of self-excitation, and it has been widely reported that this could cause severe damages to the capacitor bank and the wind turbine constructions [99][100][107].

Behaviour of Unloaded Induction Generator after Islanding

In the first case of study, an islanding scenario is simulated by disconnecting the generator from the network by opening of line 8 - 10. Following the disconnection, the generator is not connected to a load, hence it is only loaded by the capacitor bank. Figure 5.8 shows the induction generator speed and terminal voltage under different excitation level. The results indicate that the generator achieves a new point of operation at a new voltage and speed level [107][109].

When the windfarm is initially isolated from the utility network, the sudden change of balance in power flow due to load shedding causes the generator output torque to decrease rapidly to a small value, as shown in Figure 5.9. This is immediately reflected in the rise of the generator speed in Figure 5.8a as a result of the diminished output torque to retard the input torque. A balance between the input and output torque of the generator is necessary in order to establish an equilibrium point. However, this is not achieved here since the generator is still being driven by the fix input power.

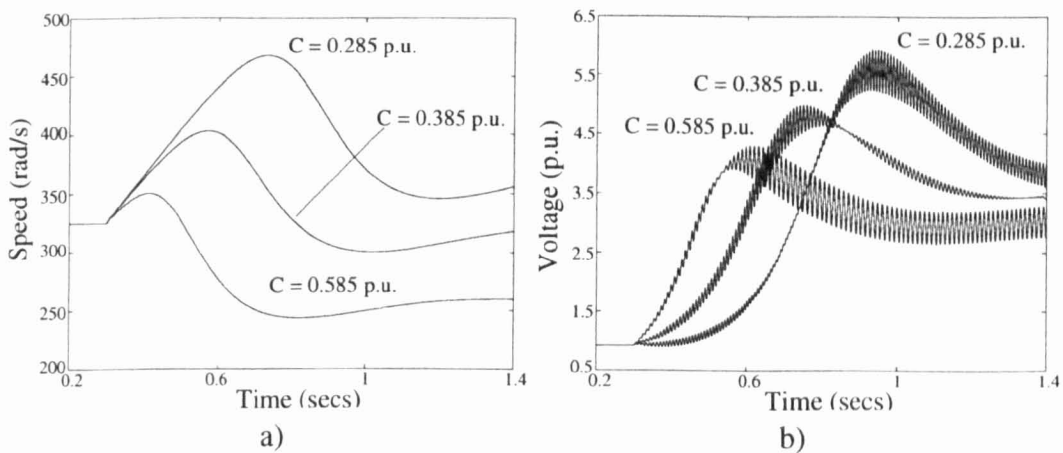


Figure 5.8.: Islanded induction generator speed and terminal voltage with no isolated load under different excitations

The capacitor bank continues to provide voltage for the self-excitation of the generator. When the voltage is large enough, the active power losses in the generator will be equal to the input power. Hence, the output torque of the generator increases to cater for such losses, retarding

5. Dynamic Behaviour of a Network with Embedded Wind Driven Fixed Speed Induction Generator

the continuous rise of the generator speed. A new steady state operating point would be established where the reactive power demanded by the generator is met by the capacitor, and the output power balances the losses of the generator as in Figure 5.9. It is observed that the value of the excitation capacitor can have a significant effect on the speed increase and voltage level of the generator. Large capacitors react faster to provide the retarding torque needed to slow down the generator. This in turn results in the steady state voltage level to be achieved at a faster rate reducing the peak voltage value. If a large enough capacitor is used then very low speed and even a complete stop can be achieved [107][109].

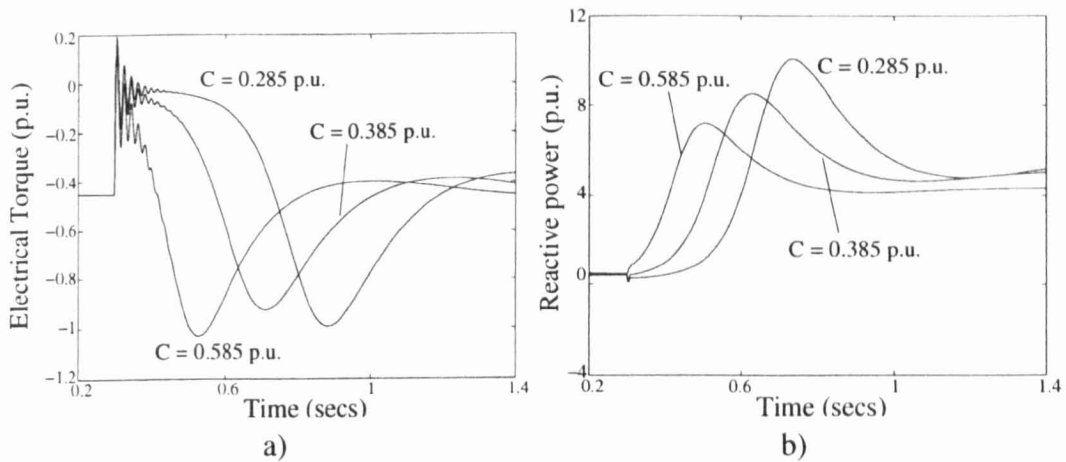


Figure 5.9.: Islanded induction generator torque and reactive power demand with no isolated load under different excitations

It is observed that the peak voltage level can be a few times in excess of the rated voltage depending on the capacitor bank rating. This value of voltage can be disastrous to the equipments especially the capacitor banks itself. Figure 5.10 shows the terminal phase voltage of the generator when one phase and two phases of the capacitor, rated at 0.585 p.u., is opened due to damage or disconnection. When one phase of the capacitor opens, the effect on the overall response is not very obvious. The generator still can maintain self-excitation although the time taken to reach the new operating point is slow. For the case when two phases are open, the reduction in the capacitor compensation level is clearly shown by the slow increase of the voltage to the new operating point resulting in higher voltage peak. The speed response is shown in Figure 5.11, where it is observed that loss of excitation, due to opening of capacitor phases, results in higher operating speed. If all three phases of the capacitor bank are disconnected the self-excitation of the generator is not possible resulting in the continuous rise in speed.

Behaviour of Loaded Generator after Islanding

Sometimes islanding can occur leaving the generator still connected to part of the network, which would happen if the induction generator in the network under study is isolated by the

5. Dynamic Behaviour of a Network with Embedded Wind Driven Fixed Speed Induction Generator

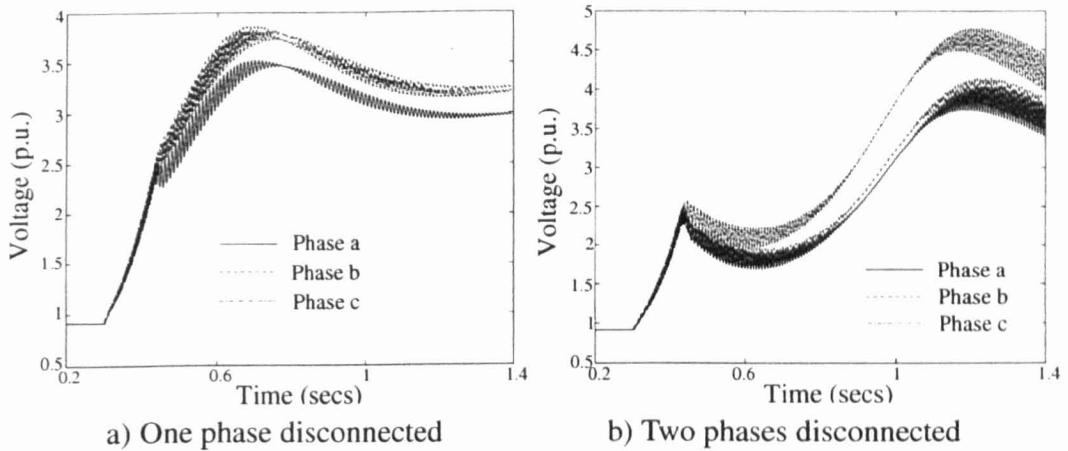


Figure 5.10.: Islanded induction generator terminal voltage with no isolated load under unbalanced excitation due to capacitor bank phases disconnection

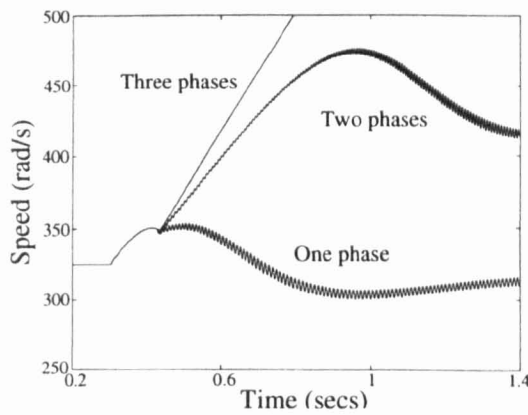


Figure 5.11.: Islanded induction generator speed with no isolated load under unbalanced excitation due to capacitor bank phases disconnection

opening of line 3 – 8 and 8 – 9. This leaves the generator loaded by the passive load at *Node 8* of the isolated network. The generator will then attempt to supply the power required by the load and in doing so increases its own reactive power demand.

Figure 5.12 shows the speed and the terminal voltage of the isolated generator under different excitation when loaded by its capacitor bank and the isolated load at *Node 8*. Upon islanding, the reactive power from the capacitor bank needs to be distributed to maintain self-excitation of the generator as well as to meet the load’s reactive power demand. This causes a deficit of reactive power which results in the voltage at the terminal of the generator to collapse after the islanding. The generator will not be able to achieve immediate self-excitation and as a result the mechanical input will drive the rotor speed up.

Depending on the rating of the excitation capacitor, a different steady state speed will be obtained at a new voltage level. Larger excitation capacitor ensures that a lower steady state speed can be obtained at a shorter duration. Under excitation due to smaller capacitor will result in a very high speed increase creating a more severe electrical transients as observed

5. Dynamic Behaviour of a Network with Embedded Wind Driven Fixed Speed Induction Generator

by the voltage level in Figure 5.12b.

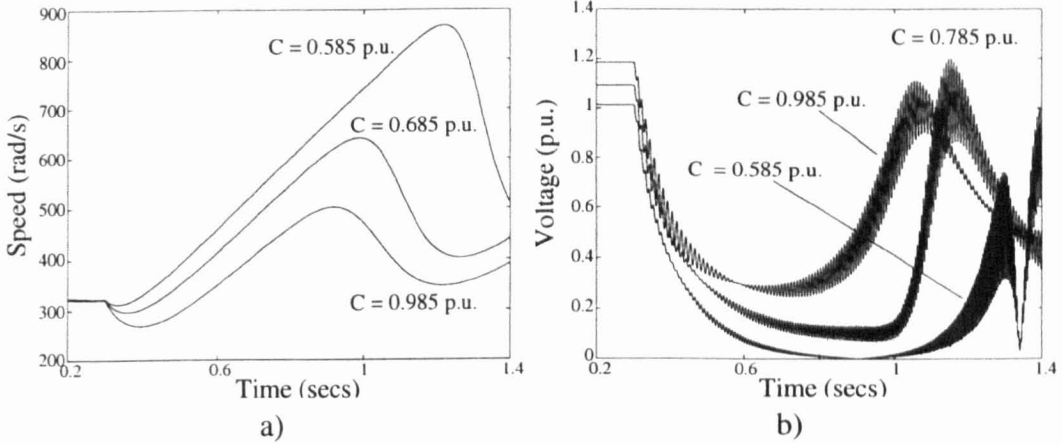


Figure 5.12.: Islanded induction generator speed and terminal voltage with isolated load under different excitation

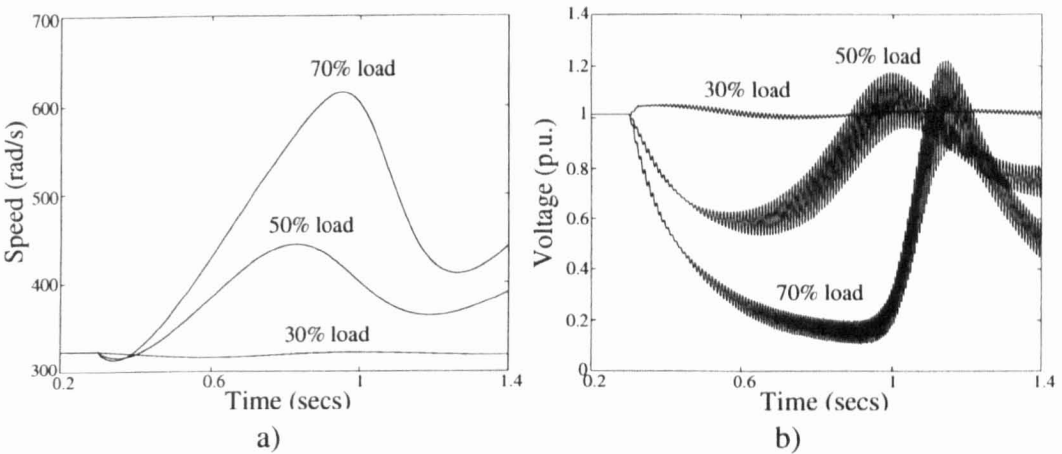


Figure 5.13.: Islanded induction generator speed and terminal voltage with isolated load under different loading condition with excitation $C = 0.585$ p.u.

The extent of the speed increase and voltage level does not depend on the excitation capacitor alone. Naturally, the isolated load plays an important role as it determines the mismatch of power flow in the isolated network. Decreasing the load will ensure more reactive power for the generator to achieve self-excitation in a shorter duration, hence, reducing the steady state speed. The effect of the loading on the response of the generator is shown in Figure 5.12.

The result presented indicates that the transient behaviour of the isolated induction generator is more critical when it is loaded. The rating or size of the excitation capacitor plays an important role in determining the duration for the generator to achieve a new operating speed and voltage level. The longer it takes the more severe is the transient behaviour of the generator. Reducing the level of load can also improve the response of the isolated generator.

5.4. Operation of the Wind-driven Induction Generator Under Unbalance Network Conditions

In this section, asymmetrical faults and network conditions are considered for transient analysis of the induction generator. Two types of asymmetrical fault in the form of single-phase-to-ground fault and phase-to-phase fault are simulated in the network at the same node. The effect of different unbalances in the network on the transient response of the generator are presented. The cases considered are unbalance load at *Node 8* and unbalance tie-line connecting the generator to the network from *Node 8 - 10*. The conditions considered may not be the most realistic but it is not the main objective here to study the induction generator behaviour under these conditions. Rather the aim is to demonstrate the effectiveness of the model that has been developed to be use in such an asymmetrical conditions.

Single-phase-to-ground fault

Figure 5.14 shows the response of the induction generator when subjected to a single-phase-to-ground fault on phase *a* of *Node 9* with different network conditions where the fault is cleared at time $CT = 0.216s$. It is observed that with the default balance network and loading conditions, the stability of the machine is less affected as compared to that incurred by the three-phase-to-ground fault. The reasons for the more stable response has to do mainly with the discharging effect of the excitation capacitor. In the case of the single-phase-to-ground fault, the loss of excitation from the capacitor is minimized as the capacitors on the healthy phases are able to keep the stator of the induction generator magnetised while the small deficit is duly obtained from the network. Hence, a new steady state speed of the generator is rapidly achieved even during the fault period. The unbalance caused by the fault can be seen from the oscillations in the generator's electrical torque which carries the negative sequence components [12][13].

Network unbalances are included in the simulation where three conditions are considered, an unbalance line connecting the induction generator to the network from *Node 8 - 10* and an severe unbalance load at *Node 8*. The unbalance of the line is simulated for two cases of single phase opening of line 8 – 10 where the parameters of phase *a* is set to a very large value for one case, and phase *b* for another. The unbalance load is created by considering the load of phase *b* to be about 90% of the total load demand at *Node 8*.

Depending on the type of unbalances, the stability of the generator can be negatively or positively affected. The opening of phase *a* in line 8 – 10 have little effect on the stability, in fact, it shows a more positive response. The reason is that the open line provides a better electrical distance between the terminal of the generator to the point of fault reducing the

5. Dynamic Behaviour of a Network with Embedded Wind Driven Fixed Speed Induction Generator

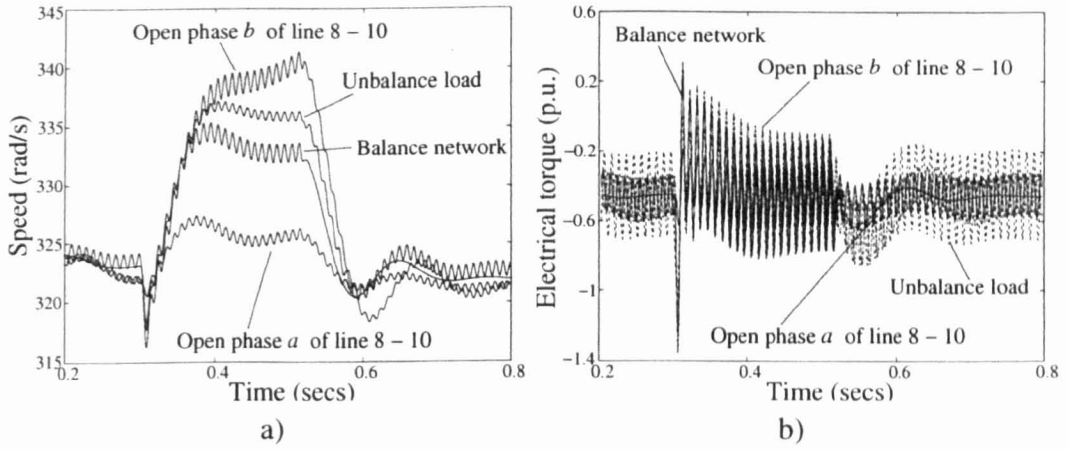


Figure 5.14.: Induction generator speed and electrical torque under a single-phase-to-ground fault in phase a with different network conditions

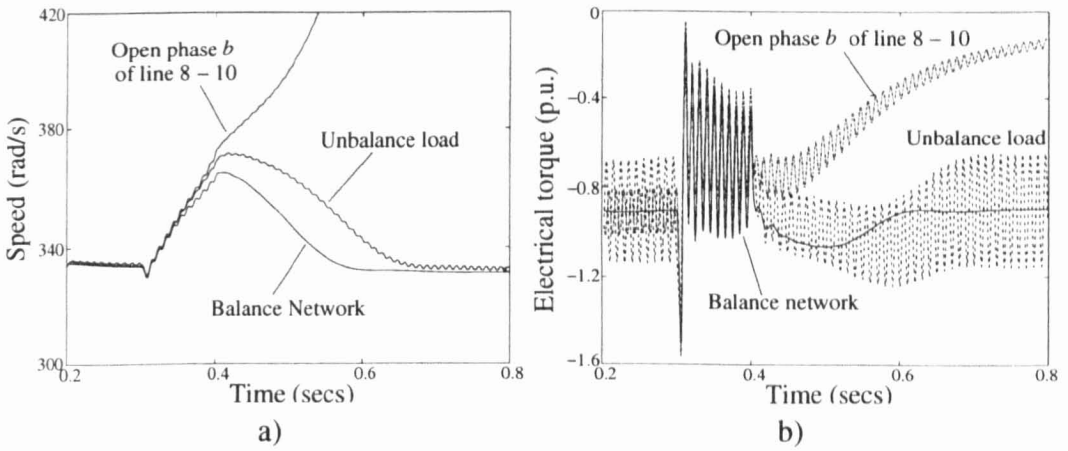


Figure 5.15.: Induction generator speed and electrical torque under a single-phase-to-ground fault on phase a with different network conditions with mechanical input torque of $P_m = 0.9 p.u.$

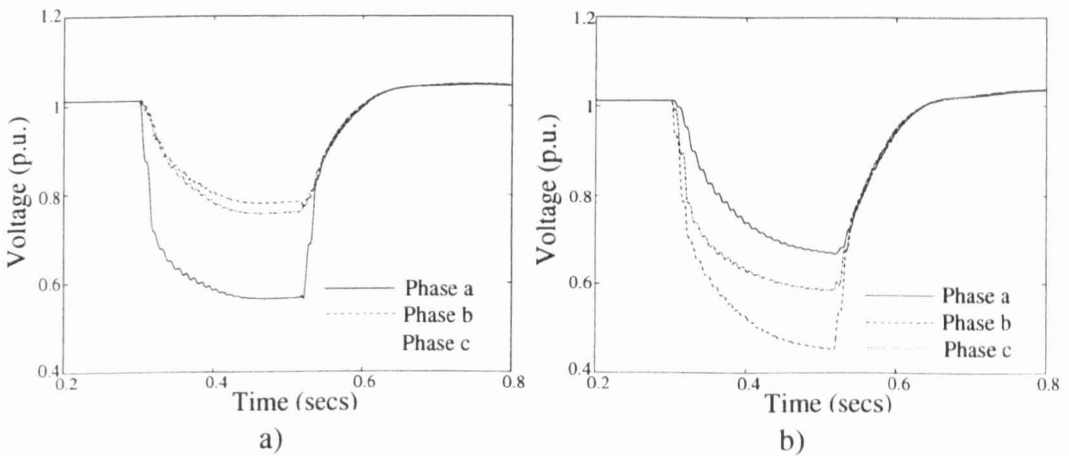


Figure 5.16.: Induction generator terminal voltage under : a) Single-phase-to-ground fault, b) Phase-to-phase fault

5. Dynamic Behaviour of a Network with Embedded Wind Driven Fixed Speed Induction Generator

discharge of the capacitor. For the large parameter on phase *b* of the line, the stability of the generator is reduced as observed by the speed increase in Figure 5.14a.

The large demand on phase *b* of the load causes the biggest unbalance in the network during the steady state where one phase of the excitation capacitor is operating nearer the limit because it has to be supplied for the generator and the load demand. Hence, during the fault the level of reactive power shortage for the generator is greater than a balanced network condition. The slight reduction in stability is observed for the small difference in the speed of the generator during the fault as shown in Figure 5.14a.

Figure 5.15 shows the similar result but this time with the mechanical torque driving the induction generator increased to $0.85 p.u.$. The CT of the simulation is reduced to $0.1 s$ because the stability of the generator is more critical under heavy loading. It can be observed that the network unbalance can have a severe effect on the stability of the network when the power penetration of the generator is high. This is a case for concern as when a wind turbine drives the generator the input power can change erratically. A combination of this situation with network unbalance during a fault can drive the generator out of stability unexpectedly.

Phase-to-phase fault

A phase-to-phase fault is simulated by short-circuiting phases *b* and *c* of Node 9 where the CT is $0.216 s$. The response of the generator loaded at $0.45 p.u.$ are as shown in Figure 5.17 where the stability of the generator under this kind of fault is more severe than the single-phase-to-ground fault. The unbalances in the network especially for the case of the opening of phase *b* can further reduce the stability of the generator.

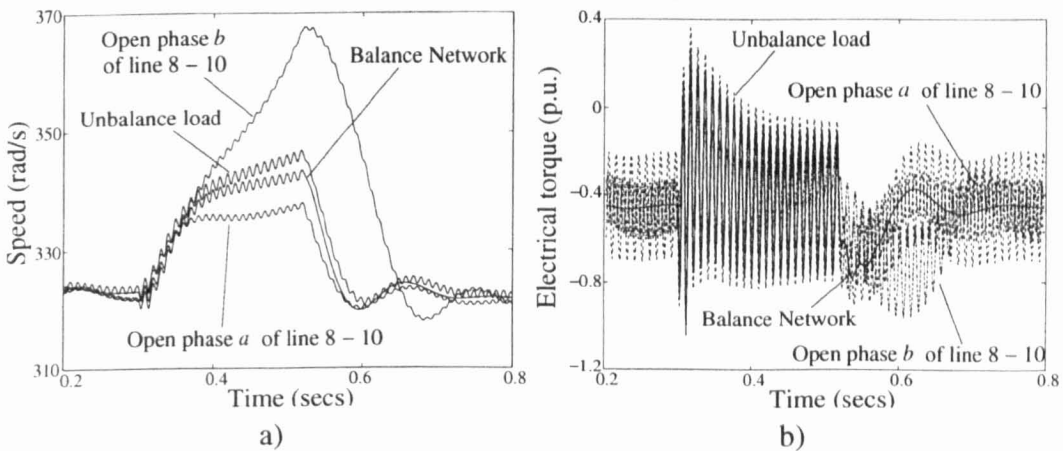


Figure 5.17.: Induction generator speed and electrical torque under a single-phase-to-ground fault on Phase *a* with different network conditions

5.5. Effect of Wind Driven Induction Generator Oscillating Output on Network Stability Margin

In wind generation, the characteristics of the generated power depend on the wind turbine driving the induction generator. It has been known that oscillations or pulsations of power output from the WECS can occur when the blades of the wind turbine pass its tower [99][100]. If the blades of a group of wind turbines pass the tower at the same instance, the oscillations of the torque at the blade passing frequency can be of significant concern. These oscillations are known to have a negative effect on the steady state power quality throughout the network. The main observations presented in the open literature are oscillations and flicker in the voltage level [101][111][112][114]. There have been limited reports on the effect of oscillations on the stability margin of the generators that are connected in the network [102].

A simulation study similar to the one conducted previously where a three-phase-to-ground fault is simulated at the terminal of the synchronous generator is carried out, but now with the induction generator input driven by an oscillating torque. The magnitude of the oscillation is set at $\pm 10\%$, $\pm 25\%$ and $\pm 50\%$ of the initial power input. The frequency of the oscillation is set at 1.6 Hz.

Magnitude	Induction Generator	Synchronous Generator
0%	0.194 s	0.246 s
$\pm 10\%$	0.194 s	0.246 s
$\pm 25\%$	0.188 s	0.236 s
$\pm 50\%$	0.176 s	0.225 s

Table 5.3.: CCT of the wind driven induction and synchronous generator with different oscillating magnitudes of the WECS power output

From Table 5.3, it is noticed that the CCT for the induction and synchronous generator remains the same for a small oscillations of $\pm 10\%$. As the magnitude of the oscillations increases, the CCT of the generators reduces. This indicates that the fault needs to be cleared faster in order to secure stability. The difference of a 10th of a millisecond may be significant in the design of protection systems. It can be concluded that oscillations can have an undesirable impact on the stability of the generators especially at higher magnitude.

5.6. Conclusions

This chapter has highlighted key aspects of the transient behaviour of networks with embedded wind driven induction generators and synchronous generators. It is observed that the stability of the induction generator is critical and highly dependent on the voltage level at its terminal. One possible explanation is the quick discharge of the capacitor bank at the

5. *Dynamic Behaviour of a Network with Embedded Wind Driven Fixed Speed Induction Generator*

terminal of the induction generator during the fault and the ensuing de-magnetisation of the generator. The effect of this de-magnetisation of the generator is not as serious in the case of asymmetrical fault conditions. The assessment of various X/R ratio of the line connecting the wind driven induction generator to the network indicates that a smaller ratio results in a more stable generator operations. However, the effect of this ratio becomes less significant if a strong line is used to connect the wind driven induction generator to the network. Results were also presented to show the dynamic behaviour of the induction generator upon islanding from the network. If the generator is sufficiently compensated by the capacitor bank it will be in a state of self-excitation where it will achieve a new operating point of power balance. The longer period required by the islanded generator to reach its new operating point results in more severe overvoltages at its terminal. Finally, analysis was performed to assess typical oscillating characteristics of a wind driven generator on the stability margin. The preliminary study indicates that the stability margin can be further limited by the oscillations depending on its magnitude. These observations provide a good indication of what to expect in the future when a more significant amount of wind powered generation will find its way into existing networks.

6. Power Electronics Controllers in the Phase-Domain

The thrust of this chapter is the development of power electronics controllers models suitable for inclusion within the direct time phase-domain multimachine environment. The following power electronics controllers receive attention, the SVC, STATCOM, DVR and HVDC-VSC station. The use of these controllers for power quality and transient stability enhancement form a very important part of this chapter. To this end, power system networks described in the previous chapters are used to perform analysis with these controllers included. A detailed description of the control strategies associated with these controllers is presented for both symmetrical and asymmetrical conditions. The HVDC-VSC station model is used for analysis in a hybrid scaled-down simulation environment. Results are presented which clearly show many advantages of using these power controllers for network operation enhancement.

6.1. Introduction

In conventional power systems, synchronous generators are the main source of electrical power, which is transmitted to points of demand via high voltage transmission lines and low voltage distribution systems. From the operational view point, the quality of power supply should meet certain standards with regards to frequency and voltage levels. These levels which should not deviate significantly from pre-specified operating values [4][5]. Various levels of control are used to meet such demands. As mentioned in Chapter 1, the generator is the main element, responsible for providing good quality power. There are several controllers that are specially designed for the generators, such as the turbine governor, the automatic voltage regulator and the power system stabiliser, to ensure this point. However, sole dependency on the generators are not enough since many points of demand are located far away from the generating units' controls. There are conventional devices such as tap-changing transformers and synchronous condensers which are installed at suitable points in the transmission system, which help to control voltage magnitude, and phase-shifting transformers whose main

6. *Power Electronics Controllers in the Phase-Domain*

function is to regulate active power flow.

With the availability of high power and high speed electronics devices, a range of advanced power electronics controllers are becoming widely available. The SVC, which was developed in the early seventies, is a good example of a first generation of controllers based on the operation of thyristor. The control of voltage magnitude using a TCR controllers is achieved by making suitable adjustments to the firing angle of the thyristor. The change in firing angle is amenable to an increase/decrease in reactive impedance of the controllers and, hence, the total reactances in the network. It may be said that the control action modifies the loading condition of the network in order to obtain the desired voltage level. However, the actual level of voltage compensation that can be provided is dependent on the network voltage level itself. If the voltage level is too low, the loading condition of the network will not change significantly by changing the reactances in the network. During transient operations, when the voltage level is greatly affected, the effectiveness of the TCR based controllers are ironically reduced.

The arrival of modern power electronics devices such as the GTO and IGBT has given rise to a new generation of power electronics controllers. The new controllers base their operation on the voltage conversion principle, deriving an AC output from a DC source using the PWM control techniques. The VSC based controllers can be operated as either a source or a sink in term of power flow by control of the modulation of the PWM signal. Such a control approach makes these controllers less dependent on network conditions and enable them to function better in time of significant voltage disturbances. The STATCOM, DVR and HVDC-VSC station are based on this technology.

This chapter starts by introducing an SVC where the TCR is the controllable element. The effectiveness of the SVC in improving adverse power quality phenomenon such as voltage sags are analysed. The modelling of the VSC is carried out in the phase-domain and based on PWM control for switching of the GTOs. The VSC model is provided with a suitable control scheme to be modelled as a STATCOM. The STATCOM is applied to solve power quality problems involving both symmetrical and asymmetrical operations relating to networks with embedded generation. The DVR, which may be seen as a series connected version of the STATCOM is also investigated with special reference to its ability to compensate voltage sags at its neighbourhood. Moreover, the application of a HVDC-VSC station for power transfer in a WECS will be investigated. The model of the power electronics controllers presented are not unduly complex but perhaps more importantly is the fact that they are suitable for simulation in the direct time phase-domain within a multimachine environment.

6.2. Static Var Compensator (SVC)

It may be argued that the proof-of-concept of application of power electronics controllers into AC power system has originated from the development and deployment of SVCs. The SVC consists of a group of shunt connected capacitor banks and inductors with fast speed of response afforded by thyristor switching. The SVC provides the required amount of reactive power compensation at its point of connection by adjusting the fundamental frequency components of the current drawn by the TCR. Depending on the equivalent reactance, i.e. capacitive or inductive, the SVC is capable of either drawing or supplying reactive power. The control of reactive power flow helps to regulate the voltage magnitude at its point of connection. Before the advent of the SVC, the control of voltage magnitude was only possible by using mechanically controlled equipments. The slow switching of mechanical devices leads to abrupt voltage changes that add to the transient already experienced by the system due to the disturbances. Conversely, the electrically controlled SVC provides rapid and smooth voltage regulation.

The two most popular SVC configurations are [48][50][51]: a system with a bank of fix capacitors and a thyristor controlled reactor (FC/TCR type) and a system with thyristor switched capacitors and a thyristor controlled reactor (TSC/TCR type). In both configurations, the thyristors are the switching elements which turn on when a forward biased voltage occurs and turn off at the natural zero-crossing of the current in the reactor. The only SVC configuration considered in this thesis is the FC/TCR type, for which the one-line schematic layout is shown in Figure 6.1.

Each phase of the TCR consists of two bi-directional valves in series with a switchable linear inductor. The reactive power contributed by the SVC is controlled by switching of the TCR, which increases or decreases the shunt inductor and in turn changes the SVC's equivalent reactances. Hence, the flow of reactive power between maximum and minimum rating of the SVC can be continuously controlled by varying the thyristor's firing angle, α , in the range of $\frac{\pi}{2} \leq \alpha \leq \pi$.

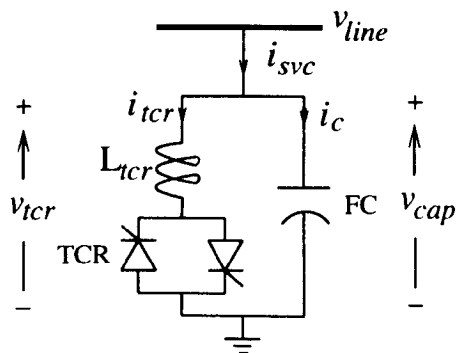


Figure 6.1.: FC/TCR configuration of SVC

6.2.1. Mathematical Model of SVC

A three-phase SVC may be described by a set of differential equations. With reference to Figure 6.1, the voltage equation for one branch of the TCR is given by,

$$v_{tcr} = L_{tcr} \frac{di_{tcr}}{dt} \quad (6.1)$$

with current conduction periods of $0 \leq \omega_s t \leq \pi - \alpha$, $0 \leq \omega_s t \leq 2\pi - \alpha$ and $\pi + \alpha \leq \omega_s t \leq 2\pi$, where $\omega_s = 2\pi f_o$ and f_o is the fundamental frequency of the system. The conduction period can be represented by means of a switching function, s_{tcr} , hence (6.1) becomes,

$$s_{tcr} v_{tcr} = L_{tcr} \frac{di_{tcr}}{dt} \quad (6.2)$$

The switching function s_{tcr} depends on the forward biased voltage and the natural zero-crossing of the current in the reactor.

The voltage equation for the capacitor branch is given as,

$$\frac{dv_{cap}}{dt} = \frac{1}{C} i_c \quad (6.3)$$

Since $v_{line} = v_{tcr} = v_{cap}$, the state equation for the SVC model can be obtained as,

$$\frac{dv_{line}}{dt} = \frac{1}{C} i_c \quad (6.4)$$

$$\frac{di_{tcr}}{dt} = \frac{1}{L_{tcr}} s_{tcr} v_{line} \quad (6.5)$$

A similar representation exist for the other phases of the SVC.

Applying the trapezoidal rule to discretise (6.4) and (6.5), as shown in Appendix B.2, a general description for the three phases SVC is obtained as,

$$[G_{c_{abc}}][v_{line}(t)] = [i_{c_{abc}}(t)] - [hist_{c_{abc}}] \quad (6.6)$$

$$[G_{tcr_{abc}}][v_{line}(t)] = [i_{tcr_{abc}}(t)] - [hist_{tcr_{abc}}] \quad (6.7)$$

The capacitor and TCR variables, including the switching functions, are included in $[G_{c_{abc}}]$ and $[G_{tcr_{abc}}]$, which in turn find their way into the network conductance matrix $[G_{abc}]$ in (3.13). The solution of the network with the SVC included is carried out in a similar manner as presented in Chapter 3.

6.2.2. Time-Step Consideration When Modelling Thyristor Switching

The solution of the phase-domain model is carried out using the trapezoidal rule where a fixed discrete time-step is used throughout the simulation. This can lead to problems when the current zero crossing falls in between two time steps as shown in Figure 6.2. If the turn-off of the thyristor occurs when the inductor is carrying current, a spike can appear in the TCR voltages, as shown in Figure 6.3a, due to the chopping of the inductive current [115].

The most direct solution to this problem is to take a sufficiently small time-step of simulation. However, this solution is not a preferred option since small time-step greatly limit the speed of the computer simulations. A good compromise adopted in this thesis is to use a variable time-step approach where the time-step is suitably reduced around the zero crossing of the current and then returned to normal at other instances [115][116].

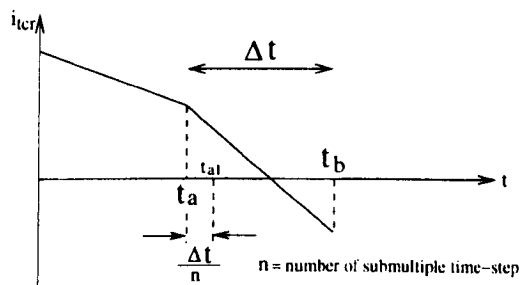


Figure 6.2.: Thyristor switching at current zero crossing

With reference to Figure 6.2, at point t_a the current in the inductor is positive but at the next time-step t_b is negative. If the zero crossing is determined by the change of sign in the current, a degree of inaccuracy would occur in detecting the natural zero crossing. In the proposed method, when the change of sign in the current is detected at t_b , the simulation reverts back to point t_a , without updating variables of the simulations. At this point, the time-step is subdivided into, n sub-steps. The switching instant is now more finely tuned depending on the number of subdivision chosen by the user. In this thesis, the time-step is subdivided by ten times. Upon arriving at point t_b again, the simulations will come back to synchronism with the original time-step. This will continue as normal until the next current zero crossing is encountered where the process will repeat itself.

The typical time-steps of $200\mu s$ would incur an error of 4° , during the zero current crossing which will be reduced by ten times with the variable time-step approach. The improvement in the voltage behaviour using the variable time-step switching method is evident in Figure 6.3b. The spike at the voltage is virtually eliminated.

6. Power Electronics Controllers in the Phase-Domain

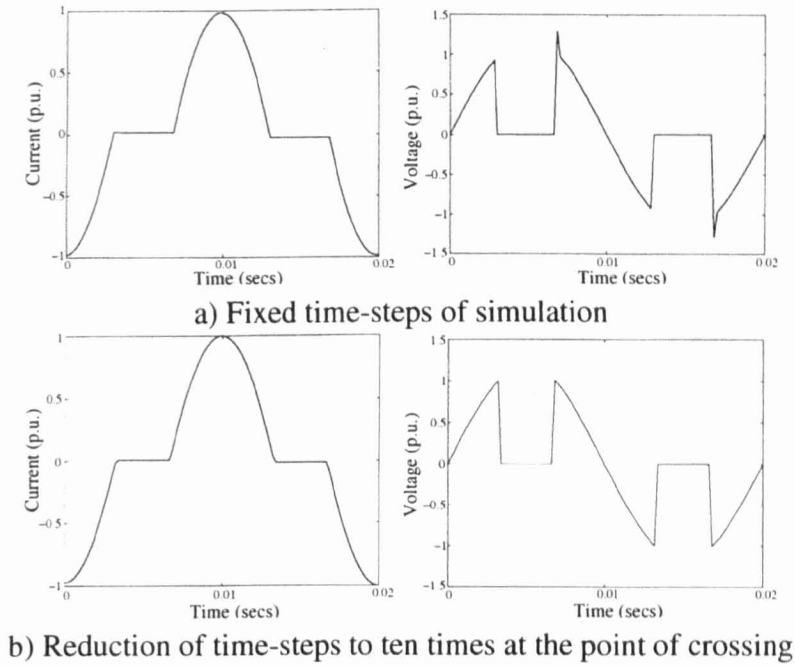


Figure 6.3.: TCR current and voltage waveforms

6.2.3. SVC Control Scheme

The SVC controllers are usually configured to meet individual system requirements. Since application requirements may differ and the control techniques offered by different equipment vendors may vary [51], often very detail controller models may not be necessary.

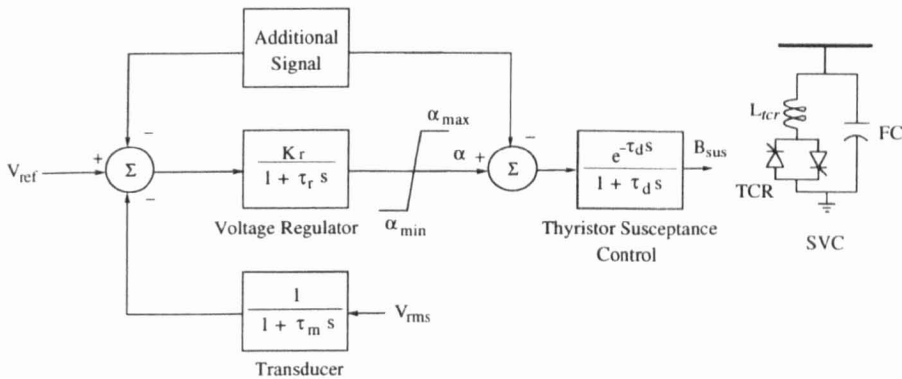


Figure 6.4.: SVC control blocks

The basic SVC controller model for general purpose studies [50][51] is as depicted in Figure 6.4. This controller model is based on the automatic voltage regulator (AVR) scheme [51]. The control block consists of a transducer to obtain the line voltage, the AVR and the thyristor susceptance control block. Further assumptions can be made on Figure 6.4, where the transducer block can be neglected unless the objective is to study the effect of the transducer response on the SVC. The thyristor susceptance control block represents the variation of reactor's susceptance as a function of the firing angle. In most cases the non-linear relationship

6. Power Electronics Controllers in the Phase-Domain

between the susceptance and firing angle is considered to be compensated, hence, leaving this block redundant. With such assumptions, the control scheme of the SVC primarily consists of only the AVR. The AVR is a simple PI control block with a gain of K_r and a time constant τ_r . The AVR takes the feedback voltage from the line and outputs the regulated firing angle for the TCR. An additional signal is sometimes used which can be a signal of speed or frequency of the system. The aim of these signals is to improve power oscillations damping when the network is subjected to severe disturbances.

6.2.4. Application of SVC to Voltage Sags Mitigation During Motor Start-Up

The effect of having the SVC as a source of compensation is analysed in this section based on a similar study case as in Section 4.4 of Chapter 4. The test network is the same as in Figure 4.18, with the SVC replacing the fix capacitor bank at *Node 8* as the compensating device. The SVC is at a *p.u.* rated value of $+1.5/ - 0.6$ *p.u.*.

Figure 6.5 shows the bus voltage at *Node 8* and the thyristor firing angle following a direct online starting of the motor. Various values of SVC controller gain, K_r , were used with a time constant, $t_r = 0.1$ s. It is observed that in the initial period of the sag, the firing angle reaches its maximum value due to the large magnitude of the sag. As the voltage level recovers to the pre-starting value, the firing angle reduces. There is a slight voltage overshoot before the steady state is reached, with the level of the overshoot being dependent on the gain used. Figure 6.6 demonstrated that if a smaller time constant is used, say $t_r = 0.05$ s, the response is faster, with less overshoot. However, a general conclusion is difficult to reach concerning the control parameters of the SVC, as it is dependent on the severity of the events which the SVC is expected to compensate. Hence, the parameters must be tuned correctly to ensure good and stable responses depending on network requirements for each study cases.

The voltage levels are significantly higher with the presence of a SVC then when a fix capacitor bank is used as the compensator. As the voltage drops, the firing angle of the thyristor increases to reduce the SVC inductance making it more capacitive. This increases the available reactive power in the network, hence, increasing the voltage level and enabling the steady state to be reached in a shorter time period. Although improved, the voltage level is still low compare to the pre-starting level. The voltage dependent operation of the SVC is responsible for the low voltage level. Even though a high capacitive reactance is available, the required reactive power cannot be generated due to the low voltage at the SVC terminal. The occurrence of overvoltages prior to reaching the steady state could be due to the delay of the SVC controller. One other major attribute of the overvoltage is the slow discharge of the capacitor, resulting in a prolonged capacitive contribution of the SVC.

The improved voltage response in the presence of a SVC is better appreciated by looking

6. Power Electronics Controllers in the Phase-Domain

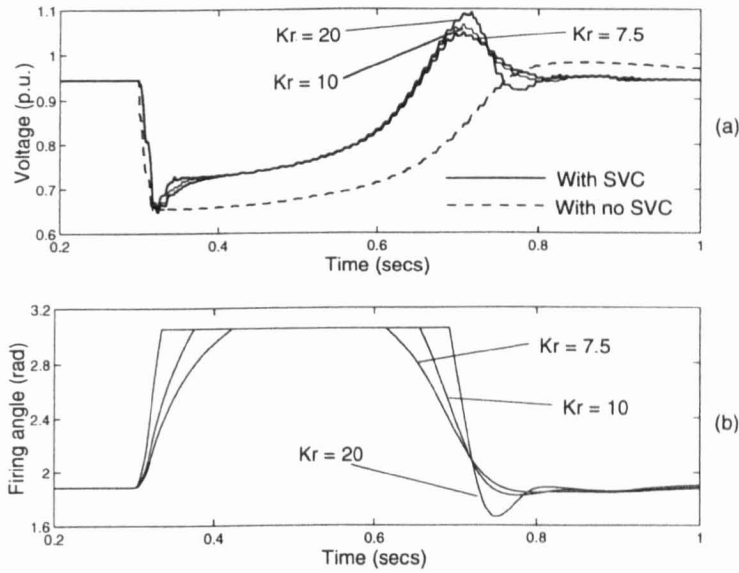


Figure 6.5.: Bus voltage at *Node 8* and the thyristor firing angle following a direct online motor starting with $t_r = 0.05$ s

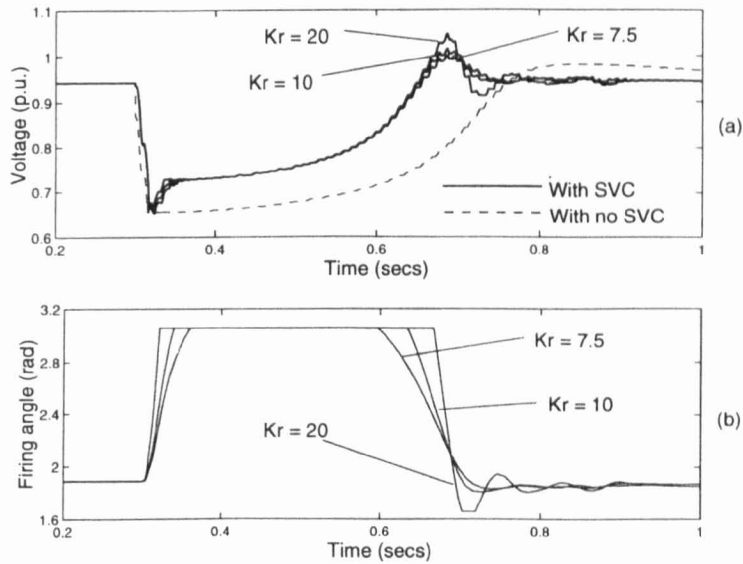


Figure 6.6.: Bus voltage at *Node 8* and the thyristor firing angle following a direct online motor starting with $t_r = 0.1$ s

at the behaviour of the motor speed and electrical torque in Figure 6.7, where it is observed that steady state is achieved in a shorter time. Since the SVC only changes the equivalent reactance and, hence, reactive power, it has little impact on the active power that will be supplied by the network to meet the demand of the motor starting torque. With a large part of the reactive power being supplied by the SVC, the contribution from the network reduces significantly as seen in Figure 6.8b. The motor current is shown in Figure 6.9a where the presence of harmonic distortion is observed in the steady state. The power factor of the motor does not change significantly, as the motor power demand is the same with or without

6. Power Electronics Controllers in the Phase-Domain

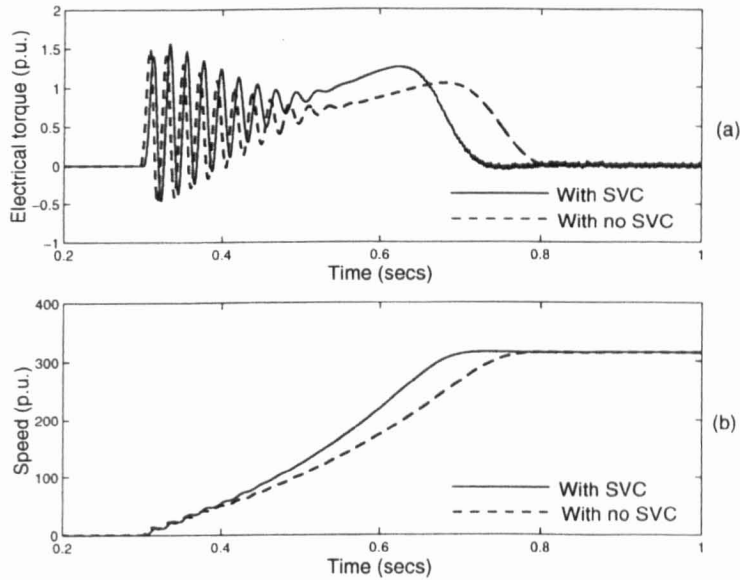


Figure 6.7.: Motor speed and electrical torque following a direct online start-up

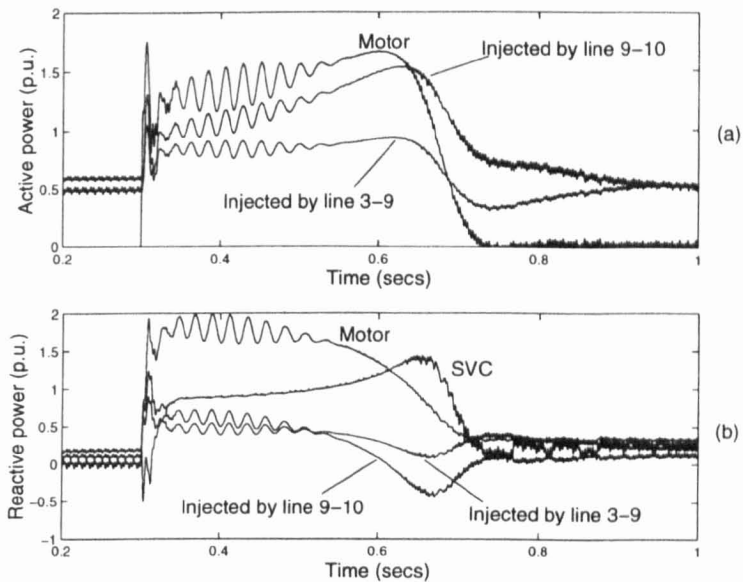


Figure 6.8.: Active and reactive power of motor following a direct online start-up with SVC
the SVC.

6.2.5. Generator Transient Stability Enhancement with SVC

The aim of reactive power compensation in dynamic studies is not limited to voltage sag mitigation but it is also aimed at maintaining network stability following the occurrence of a fault. Dynamically, any system running at the desired output power must maintain the appropriate amount of voltage level at its terminal to ensure power transfer. However, following a fault, the voltage reduces to a level which depends on the location and type of fault. As a result the

6. Power Electronics Controllers in the Phase-Domain

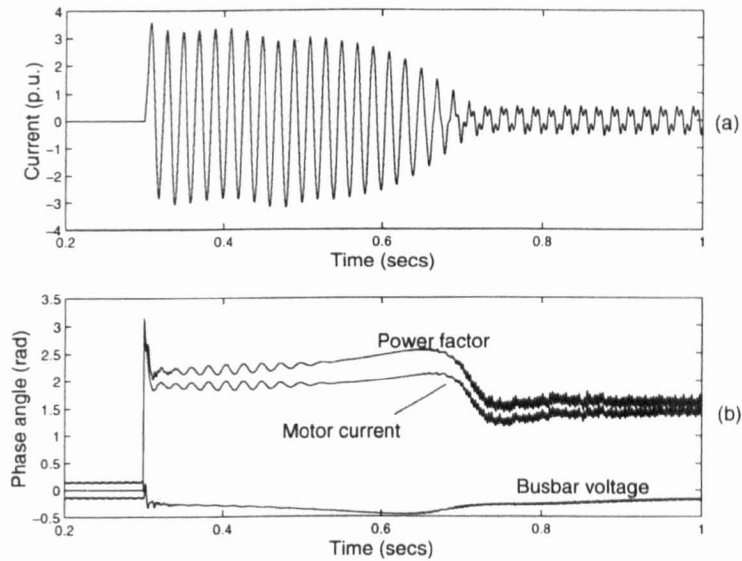


Figure 6.9.: Motor current and phase angle following a direct online start-up with SVC

power transfer between the generator and the network reduces, increasing the acceleration of the generator. The speed of the generator continues to rise until the fault is cleared and the pre-fault power increases in an attempt to decelerate the generator. If the load angle swing of the generator exceeds the maximum angular swing during the fault, stability will never be recovered even after the clearance.

Reactive power compensation can improve the stability of the network by increasing the amount of active power transfer during the fault period by maintaining a higher level of voltage magnitude at the generator's terminal. Hence, the acceleration of the generator can be reduced allowing more time before the maximum angular swing is reached.

The SVC can provide this reactive power compensation capability that helps to stabilise the generator when a fault occurs. A three-phase-to-ground fault is simulated at *Node 7*, near *Gen 2*, at time $t = 0.3s$, where the fault is not cleared for $450ms$. The SVC voltage control loop gain is increased to $K_r = 20$ with $t_r = 0.05s$. If the generator's internal controls, i.e. AVR and turbine governor, are ignored the generator becomes unstable as seen from the simulation results in Figures 6.10 and 6.11. With no AVR to increase excitation, the voltage does not recover, which in turn causes the power output to fall. This drives the load angle above the maximum swing even after the fault is cleared.

On the other hand, the presence of the SVC increases the voltage level during the fault, and more importantly during the post fault period. The higher post fault voltage provides a higher electrical torque output damping the acceleration of the generator. This helps to maintain the generator stability even when there is no generator internal control to increase its excitation. It is observed from Figure 6.12 and 6.13 that the presence of SVC does not significantly affect the stability of the generator when internal controls are available. The AVR provides the excitation required for voltage regulation while the turbine governor adjusts the mechanical

6. Power Electronics Controllers in the Phase-Domain

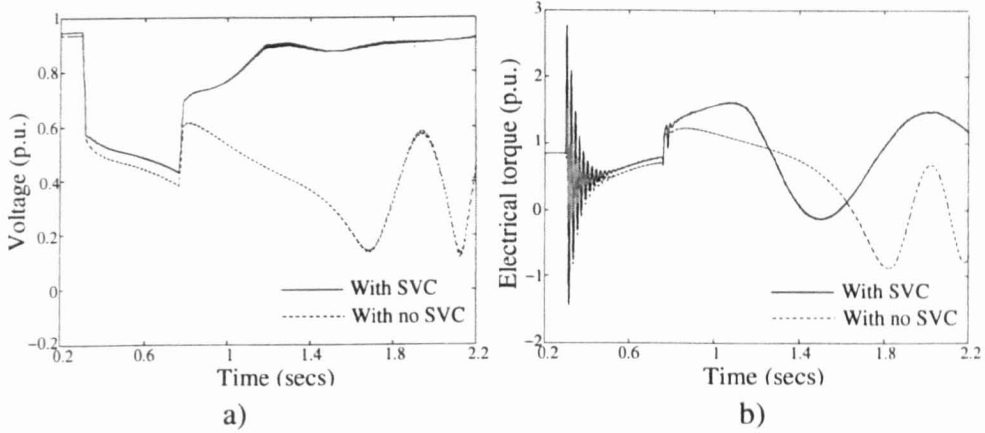


Figure 6.10.: *Gen 3* terminal voltage and electrical torque following a three-phase-to-ground fault without AVR and turbine governor control

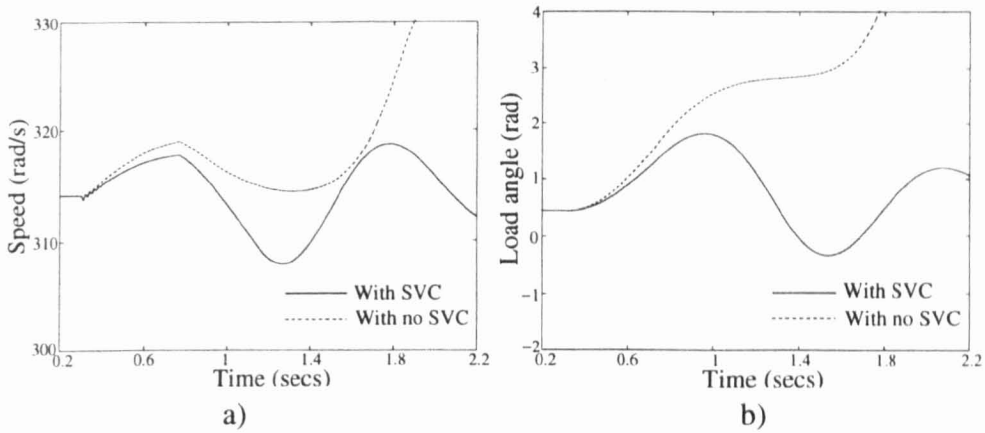


Figure 6.11.: *Gen 3* speed and load angle following a three-phase-to-ground fault without AVR and turbine governor control

torque to reduce the speed change. Nevertheless, the SVC provides additional damping to reduce the first swing of the load angle which in many cases is the most important period in the course of transient analysis.

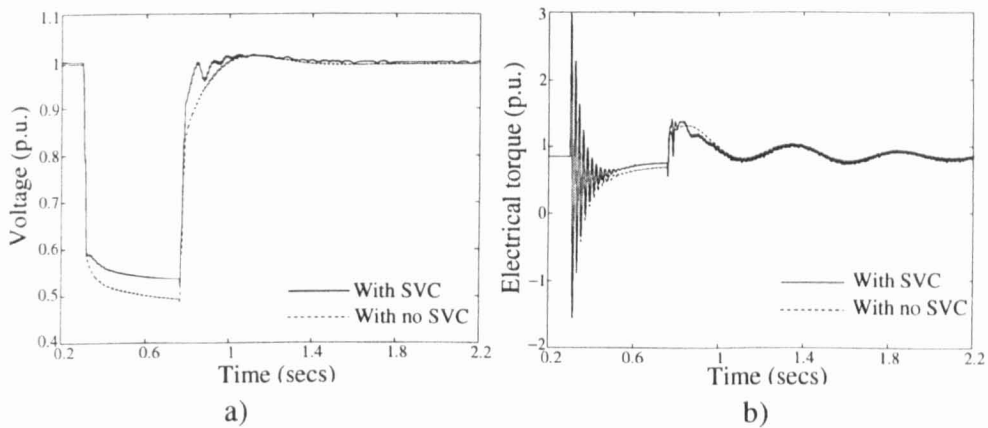


Figure 6.12.: *Gen 3* terminal voltage and electrical torque following a three-phase-to-ground fault with AVR and turbine governor control

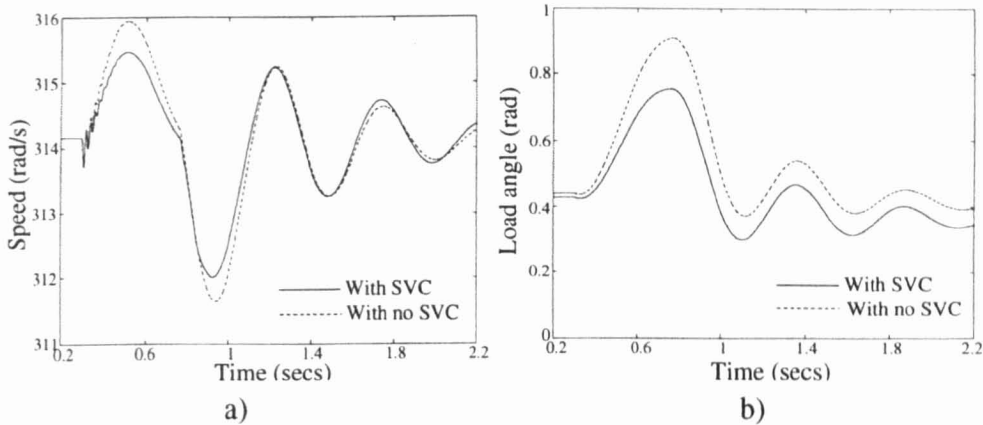


Figure 6.13.: *Gen 3* speed and load angle following a three-phase-to-ground fault with AVR and turbine governor control

6.3. Voltage Source Converter (VSC) Representation in the Phase-Domain

Various types of converter circuits have been suggested over the years for application in high rating switchable power electronics controllers. Unlike thyristor based controllers, the new generation of switchable controllers are constructed with devices such as GTOs or IGBTs with turn-on and turn-off capabilities. Although these switchable controllers may incur higher losses, they have a significant overall system cost and performance advantage [46]. There are two mainstream converter designs; the voltage source converters (VSC) and current source converters (CSC).

For reasons of performance and economics, the VSC are often preferred over the current source converters for power system applications [46]. The VSC using PWM control techniques forms the basis of most modern power electronics controllers such as the STATCOM, DVR and HVDC-VSC stations. These controllers are discussed in this thesis with emphasis on multimachine transient stability. To this end, it is best to develop a generic VSC model, which forms the basic building block with which the most advanced power electronics controllers can be constructed.

The basic idea behind VSC operation is that of AC voltage generation due to a DC source. The DC source can be a battery with constant output or a large capacitor whose output voltage can be controlled. In the VSC, a quasi-sinusoidal voltage waveform of desired magnitude, phase angle and frequency can be produced by resorting to waveform control via PWM switching techniques. The VSC output voltage measured with respect to an existing AC system voltage dictates the direction of active and reactive power exchange between the two systems.

A detailed construction of a three-phase full wave converter is shown in Figure 6.14 where the switching elements are power electronics devices with gate turn-off capabilities, e.g. GTOs

6. Power Electronics Controllers in the Phase-Domain

or IGBTs. The main elements of the VSC are the valves and the DC source. The valves are constructed by connecting in parallel a turn-on/turn-off device and a diode. The DC voltage in this case is a charged capacitor. Comprehensive information on the VSC construction and operation are widely available in the open literature [46][47] and will not be address here.

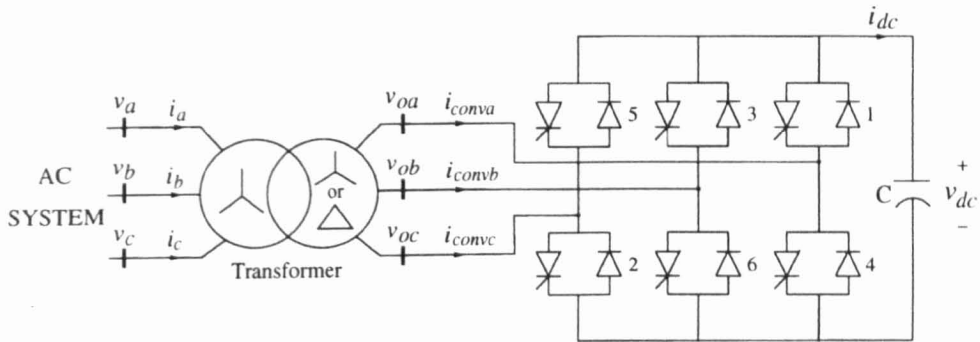


Figure 6.14.: Three phase VSC

In the modelling approach adopted here the operation of the converter valves is modelled as switching functions based on the unipolar PWM technique. The one phase switching process of the VSC's output is as shown in Figure 6.15, where v_r represents the carrier signal with a frequency of f_r and v_c the modulation signal with a frequency of f_s which in this case corresponds to the fundamental frequency. The switching frequency in this case is five times the fundamental frequency. The signal v_c has a magnitude which is determined by the modulation index, m . The switching function $s_a(t)$ is equal to ± 1 when $|v_s| > |v_r|$, and zero otherwise. The switchings for the other phases are shifted by 120° and -120° , respectively.

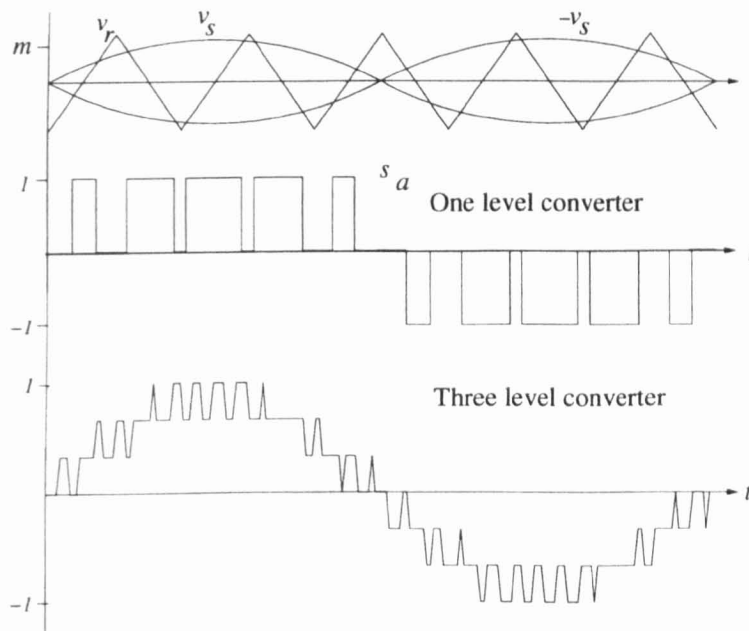


Figure 6.15.: PWM with unipolar switching

Harmonic reduction of the VSC output is possible by increasing the number of six-pulse

6. Power Electronics Controllers in the Phase-Domain

converters, thereby increasing the VSC level. In the modelling approach adopted here, this can be achieved by adding another PWM switching function with the angle of v_r shifted while v_c remains the same [117]. A three level converter can be obtained by having three individual PWM switchings with v_r shifted by 0° , 120° and -120° , respectively. The average of the three PWM switchings will be the output from the three level VSC as shown in the last plot of Figure 6.15.

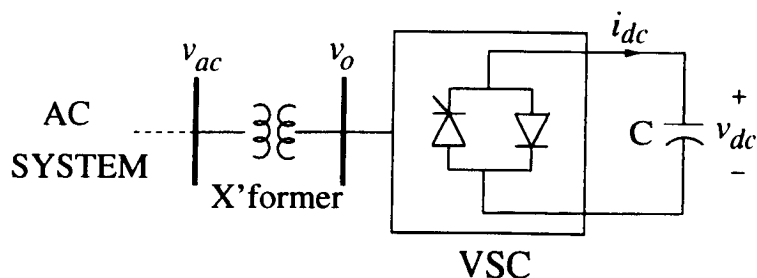


Figure 6.16.: One-line representation of a Voltage Source Converter

The equivalent one-line diagram of the VSC is shown in Figure 6.16 where the following equations are used to describe the waveform conversion process, with the magnitude of the fundamental frequency of the VSC output being a function of the modulation index, m . The voltage angle can be controlled by shifting the angle of v_c with respect to the AC voltage at the terminal of the interfacing transformer.

$$\begin{aligned} v_{oa} &= s_a v_{dc} \\ v_{ob} &= s_b v_{dc} \\ v_{oc} &= s_c v_{dc} \end{aligned} \quad (6.8)$$

The balance of instantaneous power between the AC system and the DC side of the converter is kept, $P_{ac} = P_{dc}$, hence,

$$v_{oa} i_{oa} + v_{ob} i_{ob} + v_{oc} i_{oc} = v_{dc} i_{dc} \quad (6.9)$$

Substituting (6.8) into (6.9), the DC current can be obtained as,

$$i_{dc} = s_a i_{oa} + s_b i_{ob} + s_c i_{oc} \quad (6.10)$$

The general equations describing the model of the VSC in the phase-domain is given from (6.8)-(6.10) together with the DC capacitor equation of,

$$i_{dc} = C \frac{dv_{dc}}{dt} \quad (6.11)$$

Depending on the type of controllers being considered, additional equations may become necessary to represent the connection to the network. The following sections will be dedicated to implementing the VSC model as part of power electronics controllers such as the STATCOM, DVR and HVDC-VSC Station.

6.4. Static Synchronous Compensator (STATCOM)

It has been shown that an enhanced response of power system is strongly linked to having a healthy voltage profile throughout the network [41][48]. One way of achieving this is by modifying the network impedance, which is the approach taken by the SVC. But this approach fail to respond appropriately during critical disturbances associated with slow voltages. An alternative approach to the control of voltage profile is to provide additional voltage source in the network. The rotating synchronous condenser has been used extensively in the past for this purpose. However, the rotating condenser suffers from a number of drawbacks including slow responses, possible rotational instability and lacks application flexibility [122].

The STATCOM is a new kind of compensating controller in power system. It has been designed to obey the operating principles of the rotating synchronous condenser, which has been used extensively in the past for reactive power compensation. However, the STATCOM operation differs from that of its predecessor in many ways, it provides faster responses leading to enhanced system and power quality improvements. Like the synchronous generator, the STATCOM produces three-phase voltages at its terminal. The active and reactive power are dynamically exchanged between the STATCOM and the AC system by suitable control of its output voltage.

The construction of the STATCOM consists of the VSC and a coupling transformer which connects it to the network in shunt. The schematic diagram of the STATCOM is as shown in Figure 6.17 where the transformer is represented by its leakage inductance, L_{lr} .

The exchange of reactive power between the STATCOM and the system is controlled by changing the magnitude of the converter output voltage, v_o . If the magnitude of the output voltage is greater than the AC system, $|v_o| > |v_{line}|$, the STATCOM will generate reactive power and the current flows from the STATCOM to the AC system. For the STATCOM operation with the output voltage below the AC system, $|v_o| < |v_{line}|$, reactive power is being absorbed by the STATCOM and the direction of current flow reverses.

Provided the STATCOM is fitted with an active power source/storage capability, full active power exchange between the STATCOM and the AC system can be achieved by controlling the phase difference between v_o and v_{line} . The STATCOM will provide active power from its source if its output leads the voltage of the AC system and vice versa. In normal STATCOM applications, the control of active power flow is normally performed to charge or discharge

6. Power Electronics Controllers in the Phase-Domain

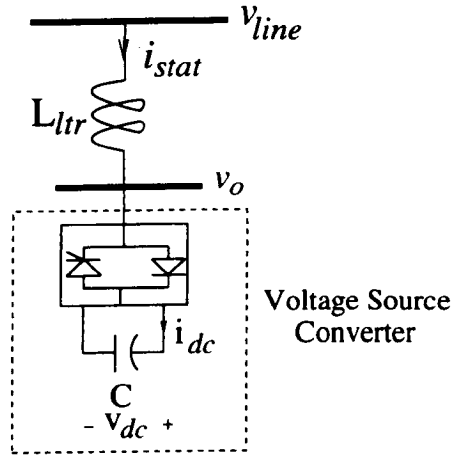


Figure 6.17.: Basic STATCOM configuration

the DC capacitor in order to ensure the DC voltage is fixed at a reference value. If the DC capacitor is very large, the DC voltage can be considered to be fixed at constant value, hence, the control of active power flow is not necessary.

6.4.1. Mathematical Model of STATCOM

The mathematical model of the STATCOM is straightforward to develop once the model of the VSC is available. The only additional equation required is for the transformer which connects the VSC to the network, in shunt. The representation of the STATCOM in Figure 6.17, suggest that the STATCOM may be considered as a controllable voltage source. Hence, the per phase representation of the STATCOM output is given by,

$$\frac{di_{stat}}{dt} = \frac{1}{L_{ltr}} (v_{line} - v_o) \quad (6.12)$$

With the other two phases having similar equations. Since the STATCOM may be seen to act as a voltage source then it may be treated as such and its equations are discretised in very much the same way as the generator model was integrated into the multimachine environment. Applying the trapezoidal rule to (6.12) and taking account of all three phases, the discretised equation is,

$$[v_{line_{abc}}(t)] = -\frac{2L_{ltr}}{\Delta t} [i_{stat_{abc}}(t)] + [hist_{stat}] \quad (6.13)$$

where

$$[hist_{stat}] = [v_{o_{abc}}(t)] + \left([v_{o_{abc}}(t - \Delta t)] - [v_{line_{abc}}(t - \Delta t)] + \frac{2L_{ltr}}{\Delta t} [i_{stat_{abc}}(t - \Delta t)] \right) \quad (6.14)$$

The state variables in the multimachine model are the voltage and the current injection of

6. Power Electronics Controllers in the Phase-Domain

the STATCOM. The term $[hist_{stat}]$ consists of preceding variables and the STATCOM output which is a function of (6.8). The representation of the STATCOM in (6.13) is similar to that of the generator in (3.7), hence its solution in the multimachine environment is carried out as discussed in Chapter 3.

If the dynamics of the DC voltage is to be accounted, for then the equations that governed the capacitor behaviour given by (6.10) and its discretised form, (6.11), are needed,

$$v_{dc}(t) = \frac{\Delta t}{2C} i_{dc}(t) + hist_{dc} \quad (6.15)$$

where

$$hist_{dc} = \frac{\Delta t}{2C} i_{dc}(t - \Delta t) + v_{dc}(t - \Delta t) \quad (6.16)$$

6.4.2. STATCOM's AVR Control

Similarly to the SVC, a general control scheme for the STATCOM can be modelled in relation to an AVR controller. This is reasonable since the action of STATCOM is to improve voltage profile of the network. The generalised control block is given Figure 6.18. The output from the controller is the modulation index, m , which governs the magnitude of the modulation signal for the PWM scheme. Since a constant DC source is assumed for the STATCOM, no controller on the DC side is necessary.

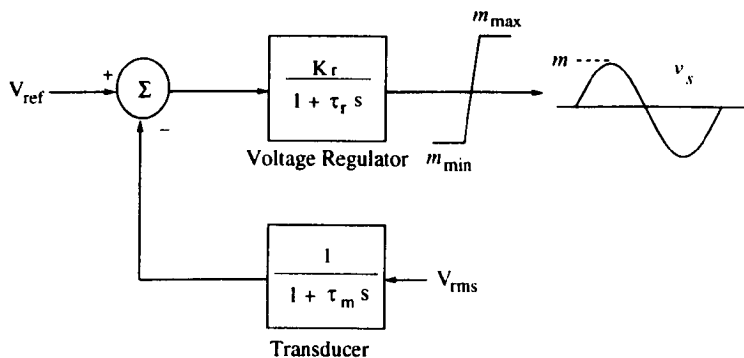


Figure 6.18.: Simplified STATCOM's AVR control blocks

This controller is very general and suitable for simple cases concerning balanced conditions. This general model will be applied to the control of the STATCOM for the case of voltage sags mitigation to enable meaningful comparisons with the SVC. A more detailed controller for asymmetrical operation and overcurrent control is presented at a later section.

6.4.3. Application of STATCOM to Voltage Sags Mitigation During Motor Start-Up

A STATCOM rated at $+1.5/-0.6$ p.u. replaces of the SVC as a shunt compensator in the network of Figure 4.18 in Section 6.2.4. The aim in this study is to correct the voltage sags caused by the motor start-up. The calculation steps to obtain the STATCOM initial parameters and operating conditions are given in reference [117]. In this study, the DC voltage of the capacitor is taken to be fixed, supported by a large capacitor.

Figure 6.19a shows that the voltage level in the initial period of motor start-up is considerably higher with the STATCOM than with the other two compensators. Unlike the SVC and FC, the level of compensation that can be afforded by the STATCOM does not depend on the voltage level of the network. Hence, it functions quite effectively even when the voltage at its terminal is low. The only restriction is that the STATCOM must function within limits depending on its rating. The voltage level also reaches the steady state at a shorter time with less, more gradual, overvoltage peak compared to the SVC. Since the reactive compensation of the STATCOM is not achieved by modifying the network capacitive reactance, no prolong overvoltages due to the discharging of capacitor is experienced unlike in the operation of the SVC.

With a healthier voltage magnitude at its terminal, the motor reaches its steady operation quicker as shown by the simulation results of electrical torque and speed in Figure 6.20. The STATCOM operation is not affected during motor start-up when low voltage levels takes place. It is observed in Figure 6.21b that the STATCOM supplies the rated reactive power which constitute a high percentage of that required by the motor starting. This in turn reduces the need for extra reactive power exported from the network. The active power response is similar to that of the SVC which clearly indicates that the STATCOM is neither providing or absorbing active power from the network. The motor steady state current in Figure 6.22 indicates that STATCOM harmonics is lesser compared to SVC operation. The STATCOM could provide more effective harmonic elimination by increasing the number of its converters and selection of the correct switching frequency.

6.4.4. STATCOM Control and Operation for Asymmetrical Operation

It has been shown that the STATCOM is a very effective tool for voltage sags mitigation, with good speed of response even under severe adverse conditions. It compares favourably with the conventional SVC covered in the previous section. However, the condition considered so far has only involved cases of symmetrical motor starting. The large number of disturbances in the network involving asymmetrical conditions has made it necessary to understand STATCOM operation under conditions when dealing with voltage unbalances, in a common basis.

6. Power Electronics Controllers in the Phase-Domain

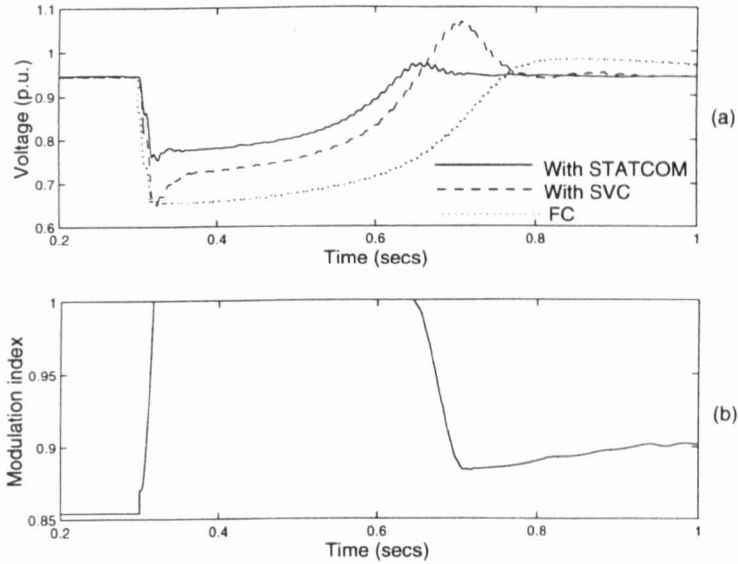


Figure 6.19.: Bus voltage at *Node 8* and converter modulation index following direct on-line motor starting with $K_r = 10$ and $t_r = 0.1s$

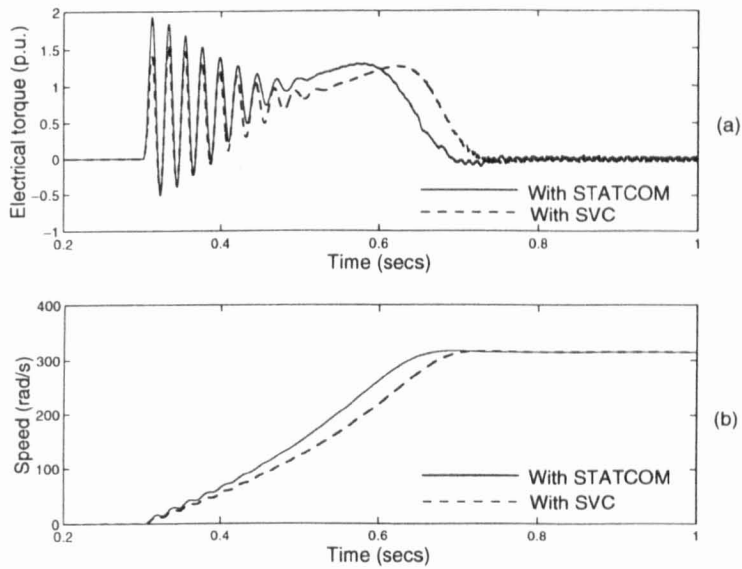


Figure 6.20.: Motor speed and electrical torque following direct on-line motor start-up with $K_r = 10$ and $t_r = 0.1s$

From the sequence domain point of view when the voltages are balanced, the current flow between the STATCOM and the network consists of only positive sequence. During an asymmetrical disturbance the voltage at the faulted phase is quite low compared to the voltages in the healthy phases. On the other hand, the current on the faulted phase will be very large. This prompts the STATCOM to react providing the necessary current to compensate the faulted phase. During unbalance operation, negative sequence components of the current flow between the STATCOM and the network. If the STATCOM is providing the rated reactive power in the positive sequence for the faulted phase, the magnitude of the total current can

6. Power Electronics Controllers in the Phase-Domain

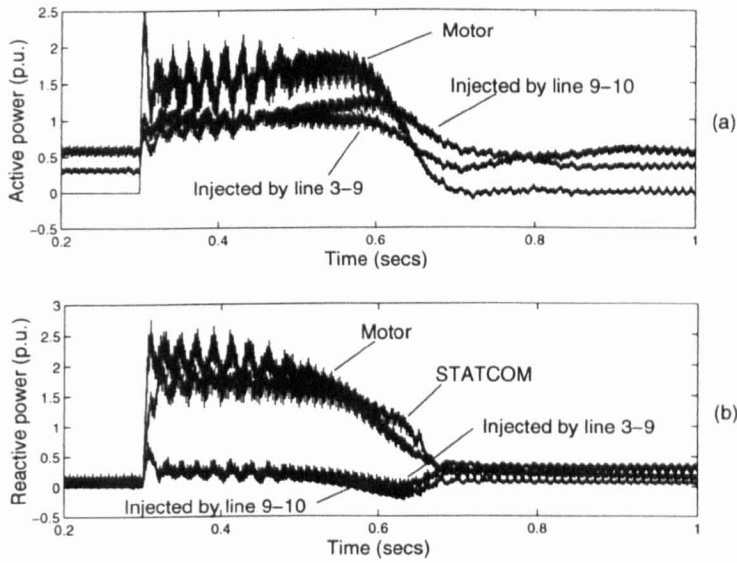


Figure 6.21.: Active and reactive power following direct on-line motor start-up with STATCOM

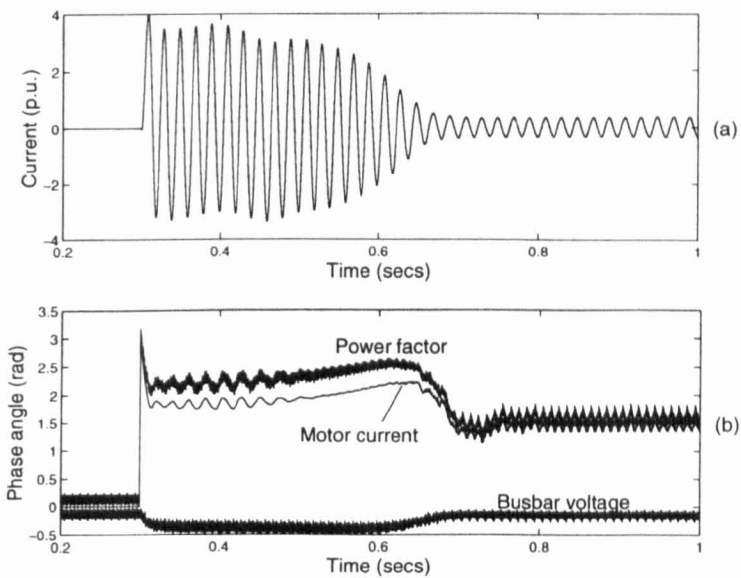


Figure 6.22.: Motor current and phase angle following direct on-line motor start-up with STATCOM

exceed the permitted rating due to the presence of its negative component. This will result in the total phase current in the converter being very large, resulting in stressful conditions that may pose as a treat to the converter [119][121]. In severe unbalanced cases the STATCOM converter is disconnected from the network and forced into a standby mode [120] [123] to prevent damage to the converter and DC capacitor. As a result of disconnection the STATCOM will be off line temporarily even after the fault is removed. Ironically, it is in cases of severe disturbances that the compensator is most needed for voltage support and speedy recovery of the AC system. Hence, a solution is needed to limit the magnitude of the faulted phase current while providing the highest possible amount of reactive compensation.

6. Power Electronics Controllers in the Phase-Domain

Since the amount of reactive power is solely provided by the positive sequence of the current, the overcurrent can be avoided by limiting the negative sequence current during the unbalanced condition. One possible solution is to limit the negative sequence voltage difference between the STATCOM and the AC system [120]. This can be achieved by making the negative sequence voltage of the STATCOM voltage to be the same as AC system's negative sequence voltage through a control loop.

Principle of Control Strategy

The general principle of this control strategy is to monitor both the positive and negative sequence components of the AC system voltage. The separation of the instantaneous voltages into its sequence domain equivalent can be achieved in several ways but the fastest approach is to transform the instantaneous three phase variables into $\alpha\beta$ components and then into dq components where the positive and negative sequence can be easily segregated. The general block diagram of the transformation technique for the transformation is shown in Figure 6.23. The transformation of the instantaneous variables into the two phase reference is given by,

$$\begin{bmatrix} v_\alpha \\ v_\beta \end{bmatrix} = \frac{2}{3} \begin{bmatrix} 1 & -\frac{1}{2} & -\frac{1}{2} \\ 0 & \frac{\sqrt{3}}{2} & -\frac{\sqrt{3}}{2} \end{bmatrix} \begin{bmatrix} v_a \\ v_b \\ v_c \end{bmatrix} \quad (6.17)$$

The transformation from the stationary $\alpha\beta$ reference frame to the synchronous dq reference frame in order to obtain the positive and negative sequence components according to Figure 6.23, is completed by,

$$\begin{bmatrix} v_{pd} \\ v_{pq} \\ v_{nd} \\ v_{nq} \end{bmatrix} = \begin{bmatrix} \cos\omega_s t & \sin\omega_s t & & \\ -\sin\omega_s t & \cos\omega_s t & & \\ & & \cos\omega_s t & -\sin\omega_s t \\ & & \sin\omega_s t & \cos\omega_s t \end{bmatrix} \begin{bmatrix} v_{p\alpha} \\ v_{p\beta} \\ v_{n\alpha} \\ v_{n\beta} \end{bmatrix} \quad (6.18)$$

Figure 6.24 shows the dynamic control scheme for the STATCOM with consideration to both positive and negative sequences [119]. A separate AVR control loop is applied on the individual sequence components. Once the voltages is segregated into their positive and negative dq components, it is converted to its phasor equivalent. The magnitude of the phasor is used in the regulation of the reactive power while the angle is used for active power control.

The control objective of the AVR in the positive sequence is to drive the voltage magnitude to a specified reference value where the error signal is fed into a PI controller. The output from the PI controller corresponds to the voltage drop across the STATCOM transformer leakage reactance. This voltage drop is added to the magnitude of the network voltage to give the desired positive sequence output voltage of the STATCOM. By placing a limiter on the PI

6. Power Electronics Controllers in the Phase-Domain

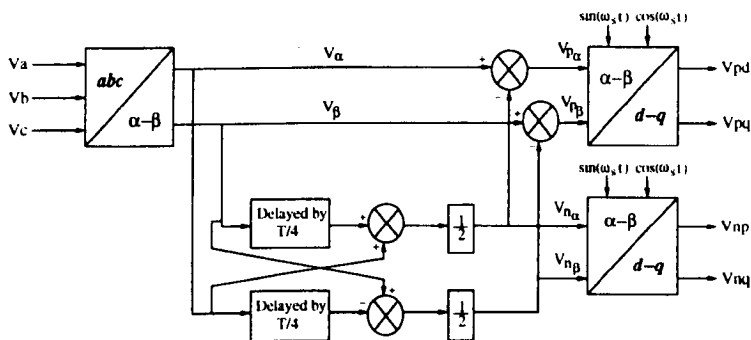


Figure 6.23.: Segregation of instantaneous variables into positive and negative sequence

controllers the magnitude of the inverter current can be controlled to within the permitted value. The phase angle control is not necessary as a simpler separate control loop can be used for regulation of active power exchanged between the AC system and the STATCOM [120][124], as shown in the lower left corner of Figure 6.24. If the active power control loop is ignored the angle of the STATCOM output voltage will be the same as the AC system voltage at all time.

The negative sequence control loop functions in a slightly different manner than the positive sequence. In order to minimise the negative sequence current the voltage of the STATCOM output would need to be the same as the AC system voltage. The magnitude of the AC system negative sequence voltage is compared to a reference value of zero and the error is fed into the PI controller. The output from the PI controller represents the change in the magnitude of the AC system negative sequence voltage, which will be used as the voltage for the STATCOM output.

Once the sequence components have been compensated, the phasor representation of the three phase voltages for the STATCOM output can be obtained by inverse decomposition. The magnitude of the phase voltages are used to obtain the appropriate amplitude of the modulation indices required by the PWM control of the individual phases of the converter. The modulation index is kept within a specified range to avoid over-modulation.

Simulations

The control scheme discussed above is applied to the asymmetrical fault situation considered in Section 4.4.2 based on Figure 4.18, where a single-phase-to-ground fault was simulated near a loaded induction motor. Two control options are considered, in the first instance the negative sequence control loop is neglected and in the second case it is used for overcurrent control. Figure 6.25 shows the voltage response, per-phase, at the terminal of the induction motor. The response with no STATCOM is shown in Figure 4.31a in the previous chapter where the voltage in the faulted phase drops by 70% and the voltage in the other two phases dropping by 20%. With the STATCOM, the voltage drop is less severe where the faulted

6. Power Electronics Controllers in the Phase-Domain

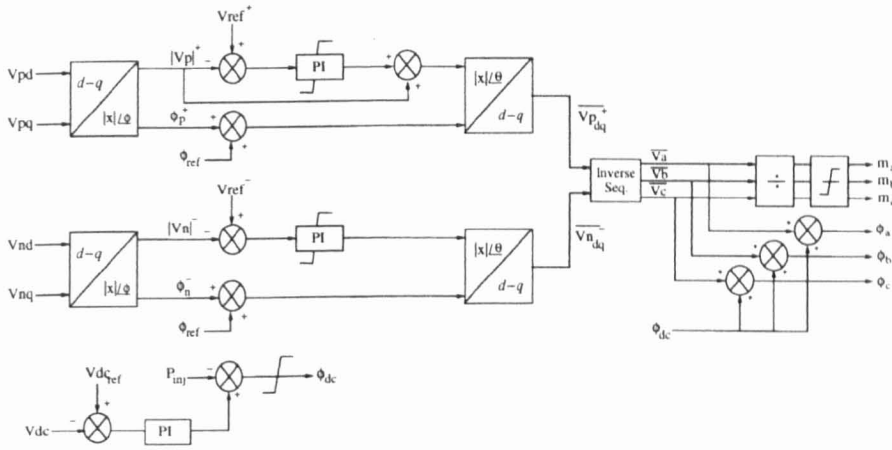


Figure 6.24.: Block diagram of the dynamic control scheme for the STATCOM

phase sags by 25% without the overcurrent control and 36% with the overcurrent control. The other two phases maintained an almost constant voltage throughout the whole period of fault. The speed of response of the motor also improves, as shown in Figure 6.26a where its speed drop is insignificant when the STATCOM is included in the simulation, making the effect of motor re-acceleration less drastic after the fault is removed.

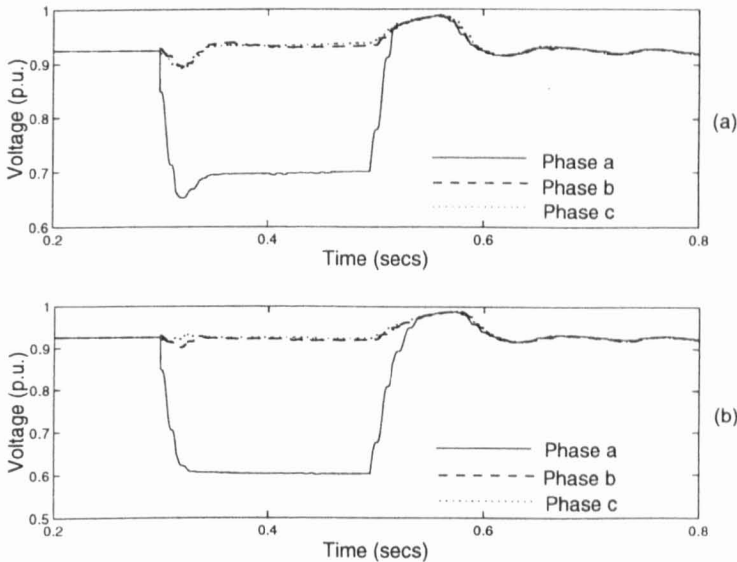


Figure 6.25.: Bus voltage at *Node 8*: a) without overcurrent control; and b) with overcurrent control

It can be observed from Figure 6.27a that the magnitude of the positive sequence voltage is better without the overcurrent control. This is because overcurrent control limits the magnitude of required compensating current that can be supplied by the STATCOM in order to ensure that it is within the permissible limit of the inverter. This is evident in Figure 6.27b where the negative sequence current, with overcurrent control, is almost zero throughout the fault except for the initial transient period and immediately after the fault is cleared. However, without the overcurrent control the negative sequence current is high resulting in

6. Power Electronics Controllers in the Phase-Domain

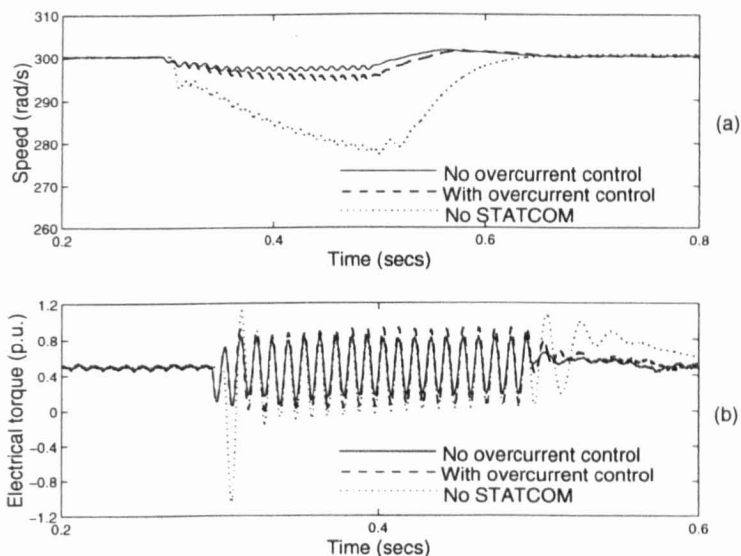


Figure 6.26.: Motor speed and electrical torque with and without overcurrent control

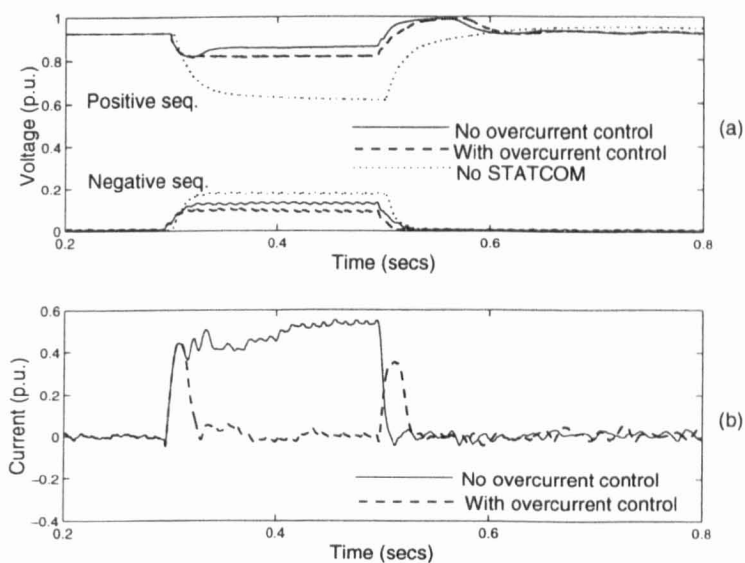


Figure 6.27.: a) Magnitude of positive and negative sequence bus voltage at *Node 8*; and b) Magnitude of negative sequence STATCOM compensating current

the magnitude of the compensating current being large. It is observed from the three-phase instantaneous current response in Figure 6.28 where the faulted phase current can be very high, compared to the other two phases, without the overcurrent control. With overcurrent control the magnitude of the current can be maintained almost level with the other phases. It can be argued that the STATCOM can provide higher compensating current without the overcurrent control but this would be at the expense of putting at risk the converter due to the high unbalances in the phase currents. In such a situation the STATCOM would have to be disconnected from the network if it is not protected by an overcurrent control scheme.

6. Power Electronics Controllers in the Phase-Domain

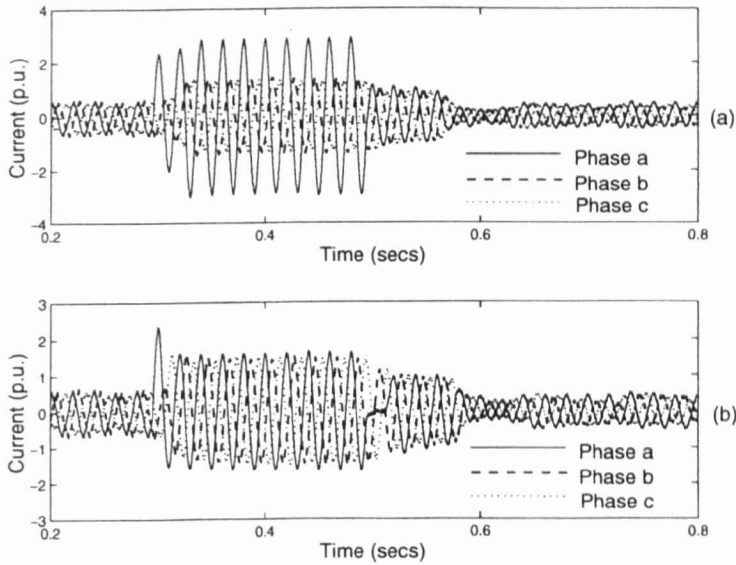


Figure 6.28.: STATCOM compensating current: a) Without overcurrent control; and b) With overcurrent control

6.4.5. Application of STATCOM to a network with fixed speed wind driven induction generator

The interest in distribution network has seen an increase over the last years. One reason for this is that the renewable energy, which is deemed to be the resource of the future, can be connected and integrated with existing generating plants at low voltage distribution level. It is mentioned in Chapter 5 that a dispersed generation scheme involving the particularly popular wind generator still post many problems to the current distribution system.

A major attribute to the problem of power generation using asynchronous generator is its reactive power demand from the network. Unlike the synchronous generator, it does not have complicated internal control that can help to regulate its terminal voltage or to maintain its damping after a disturbance. Voltage compensation is especially important since the induction generator relies on the voltage support at its terminal to provide the reactive power required for its magnetisation. Hence, an external device is necessary to provide for this type of control in order to enhance the performance of the connected induction generator.

The STATCOM, which is both simple and economical, and yet able to operate in both low and high voltage transmission systems, is an ideal choice for voltage compensation in a distribution network. This section emphasise on applying the STATCOM into a distribution network with co-generation scheme, described in Chapter 5, where it is use to improve the transient response of the induction generator.

Transient stability of induction generator with STATCOM

The STATCOM is installed at *Node 8* of the study network in Figure 5.1 where it is the point of connection between the induction generator and the network. A similar analysis where a three-phase-to-ground fault is applied to *Node 9* is performed. Figure 6.29 shows the response of the induction generator's speed and voltage for a clearing time of $CT = 0.217s$. The generator is stable at a clearing time that would have resulted in it being unstable without the presence of the STATCOM as shown in Figure 5.2. The STATCOM helps to regulate the voltage at the terminal of the generator to maintain a significantly higher level during the fault. This provide enough reactive power for the generator to be magnetised throughout the fault period, and hence, reducing the acceleration of its rotor. The additional supply of the STATCOM makes the connection of the generator to the network stronger, hence, the X/R ratio of the connecting line has no significant importance in the stability of the generator as shown by its responses.

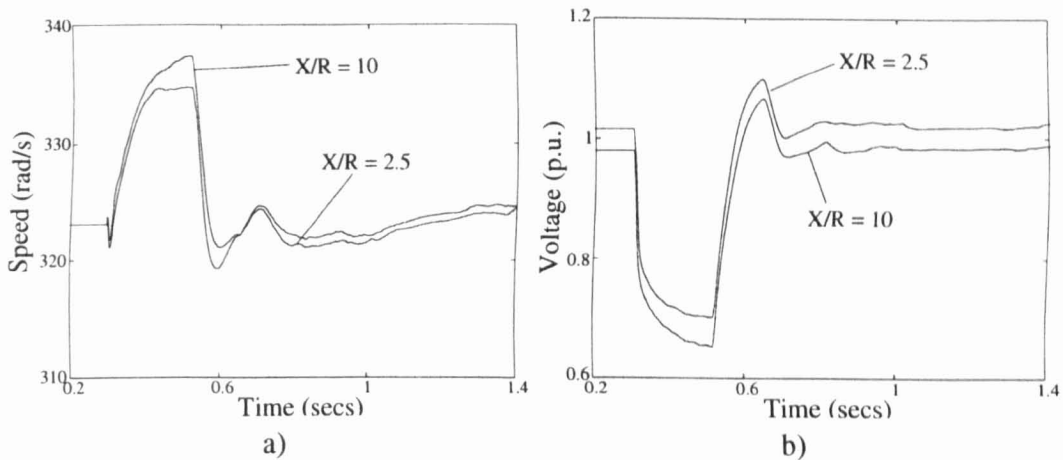


Figure 6.29.: Induction generator speed and terminal voltage cleared at $CT = 0.247s$ with STATCOM in the network

Behaviour of islanded induction generator with STATCOM

In the previous example, the STATCOM has been used to supply the reactive power demand for the induction generator. By doing so the voltage level at the terminal of the generator can be maintain at a higher level in event of a fault. However, when the generator is in self-excitation, due to isolation from the main grid, the STATCOM can be used to absorb the additional reactive power which would cause overvoltages.

The STATCOM was used to stabilise the response of the generator when islanded from the network. The speed and the terminal voltage of the generator and STATCOM are shown in Figure 6.30. It is observed that the speed and voltage level at the terminal of the generator are maintained close to its steady state level. Upon islanding, the STATCOM reacts to absorb the

6. Power Electronics Controllers in the Phase-Domain

reactive power supplied by the capacitor bank, which regulates the reactive power available for the generator. This limits the self-excitation of the generator avoiding any overvoltages at its terminal. The right amount of retarding torque are then produced by the generator to avoid further acceleration.

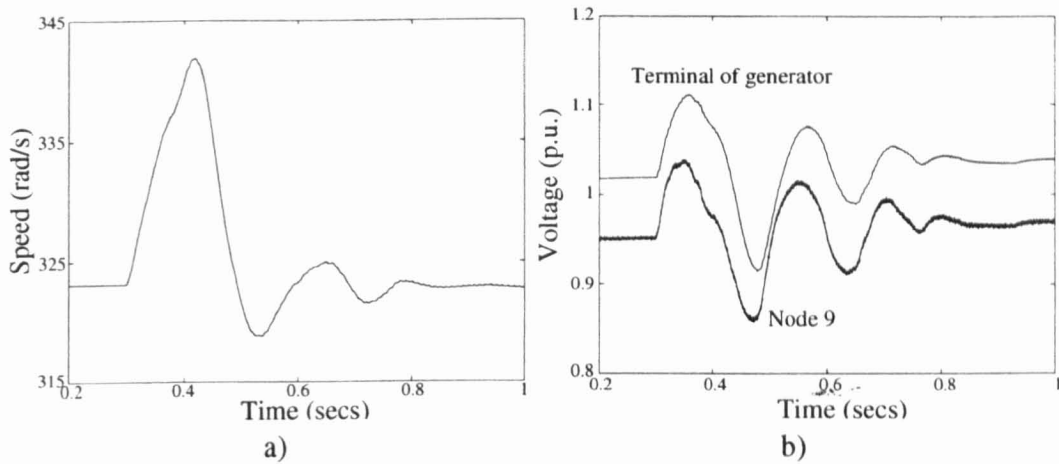


Figure 6.30.: Islanded induction generator speed and terminal voltage with no isolated load with STATCOM

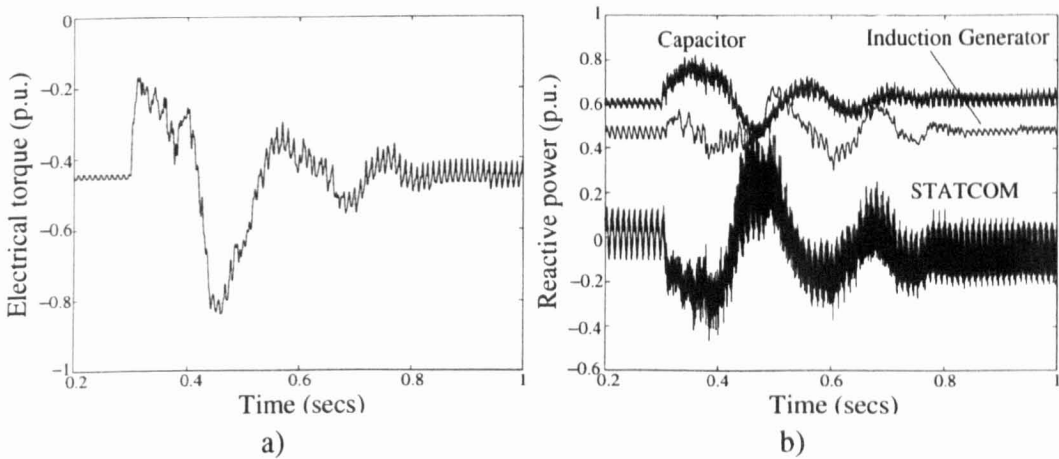


Figure 6.31.: Islanded induction generator torque and reactive power with no isolated load with STATCOM

6.5. The Dynamic Voltage Restorer (DVR)

The increased use of electronics loads in our everyday activities, which are highly sensitive to even very minor supply disruptions, has drawn attention from both customers and suppliers to the issue of power quality. Voltage sags, which are known to cause heavy disruptions resulting in substantial financial losses [91], are among the most prominent of all power quality problems. The high frequency occurrence of voltage sags has led to the development of a variety of power electronics controllers to overcome the problem. The SVC and STATCOM

6. Power Electronics Controllers in the Phase-Domain

have been shown to provide a source of voltage compensation but they do not have the ability to maintain constant voltage profile at the load throughout the period of the fault.

A more suitable approach is to use a series voltage source connected directly to the terminal of the load. Ideally, this compensator should provide the exact amount of voltage deficit during a sag in order to ensure uninterrupted supply to the load. Unlike conventional series compensators that are based on thyristor control of passive elements to change the X/R ratio of a line, the DVR is based on the VSC technology. The DVR in fact may be seen as a STATCOM connected in series with the network through its coupling transformer.

The schematic layout of the DVR is shown in Figure 6.32, where its function is to protect the load voltage as indicated in the picture. The DVR functions by injecting three single phase AC voltages in series with the three phase incoming network voltages during a voltage sags. The action of the DVR is to compensate for the difference between the faulty and normal voltages [126][127]. All three phases of the injected voltages are of controllable amplitude and phase. During steady operation, the DVR is in standby mode and its series transformer functions as a short-circuited current transformer [127].

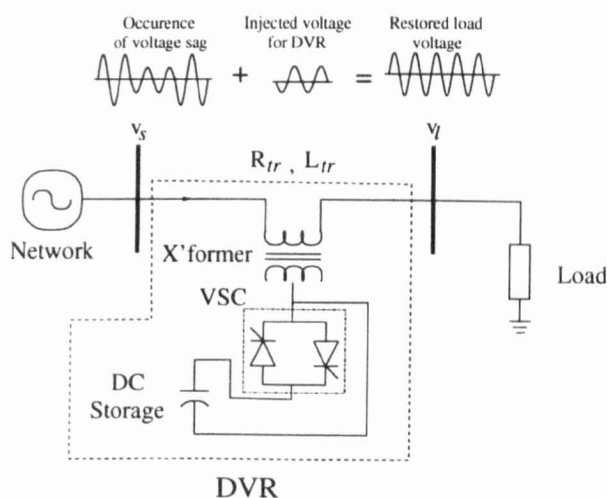


Figure 6.32.: Basic DVR configuration and connection to the network

6.5.1. Mathematical Model of DVR

The basic model of the DVR has been addressed in the previous sections, as it is based on the operation of the VSC. The challenge now is to find a way to integrate the model into the existing multimachine network environment. This can be achieved by treating the DVR as an embedded voltage source at the point of connection.

In connection with Figure 6.32, the voltage state relationship can be expressed as,

$$v_s + v_{dvr} - v_l = R_{tr}i_l + L_{tr}\frac{di_l}{dt} \quad (6.19)$$

6. Power Electronics Controllers in the Phase-Domain

Discretising this equations using the trapezoidal rule the following equation is obtained,

$$v_s(t) - v_l(t) = \left(R_{tr} + \frac{2}{\Delta t} L_{tr} \right) i_l(t) + hist_{sl} \quad (6.20)$$

where

$$hist_{sl} = \left(R_{tr} - \frac{2}{\Delta t} L_{tr} \right) i_l(t - \Delta t) - (v_s(t - \Delta t) - v_l(t - \Delta t)) - (v_{dvr}(t) - v_{dvr}(t - \Delta t)) \quad (6.21)$$

The discretised equations (6.20) and (6.21) are similar in form to those of a given network branch presented in Appendix B.2. By making $i_l(t)$ the subject, it can then be incorporated into the complete network representation as in (3.13). The exception being the additional term within $hist_{sl}$ which represents the injected voltage of the DVR. The inclusion of the DVR voltage does not complicate the multimachine network representation as it can be added as an input vector within the preceding terms of $[hist_{abc}]$ in (3.13) for branches where a DVR exist.

6.5.2. Dynamic Voltage Restorer Control Scheme

The control of the DVR is based on the tracking of the load side voltage [128][129]. The main objective is to maintain the voltage $v_l(t)$ at the desired reference value. The tracking error between the reference and the actual load voltage must be minimised during a disturbance. Manipulating equation (6.19) to make v_l the subject and representing the current flow across the reactances as a voltage drop we obtain,

$$v_l = v_s + v_{dvr} - v_{drop} \quad (6.22)$$

The tracking reference voltage is introduced into (6.22) where the difference between the reference and the load voltage should be zero, hence,

$$\begin{aligned} V_{ref} - v_l &= V_{ref} - (v_s + v_{dvr} - v_{drop}) \\ 0 &= V_{ref} - (v_s + v_{dvr} - v_{drop}) \end{aligned} \quad (6.23)$$

The desired instantaneous value for the DVR output is thus obtained as,

$$v_{dvr} = V_{ref} - (v_s - v_{drop}) \quad (6.24)$$

The instantaneous representation can be decoupled into their phasor equivalents by performing frame-of-reference transformations as described for the STATCOM. The DVR control in the transformed domain is as shown in Figure 6.33. The instantaneous voltage drop across

6. Power Electronics Controllers in the Phase-Domain

the line is obtained by multiplying the branch current and the reactances. The reference value for the positive sequence component is obtained from decoupling the instantaneous reference. The summation point is designed to replicate the operation of equation (6.24) in the decoupled parameters. The PI controllers is added to ensure smooth output from the DVR.

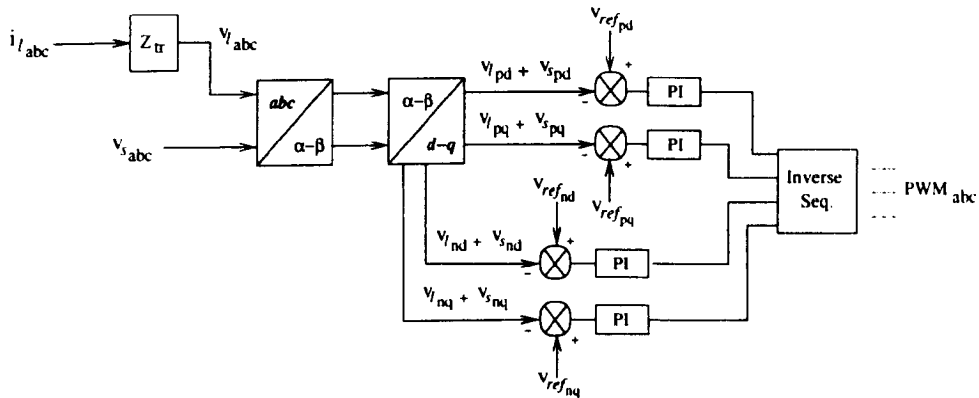


Figure 6.33.: DVR control scheme

6.5.3. DVR Simulations and Results

A DVR is assumed to exist in the test circuit used in Section 4.4.2 based on Figure 4.18 of Chapter 4, where it is installed in the line connecting the terminal of the induction motor to *Node 8* which acts as a common coupling point of the motor to the rest of the network. The section of the network where the DVR is installed is shown in Figure 6.34. The purpose of installing the DVR at this location is to protect the induction motor from any possible voltage sags that might occur in the network. The application of the DVR is ideal in this case since the operation of the induction motor is highly sensitive to voltage disturbances.

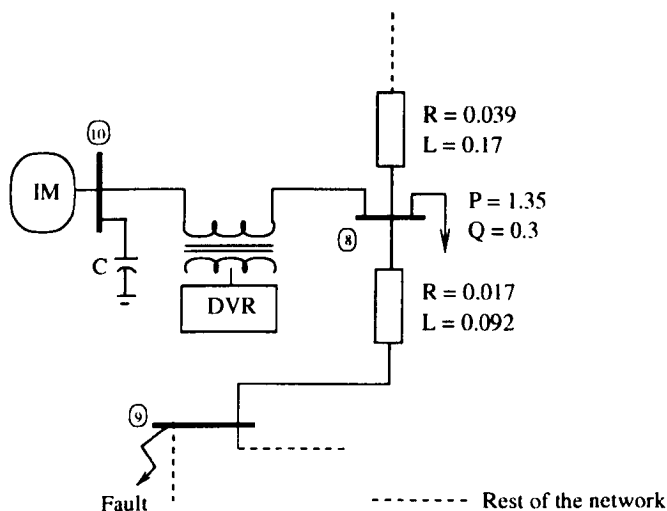


Figure 6.34.: Section of test network as in Figure 4.18 with DVR installed between the induction motor and common coupling point

6. Power Electronics Controllers in the Phase-Domain

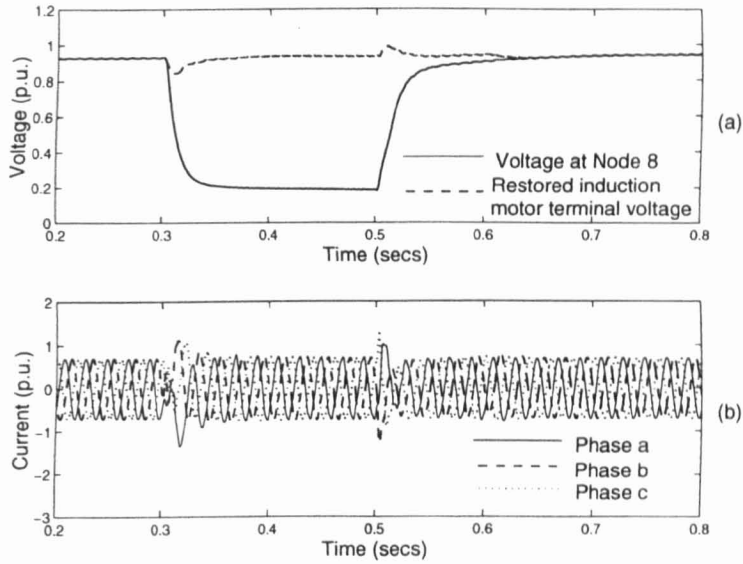


Figure 6.35.: a) Common coupling point voltage and motor terminal voltage; and b) Motor current when subjected to a three-phase-to-ground fault with DVR

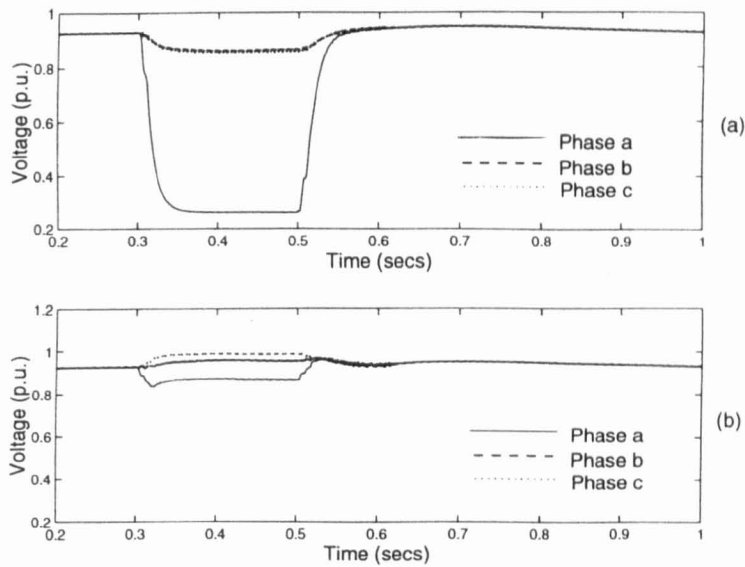


Figure 6.36.: Single-phase-to-ground fault with DVR; a) Common coupling point voltage at *Node 8*; and b) Motor terminal voltage

Different fault conditions are simulated where the fault is applied at a time $t = 0.3$ s for a duration of 200ms. The voltage at the terminal of the induction motor and at *Node 8* is shown in Figure 6.35a. It is observed that the voltage at *Node 8* will experience a sag in the event of a three-phase-to-ground fault in the network. However, due to the restoring action of the DVR the voltage at the terminal of the motor maintains an almost constant profile throughout the period of the fault. The improved response of the motor terminal voltage also reduces the post-sag duration of the voltage as compared to the case where no DVR is used as shown in Figure 4.26a. The constant voltage profile at its terminal enables the motor to maintain its operating speed as shown in Figure 6.38 where during the post-fault period, the

6. Power Electronics Controllers in the Phase-Domain

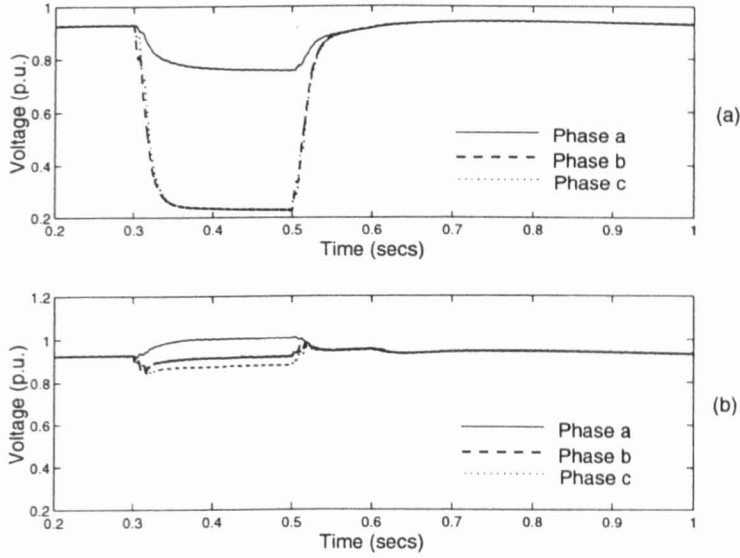


Figure 6.37.: Phase-to-phase fault with DVR; a) Common coupling point voltage at *Node 8*; and b) Motor terminal voltage

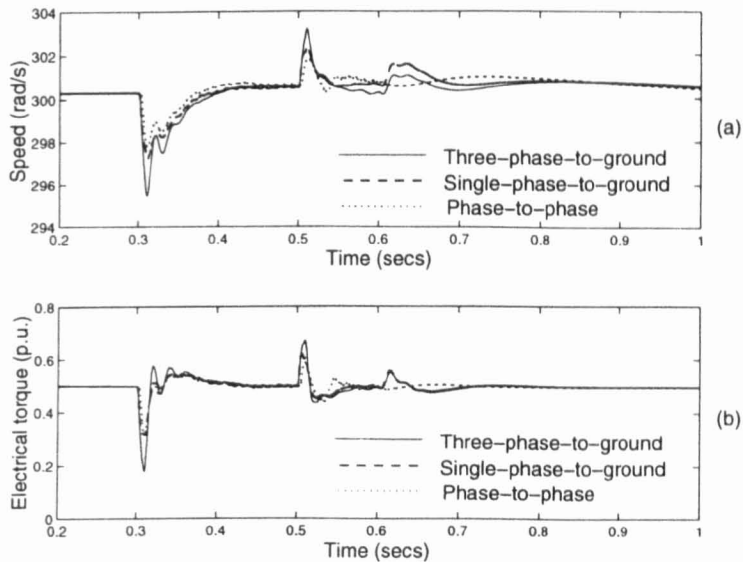


Figure 6.38.: Loaded motor speed and electrical torque subjected to various fault conditions with DVR

re-acceleration time of the motor is negligible. This provides for the faster recovery of the voltage since no extra reactive power is required from the network for the re-magnetisation of the motor.

The operation of the DVR under asymmetrical condition is also investigated where it is used to restore unbalanced voltage sag. A single-phase-to-ground and a phase-to-phase fault are performed and the results are as shown in Figure 6.36 and 6.37. It is observed in both cases that the voltage at the terminal of the motor is not greatly affected by the sags at the coupling point. The presence of the DVR almost eliminates the effects of the motor voltage unbalances present in Figure 4.31 and 4.33 of the previous chapter. The post-fault recovery period

6. Power Electronics Controllers in the Phase-Domain

of the coupling voltage also improves due to the small change in the motor speed. More significant is the observation that the second harmonic of the electrical torque that exists under unbalanced voltage conditions is totally cancelled out when the DVR operates to restore the voltage balance.

The observations reveal that the DVR is very effective in restoring voltage at the terminal of the motor under all fault conditions. The presence of the DVR also improves the coupling point voltage especially during the post-fault period where the recovery time is significantly reduced. While SVC and STATCOM are effective in achieving voltage compensation in the network, the DVR should be the ideal choice when direct protection of a sensitive load is of concern.

6.6. HVDC-VSC Station

Interest in the use of VSCs for HVDC stations is increasing rapidly due to their economical and technical advantages. The HVDC-VSC is based on the operation of the VSC technology as is in the STATCOM and DVR. The basic building blocks of a HVDC-VSC are as shown in Figure 6.39, where two VSC stations are linked together by a DC-link cable. As mentioned earlier, the switching elements used in the converters are high speed switches capable of turn-on and turn-off by applying gating signals at a frequency rate higher than the fundamental frequency. The gating signals are controlled by PWM technique. The AC system is connected to the terminal of the HVDC-VSC station through the interfacing transformers.

6.6.1. Phase Domain HVDC-VSC Model

The AC output of the HVDC-VSC system is similar to that of the VSC described in earlier sections. The per-phase voltage output for both VSCs are hence given by,

$$v_{o1} = s_{a1}v_{dc1} \quad (6.25)$$

$$v_{o2} = s_{a2}v_{dc2} \quad (6.26)$$

The DC-link connection between the two VSC stations can be represented by an equivalent DC network resembling a π – circuit as shown in Figure 6.39. It should be remarked that there exist an instantaneous power balance between the AC and DC systems, giving rise to the following equations for VSC1,

$$P_{ac1} = P_{dc1} \quad (6.27)$$

$$v_{oa1}i_{a1} + v_{ob1}i_{b1} + v_{oc1}i_{c1} = i_{dc1}v_{dc1} \quad (6.28)$$

6. Power Electronics Controllers in the Phase-Domain

Substituting (6.25), with the other phases represented in similar manner, into (6.28), i_{dc1} can be obtained as,

$$i_{dc1} = s_{a1}i_{a1} + s_{b1}i_{b1} + s_{c1}i_{c1} \quad (6.29)$$

Similarly the DC current for VSC2 can be obtained as,

$$i_{dc2} = s_{a2}i_{a2} + s_{b2}i_{b2} + s_{c2}i_{c2} \quad (6.30)$$

The following network equations are obtained from the DC network for VSC1,

$$i_{dc1} = i_{dx} + i_{c1} \quad (6.31)$$

$$i_{c1} = C_1 \frac{dv_{dc1}}{dt} \quad (6.32)$$

With (6.31) substituted into (6.32),

$$\frac{dv_{dc1}}{dt} = \frac{1}{C_1} (i_{dc1} - i_{dx}) \quad (6.33)$$

For the DC-link of VSC2,

$$i_{dc2} = i_{c2} - i_{dx} \quad (6.34)$$

$$i_{c2} = C_2 \frac{dv_{dc2}}{dt} \quad (6.35)$$

With (6.34) substituted into (6.35),

$$\frac{dv_{dc2}}{dt} = \frac{1}{C_2} (i_{dc2} + i_{dx}) \quad (6.36)$$

The current flowing in the DC-link cable is given by,

$$\frac{di_{dx}}{dt} = \frac{1}{L_x} (v_{dc1} - v_{dc2} - R_x i_{dx}) \quad (6.37)$$

It can be observed that the variables are the DC voltages across the capacitors of the two VSCs and the current in the cable. In order to keep the model of the HVDC-VSC consistent with the multimachine model, a discretisation representation must be developed. Hence, equations (6.33), (6.36) and (6.37) are discretised using the trapezoidal rule of integration,

$$v_{dc1} = \frac{\Delta t}{C_1} \left(i_{dc1} - \frac{i_{dx}}{2} \right) + hist_{dc1} \quad (6.38)$$

$$v_{dc2} = \frac{\Delta t}{C_2} \left(i_{dc2} + \frac{i_{dx}}{2} \right) + hist_{dc2} \quad (6.39)$$

$$i_{dx} = \left(1 + \frac{R_x \Delta t}{2L_x} \right)^{-1} \left(\frac{\Delta t}{2L_x} v_{dc1} - \frac{\Delta t}{2L_x} v_{dc2} + hist_{dx} \right) \quad (6.40)$$

6. Power Electronics Controllers in the Phase-Domain

The term *hist* represents the variables known from preceding time steps. The DC-link network equations are solved simultaneously with the equations describing the VSCs to obtain the output in a discretised form suitable for general network solution.

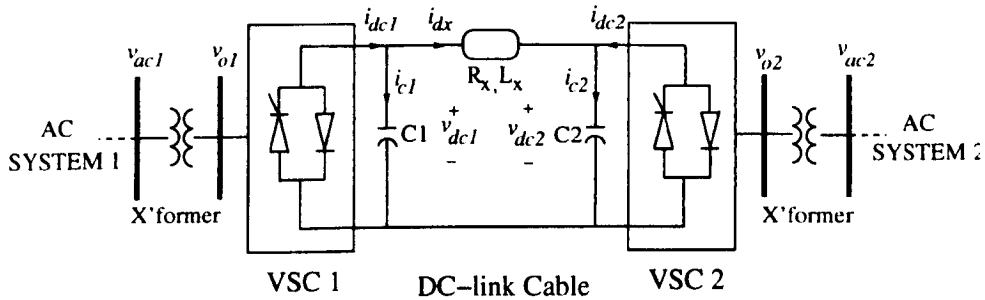


Figure 6.39.: HVDC-VSC configuration

6.6.2. Operations and Control of the HVDC-VSC

The power exchanged between the AC and DC system in an HVDC-VSC is defined by the fundamental voltage across the VSC. The active power flow between the converter and the AC system is controlled by the voltage angles and the reactive power flow is controlled by the magnitude of the voltages. The application of PWM techniques enables the control of the voltage angle and magnitude of the VSCs to be varied almost instantaneously.

There are two required functions of the HVDC-VSC in order to ensure that the AC and the DC systems connect robustly. The required functions are the active power dispatch control and the DC-link voltage regulation [130]. The individual VSC stations can be selected to control either of the assigned functions.

The control of the active power dispatch involves maintaining a reference point for active power in the converter station. The selected VSC must vary its output voltage angle to function as an inverter or rectifier based on the direction of power flow. The error between the reference power and the actual power of the VSC must be minimal. The control block is as shown in Figure 6.40 where VSC1 is selected for power dispatch control.

The exchange of active power between the AC system and the VSC will result in a variation of the DC-link voltage. If the AC system provides more active power than that demanded by the load and the converter losses, the excess power will be absorbed by the VSC resulting in an increase in the DC-link capacitor voltage. If this active power is less than the load demand and the converter losses, the DC-link capacitor voltage will decrease. It is important to maintain the voltage across the capacitor constant for the HVDC-VSC to ensure a continuous power flow.

Hence, one of the VSC stations will be needed to regulate the DC-link voltage of the HVDC-VSC stations at a given reference point. The DC voltage regulation control loop is as shown in

6. Power Electronics Controllers in the Phase-Domain

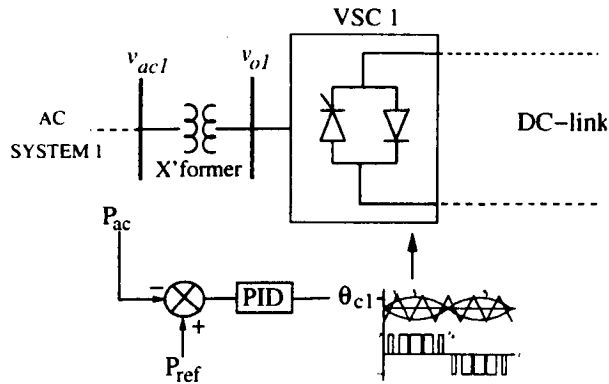


Figure 6.40.: Power dispatch control

Figure 6.41. The voltage angle of VSC2 is adjusted to ensure that the power flow is enough to maintain the DC-link capacitor charged at a desired level. In other words, the voltage regulator control ensures that the right amount of AC power is converted in one VSC from an AC system to satisfy the power requirements to be dispatched onto the other AC system.

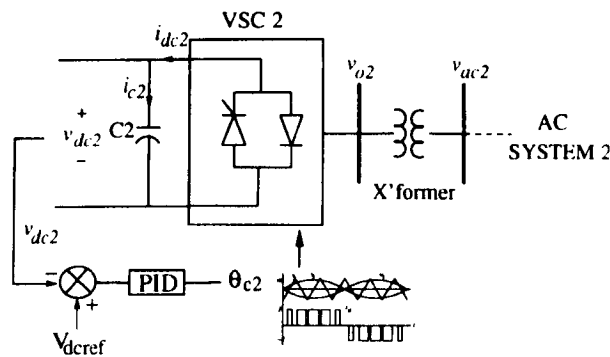


Figure 6.41.: DC voltage regulation control

6.6.3. Real-time Implementation of the HVDC-VSC Model for Application in a Scaled-Down WECS

The application of the HVDC-VSC model is well suited for the connection of off-shore wind-farm as its VSC based technology allow for continuous operation of the DC-link even if one side of the AC system is disconnected [132]-[134]. This is in contrast to the current source converter technology, which needs to be shut down if one side of the AC system becomes disconnected.

This section covers the implementation of the HVDC-VSC model in an application study involving an actual WECS through real-time simulation. A scaled-down laboratory model of a WECS is used to represent the wind generator and the HVDC-VSC is applied to control the power flow between the WECS and the AC system.

Scaled-down Laboratory WECS Model

The scaled-down model of the WECS is constructed using a three-phase induction machine coupled to a DC servomotor. The speed of the servomotor, which drives the induction machine, can be adjusted by its excitation voltage. Hence, this excitation voltage is assumed to be equivalent to the wind speed. The induction machine runs at synchronous speed until the servomotor driving it reaches a cut-in speed where it will then run as a generator. The schematic of the scaled-down WECS setup is as shown in Figure 6.42. The power output from the induction generator is monitored by acquiring the voltage and current generated using the respective transformers.

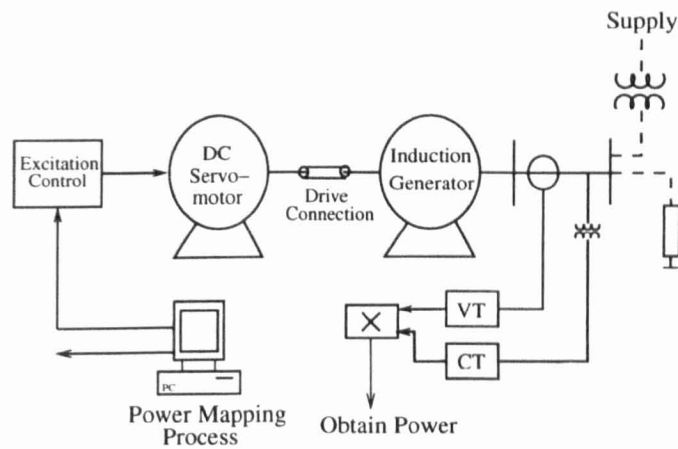


Figure 6.42.: Schematic diagram of the scaled-down WECS

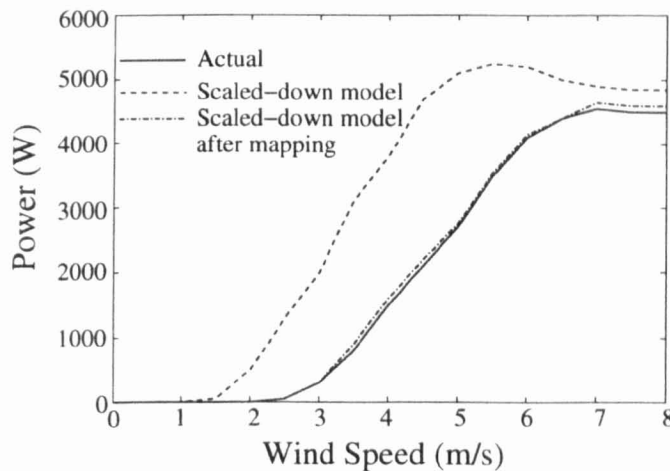


Figure 6.43.: Scaled-down WECS power characteristics

In order to study the behaviour of an actual wind generator using this scaled-down modelling approach, the output of the generator must reflect the actual characteristic of the wind generator. This can be achieved by first studying the power vs. speed characteristics of the scaled-down model [135] where the speed corresponds to the servomotor excitation voltage and the power is the output from the induction machine. A transfer function is developed

6. Power Electronics Controllers in the Phase-Domain

to illustrate the relationship between this input excitation voltage and the output power. The characteristics of the scaled-down model can then be obtained as shown in Figure 6.42. The value of the power is scaled to the actual characteristic in the range of kW.

It is observed that a mismatch occurs between the characteristics of the scaled-down model and the actual system. This can be overcome by mapping the characteristics of the scaled-down model to the actual system as shown in Figure 6.43. With this mapped characteristic, which correctly represents the actual system, a new set of excitation voltages for the servomotor can be obtained using the transfer function approach.

With the flexibility in the transfer function approach to characterise the input and output, the scaled-down model can be constructed with any type and rating of DC servomotor and induction machine. The mapping process allows the actual generator characteristic of any system to be represented accurately with this transfer function approach [135].

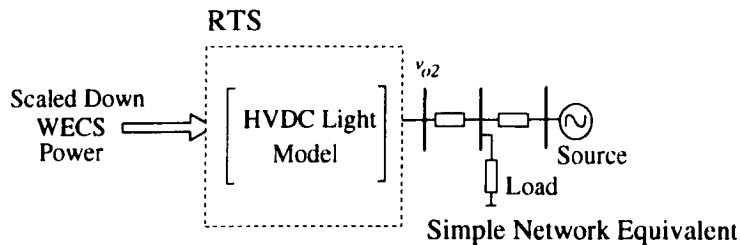


Figure 6.44.: Test setup

Real-time Simulation Approach

In the real-time simulation, the HVDC-VSC model is implemented in the RTS. The WECS is considered to be connected directly to the terminal of VSC1 in the HVDC-VSC model. The general block diagram of the test setup is as shown in Figure 6.44.

In (6.25)-(6.30) the DC currents, i_{dc1} and i_{dc2} , are derived from the power balance equation between the AC and DC system. Hence, it can be assumed that the DC current of the two VSCs corresponds to the instantaneous power of the two AC systems. In this case, the power into the terminal of VSC1 is the power generated by the WECS. With this consideration, the current equation for i_{dc1} is equal to the power from the WECS. The remaining DC-link cable model is unchanged in the real-time simulation.

The terminal of VSC2 in the HVDC-VSC model is connected to a simple physical network via the DAC of the RTS. The voltage profile at the load point of the network is monitored.

Simulations and Results

Simulations are conducted to show the real-time capability of the HVDC-VSC model in the study of the WECS connection. The ability of the HVDC-VSC to transfer the power

6. Power Electronics Controllers in the Phase-Domain

generated is demonstrated by starting the WECS from standstill through the cut-in period and to full generation. The assessment of the HVDC-VSC to maintain voltage and frequency regulation is performed by oscillating the power output from the WECS.

In these simulations certain assumptions are made on the system. The power of the WECS is assumed to be at the rated value at full generation. The power is represented in the equivalent p.u. value. The power vs. speed characteristic in Figure 6.43 is scaled in proportion to an equivalent time frame of 2s. Finally, DC values of the HVDC-VSC model are represented in p.u. assuming that an accurate base value exists for both the AC and DC system. The detailed rating and component values of the HVDC-VSC can also be included. These assumptions are made in the interest of the current work, since the main objective here is to demonstrate the ability of the HVDC-VSC model to operate in real-time with physical interactions.

WECS Run-Up to Full Generation

The power output from the WECS is as shown in Figure 6.45. The initial period represents the wind speed where the WECS is not generating any power. The cut-in instant is at 0.8s. The power transferred to the load network side or the output power, P_{ac2} , from VSC2 is slightly less than the WECS power input due to the losses in the cable.

It is observed that as the power from the WECS increases, the power transfer across the DC-link cable also increases as shown by the current in the cable. The DC voltage of VSC1 increases slightly as a result of this power input. The DC voltage of VSC2, where the voltage regulation control is taking place, is maintained at an almost constant level. The difference in the DC voltage level is to facilitate the current flow in the DC-link cable. As the voltage level at the terminal of VSC2 is dependent on the DC voltage, it will also maintain a constant profile throughout the transfer of power. This will in turn keep the voltage at the load point constant ensuring constant supply.

Oscillations in WECS Generated Power

In wind generation, the characteristics of the output power is dependent on the wind turbine driving the generator. It has been known that pulsations or oscillations of the power output can occur when the blades of the wind turbine passes its tower. In this simulation, the output of the WECS is assumed to contain low frequency oscillations. This can be achieved by changing the power characteristics of the WECS which involves adding an oscillation signal to the excitation voltage of the servomotor.

It is observed from Figure 6.46, that the DC voltage at both terminals is not very much affected by the oscillations in the power input and output. Hence, from the previous explanation, the voltage profile at the load point also maintains its level. This shows the effectiveness of the HVDC-VSC in maintaining a constant voltage profile at its point of connection with the AC system.

6. Power Electronics Controllers in the Phase-Domain

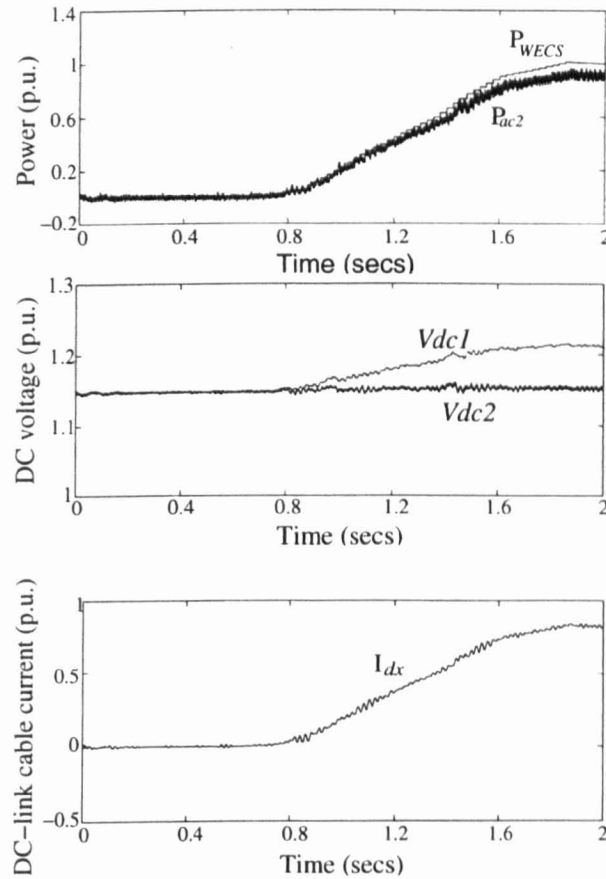


Figure 6.45.: HVDC-VSC response during WECS run-up to rated power

Frame Time of Simulations

The main parameter that needs monitoring when performing real-time simulations is the Actual Frame Time (AFT) of the RTS. The AFT allows the user to observe the time taken by the RTS to compute each time step of the simulation. The AFT must not exceed the Desired Frame Time (DFT) at any point in the simulation. The DFT is always given by the simulation time step.

In the study cases, the simulations were undertaken with a time step of 100 ms. It is observed from Figure 6.47, that the AFT of both study cases are below the DFT of 100 ms. Hence, the real-time capability of the simulations is demonstrated.

6.7. Conclusions

This chapter has addressed the development of power electronics controllers models in the direct time phase-domain which are well suited for incorporation into the existing multi-machine environment. Both the conventional thyristor based and modern turn-on turn-off controllers are carefully modelled and implemented within the multimachine environment.

6. Power Electronics Controllers in the Phase-Domain

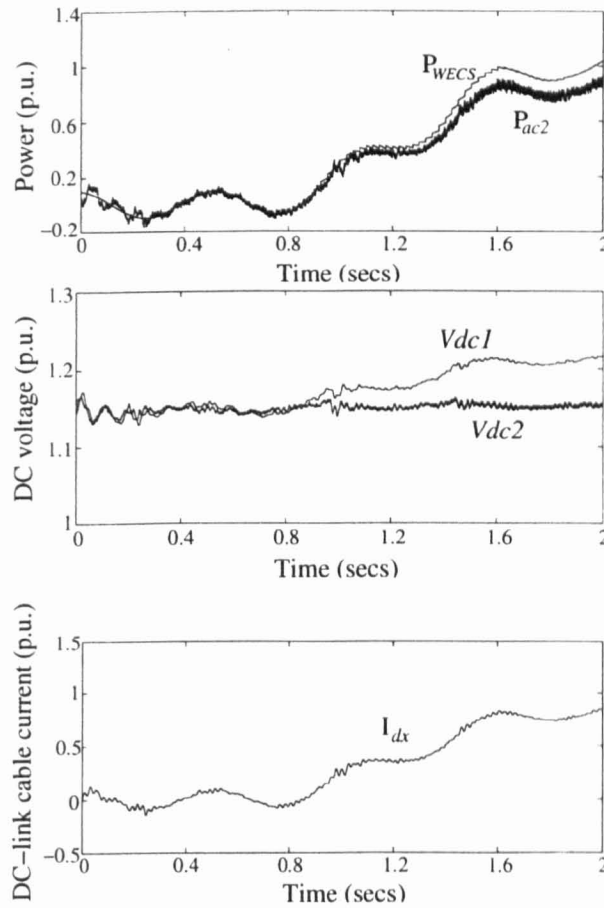


Figure 6.46.: HVDC-VSC response when carrying oscillating power

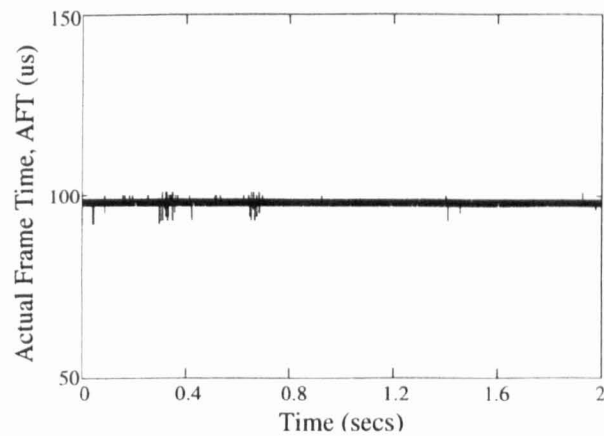


Figure 6.47.: AFT of simulations

The flexibility of the models in studies involving asymmetrical conditions has further shown the potential of the phase-domain method to conduct comprehensive power system analyses.

Based on the model proposed, the impact of the SVC in the mitigation of voltage sags during starting of motor and transient stability enhancement was investigated. It was found that the presence of SVCs can improve the performance of the network. However, the SVC which function by modifying the network reactances has certain limitations, namely its ineffective-

6. *Power Electronics Controllers in the Phase-Domain*

ness to respond under severe low voltage conditions and the slow discharging of its capacitor which can result in overvoltages at post steady state period. Modern VSC-based controllers like the STATCOM can overcome this problem. The STATCOM which functions very much like a synchronous source performs better than the SVC for the conditions considered in this chapter. It provides effective compensation even at low voltage levels and its PWM control technique is fast and flexible. The STATCOM is sensitive to high level of unbalance in its phase current, hence, to operate effectively under this conditions an overcurrent control scheme needs to be implemented. The STATCOM with its low voltage ability is suitable to be installed at distribution systems with embedded wind driven induction machines. The STATCOM can overcome the transient problems associated with the operation of this embedded generators.

The DVR, which is a series compensator, has been demonstrated to be an effective device for load protection in the event of network faults. It functions by injecting the voltage deficit between the load demand and the network to ensure a smooth supply to the load. Results presented shows that the DVR can provide voltage stability at the terminal of a voltage sensitive load, such as an induction motor, under both symmetrical and asymmetrical operations. An HVDC-VSC station model is implemented where it is used to perform study in a practical situation involving the operation of a WECS. The HVDC-VSC station functions as a transmission component to transfer power from the WECS to the network. The implementation of the HVDC-VSC model in real-time has highlighted the capability of the power electronics controllers model developed in this chapter as a flexible and effective study tools to be used in conjunction with the multimachine system.

7. General Conclusions and Suggestions for Future Research Work

7.1. General Conclusions

The research work presented in this thesis has been directly oriented towards the development of a new multimachine power system model with power electronics controllers for transient analysis in the direct time phase-domain. The flexibility and practical usage of the model has been thoroughly investigated for different network conditions. The motivation of this work stems from the need to improve on the models of power system components and solution techniques to assess potential transient stability problem involving severe asymmetrical conditions. The reason for modelling in the direct time phase-domain is that it can analyse asymmetrical conditions with great effect.

Comprehensive direct time phase-domain model of AC machine has been developed. The reliability of the model should not be in doubt as it has been validated against an industry power system package and available experimental results. The model does not require any form of mathematical domain transformation and as such can be truly evaluated in time based phase co-ordinates. The flexibility afforded by this model is unchallenged, especially in dealing with asymmetrical operations.

The main original contribution of this thesis is the development of a new method for efficient solution of a multimachine power system network using the comprehensive direct time phase-domain AC machine model.

With this new method of approach, the application of the AC machine model is no longer limited to the analysis of one machine system. The analysis of large network using this model, which has not been feasible in the past due to lack of computing capability and solution techniques, is now possible with the solution method proposed in this thesis. The non-linear differential equations governing the machine model and network were discretised using the trapezoidal rule of integration to form sets of algebraic equations. With careful manipulation, the algebraic equations were then effectively solved with a direct simultaneous solu-

7. *General Conclusions and Suggestions for Future Research Work*

tion. This new algorithm is numerically stable, and fast when compared to the conventional method, hence, reducing the computing time. Good comparison of responses for symmetrical operating conditions with a commercial power system package, PSCAD/EMTDCTM, has established confidence in the new model and solution technique.

The successful implementation of the multimachine model in the real-time environment is another contribution in this context.

The value of the proposed model and solution technique is enhanced by the capability to perform real-time studies. The results clearly indicate that the multimachine model is indeed able to output responses in actual world time when implemented in a multi-purpose real-time station. This original idea of using a multi-purpose real-time station for power system studies has open up doors to many research possibilities including physical equipment testing in a HIL configuration.

The new method of coherency-based multimachine approach based on the direct time phase-domain model developed in this thesis is another major contribution to the area of multimachine studies. The approach allows a group of coherent generators to be aggregated, and represented by an equivalent unit, which greatly reduces the complexity of the network. Results show that the computing time of the simulation is cut down, while the responses of the network, in the area of interest, is not affected. This will enable real-time simulation of larger networks to be conducted.

The application of the multimachine model in the analysis of power system stability problems involving asynchronous machines has also been successfully carried out.

The effect of dynamic loads within the multimachine network has been thoroughly investigated. A range of analysis on the transient and power quality issues relating to dynamic loads, in the form of asynchronous motors was performed. It was observed that the direct on-line starting of the motor could have severe adverse effects on the voltage quality of the network. Also, under faulted conditions the presence of motor can influence the duration of voltage disruption due to the high reactive power it requires for re-acceleration. This reactive power is obtained from the network creating a deficit of reactive power resulting in a prolonged voltage disruption.

The reverse operating mode of the asynchronous motor, to function as a generator, was also presented in the thesis. This is a timely topic as power generation involving asynchronous generators is on the increase due to the dissemination of renewable generation sites which favour the use of asynchronous generators such as WECS. It has been shown that in a dispersed generation scheme, the voltage level and parameters of the network can affect the stability of the asynchronous generator. The oscillations of the power output from such wind driven generator have a negative impact on the stability of the dispersed generation system. The islanding scenario involving the operation of wind generators was analysed and it was

7. *General Conclusions and Suggestions for Future Research Work*

observed that the terminal voltage of the generator could increase to a very high value depending on the excitation capacitor installed at the terminal.

The thesis has also contributed to the development of power electronics controllers model in the direct time phase-domain for transient analysis. The integration of these controllers into the direct time phase-domain multimachine network is an original idea of the research work. The power electronics controllers developed are:

- SVC
- STATCOM
- DVR
- HVDC-VSC

The controllers were introduced into the multimachine network to improve the response of the network when subjected to operational problems as a result of dynamic loads and asynchronous generators. The SVC and STATCOM proved to produce good compensation for the network, reducing voltage disruptions resulting from the operations of the dynamic loads and asynchronous generators. The DVR was used in a severe fault situation to protect the voltage level at the terminal of a sensitive load where it was shown to be effective in both symmetrical and asymmetrical conditions.

Another important contribution of the thesis is the application of the HVDC-VSC model in the study of a practical situation involving a laboratory scaled down model of a WECS. This is an analysis involving the interaction of physical devices to mathematical model in a real-time environment.

A scaled down WECS was interface to the model of the HVDC-VSC station embedded in the real-time station. It was observed that the HVDC-VSC station can continuously transmit power from the WECS to the network without affecting the voltage level of the network even when the output of the WECS changes as a result of the wind speed.

7.2. Suggestions for Future Research Work

An integrated, novel approach to power system components modelling for transient stability analysis has been presented in this thesis. The direct time phase-domain yields unique flexibility in the development of transient analysis tools. Further research work that would enhance further this approach include the following research points:

- Include equations representing the saturation effect of the rotating machines in order to study the effect of resonance in cases of overvoltages involving isolation of wind generators.

7. *General Conclusions and Suggestions for Future Research Work*

- The proposed multimachine network models have been used to investigate asymmetrical operating conditions with great effectiveness. One other benefit of this model which need to be explored further is the possibility to simulate internal faults of generators in the multimachine environment. Although published literatures are available for internal fault studies [136][137], it has been limited to cases of one generator connected to an infinite busbar system.
- The coherency-based approach to aggregate the coherent generators has, in this thesis, been implemented for synchronous generators. A similar approach would need to be developed for cases of asynchronous machines, especially in its generating mode. This will be important to the analysis of large wind farms where closely knitted groups of asynchronous generators are located close to each other. The coherent approach could be used to represent the group of generators in order to reduce computing overheads.
- A wide range of power electronics controllers are available for use in today's power system. One of the device which has not been researched in this thesis is the unified power flow controller (UPFC). The modelling of this controller in the direct time phase-domain should be given priority in the near future.

Bibliography

- [1] B.M. Weedy, *Electric Power System*, John Wiley & Sons 1979.
- [2] J.J Grainger and W.D. Stevenson, *Power System Analysis*, McGraw-Hill 1994.
- [3] A Gross, *Power System Analysis*, John Wiley & Sons 1979.
- [4] P. Kundur, *Power System Stability and Control*, McGraw-Hill 1994.
- [5] P.M. Anderson and A.A. Fouad, *Power System Control and Stability*, IEEE Press 1994.
- [6] E.W. Kimbark, *Power System Stability*, John Wiley & Sons 1962.
- [7] P.W. Sauer and M.A. Pai, *Power System Dynamics and Stability*, Prentice Hall 1998.
- [8] J. Machowski, J.W. Bialek and J.R. Bumby, *Power System Dynamics and Stability*, John Wiley & Sons, 1997.
- [9] Mania Pavella, "Power system transient stability assessment - traditional vs modern methods", *Control Engineering Practice*, vol. 6, no. 10, 1998, pp. 1233-1246.
- [10] R.H. Park, "Two reaction theory of synchronous Machines - I", *AIEE Trans*, vol. 48, 1929, pp. 716-730.
- [11] R.H. Park, "Two reaction theory of synchronous Machines - II", *AIEE Trans*, vol. 51, 1933, pp. 352-355.
- [12] B. Adkins and R.G. Harley, *The General Theory of Alternating Current Machines*, Chapman and Hall, 1975.
- [13] P.C. Krause, *Analysis of Electric Machinery*, McGraw-Hill, 1987.
- [14] A.E. Fitzgerald and C. Kingsley, *Electric Machinery*, McGraw-Hill, 1961.
- [15] T.J. Hammons and D.J. Winning, "Comparison of Synchronous Machine Models in the Study of transient Behaviour of Electrical System", *Proc. IEE*, vol. 118, no. 10, October 1971, pp. 1142-1458.

Bibliography

- [16] G.W. Stagg and A.H. El-Abiad, *Computer Methods in Power System Analysis*, McGraw-Hill, 1968.
- [17] H.H. Hwang, "Unbalanced Operation of AC machines", *IEEE Trans. on Power Apparatus and Systems*, PAS-84, , 1965, pp. 1054-1066.
- [18] D.B. Mehta and B. Adkins, "Transient torque and load angle of synchronous generator following several types of system disturbance", *Proc. IEE*, 107, Part A, 1960, pp. 61-74.
- [19] B. Adkins, "Transient theory of synchronous generators connected to power systems", *JIEE*, vol. 98, 1951, pp. 510-528.
- [20] R.G. Harley and B. Adkins, "Calculation of the angular back swing following a short circuit of a loaded alternator", *Proc. IEE*, vol. 117, no. 2, February 1970, pp. 377-386.
- [21] G. Shackshaft, "New Approach to the determination of synchronous machine parameters from tests", *Proc. IEE*, vol. 121, no. 12, November 1974, pp. 1385-1392.
- [22] IM Canay, "Causes of Discrepancies on calculation of rotor quantities and exact equivalent diagrams of synchronous machine", *IEEE Trans. on Power Apparatus and Systems*, PAS-88, July 1969, pp. 1114-1120.
- [23] P.L. Dandeno, R.L. Hauth and R.P. Schulz, "Effects of synchronous machine modelling in large scale stability studies", *IEEE Trans. on Power Apparatus and Systems*, PAS-92, March/April 1973, pp. 574-582.
- [24] P. Kundur and P.L. Dandeno, "Implementation of advanced generator models into power system stability programs", *IEEE Trans. on Power Apparatus and Systems*, PAS-102, no. 7, July 1983, pp. 2047-2054.
- [25] P. Subramaniam and O.P. Malik, "Digital Simulation of a synchronous generator in the direct phase quantities", *Proc. IEE*, vol. 118, no. 1, January 1971, pp. 153-160.
- [26] T.J.H. Hammons, "Simulation of a Synchronous generator in the Direct time phase quantities - Sequential Interruption of fault currents and their effect on transient electromagnetic torque", *Proc. International Conference on Electrical Machine, ICEM 1984*, Lausanne, September 1984, pp. 439-442.
- [27] A.K. Desarkar and Gunnar J. Berg, "Digital Simulation of Three-Phase Induction Motors", *IEEE Trans. on Power Apparatus and Systems*, PAS 89, no. 6, 1970, pp. 1031-1037.
- [28] M. Rafian and M.A. Laughton, "Determination of Synchronous-machine phase coordinate parameters", *Proc. IEE*, vol. 123, 1976, pp. 818-824.

Bibliography

- [29] M. Rafian, *Power System Dynamic Modelling and Parameter Identification in Phase Co-ordinates*, Ph.D Thesis, Queen Mary College, University of London, 1976.
- [30] M.J. Chen, *Phase Coordinates Representation on Interconnected Machine System*, Ph.D Thesis, University of Strathclyde, UK, 1992.
- [31] J.R. Marti and K.W. Louie, "A Phase Domain Synchronous Generator Model Including Saturation Effect", *IEEE Trans. on Power System*, vol 112, no. 1, February 1997, pp. 222-229.
- [32] K.L. Lo and H. El-Khatroushi, "Dynamic Stability System Analysis using Phase Frame of reference Quantity", *Universities Power Engineering Conference, UPEC '94*, September 1994, pp. 298-301.
- [33] K.H. Chan, E. Acha, M. Madrigal and J.A. Parle, "The use of Direct Time-Phase Domain Synchronous Generator Model in Standard EMTP-Type Industrial Packages", *IEEE Power Engineering Review*, vol. 21, no. 6, June 2001, pp. 63-65.
- [34] Dommel H.W., *Electromagnetic Transient Program (EMTP) Rule Book*, EPRI EL 642-1, vol. 1 and 2, June 1989.
- [35] PSCAD/EMTDC V3.0.4, *User's Guide [Educational Edition]*, Manitoba HVDC Research Centre, April 2000.
- [36] IEEE Committee Report, "Excitation System Models for Power System Stability Studies", *IEEE Trans. on Power Apparatus and Systems*, PAS-100, no. 2, February 1981, pp. 497-509.
- [37] IEEE Committee Report, "Dynamic Models for Steam and Hydro-turbine in Power System Studies", *IEEE Trans. on Power Apparatus and Systems*, PAS-92, no. 6, November 1973, pp. 1904-1915.
- [38] IEEE Committee Report, "Proposed Excitation System Definitions for Synchronous Machines", *IEEE Trans. on Power Apparatus and Systems*, PAS-88, 1981, pp. 1248-1258.
- [39] F.P. Demello and C. Concordia, "Concepts of Synchronous Machine Stability as Affected by Excitation Control", *IEEE Trans. on Power Apparatus and Systems*, PAS-88, no. 4, April 1969, pp. 189-202.
- [40] A.A Fouad, V. Vittal, Y.X. Ni, H.M. Zein and E. Vaahedi, "Direct Transient Stability Assessment with Excitation Control", *IEEE Trans. on Power System*, vol. 14, no. 1, 1989, pp. 75-82.

Bibliography

- [41] N.G. Hingorani, "Flexible AC Transmission Systems", *IEEE Spectrum*, vol. 30, Issue 4, April 1993, pp. 40-45.
- [42] D. Povh, "Applications of FACTS to systems", *Proc. EPSOM 98, Zurich*, vol. 2, September 1998.
- [43] EPRI, "Flexible AC Transmission System (FACTS)", *EPRI Workshop, Boston*, May 1992.
- [44] IEEE Power Engineering Society, "FACTS Overview", *CIGRE International Conference on Large High Voltage Electric Systems*, 1995.
- [45] N.G. Hingorani, "Introducing Custom Power", *IEEE Spectrum*, vol. 32, Issue 6, June 1995, pp. 41-48.
- [46] N.G. Hingorani and L. Gyugyi, *Understanding FACTS: Concepts and Technology of Flexible AC Transmission Systems*, IEEE Press Inc., New York, 2000.
- [47] Y.H. Song and A.T. Johns, *Flexible AC Transmission System (FACTS)*, IEE, England 1999.
- [48] T.J.E. Miller, *Reactive Power Control in Electric Systems*, Wiley-Interscience, New York, 1982.
- [49] R. Dilger and D. Nelles, "Improvement of network damping and transient stability by active and reactive power control", *Proc. IEE - Gener. Transm. and Distrib.*, vol. 144, no. 2, March 1997, pp. 125-128.
- [50] A.E. Hammad, "Analysis of Power System Stability Enhancement by Static Var Compensator", *IEEE Trans. on Power Systems*, vol. 1, no. 4, November 1986, pp. 222-227.
- [51] IEEE Special Stability Controls Working Group, "Static Var Compensator Models for Power Flow and Dynamic Performance Simulation", *IEEE Trans. on Power Systems*, vol. 9, no. 1, February 1994, pp. 229-240.
- [52] L. Anquist, B. Lundin and J. Samuelson, "Power Oscillation Damping Using Controlled Reactive Power Compensation: A comparison between series and shunt approaches", *IEEE Trans. on Power Systems*, vol. 8, no. 2, May 1993, pp. 687-699.
- [53] E. Lerch, D. Povh and L. Xu, "Advanced SVC Control for Damping Power Oscillations", *IEEE Trans. on Power Systems*, vol. 6, no. 2, May 1991, pp. 524-535.
- [54] H.F. Wang and F.J. Swift, "A Unified Model for the analysis of FACTS devices in Damping Power System Oscillations Part I: Single-machine Infinite-bus Power Systems", *IEEE Trans. on Power Delivery*, vol. 12, no. 2, April 1997, pp. 941-946.

Bibliography

- [55] H.F. Wang, F.J. Swift and M. Li, "A Unified Model for the analysis of FACTS devices in Damping Power System Oscillations Part II: Multi-machine Power Systems", *IEEE Trans. on Power Delivery*, vol. 13, no. 4, October 1998, pp. 1355-1360.
- [56] S. Arabi and P. Kundur, "A Versatile FACTS Device Model for Power flow and Stability Simulations", *IEEE Trans. on Power Systems*, vol. 11, no. 4, November 1996, pp.1944-1950.
- [57] L. Gyugyi, "Dynamic Compensation of AC Transmission Lines by Solid-State Synchronous Voltage Source", *IEEE Trans. on Power Delivery*, vol. 9, no. 1, February 1994, pp. 229-240.
- [58] C. Shauder and H. Mehta, "Vector Analysis and Control of Advanced Static Var Compensators", *Proc. IEE Part C*, vol. 140, no. 4, July 1993, pp. 299-306.
- [59] C. Shauder, M. Gernhart, E. Stacey, T. Lemak, L. Gyugyi et al, "Development of a ± 100 MVAR Static Condenser for Voltage Control of Transmission Systems", *IEEE Trans. on Power Delivery*, vol. 10, no. 3, July 1995, pp. 1486-1496.
- [60] C. Shauder, M. Gernhart, E. Stacey, T. Lemak, L. Gyugyi et al, "Operation of a ± 100 MVAR STATCOM", *IEEE Trans. on Power Delivery*, vol. 12, no. 3, Oct. 1997, pp. 1805-1811.
- [61] J.B. Ekanayake and N. Jenkins, "Mathematical Model of a Three-level Advanced Static Var Compensator", *Proc. IEE - Gener., Trans. & Distrib.*, vol. 4, no. 2, March 1997, pp. 201-206.
- [62] L. Gyugyi, "Static Synchronous Series Compensator: A solid-state series approach to the series compensation of transmission lines", *IEEE Trans. on Power Delivery*, vol. 12, no. 1, January 1997, pp. 406-417.
- [63] R.P. Wierckx, "Fully Digital Real-Time Electromagnetic Transients Simulator", *IERE International Electric Research Exchange, Workshop on New Issues in Power System Computation*, Caen, France, March 1992.
- [64] R. Kuffel, J. Giesbrecht, T. Maguire, R.P. Wierckx and P. McLaren, "RTDS - A Fully Digital Power System Simulator Operating in Real-Time", *1st International Conference on Digital Power System Simulators, ICDS '95*, College Station, USA, April 1995.
- [65] X. Wang, J. Giesbrecht, D. Woodford, L. Arendt, R.P. Wierckx and R. Kuffel, "Enhanced Performance of Conventional HVDC Analogue Simulator with a Real-Time Digital Simulator", *11th Power Systems Computation Conference, PSCC '93*, Avignon, France, August 1993.

Bibliography

- [66] H. Duchon, M. Lagerkvist, R. Kuffel and R.P. Wierckx, "HVDC Simulation and Control System Testing Using a Real-Time Digital Simulator (RTDS)", *1st International Conference on Digital Power System Simulators, ICDS '95*, College Station, USA, April 1995.
- [67] R. Kuffel, R.P. Wierckx, H. Duchon, M. Lagerkvist and X. Wang, "Expanding an Analogue HVDC Simulator's Modelling Capability Using a Real-Time Digital Simulator (RTDS)", *1st International Conference on Digital Power System Simulators, ICDS '95*, College Station, USA, April 1995.
- [68] J.A. Parle, E.Acha and C.R. Fuerte-Esquivel, "Real-Time Implementation of Transmission Line Models for Electromagnetics Transient Studies", *International Conference on Digital Power System Simulators, ICDS 1999*, May 1999.
- [69] J.A. Parle, *Phase Domain Transmission Line Modelling for EMTP-Type Studies with Application to Real-Time Digital Simulation*, Ph.D Thesis, University of Glasgow, April 2000.
- [70] P. Aree, *Small-Signal Stability Modelling and Analysis of Power Systems with Electronically Controlled Compensation*, Ph.D Thesis, University of Glasgow, April 2000.
- [71] R.B.I. Johnson, M.J. Short and B.J. Cory, "Improved Simulation Techniques for power system dynamics", *IEEE Trans. on Power Systems*, vol. 3, no. 4, November 1988, pp. 1691-1698.
- [72] R.B.I. Johnson, B.J. Cory and M.J. Short, "A tunable integration method for the simulation of power system dynamics", *IEEE Trans. on Power Systems*, vol. 3, no. 4, November 1988, pp. 1530-1537.
- [73] H.W. Dommel and N. Sato, "Fast Transient stability solutions", *IEEE Trans. on Power Apparatus and Systems*, PAS-91, July/Aug 1972, pp. 219-241.
- [74] K. Saikawa, M. Goto, Y. Inamura, M. Takato and T. Kanke, "Real time simulation system of large-scale power system dynamics for dispatcher training simulator", *IEEE Trans. on Power Apparatus and Systems*, PAS-103, December 1984, pp. 3496-3501.
- [75] G. Gross and A.R. Gergen, "A class of new multi step integration algorithms for the computation of power system dynamical response", *IEEE Trans. on Power Apparatus and Systems*, PAS-96, no. 1, Jan/Feb 1977, pp. 293-306.
- [76] T. Berry, L.A. Dale, A.R. Daniels and R.W. Dunn, "Real time modelling of multimachine power systems", *Proc. IEE, Part C*, vol. 140, no. 4, July 1993, pp. 241-248.
- [77] T. Berry, K. Chan, R.W. Dunn and F. Ng, "Real time power system simulator", *25th Universities Power Engineering Conference, UPEC 1990*, pp. 671-674.

Bibliography

- [78] P.C. Krause and C.H. Thomas, "Simulation of Symmetrical Induction Machinery", *IEEE Trans. on Power Apparatus and Systems*, PAS-84, no. 11, November 1965, pp. 1038-1053.
- [79] R.W. de Mello, R. Podmore and K.N. Stanton, "Coherency-based Dynamic Equivalents: Applications in Transient Stability Studies", *PICA Conference Proceedings, 1975*, pp. 23-31.
- [80] R. Podmore, "Identification of Coherent Generators For Dynamic Equivalents", *IEEE Trans. Power Apparatus and Systems*, PAS-97, no. 4, July 1978, pp. 1344-1354.
- [81] A.J. Germond and R. Podmore, "Dynamic Aggregation of Generating Unit Models", *IEEE Trans. Power Apparatus and Systems*, PAS-97, no. 4, July 1978, pp. 1060-1069.
- [82] A. Ghafurian and G.J. Berg, "Coherency-based multimachine stability study", *Proc. IEE, Part C*, vol 129, 1982, pp. 153-160.
- [83] R. Nath and SS. Lamba, "Development of coherency-based time-domain equivalent model using structure constraints", *Proc. IEE, Part C*, vol 133, May 1986, pp. 165-175.
- [84] Y. Xue, T. Van Cutsem and M.R. Pavella, "A simple direct method for fast transient stability assessment of large power systems", *IEEE Trans. on Power Systems*, vol. 3, no. 2, May 1988, pp. 400-412.
- [85] A.M. Miah, "Simple dynamic equivalent for fast online transient stability assessment", *Proc. IEE - Gener., Trans. & Distrib.*, vol. 145, no. 1, Jan. 1998, pp. 49-55.
- [86] J.H. Chow, P. Accari and W.W. Price, "Inertial and Slow Coherency Aggregation Algorithms for Power System Dynamic Model Reduction", *Trans. IEEE on Power Systems*, vol 10, no. 2, May 1995, pp. 680-685.
- [87] A. Chang and M.M. Adibi, "Power System Dynamic Equivalents", *IEEE Trans. Power Apparatus and Systems*, PAS-89, no. 8, Nov 1970, pp. 1737-1744.
- [88] A.M. Miah, J. Meisel and B.J. Cory, "Transient stability assessment using a dynamic equivalent for undisturbed generators", *Proceedings of 10th PSCC*, Graz Austria, 1990, pp. 501-508.
- [89] R.G. Harley, E.B. Makram and E.G. Duran, "The Effects of Unbalanced Networks and Unbalanced Faults on Induction Motor Transient Stability", *IEEE Trans. on Energy Conversion*, Vol. 3, no. 2, June 1988, pp. 398-403.

Bibliography

- [90] R.G. Harley, J.M. Correia, G.D. Jennings and E.B. Makram, "Induction motor model for the study of transient stability in both balanced and unbalanced multi-machine networks", *IEEE Trans. on Energy Conversion*, vol. 7, no. 1, March 1992, pp. 209-215.
- [91] M.H.J. Bollen, *Understanding Power Quality Problems: Voltage Sags and Interruptions*, IEEE Press, 1999.
- [92] M.H.J. Bollen, "Characterization of voltage sags experienced by three-phase adjustable-speed drives", *IEEE Trans. on Power Delivery*, vol. 12, no. 4, Oct 1997, pp. 1666-1671.
- [93] M.H.J. Bollen, "The Influence of Motor Re-acceleration on Voltage Sags", *IEEE Trans. on Industry Applications*, vol. 31, no. 4, July/August 1995, pp. 667-674.
- [94] M.H.J. Bollen, "Simple model for post-fault motor behaviour for reliability/power quality assessment of industrial power systems", *Proc. IEE - Gener., Trans. & Distrib.*, vol. 143, no. 1, Jan 1996, pp. 56-60.
- [95] J.C. Das, "Effects of Momentary Voltage Dips on the Operation of Induction and Synchronous Motors", *IEEE Trans. on Industry Applications*, vol. 26, no. 4, July/August 1990, pp. 711-718.
- [96] J.W. Shaffer, "Air conditioner response to transmission fault", *IEEE Trans. on Power Systems*, vol. 12, no. 2 May 1996, pp. 614-621.
- [97] C.S Chang and Y.S. Ho, "The Influence of Motor Loads on the Voltage Restoration Capability of the Dynamic Voltage Restorer", *Proc. of International Conference on Power System Technology*, PowerCon 2000, vol. 2, 2000, pp. 637-642.
- [98] G. Yalcinkaya, M.H.J. Bollen and P.A. Crossley, "Characterization of voltage sags in industrial distribution systems", *IEEE Trans. of Industry Applications*, vol. 34, no. 4, July 1998, pp. 682-688.
- [99] S. Heier, *Grid Integration of Wind Energy Conversion Systems*, John Wiley, New York 1998.
- [100] Z. Saad-Saoud, M.L. Lisboa, J.B. Ekanayake, N. Jenkins and G. Strbac, "Application of STATCOMs to wind farms", *Proc. IEE Gener Trans and Distr*, vol. 45, no. 5, September 1998, pp. 511-516.
- [101] A. Feijoo and J. Cidras, "Analysis of mechanical power fluctuations in asynchronous WECS", *IEEE Trans. Energy Conversion*, vol. 14, no. 3, September 1999, pp. 284-291.

Bibliography

- [102] K.H. Chan and E. Acha, "Transient Stability Behaviour of a Distribution Network with Embedded Wind-driven Induction generator", *Procs. of the Sixth IASTED International Conference EUROPES 2001*, Rhodes, Greece, July 2001, pp. 663-668.
- [103] C.S. Demoulias and P. Dokopoulos, "Electrical Transients of Wind Turbines in a Small Power Grid", *IEEE Trans on Energy Conversion*, vol. 11, no. 3, September 1996, pp. 636-642.
- [104] F.P. de Mello, J.W. Feltes, L.N. Hannett and J.C. White, "Application of Induction Generator in Power Systems", *IEEE Trans PAS*, vol. 101, no. 9, September 1982, pp. 3385-3393.
- [105] E. Santos, T.I. Asian, D. Ruiz and D. Olguin, "The effect of load characteristics on the transient stability studies of a laboratory electric power system including induction generators", *Proc. Electric Power Engineering PowerTech Budapest International Conference 1999*, 1999, pp. 81-84.
- [106] L. Holdsworth, N. Jenkins and G. Strbac, "Electrical Stability of Large, Offshore wind farms", *Procs. 7th International Conference on AC-DC Power Transmission*, London, November 2001, pp. 156-161.
- [107] L. Tang and R. Zavadil, "Shunt Capacitor Failures due to Windfarm Induction Generator Self-Excitation Phenomenon", *IEEE Trans. on Energy Conversion*, vol. 8, no. 3 September 1993, pp. 513-519.
- [108] L. Wang and R.Y. Deng, "Transient Performance of an Isolated Induction Generator Under Unbalanced Excitation Capacitors", *IEEE Trans. on Energy Conversion*, vol. 14, no. 4, December 1999, pp. 887-893.
- [109] M.A. Ouhrouche, X.D. Do, Q.M. Le and R. Chaine, "EMTP Based Simulation of a self-excited Induction Generator after its disconnection from the grid", *IEEE Trans. on Energy Conversion*, vol. 13, no. 1, March 1998, pp. 7-13.
- [110] L. Wang and C.M. Cheng, "Excitation capacitance required for an isolated three-phase induction generator under single-phasing mode of operation", *Power Engineering Society Winter Meeting 2000*, vol. 1, 2000, pp. 299-303.
- [111] H. Sharma, S. Islam and C.V. Nayar, "Power Quality Simulation of a variable speed wind generator connected to a weak grid", *Procs. 9th International Conference on Harmonic and Quality of Power ICHQP 2000*, Florida, October 2000, pp. 988-993.
- [112] Z. Saad Saoud and N. Jenkins, "Models for predicting flicker induced by large wind turbines", *IEEE Trans. on Energy Conversion*, vol. 14, no. 3, September 1999, pp. 743-748.

Bibliography

- [113] A.H. Ghorashi, S.S. Murthy, B.P. Singh and B. Singh, "Analysis of wind driven grid connected induction generators under unbalanced grid conditions", *IEEE Trans. on Energy Conversion*, vol. 9, no. 2, June 1994, pp. 217-223.
- [114] H. Amaris, C. Villar, J. Usaola and J.L. Rodriguez, "Frequency Domain Analysis Produced by Wind Energy Conversion Systems", *Procs. 8th International Conference on Harmonic and Quality of Power ICHQP 1998*, Greece, October 2000, pp. 1162-1167.
- [115] A.M. Gole and V.K. Sood, "A Static Compensator Model for use with Electromagnetic Transients Simulation Programs", *IEEE Trans. on Power Delivery*, vol. 5, no. 3, July 1990, pp. 1398-1407.
- [116] I.T. Fernando, W.T. Kwasnicki and A.M. Gole, "Modelling of conventional and advanced static var compensator in electromagnetic transients simulation program", [Online], Available: <http://www.ee.unmanitoba.ca/~hvdc>.
- [117] M. Madrigal, O. Anaya, E. Acha et al, "Single-phase PWM Converters Array for Three-Phase Reactive Power Compensation. Part 1: Time Domain Studies", *Proc. 2000 International Conference on Harmonics and Quality of Power, ICHQP 2000*, October 2000, pp. 541-547.
- [118] K.H. Chan and M. Madrigal, "Phase Domain Dynamic Analysis of Conventional and Advanced Static Var Compensator in Voltage Sag due to Motor Start-Up", *Proc. of the Sixth IASTED International Conference on Power and Energy Systems, EUROPE 2001*, Rhodes, Greece, July 2001, pp. 394-400.
- [119] C. Hockgraf and R.H. Lasseter, "Statcom Controls for Operation with Unbalanced Voltages", *IEEE Trans. on Power Delivery*, vol. 13, no. 2, April 1998, pp. 538-544.
- [120] Y. Jiang and A. Ekstrom, "Applying PWM to Control Overcurrents at Unbalanced Faults of Forced-Commutated VSCs Used as Static VAR Compensators", *IEEE Trans. on Power Delivery*, vol 12, no. 1, January 1997, pp. 273-278.
- [121] S. Mori and K. Matsuno, M. Takeda and M. Seto, "Development of Large Static VAR Generator Using Self-Commutated Inverter For Improving Power System Stability", *IEEE Trans. Power Systems*, vol. 8, no. 1, February 1993, pp. 371-377.
- [122] L. Gyugyi, "Dynamic Compensation of AC Transmission Lines By Solid-State Synchronous Voltage Sources", *IEEE Trans. on Power Delivery*, vol. 9, no. 2, April 1994, pp. 904-911.
- [123] Y. Sumi, Y. Harumoto, T. Hasegawa and M. Yano, "New Static Var Control Using Forced-commutated Inverters", *IEEE Trans. on Power Apparatus and System*, PAS-100, no. 9, September 1981, pp. 4216-4224.

Bibliography

- [124] Y. Liang and C.O. Nwankpa, "Power-Line Conditioner Based on Flying-Capacitor Multilevel Voltage-Source Converter with Phase-Shift PWM", *IEEE Trans. on Industry Applications*, vol. 36, No. 4, July/August 2000, pp. 965-971.
- [125] L. Gyugyi, "Static Synchronous Series Compensator: A solid-state series approach to the series compensation of transmission lines", *IEEE Trans. on Power Delivery*, vol. 12, No. 1, January 1997, pp. 406-417.
- [126] S.W. Middlekauff and E.R. Collins, "System and Customer Impact: Considerations for Series Custom Power Devices", *IEEE Trans. on Power Delivery*, vol. 13, no. 1, January 1998, pp. 278-282.
- [127] N.H. Woodley, L. Morgan and A. Sundaram, "Experience with an Inverter-Based Dynamic Voltage Restorer", *IEEE Trans. on Power Delivery*, vol. 14, no. 3, July 1999, pp. 1181-1186.
- [128] M. Fang, A.I. Gardiner, A. MacDougall and G.A. Mathieson, "A novel series dynamic voltage restorer for distribution systems", *Procs. POWERCON 1998*, Australia, vol. 1, 1998, pp. 38-42.
- [129] M.H. Haque, "Voltage Sag Correction by Dynamic Voltage Restorer with Minimum Power Injection", *IEEE Power Engineering Review*, vol. 21, no.5, May 2001, pp. 56-58.
- [130] B.T. Ooi and X. Wang, "Boost Type PWM HVDC Transmission System", *IEEE Trans. on Power Delivery*, vol. 6, no. 4, October 1991, pp. 1557-1563.
- [131] B.T. Ooi and X. Wang, "Voltage Angle Lock Loop Control of Boost Type PWM Converter for HVDC Application", *IEEE Trans. on Power Electronics*, vol. 5 no. 2, April 1990, pp. 229-235.
- [132] G. Asplund, "Application of HVDC Light to Power System Enhancement", *IEEE PES Winter Meeting 2000*, vol. 4, pp. 2498-2503.
- [133] G. Asplund, K. Eriksson and O. Tollerz, "Land and sea Cable Interconnections with HVDC Light", *CEPSI Conference 2000*, Manila, Philippines, October 2000.
- [134] L. Weimers, "HVDC Light: A new technology for a better environment", *IEEE Power Engineering Review*, August 1998, pp. 19-20.
- [135] NP Johnson , T.L. Tan, P. Miller and E. Acha, "A Laboratory Model for Harmonic Measurements in Windpower Generators", *IEEE Power Engineering Review*, August 1998, pp. 19-20.

Bibliography

- [136] A.I. Megahed and O.P. Malik, "Synchronous generator internal fault computation and experimental verification", *Proc. IEE Gener Trans and Distr.*, vol. 145, September 1998, pp. 604-610.
- [137] A.I. Megahed and O.P. Malik, "Simulation of Internal Faults in Synchronous Generator", *IEEE Trans. on Energy Conversion*, vol. 14, no. 4, December 1999, pp. 1306-1311.
- [138] C.W. Evans, *Engineering Mathematics: A Programmed Approach*, VNR International, 1989.

A. Generator Data and PSCAD/EMTDCTM Schematic Diagrams

A.1. Synchronous Generator Data Used for Validation with PSCAD/EMTDCTM

The generator data used for validation studies with PSCAD/EMTDCTM in Chapters 2 and 3 is obtained from reference [28]. The respective direct time phase-domain and the transformed axis $d - q - 0$ generator quantities are given as follow:

Phase Domain Parameters in $p.u.$:

$L_{a0} = 0.511$	$L_{kd} = 0.876$
$L_{a2} = 0.154$	$L_{kq} = 0.556$
$M_{s0} = -0.221$	$M_{fkd} = 0.674$
$M_{af} = 0.656$	$R_s = 0.0135$
$M_{ad} = 0.565$	$R_f = 0.00101$
$M_{aq} = 0.292$	$R_{kd} = 0.0207$
$L_{ff} = 0.980$	$R_{kq} = 0.065$

Transformed Axis Parameters :

$X_d = 0.969 p.u.$	$T_d' = 0.998 s$
$X_d' = 0.310 p.u.$	$T_d'' = 0.023 s$
$X_d'' = 0.213 p.u.$	$T_{d0}' = \frac{X_d}{X_d'} T_d' s = 3.1195 s$
$X_q = 0.492 p.u.$	$T_{d0}'' = \frac{X_d}{X_d''} T_d'' s = 0.0335 s$
$X_q'' = 0.271 p.u.$	$T_a = 0.013 s$

Standard Generator Base Value :

Base power = 1.29 MVA	Base Zbase = 27.9 ohm
Base voltage = 6 kV	Base Lbase = 0.088 H
Base frequency = 50 Hz	
Base speed = 314.159 rad/s	

A.2. Synchronous Generator and Asynchronous Machine Data for Other Simulation Studies

1) The generator data for simulations conducted in Chapter 4, 5 and 6 are [25]:

Phase Domain Parameters in *p.u.* :

$L_{a0} = 0.7415$	$L_{kd} = 0.93719$
$L_{a2} = 0.2455$	$L_{kq} = 0.43566$
$M_{s0} = -0.3335$	$M_{fkd} = 0.892$
$M_{af} = 0.8919$	$R_s = 0.0026$
$M_{ad} = 0.8919$	$R_f = 0.000426$
$M_{aq} = 0.4013$	$R_{kd} = 0.00526$
$L_{ff} = 0.9786$	$R_{kq} = 0.00406$

Standard Generator Base value :

Base power = 30MVA	Base speed = 314.159 rad/s
Base voltage = 13.8 kV	Base Zbase = 6.348 ohm
Base frequency = 50 Hz	Base Lbase = 0.02021 H
Inertia constant, $H = 4.6s$	

2) The data for *Gen 5* of Figure 4.1 in Chapter 4 at base of 30MVA:

Phase Domain Parameters in *p.u.* :

$L_{a0} = 0.736$	$L_{kd} = 0.7287$
$L_{a2} = 0.096$	$L_{kq} = 0.5381$
$M_{s0} = -0.269$	$M_{fkd} = 0.7026$
$M_{af} = 0.7026$	$R_s = 0.0069$
$M_{ad} = 0.7026$	$R_f = 0.000733$
$M_{aq} = 0.5107$	$R_{kd} = 0.01063$
$L_{ff} = 0.7706$	$R_{kq} = 0.0080$
$H = 5.4s$	

3) The *p.u.* asynchronous/induction machine data for the motor and generator modes studies in Chapter 4, 5 and 6, at a base of 30MVA are as follow:

Phase Domain Parameters in *p.u.* :

$L_{ss} = 1.7450$
$L_{rr} = 1.7450$
$L_{sm} = 0.825$
$L_{rm} = 0.825$
$M_{sr} = 1.650$
$R_{sm} = 0.0642$
$R_{rm} = 0.0637$
$H_m = 0.5s$

A.3. Schematic Diagrams in PSCAD/EMTDCTM

PSCAD/EMTDCTM is a general purpose time domain simulation tool for examining the behaviour of electrical networks. The operation of this industry standard power system package is based on a graphical user interface layout [35]. A library of power system components are readily available where they can be used to construct any desire circuits. The parameters for the network in PSCAD/EMTDCTM are represented in the actual unit. The *p.u.* value used in Figure 2.4, 2.9 and 3.2 are converted to their actual equivalent by multiplying by the base value. The *p.u.* field and rotor damper windings' responses produce by PSCAD/EMTDCTM are $\frac{3}{2}$ times the corresponding value in the direct time phase-domain.

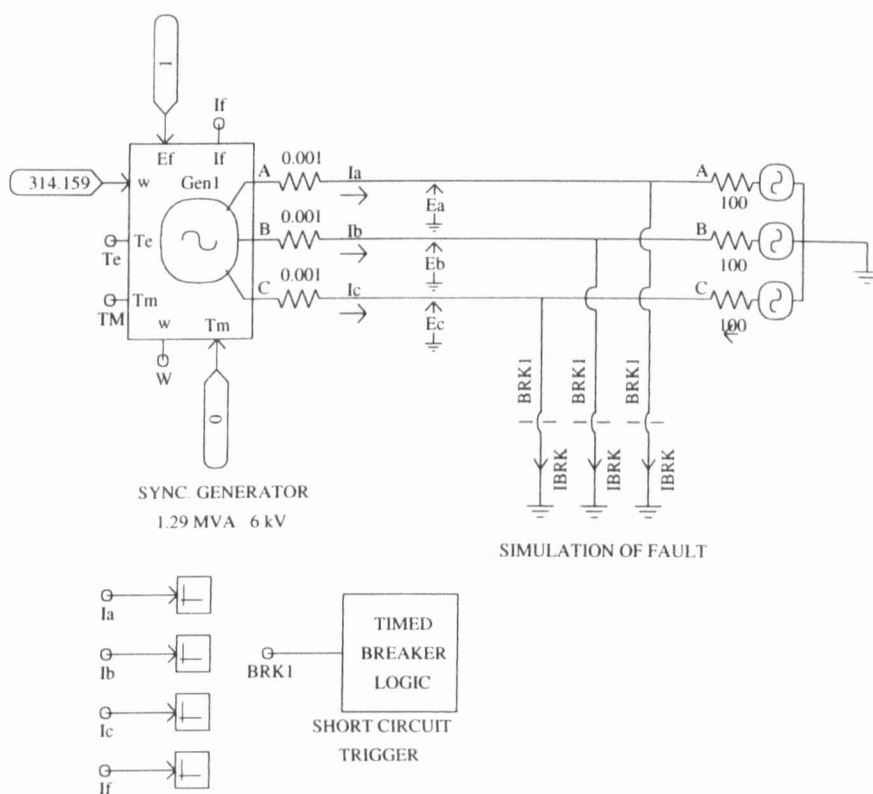


Figure A.1.: Generator connected to an infinite bus for short circuit fault analysis using PSCAD/EMTDCTM; corresponding results in Figure 2.2

A. Generator Data and PSCAD/EMTDCTM Schematic Diagrams

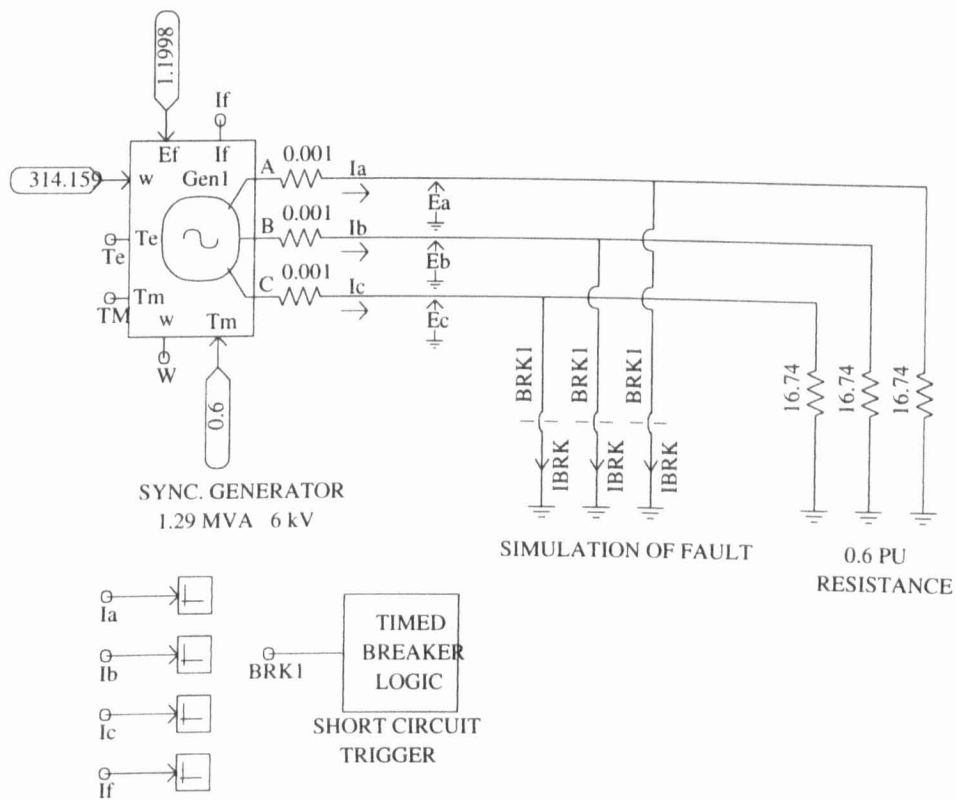


Figure A.2.: Generator connected to a load for short circuit fault analysis in PSCAD/EMTDCTM; corresponding results in Figure 2.5

A. Generator Data and PSCAD/EMTDCTM Schematic Diagrams

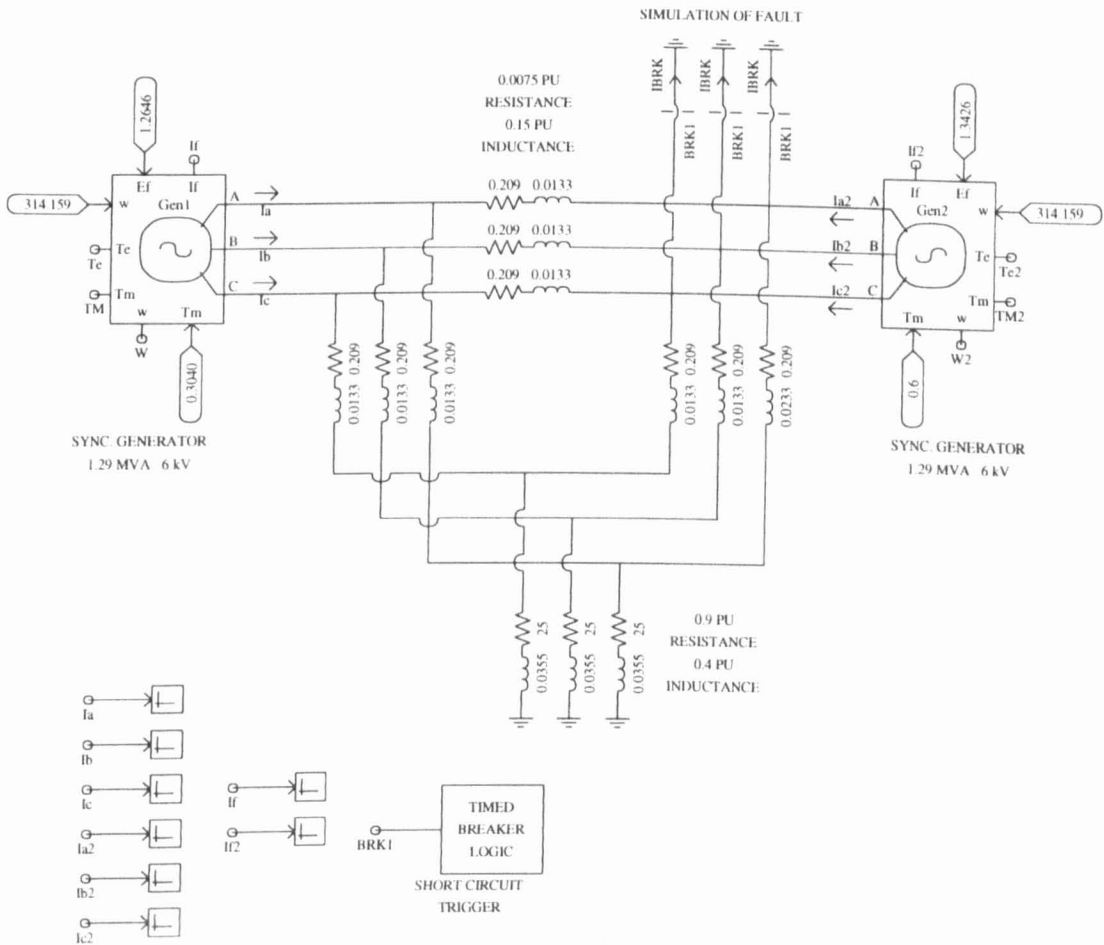


Figure A.3.: Multimachine network for short circuit fault analysis using PSCAD/EMTDCTM, corresponding results in Figure 3.3

A. Generator Data and PSCAD/EMTDCTM Schematic Diagrams

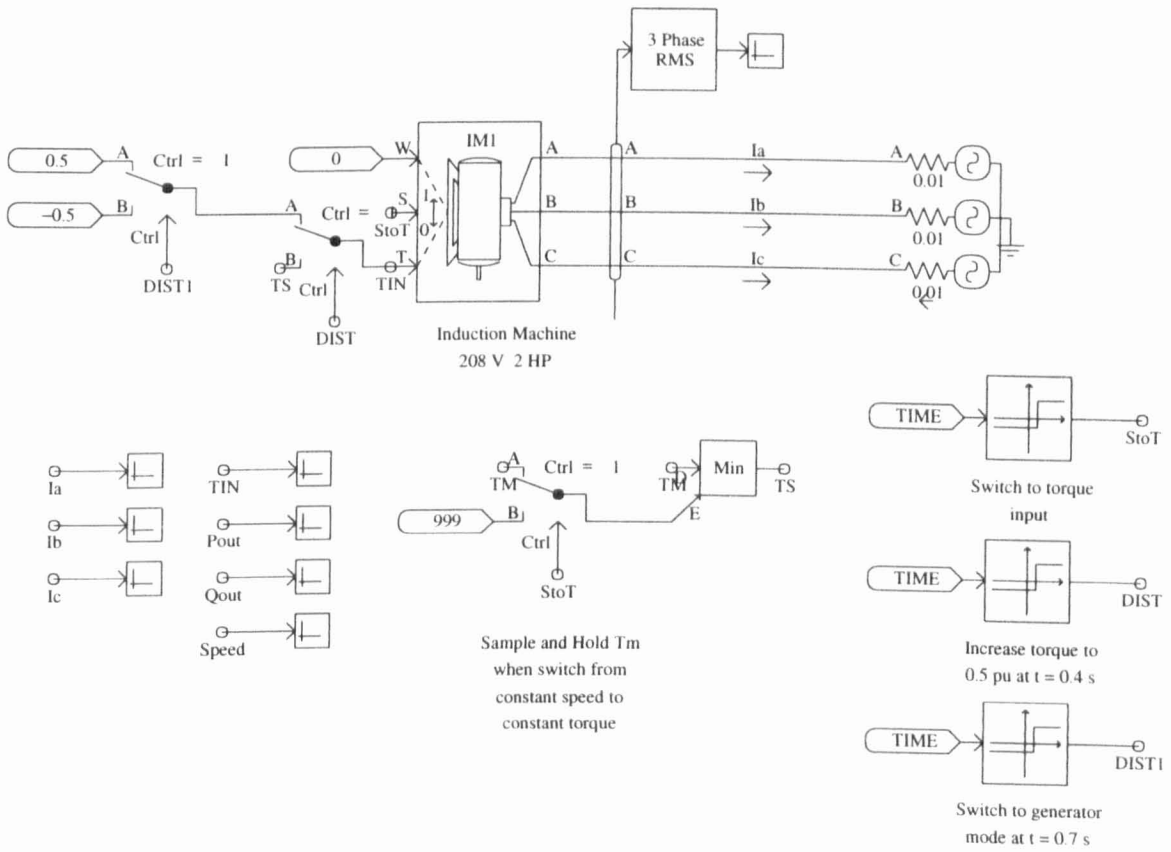


Figure A.4.: Asynchronous machine connected to a source for operational analysis using PSCAD/EMTDCTM; corresponding results in Figure 2.9

B. Trapezoidal Rule of Integration and Discretisation of Network and Generator Controllers Equations

B.1. Trapezoidal Rule

The trapezoidal rule is an implicit integration technique for that can be applied to solve ordinary differential equations [34][138]. Consider the curve $f(t)$ in Figure B.1 on the interval of Δt . The integral of the function between the interval can be represented by,

$$\int_{t-\Delta t}^t f(t) dt \quad (\text{B.1})$$

To determine the definite integral we need to know the area of the region enclosed by the function within that time interval. This can be done by using the trapezoids approximation where the area of the trapezium is given by,

$$A = \frac{\Delta t}{2} (f(t) + f(t - \Delta t)) \quad (\text{B.2})$$

The trapezoidal rule is hence derive as,

$$\int_{t-\Delta t}^t f(t) dt = \frac{\Delta t}{2} (f(t) + f(t - \Delta t)) \quad (\text{B.3})$$

An example of application of the trapezoidal rule in the solution of a differential equation is given as follow,

$$\frac{dy(t)}{dt} = f(t) \quad (\text{B.4})$$

where integrating both sides and applying the trapezoidal rule,

$$y(t) - y(t - \Delta t) = \frac{\Delta t}{2} (f(t) + f(t - \Delta t))$$

B. Trapezoidal Rule of Integration and Discretisation of Network and Generator Controllers Equations

$$y(t) = \frac{\Delta t}{2} f(t) + y(t - \Delta t) + \frac{\Delta t}{2} f(t - \Delta t) \tag{B.5}$$

The solution is based on assumption that the value of y and f are known at time t thereby making the method implicit. If more than one equations exist in this form for y and f then direct simultaneous solution can be applied to obtain the value of the variables.

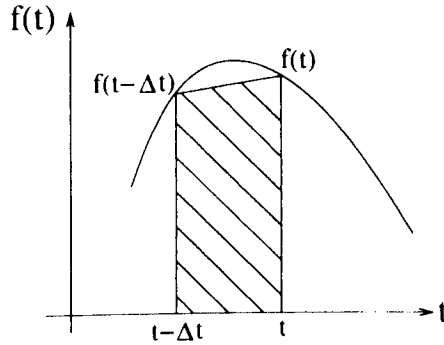


Figure B.1.: The trapezoidal rule

B.2. Discretisation of the Network Equations

The power network in this thesis is represented by interconnections of resistances, inductances and capacitances where a general representation is given in Figure B.2.

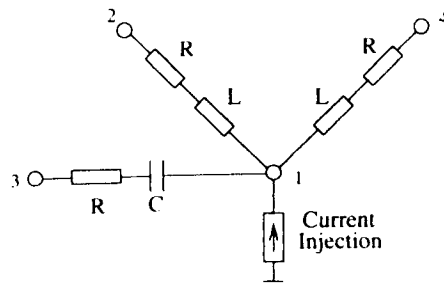


Figure B.2.: Connection of simple network to node

The network branches can be represented mathematically by simple AC circuit analysis where in one phase they are given by,

$$v_1(t) - v_2(t) = R_{12}i_{12}(t) + L_{12} \frac{di_{12}(t)}{dt} \tag{B.6}$$

$$v_1(t) - v_3(t) = R_{13}i_{13}(t) + \frac{1}{C_{13}} \int i_{12}(t) dt \tag{B.7}$$

$$v_1(t) - v_4(t) = R_{14}i_{14}(t) + L_{14} \frac{di_{14}(t)}{dt} \tag{B.8}$$

B. Trapezoidal Rule of Integration and Discretisation of Network and Generator Controllers Equations

Discretising the above network equations results in,

$$i_{12}(t) = \left(R_{12} + \frac{2}{\Delta t} L_{12} \right)^{-1} (v_1(t) - v_2(t)) + hist_{12} \quad (\text{B.9})$$

$$i_{13}(t) = \left(R_{13} + \frac{\Delta t}{2C_{13}} \right)^{-1} (v_1(t) - v_3(t)) + hist_{13} \quad (\text{B.10})$$

$$i_{14}(t) = \left(R_{14} + \frac{2}{\Delta t} L_{14} \right)^{-1} (v_1(t) - v_4(t)) + hist_{14} \quad (\text{B.11})$$

where

$$hist_{12} = \left(R_{12} + \frac{2}{\Delta t} L_{12} \right)^{-1} \left((v_1(t - \Delta t) - v_2(t - \Delta t)) - \left(R_{12} - \frac{2}{\Delta t} L_{12} \right) i_{12}(t - \Delta t) \right)$$

$$hist_{13} = \left(R_{13} + \frac{\Delta t}{2C_{13}} \right)^{-1} \left(-(v_1(t - \Delta t) - v_3(t - \Delta t)) + \left(R_{13} - \frac{\Delta t}{2C_{13}} \right) i_{13}(t - \Delta t) \right)$$

$$hist_{14} = \left(R_{14} + \frac{2}{\Delta t} L_{14} \right)^{-1} \left((v_1(t - \Delta t) - v_4(t - \Delta t)) - \left(R_{14} - \frac{2}{\Delta t} L_{14} \right) i_{14}(t - \Delta t) \right)$$

Using Kirchoff's current law on *Node 1* of Figure B.2, the current injected by the node can be represented by,

$$i_1(t) = i_{12}(t) + i_{13}(t) + i_{14}(t) \quad (\text{B.12})$$

where by direct substitution,

$$\begin{aligned} & \left(\left(R_{12} + \frac{2}{\Delta t} L_{12} \right)^{-1} + \left(R_{13} + \frac{\Delta t}{2C_{13}} \right)^{-1} + \left(R_{14} + \frac{2}{\Delta t} L_{14} \right)^{-1} \right) v_1(t) - \left(R_{12} + \frac{2}{\Delta t} L_{12} \right)^{-1} v_2(t) \\ & - \left(R_{13} + \frac{\Delta t}{2C_{13}} \right)^{-1} v_3(t) - \left(R_{14} + \frac{2}{\Delta t} L_{14} \right)^{-1} v_4(t) \\ & = i_1(t) - hist_{12} - hist_{13} - hist_{14} \end{aligned} \quad (\text{B.13})$$

The matrix and vector of equations (3.13) is obtained using the similar approach to discretise a three-phase *n-node* network.

B.3. Discretisation of Generator Controllers Equations

B.3.1. Generator Excitation Control

The discretisation of the excitation control state equations (3.18)-(3.20) for the exciter, automatic voltage regulator and stabiliser block is presented as follow,

B. Trapezoidal Rule of Integration and Discretisation of Network and Generator Controllers Equations

The exciter block:

$$\left(1 + \frac{\Delta t}{2\tau_{ex}}\right) E_{fd}(t) = \frac{\Delta t}{2\tau_{ex}} V_r(t) + E_{fdhis} \quad (\text{B.14})$$

where

$$E_{fdhis} = \frac{\Delta t}{2\tau_{ex}} V_r(t - \Delta t) + \left(1 - \frac{\Delta t}{2\tau_{ex}}\right) E_{fd}(t - \Delta t)$$

The regulator block:

$$\left(1 + \frac{\Delta t}{2\tau_a}\right) V_r(t) = \frac{\Delta t}{2\tau_a} K_a V_{ef}(t) + V_{rhis} \quad (\text{B.15})$$

where

$$V_{rhis} = \frac{\Delta t}{2\tau_a} K_a V_{ef}(t - \Delta t) + \left(1 - \frac{\Delta t}{2\tau_a}\right) V_r(t - \Delta t)$$

The stabiliser block:

$$\left(1 + \frac{\Delta t}{2\tau_f}\right) V_f(t) = \frac{\Delta t}{2\tau_f} K_f E_{fd}(t) + V_{fhis} \quad (\text{B.16})$$

where

$$V_{fhis} = \frac{\Delta t}{2\tau_f} K_f E_{fd}(t - \Delta t) + \left(1 - \frac{\Delta t}{2\tau_f}\right) V_f(t - \Delta t)$$

These equations can be solve simultaneously with the known variables of the generator terminal voltages.

B.3.2. Turbine Governor

The discretisation of the turbine governor state equations (3.28) and (3.29) for the exciter, automatic voltage regulator and stabiliser block is presented as follow,

The turbine block:

$$\left(1 + \frac{\Delta t}{2\tau_{tr}}\right) P_m(t) = \frac{\Delta t}{2\tau_{tr}} P_g(t) + P_{mhis} \quad (\text{B.17})$$

where

$$P_{mhis} = \frac{\Delta t}{2\tau_{tr}} P_g(t - \Delta t) + \left(1 - \frac{\Delta t}{2\tau_{tr}}\right) P_m(t - \Delta t)$$

The governor block:

$$\left(1 + \frac{\Delta t}{2\tau_{gv}}\right) P_g(t) = \frac{\Delta t}{2\tau_{gv}} P_{gv}(t) + P_{ghis} \quad (\text{B.18})$$

where

$$P_{ghis} = \frac{\Delta t}{2\tau_{gv}} P_{gv}(t - \Delta t) + \left(1 - \frac{\Delta t}{2\tau_{gv}}\right) P_g(t - \Delta t)$$

C. Network Reduction of Coherent Generators Bus

In order to demonstrate the network reduction method for the coherent generators bus, consider the 4 generators power system of Figure C.1. The approach adopted here is similar to that in [85] with exception that the voltage of the coherent generators are deemed the same.

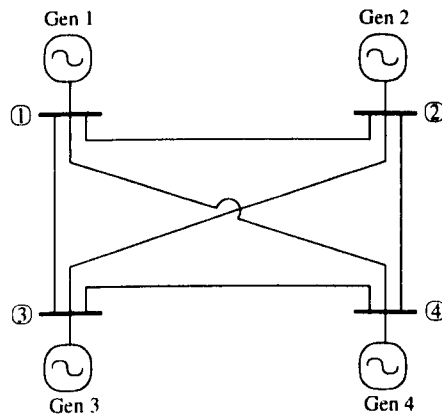


Figure C.1.: Actual power system network

Assume that for a particular fault condition *Gen 3* and *4* are coherent and to be replace by an equivalent generator. The coherency criterion is defined by a group of generators oscillating with same angular speed and voltage ratio. Applying the above definition to *Gen 3* and *4* gives the following,

$$\delta_3(t) - \delta_4(t) = c \quad (\text{C.1})$$

$$V_4/V_3 = b \quad (\text{C.2})$$

where c is constant and b is equal to 1.

It is desired to replace the coherent *Gen 3* and *4* with an equivalent unit and thus reduce the system of Figure C.1 to a simpler 2 generators system as in Figure C.2. To achieve this, the steady state the network equations for Figure C.1 is considered first as,

C. Network Reduction of Coherent Generators Bus

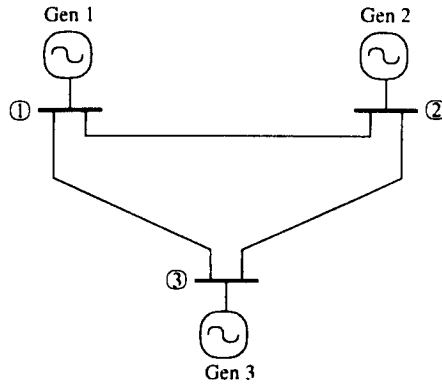


Figure C.2.: Reduced equivalent power system network

$$\begin{aligned}
 I_1 &= y_{11}V_1 + y_{12}V_2 + y_{13}V_3 + y_{14}V_4 \\
 I_2 &= y_{21}V_1 + y_{22}V_2 + y_{23}V_3 + y_{24}V_4 \\
 I_3 &= y_{31}V_1 + y_{32}V_2 + y_{33}V_3 + y_{34}V_4 \\
 I_4 &= y_{41}V_1 + y_{42}V_2 + y_{43}V_3 + y_{44}V_4
 \end{aligned} \tag{C.3}$$

Substituting for V_4 with V_3 in equation (C.3) gives,

$$\begin{aligned}
 I_1 &= y_{11}V_1 + y_{12}V_2 + (y_{13} + y_{14})V_3 \\
 I_2 &= y_{21}V_1 + y_{22}V_2 + (y_{23} + y_{24})V_3 \\
 I_3 &= y_{31}V_1 + y_{32}V_2 + (y_{33} + y_{34})V_3 \\
 I_4 &= y_{41}V_1 + y_{42}V_2 + (y_{43} + y_{44})V_3
 \end{aligned} \tag{C.4}$$

The equivalent model will have the total current injection of *Gen 3* and *4*, thus adding I_3 and I_4 and rewriting the new sets of equations,

$$\begin{aligned}
 I_1 &= Y_{11}V_1 + Y_{12}V_2 + Y_{13}V_3 \\
 I_2 &= Y_{21}V_1 + Y_{22}V_2 + Y_{23}V_3 \\
 I_e &= Y_{31}V_1 + Y_{32}V_2 + Y_{33}V_3
 \end{aligned} \tag{C.5}$$

where

C. Network Reduction of Coherent Generators Bus

$$\begin{aligned} I_e &= I_3 + I_4 \\ Y_{11} &= y_{11}; Y_{12} = y_{12}; Y_{13} = y_{13} + y_{14} \\ Y_{21} &= y_{21}; Y_{22} = y_{22}; Y_{23} = y_{23} + y_{24} \\ Y_{31} &= y_{31} + y_{41}; Y_{32} = y_{12} + y_{42}; Y_{33} = y_{33} + y_{34} + y_{43} + y_{44} \end{aligned} \tag{C.6}$$

The network equation for Figure C.1 has now been reduced to the equivalent for the network of Figure C.2. The new admittance matrix for this system is obtained by modifying the elements according to equation (C.6). The voltages and current for *Gen 1* and *2* is the same for the original and equivalent systems. The voltage of *Gen 3* and *4* is also the same and an equivalent current of I_e is fed from the equivalent generator into the busbar.

Even though the network reduction is carried out during the steady state, the result obtained for the network impedances, which are reciprocal of the admittance, are equal to the actual resistances and inductances in the direct time phase-domain since the rated speed of 1 *p.u.* is considered.

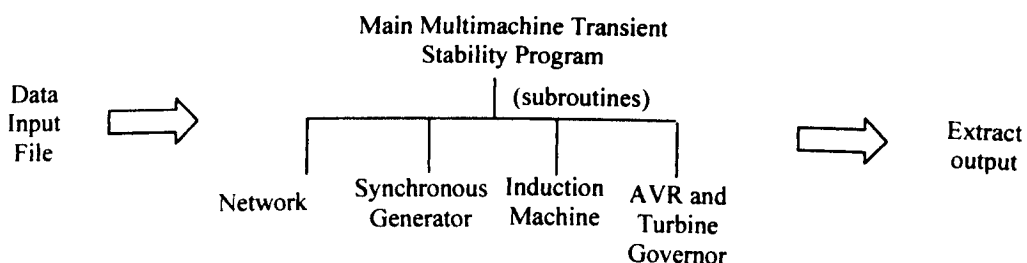
D. Computer Program Code Listing

The program codes listed in this appendix are solely written to test the solution of the multimachine model proposed in this thesis. The program is written using MatlabTM version 5.3. MatlabTM is selected as the programming language as it offers the most convenient way to test the proposed multimachine model. A wide range of mathematical toolboxes are available within MatlabTM, hence, making the programming development straightforward where effort can be focus on building of the model.

An overview of the general transient stability program and the program listings of its main building blocks are given in Section D.1. Descriptions of each building block and its respective code listing can be found in the relevant program files. Power electronics controllers subroutines are provided in Section D.2.

D.1. General Transient Stability Program Listing

The structure of the general transient stability program can be summarise as follow:



The program is divided into three general blocks:

- 1) The data input file where the relevant data for the network under study are to be entered. (**DATAIN.m**)
- 2) The main transient stability program solves the network and make call to the relevant subroutines throughout the simulation process. (**Main_TS.m**)
- 3) The extraction of simulation responses from the main transient stability program. (**call_store.m** and **call_plot.m**)

D. Computer Program Code Listing

In order to use the program, the user needs to provide the relevant data of the network under study in the data input file, **DATAIN.m**.

Once the complete network data has been entered, the transient stability program can be executed by running the main file, **Main_TS.m**, where the input data from the **DATAIN.m** file are read in automatically. Any disturbances to the network can be set by modifying an auxiliary file, **call_disturbances.m**.

The simulation responses that are of interest can be stored by modifying the **call_store.m** file. In this file, the simulation response of every time step is stored as an array, where upon completion of the simulation, this stored data can be plotted using the MatlabTM plot command. Plotting is carried out in the **call_plot.m** file.

Files that need to be modify by the user:

- **DATAIN.m**
- **call_disturbances.m**
- **call_store.m**
- **call_plot.m**

D. Computer Program Code Listing

```

Lgenhis = [ ]; % matrix of generator inductances at t = tstart-dt. For network with two generators:
%           Lgenhis = [ [L_1] [L_2] ] ;
%
%           
%
%
Rgen = % matrix of generator resistance. Refer to Lgenhis for format.

%% The program allows user to define a generator node as a fixed source to represent an infinite supply.
FGEN = ; % A flag to indicate that there are generator nodes with fixed source. 1) Fgen=1, there are fixed
% source in the network. 2) Fgen=0, there are no fixed source in the network

FGENO = [ ]; % which generator node is a fixed source. For the example network if Node 2 is a fixed source,
%           FGENO = [ 2 ] ;

FGENMAG = [ ]; % magnitude of the fixed source voltage.
FGENANG = [ ]; % angle of the fixed source voltage.

%% ===== Mandatory Induction Machine Data ===== %%
%% Include data only if there are induction machine in the network

VrotorIM = [ ]; % vector of induction machine rotor voltage. The induction machine rotor voltage is always
% zero. Same format as synchronous generator.

IrotorIM = [ ]; % vector of induction machine rotor current. Same format as synchronous generator

Lss = [ ]; % vector of induction machine inductance Lss. Same format as synchronous inductance, eg Lao

Lrr = [ ]; % vector of induction machine inductance Lrr. Refer to Lss for format.

Lsm = [ ]; % vector of induction machine inductance Lsm. Refer to Lss for format.

Lrm = [ ]; % vector of induction machine inductance Lrm. Refer to Lss for format.

Msr = [ ]; % vector of induction machine inductance Msr. Refer to Lss for format.

ZIM = [ ]; % vector of induction machine inertia constant. ZIM = 1/2H. Refer to Lss for format.

PmIM = [ ]; % vector of induction machine mechanical power/torque

PeIMhis = [ ]; % vector of induction machine electrical power/torque at t = tstart - dt.

wrIMhis = [ ]; % vector of induction machine speed at t = tstart - dt.

wrIMhisec = [ ]; % vector of induction machine speed at t = tstart - 2*dt

thetaIMhis = [ ]; % vector of induction machine rotor angle at t = tstart - dt.

LIMhis = [ ]; % matrix of induction machine inductances at t = tstart - dt.

RIM = [ ]; % matrix of induction machine resistances

```

D. Computer Program Code Listing

=====
 %% Mandatory Generator Excitation Control Data =====%%
 %% Please refer to excitation block model for terms

```

FAVR = [ ];           % vector of flags to indicate that the respective generators in the network has AVR control. For
                    % the example network, if only generator Gen 1 has an AVR control,
                    %           FAVR = [1 ; 0 ] ;
                    %           |
                    %           |-----> '0' because Gen 2 has no AVR
                    %           |
                    %           |-----> '1' because Gen 1 has AVR
KA = [ ];             % vector of AVR propotional gain. For the example network if gain Ka of Gen 1 AVR is 100,
                    %           KAAVR = [100 ; 0] ;
Ta = [ ];             % vector of AVR time-constant. For the example network if  $\tau_a$  of Gen 1 AVR is 0.01,
                    %           TaAVR = [0.01 ; 0] ;
Tex = [ ];            % vector of exciter time constant. For the example network if  $\tau_{ex}$  of Gen 1 AVR is 0.05,
                    %           TexAVR = [0.05 ; 0] ;
Vrhis = [ ];          % vector of AVR output, Vr, at t = tstart - dt. Refer to KAAVR for format
Efdhis = [ ];         % vector of exciter output, Efd, at t = tstart - dt. Refer to KAAVR for format
Vthis = [ ];          % vector of Vt at t = tstart - dt. Refer to KAAVR for format.
Vref = [ ];           % vector of excitation system reference voltage. Refer to KAAVR for format.
Vmax = [ ];           % vector of AVR maximum limiter. Refer to KAAVR for format.
Vmin = [ ];           % vector of AVR minimum limiter. Refer to KAAVR for format.
CRL = [ ];            % vector of scale factor of excitation output, efd = CRL*Efd. Refer to KAAVR for format.
  
```

=====
 %% Mandatory Generator Turbine Governor Data =====%%
 %% Please refer to turbine governor block model for terms. The format of the data are similar to that of the AVR.

```

FTG = [ ];            % vector of flags to indicate that the respective generators in the network has turbine governor
control.
REG = [ ];            % vector of speed regulation, R.
Tgv = [ ];            % vector of governor time-constant
Ttr = [ ];            % vector of turbine time-constant.
TGmax = [ ];          % vector of governor maximum limiter.
TGmin = [ ];          % vector of governor minimum limiter.
Pgvhis = [ ];         % vector of governor input at t = tstart - dt.
Pghis = [ ];          % vector of governor output at t = tstart - dt.
Pref = [ ];           % vector of reference power, Pref.
wref = [ ];           % vector of reference speed, wref
  
```

D. Computer Program Code Listing

```

%%=====
%%
%% File      :      Main_TS.m
%% Description :      Main transient stability program. Input data in DATAIN m file are read in and transient
%%                  stability solutions to the network under study are obtained.
%%
%%=====
%%
DATAIN; % a call to execute the datain m file
count=1; % a counter to record simulation responses to be stored for plotting

% Start simulation
for t = tstart:dt:tstop

%% Interpolation to predict load angle of generators at the beginning of each time step using preceding values %%

for j=1:1:Ngen
beta(j) = 2*betahisec(j) - betahisec(j) + ws*Z(j)*(Pm(j)-Pehis(j))*dt^2;
end

%% Interpolation to predict rotor angle of induction machines at the beginning of each time step using preceding values %%

for j=1:1:Nind
thetaIM(j) = 3*dt/2 * (wriMhis(j)+wriMhisec(j))+thetaIMhis(j);
end

%% Check to see if there is any network disturbances %%

[t,R,L] = call_disturbances(t,R,L);

%% Discretisation of network %%

[B,A,G,Ggg,Ggl,Glg,Gll,Histg,Histl,Vhis] =
call_networkwithcap(lbranch,Vnode_mac,Vnode_load,R,L,C,Ct,Nmac,Nnode,t,dt,ws, Ncap,brcap,brcapno,brcapval,Nbranch);

%% Discretisation of synchronous generator %%
k = 1;
n = 1;
Requ(Nmac*3,Nmac*3)=0;
U(Nmac*3,Nmac*3) = 0;
for j=1:1:Ngen
[Es(k:k+2),Requ(k:k+2,k:k+2),theta(j),Vhiss(k:k+2),Vhisr(k:k+2),RRrr(1:3,k:k+2),RRrs(1:3,k:k+2),Lgen(1:6,n:n+5)] =
call_generator(Lao(j),La2(j),Mso(j),Maf(j),Mad(j),Maq(j),Lff(j),Lkkd(j),Lkkq(j),Mfkd(j),Lgenhis(1:6,n:n+5),Rgen(1:6,n:n+5),Vn
ode_mac(k:k+2),Inode_mac(k:k+2),Vrotor(k:k+2),Irotor(k:k+2),beta(j),ws,dt,t,teuler,teuler2,teuler2end);
U(k,k)=1;
U(k+1,k+1)=1;
U(k+2,k+2)=1;
k=k+3;
n=n+6;
end

%% Define machine nodes with fixed source %%
if(FGEN==1)
for j=1:1:size(FGENO)
Es(FGENO(j)*3-2:FGENO(j)*3) = -FGENMAG(j)*[sin(ws*t+FGENANG(j)),sin(ws*t+FGENANG(j)-
2.0944),sin(ws*t+FGENANG(j)+2.0944)];
Requ(FGENO(j)*3-2:FGENO(j)*3,FGENO(j)*3-2:FGENO(j)*3) = [0 0 0; 0 0 0; 0 0 0];
end
end

%% Discretisation of induction machine %%
m = 1;
p = 1;
for j=1:1:Nind

```

D. Computer Program Code Listing

```

[Es(k:k+2),Requ(k:k+2,k:k+2),VhissIM(m:m+2),VhisrIM(m:m+2),RRrrIM(1:3,m:m+2),RRrsIM(1:3,m:m+2),LIM(1:6,p:p+5)] =
call_induction(Lss(j),Lrr(j),Lsm(j),Lrm(j),Msr(j),LIMhis(1:6,p:p+5),RIM(1:6,p:p+5),Vnode_mac(k:k+2),Inode_mac(k:k+2),VrotorIM(m:m+2),IrotorIM(m:m+2),thetaIM(j),ws,dt,t,teuler,teuler2,teuler2end) ;
U(k,k)=1;
U(k+1,k+1)=1;
U(k+2,k+2)=1;
k=k+3;
m=m+3;
p=p+6;
end

%% Solution of the multimachine network for current time step %%

N = Requ * (Ggg-Ggl*inv(Gll)*Glg) - U ;

M = Requ * (Ggl*inv(Gll)*Histl-Histg) - Es' ;

Vnode_mac = inv(N)*M ;
Vnode_load = -inv(Gll)*Glg*Vnode_mac - inv(Gll)*Histl ;
Inode_mac = (Ggg - Ggl*inv(Gll)*Glg)*Vnode_mac - Ggl*inv(Gll)*Histl + Histg ;
Inode_load = Glg*Vnode_mac + Gll*Vnode_load + Histl ;
Ibranch = inv(A)*C*[Vnode_mac ; Vnode_load] - inv(A)*Vhis ;

%% Calculate generator rotor current and flux %%
k = 1;
n = 1;
for j=1:1:Ngen
Irotor(k:k+2)=inv(RRrr(1:3,k:k+2)) * (Vrotor(k:k+2)-RRrs(1:3,k:k+2)*Inode_mac(k:k+2)+Vhisr(k:k+2)) ;
flux(n:n+5) = Lgen(1:6,n:n+5) * [Inode_mac(k:k+2);Irotor(k:k+2)] ;
k=k+3;
n=n+6;
end

%% Calculate induction machine rotor current and flux %%
m = 1;
n = 1;
for j=1:1:Nind
IrotorIM(m:m+2)=inv(RRrrIM(1:3,m:m+2)) * (VrotorIM(m:m+2)+RRrsIM(1:3,m:m+2)*Inode_mac(k:k+2)+VhisrIM(m:m+2)) ;
fluxIM(n:n+5) = LIM(1:6,n:n+5) * [-1*Inode_mac(k:k+2) ; IrotorIM(m:m+2) ] ;
n=n+6;
m=m+3;
k=k+3 ;
end

%% Calculating the electrical torque/power, speed and load angle of generators for the current time-step %%
k=1 ;
n=1 ;
for j=1:1:Ngen
Pe(j) = 2/(3*sqrt(3)) * ( flux(n)*(Inode_mac(k+1)-Inode_mac(k+2)) + flux(n+1)*(Inode_mac(k+2)-Inode_mac(k)) +
flux(n+2)*(Inode_mac(k)-Inode_mac(k+1))) ;
if(t<0.0)
Pe(j)=Pm(j);
end
wr(j) = ws*(-Z(j) * dt/2 * Pe(j)) + Z(j) * dt/2 * (2 *ws*Pm(j) + (2/(Z(j)*dt))*wrhis(j) - ws*Pehis(j));
k=k+3;
n=n+6;
end

%% Calculating the electrical torque/power, speed and rotor angle of inductions machines for the current time-step %%
m=1;
for j=1:1:Nind
PeIM(j) = -Msr(j)* ((
Inode_mac(k)*IrotorIM(m)+Inode_mac(k+1)*IrotorIM(m+1)+Inode_mac(k+2)*IrotorIM(m+2))*sin(thetaIM(j)) +
(Inode_mac(k)*IrotorIM(m+1)+Inode_mac(k+1)*IrotorIM(m+2)+Inode_mac(k+2)*IrotorIM(m))*sin(thetaIM(j)+2.0944) +
(Inode_mac(k)*IrotorIM(m+2)+Inode_mac(k+1)*IrotorIM(m)+Inode_mac(k+2)*IrotorIM(m+1))*sin(thetaIM(j)-2.0944) ) ;

```

D. Computer Program Code Listing

```

if(t<10.0)
PeIM(j)=PmIM(j);
end
wrIM(j) = ws * ZIM(j) * dt/2 * PeIM(j) + ws*dt/2 * ZIM(j) * PeIMhis(j) - ws*ZIM(j)*PmIM(j)*dt + wrIMhis(j);
m=m+3;
k=k+3;
end

%% Calculating of generator load angle and induction machine rotor angle %%

beta = dt/2 * wr' + dt/2 * (wrhis - 2*ws + 2/dt * betahis) ;
if(Nind==0)
thetalM = dt/2 * (wrIM' + wrIMhis ) + thetalMhis ;
end

%% Data for the AVR %%
%% Vt is the magnitude of one phase of the generator terminal voltage. It needs to be obtained from the sinusoidal voltage
waveform by
%% calculation.

k=1;
for j=1:Ngen
if(FAVR(j)==1)
[Vrotor(k),Efdhis(j),Vrhis(j)]=call_AVR(KA(j),Ta(j),Tex(j),Efdhis(j),Vrhis(j),Vthis(j),Vt,Vref(j),Vmax(j),Vmin(j),CRL(j),dt) ;
end
k=k+3;
end

%% Data for the turbine governor %%

for j=1:Ngen
if(FTG(j)==1)
[Pm(j),Pgphis(j),Pgvhis(j)] =
call_turgov(Tgv(j),Ttr(j),REG(j),wref(j),wr(j)/ws,wrhis(j)/ws,Pghis(j),Pm(j),Pgvhis(j),Pref(j),TGmax(j),TGmin(j),dt) ;
end
end

%%%%%%%%%%%%%%%%%%%%%%%%%%%%%%%%%%%%%%%%%%%%%%%%%%%%%%%%%%%%%%%%%%%%%%%%

%% Updating of history ( t = t - dt) term of generator before the next time-step %%
betahisec = betahis ;
betahis = beta ;
Pehis = Pe' ;
wrhis = wr' ;
Lgenhis = Lgen ;

%% Updating of history ( t = t- dt) term of induction machine before the next time-step%%
if(Nind==0)
wrIMhisec = wrIMhis ;
wrIMhis = wrIM' ;
thetalMhis = thetalM ;
PeIMhis = PeIM' ;
LIMhis = LIM ;
end

%% Storing of data to be plotted

[count] = call_store(count)

end %% end simulation when tstop is reached

%% Plotting the stored data after the simulation is completed

call_plot ;

```

D. Computer Program Code Listing

```
%% ===== %%
%% File      :      call_disturbances.m      %%
%% Description :      This subroutine is called by Main_TS to check if there are any network disturbances. %%
%%              Network disturbances are simulated by changing the network R and L matrix. This file is %%
%%              not generic.. The user needs to modify this file according to the type of disturbances that %%
%%              is of interest.                %%
%% ===== %%

tfault = ;          % user need to define the start time of fault
tclear = ;         % user need to define the end time of fault

function[R,L] = call_disturbances(t,R,L)

%% For the example network in the DATAIN.m file, if a three-phase fault occurs at Node 3 it can be simulated by changing the
%% network R and L parameter by shorting out the load to ground,

if(t>tfault)
R(10,10) = 0.0001; R(11,11) = 0.0001 ; R(12,12) = 0.0001 ;
L(10,10) = 0.0001; L(11,11) = 0.0001 ; L(12,12) = 0.0001 ;
end

if(t>tclear)
R(10,10) = R30a; R(11,11) = R30a ; R(12,12) = R30a ;
L(10,10) = L30a ; L(11,11) = L30a ; L(12,12) = L30a ;
end

%% If it is a single-phase-to-ground fault, just short one phase

if(t>tfault)
R(10,10) = 0.0001;
L(10,10) = 0.0001;
end

if(t>tclear)
R(10,10) = R30a;
L(10,10) = L30a;
end
```

D. Computer Program Code Listing

```

%%=====%%
%% File      :      call_network.m                %%
%% Description :      This subroutine is called by Main_TS to obtain the discretised representation of the network. %%
%%=====%%

function[B,A,G,Ggg,Ggl,Glg,Gll,Histg,Histl,Vhis] =
call_network(Ibranch,Vnode_mac,Vnode_load,R,L,C,Ct,Nmac,Nnode,t,dt,ws,teuler,teuler2,teuler2end,Ncap,brcap,brcapno,
brcapval,Nbranch) ;

Ibranches_his = Ibranch ;

Vnode_his = [Vnode_mac; Vnode_load] ;

B = (dt*R - 2*L)/dt;

%% Discretisation of the shunt branches where the active element is a capacitor %%
if(brcap==1)
for j=1:size(brcapno)
B(brcapno(j)*3-2, brcapno(j)*3-2) = B(brcapno(j)*3-2, brcapno(j)*3-2) + dt*ws/(2*brcapval(j)) ;
B(brcapno(j)*3-1, brcapno(j)*3-1) = B(brcapno(j)*3-1, brcapno(j)*3-1) + dt*ws/(2*brcapval(j)) ;
B(brcapno(j)*3, brcapno(j)*3) = B(brcapno(j)*3, brcapno(j)*3) + dt*ws/(2*brcapval(j)) ;
C(brcapno(j)*3-2,Ncap(j)*3-2) = -C(brcapno(j)*3-2, Ncap(j)*3-2) ;
C(brcapno(j)*3-1, Ncap(j)*3-1) = -C(brcapno(j)*3-1, Ncap(j)*3-1) ;
C(brcapno(j)*3, Ncap(j)*3) = -C(brcapno(j)*3, Ncap(j)*3) ;
end
end
%%%%%%%%%%%%%%%%%%%%%%%%%%%%%%%%%%%%%%%%%%%%%%%%%%%%%%%%%%%%%%%%%%%%%%%%

Vhis = B * Ibranches_his - C*Vnode_his ;

%% Discretisation of the shunt branches where the active element is a capacitor %%
if(brcap==1)
for j=1:size(brcapno)
C(brcapno(j)*3-2,Ncap(j)*3-2) = -C(brcapno(j)*3-2,Ncap(j)*3-2) ;
C(brcapno(j)*3-1,Ncap(j)*3-1) = -C(brcapno(j)*3-1,Ncap(j)*3-1) ;
C(brcapno(j)*3, Ncap(j)*3) = -C(brcapno(j)*3,Ncap(j)*3) ;
end
end
%%%%%%%%%%%%%%%%%%%%%%%%%%%%%%%%%%%%%%%%%%%%%%%%%%%%%%%%%%%%%%%%%%%%%%%%

A = (dt*R + 2*L)/dt ;

%% Discretisation of the shunt branches where the active element is a capacitor %%
if(brcap==1)
for j=1:size(brcapno)
A(brcapno(j)*3-2, brcapno(j)*3-2) = A(brcapno(j)*3-2, brcapno(j)*3-2) + dt*ws/(2*brcapval(j)) ;
A(brcapno(j)*3-1, brcapno(j)*3-1) = A(brcapno(j)*3-1, brcapno(j)*3-1) + dt*ws/(2*brcapval(j)) ;
A(brcapno(j)*3, brcapno(j)*3) = A(brcapno(j)*3, brcapno(j)*3) + dt*ws/(2*brcapval(j)) ;
end
end
%%%%%%%%%%%%%%%%%%%%%%%%%%%%%%%%%%%%%%%%%%%%%%%%%%%%%%%%%%%%%%%%%%%%%%%%

G = Ct*inv(A)*C ;
Hist = -Ct*inv(A)*Vhis ;

Ggg = G(1:Nmac*3, 1:Nmac*3);
Ggl = G(1:Nmac*3, Nmac*3+1:Nnode*3);
Glg = G(Nmac*3+1:Nnode*3, 1:Nmac*3);
Gll = G(Nmac*3+1:Nnode*3, Nmac*3+1:Nnode*3);
Histg = Hist(1:Nmac*3);
Histl = Hist(Nmac*3+1:Nnode*3);

```

D. Computer Program Code Listing

```

%% ===== %%
%% File      :      call_generator.m      %%
%% Description :      This subroutine is called by the Main_TS to obtain the discretised representation of the %%
%%              :      synchronous generator.      %%
%% ===== %%

function[Es,Requ,theta,Vhiss,Vhisr,RRrr,RRrs,L] =
call_generator(Lao,La2,Mso,Maf,Mad,Maq,Lff,Lkkd,Lkkq,Mfkd,L_his,R,Vnode_mac,Inode_mac,Vrotor,Irotor,beta,ws,dt,t,teuler
,teuler2,teuler2end)

phase = 120*pi/180 ;
theta = ws*t + beta ;

L = [ -Lao-La2*cos(2*theta)      Mso-La2*cos(2*theta - phase)  Mso-La2*cos(2*theta + phase)  Maf*cos(theta)      Maf*cos(theta)      -Maq*sin(theta)
      Mso-La2*cos(2*theta - phase)  -Lao-La2*cos(2*theta + phase)  Mso-La2*cos(2*theta)      Maf*cos(theta-phase)  Maf*cos(theta-phase)  -Maq*sin(theta-phase)
      Mso-La2*cos(2*theta + phase)  Mso-La2*cos(2*theta)      -Lao-La2*cos(2*theta - phase)  Maf*cos(theta+phase)  Maf*cos(theta+phase)  -Maq*sin(theta+phase)
      -Maf*cos(theta)      -Maf*cos(theta-phase)      -Maf*cos(theta+phase)      Lff      Mfkd      0
      -Maf*cos(theta)      -Maf*cos(theta-phase)      -Maf*cos(theta+phase)      Mfkd      Lkkd      0
      -Maq*sin(theta)      Maq*sin(theta-phase)      Maq*sin(theta+phase)      0      0      Lkkq ] ;

Vhis_mc = [Vnode_mac; Vrotor] + 2/dt * ( 1/ws * L_his + dt/2 * R) * [Inode_mac ; Irotor] ;

RR = (2* 1/ws * L - dt*R)/dt ;

RRss = RR(1:3,1:3) ;
RRsr = RR(1:3,4:6) ;
RRrs = RR(4:6,1:3) ;
RRrr = RR(4:6,4:6) ;

Vhiss = Vhis_mc(1:3) ;
Vhisr = Vhis_mc(4:6) ;

Requ = RRss - RRsr*inv(RRrr)*RRrs ;

Es = (RRsr * inv(RRrr) ) * (Vrotor + Vhisr) - Vhiss ;

```

D. Computer Program Code Listing

```

%% ===== %%
%%                               %%
%% File       :      call_induction.m           %%
%% Description :      This subroutine is called by Main_TS to obtain the discretised representation of the %%
%%                               induction machine.                                     %%
%%                               %%
%% ===== %%

function[EsIM,RequIM,VhissIM,VhisrIM,RRrrIM,RRrsIM,LIM] =
call_induction(Lss,Lrr,Lsm,Lrm,Msr,LIMhis,RIM,Vnode_mac,Inode_mac,VrotorIM,IrotorIM,thetaIM,ws,dt,t,teuler,teuler2,teuler
2end) ;

ph = 120 * pi/180 ;

LIM = [Lss Lsm Lsm      Msr*cos(thetaIM)      Msr*cos(thetaIM + ph) Msr*cos(thetaIM - ph)
        Lsm Lss Lsm      Msr*cos(thetaIM-ph) Msr*cos(thetaIM )      Msr*cos(thetaIM + ph)
        Lsm Lsm Lss      Msr*cos(thetaIM+ph) Msr*cos(thetaIM- ph) Msr*cos(thetaIM )
        Msr*cos(thetaIM) Msr*cos(thetaIM - ph) Msr*cos(thetaIM + ph) Lrr Lrm Lrm
        Msr*cos(thetaIM+ph) Msr*cos(thetaIM )      Msr*cos(thetaIM - ph) Lrm Lrr Lrm
        Msr*cos(thetaIM-ph) Msr*cos(thetaIM + ph) Msr*cos(thetaIM )      Lrm Lrm Lrr ] ;

Vhis_mclIM = [Vnode_mac; VrotorIM] + 2/dt * ( 1/ws * LIMhis - dt/2 * RIM) * [-Inode_mac ; IrotorIM];

RRIM = (2* 1/ws * LIM + dt*RIM)/dt ;

RRssIM = RRIM(1:3,1:3) ;
RRsrIM = RRIM(1:3, 4:6) ;
RRrsIM = RRIM(4:6, 1:3) ;
RRrrIM = RRIM(4:6 , 4:6) ;

VhissIM = Vhis_mclIM(1:3) ;
VhisrIM = Vhis_mclIM(4:6) ;

RequIM = RRssIM - RRsrIM*inv(RRrrIM)*RRrsIM ;

EsIM = (RRsrIM * inv(RRrrIM) ) * (VrotorIM + VhisrIM) - VhissIM ;

RequIM = -1*RequIM ;

```

D. Computer Program Code Listing

```
%%  
%%  
%% File      :      call_AVR.m      %%  
%% Description :      This subroutine is called by Main_TS to obtain the response of generator AVR control. %%  
%%  
%%
```

```
function[efd,Efd,Vr]=call_AVR(Ka,Ta,Tex,Efdhis,Vrhis,Vthis,Vt,Vref,Vmax,Vmin,CRL,dt)
```

```
VRHIS = dt*Ka/Ta * Vref - dt*Ka/(2*Ta) * Vthis + (1 - dt/(2*Ta)) * Vrhis ;
```

```
EFDHIS = dt/(2*Tex) * Vrhis + (1-dt/(2*Tex))*Efdhis .
```

```
Vr = (-dt*Ka/(2*Ta))/(1 + dt/(2*Ta)) * Vt + VRHIS/(1+dt/(2*Ta)) ;
```

```
if(Vr>Vmax)
```

```
Vr=7;
```

```
end
```

```
if(Vr<Vmin)
```

```
Vr=-7;
```

```
end
```

```
Efd = (dt/(2*Tex))/(1+dt/(2*Tex)) * Vr + EFDHIS/(1+dt/(2*Tex)) ;
```

```
efd = CRL * Efd ;
```

D. Computer Program Code Listing

```

%%
%%
%% File      :      call_turgov.m
%% Description :      This subroutine is called by Main_TS to obtain the response of generator turbine governor
%%               :      control.
%%
%%
%%

```

```
function[Pm,Pg,Pgv] = call_turgov(Tgv,Ttr,REG,wref,wr,wrhis,Pghis,Pmhis,Pgvhis,Pref,TGMax,TGMin,dt) ;
```

```
PMHIS = dt/(2*Ttr) * Pghis + (1 - dt/(2*Ttr)) * Pmhis;
```

```
PGHIS = dt/(2*Tgv) * Pgvhis + (1 - dt/(2*Tgv)) * Pghis ;
```

```
PGVHIS = 2*Pref - Pgvhis - wrhis/REG + 2*wref/REG ;
```

```
Pgv = -wr/REG + PGVHIS ;
```

```
Pg = (dt/(2*Tgv))/(1+dt/(2*Tgv)) * Pgv + 1/(1+dt/(2*Tgv)) * PGHIS ;
```

```
if(Pg>TGMax)
```

```
    Pg=1.8;
```

```
end
```

```
if(Pg<TGMin)
```

```
    Pg=0;
```

```
end
```

```
Pm = (dt/(2*Ttr))/(1 + dt/(2*Ttr)) * Pg + 1/(1 + dt/(2*Ttr)) * PMHIS ;
```

D. Computer Program Code Listing

```
%%=====%%
%%
%% File      :      call_store.m                %%
%% Description :      This subroutine is called by Main_TS to store the simulation responses. This file is not %%
%% generic and the user will need to make necessary modifications to store the required data. %%
%%=====%%

function[count] = call_store(count)

%% For the example network in datain.m, if the response of interest is the load angle of generator 1 and the phase a voltage of
%% Node 2, then %% the following commands will store these data,

load_angle_generator1(count) = beta(1) ;          % the name of the stored data 'load_angle_generator1' can be arbitrarily
chosen by the                                     % user

phase_a_voltage_of_node2(count) = Vnode_mac(4) ;

time(count) = t ;

count = count + 1 ;
```

D. Computer Program Code Listing

```
%%=====%%  
%%  
%% File      :      call_plot.m      %%  
%% Description :      This file is called by Main_TS to plot the simulation responses that are stored in %%  
%%              :      call_store.m. This is not a generic file and the user will need to make the necessary %%  
%%              :      modifications depending on the response to be plotted. %%  
%%  
%%=====%%
```

```
%% To plot the example network simulation response stored in call_store.m ,
```

```
plot(time , load_angle_generator1) ;  
plot(time , phase_a_voltage_of_node2) ;
```

D.2. Power Electronics Controllers Subroutine

In this section, program code listing for the power electronics controllers subroutines for non-real time simulation namely, the SVC, STATCOM and DVR are given. These subroutines are written as case specific blocks and modifications to the general transient stability program (Main_TS.m) are required when the network being studied involves power electronic controllers. Hence, if power electronics controllers are not the main transient stability program become non-generic, and as such it is difficult to present a general layout of the program. The implementation of the power electronics controllers within the transient stability is not presented in detail. However, commented subroutines of these controllers are presented in the following listing.

D. Computer Program Code Listing

```

%%
%%
%% File      :      call_svc.m
%% Description :      Generate the switching function of the SVC with respect to its terminal voltage and
%%                   :      current flow across the TCR
%%
%%

```

```

%%%%%%%%%%%%%%%%%%%%%%%%%%%%%%%%%%%%%%%%%%%%%%%%%%%%%%%%%%%%%%%%%%%%%%%% Data Required by the call_svc subroutine to produce the switching functions %%%%%%%%%%
%%
%% 1) sa , sb and sc are the switching function of the SVC phase a, b and c. Set initial value to either 0 or 1
%%
%% 2) seta,set2a,setb,set2b,setc,set2c,t_Vas,t_Vbs,t_Vcs and trig are programming flags used by the author to obtain the
%%    switching functions. They carry no mathematical meaning. Set initial value of flags value to zero.
%%
%% 3) Vnode is the SVC terminal three-phase voltage at t. Vnode is a vector, eg Vnode = [VSVCa ; VSVCb ; VSCc ]
%%    Vnodehis is the SVC terminal voltage at t = t-dt.
%%
%% 4) Inode the TCR three-phase current at t. Inode is a vector, eg Inode = [ITRCa ; ITRCb ; ITRCc]
%%    Inodehis the TCR current at t = t-dt
%%
%% 5) fireangle is the firing angle of the thyristor
%%
%% 6) ws is the system synchronous speed
%%
%% To make use of this subroutine the user must construct the network and pass the required argument to the
%% subroutine. The switching functions are obtained and applied in the network solution. The switching functions
%% are incorporated into the incidence matrix relating the TCR branch.
%%
%%%%%%%%%%%%%%%%%%%%%%%%%%%%%%%%%%%%%%%%%%%%%%%%%%%%%%%%%%%%%%%%%%%%%%%%

```

```

function[sa,sb,sc,seta,set2a,setb,set2b,setc,set2c,t_Vas,t_Vbs,t_Vcs,trig] =
call_SVC(Vnode,Vnodehis,Inode,Inodehis,sa,sb,sc,seta,set2a,setb,set2b,setc,set2c,t_Vas,t_Vbs,t_Vcs,fireangle,trig,t,ws) ;

```

```

trig=0;

if(sign(Inode(1))~=sign(Inodehis(1))) % detect zero crossing of TCR phase a current
trig=1; % trig sets the flag to let the program know that a zero crossing has been detected.
If the % this functions as a flag to instruct the program to reduce step time.

if(set2a==1)
set2a=0; % set phase a switching function to zero
sa=0;
end
end
if( sign(Inode(2))~=sign(Inodehis(2))) % detect zero crossing of TCR phase b current
trig=1;
if(set2b==1)
set2b=0; % set phase b switching function to zero
sb=0;
end
end
if( sign(Inode(3))~=sign(Inodehis(3))) % detect zero crossing of TCR phase c current
trig=1;
if(set2c==1)
set2c=0; % set phase c switching function to zero
sc=0 ;
end
end

if(sign(Vnodehis(1)) ~= sign(Vnode(1))) % detect zero crossing of SVC phase a terminal voltage
if(seta==1)
seta=0;
set2a=1;
t_Vas = t;
end
end
if( t >= ( t_Vas + 1/ws * fireangle ) % set phase a switching function to one after elapse of the firing angle
sa=1;
seta=1;

```

D. Computer Program Code Listing

```
end
if(sign(Vnodehis(2)) ~= sign(Vnode(2))) % detect zero crossing of SVC phase b terminal voltage
if(setb==1)
setb=0;
set2b=1;
t_Vbs = t;
end
end
if( t >= ( t_Vbs + 1/ws * fireangle ) ) % set phase b switching function to one after elapse of the firing angle
sb=1;
setb=1;
end
if(sign(Vnodehis(3)) ~= sign(Vnode(3))) % detect zero crossing of SVC phase c terminal voltage
if(setc==1)
setc=0;
set2c=1;
t_Vcs = t;
end
end
if( t >= ( t_Vcs + 1/ws * fireangle ) ) % set phase c switching function to one after elapse of the firing angle
sc=1;
setc=1;
end
end
```

D. Computer Program Code Listing

```

%%=====%%
%%                                     %%
%% File      :      call_svcontrol.m   %%
%% Description :      AVR control of the SVC to output the required firing angle %%
%%                                     %%
%%=====%%

```

```

%% Data Required by the call_svcontrol subroutine %%%
%%
%% 1) Vs is the magnitude of the SVC terminal voltage. %%
%%     Vshis is the magnitude of the SVC terminal voltage at t = t - dt. %%
%%
%% 2) Vref, Ka and Ta are the controllers parameters. Vref is the reference voltage, Kr the regulator gain and Tr the %%
%%     regulator time constant. %%
%%
%% %%%

```

```

function[fireangle] = call_svcontrol(fireangle,Vs,Vshis,Vref,Kr,Tr,dt) ;

VRHIS = dt*Kr/Tr * Vref - dt*Kr/(2*Tr) * Vshis + ( 1- dt/(2*Tr)) * fireangle ;

fireangle = (-dt*Kr/(2*Tr))/(1+dt/(2*Tr))* Vs +VRHIS/(1+dt/(2*Tr)) ;

if(fireangle >= 180*pi/180)          % limit the maximum output to pi rad
fireangle =180*pi/180;
end

if(fireangle <=(pi/2 ))          % limit the mimimum output to pi/2 rad
fireangle =( pi/2 );
end

```

D. Computer Program Code Listing

```

%%=====%%
%% File      :      call_statcom.m      %%
%% Description :      Generate the three-phase voltage output of the statcom. %%
%%=====%%

```

```

%%%%%%%%%%%%%%%%%%%%%%%%%%%%%%%%%%%%%%%%%%%%%%%%%%%%%%%%%%%%%%%%%%%%%%%% Data Required by the call_statcom subroutine %%%%%%%%%
%%
%% 1)  V1 , V2 and V3 are the STATCOM three-phase terminal voltage. V1 is phase a, V2 is phase b and V3 is phase c %%
%%
%% 2)  ma , mb and mc are the modulation index of the three-phase STATCOM. Set initial value to 1. %%
%%
%% 3)  Vdc is the STATCOM dc voltage %%
%%
%% 4)  ka, kb , kc and count are programming flags used by the author to obtain the STATCOM output. They carry no %%
%%      mathematical meaning. Set initial value of ka, kb and kc to zero. Set initial value of count to 1. Count must be %%
%%      increased by one in the main program at each time-step. %%
%%
%% 5)  w is the triangular wave to act as the carrier signal. The triangular wave can be generated using a Matlab function %%
%%      'triang'. %%
%%
%% 6)  Vstat returns the three-phase STATCOM voltage. Vstat is a vector, eg Vstat = [Vstata ; Vstadb ; Vstadc] ; %%
%%
%%      To make use of this subroutine the user must construct the network and pass the required argument to the %%
%%      subroutine. The STATCOM three-phase output in PWM signals are obtained and applied in the network %%
%%      solution. The node in the network where STATCOM is connected is considered a generator node with fixed source %%
%%      where the apply is the STATCOM three-phase voltage. %%
%%
%%%%%%%%%%%%%%%%%%%%%%%%%%%%%%%%%%%%%%%%%%%%%%%%%%%%%%%%%%%%%%%%%%%%%%%%

```

```

function[Vstat,ka,kb,kc] = call_statcom(V1,V2,V3,ma,mb,mc,Vdc,w,ka,kb,kc,t,dt,ws,count)

%%%%%%%%%%%%%%%%%%%%%%%%%%%%%%%%%%%%%%%%%%%%%%%%%%%%%%%%%%%%%%%%%%%%%%%% Phase a %%%%%%%%%

V1store(count) = V1;
V2store(count) = V2;
V3store(count) = V3;

if(t > 2*(120*0.02/360))
[mag,ang,Va,Vb,Vc] = call_getphase(V1store,ws,t,count,dt); % obtain the phase angle of
% the STATCOM phase
% a terminal voltage, in order to produce
% modulation % signal that is in phase
% with the terminal voltage
% obtain STATCOM phase a voltage

[pwmout,pwmout_2nd,pwmout_3nd,ka] = call_PWM(-sin(ws*t+ang),dt,w,ka,Vdc,ma);
Vstat(1) = (pwmout+pwmout_2nd+pwmout_3nd)/3 ;

[mag,ang,Va,Vb,Vc] = call_getphase(V2store,ws,t,count,dt); % obtain the phase angle of the
% STATCOM phase
% b terminal voltage
% obtain STATCOM phase b voltage

[pwmout,pwmout_2nd,pwmout_3nd,kb] = call_PWM(-sin(ws*t+ang),dt,w,kb,Vdc,mb);
Vstat(2) = (pwmout+pwmout_2nd+pwmout_3nd)/3 ;

[mag,ang,Va,Vb,Vc] = call_getphase(V3store,ws,t,count,dt); % obtain the phase angle of the
% STATCOM phase
% c terminal voltage
% obtain STATCOM phase c voltage

[pwmout,pwmout_2nd,pwmout_3nd,kc] = call_PWM(-sin(ws*t+ang),dt,w,kc,Vdc,mc);
Vstat(3) = (pwmout+pwmout_2nd+pwmout_3nd)/3 ;

else
Vstat = [0;0;0];
end

```

D. Computer Program Code Listing

```

%%
%%
%% File      :      call_PWM.m
%% Description :      Generate a three level PWM signal with respect to a given carrier and modulation signal.
%%
%%
%%

```

```

%%%%%%%%%%%%%%%%%%%%%%%%%%%%%%%%%%%%%%%%%%%%%%%%%%%%%%%%%%%%%%%%%%%%%%%% Data Required by the call_PWM subroutine %%%%%%%%%
%%
%% 1)  vfund is act as the modulation signal.
%%
%% 2)  m is the modulation index.
%%
%% 3)  VDC is the STATCOM dc voltage
%%
%% 4)  w is the triangular wave to act as the carrier signal. The triangular wave can be generated using a Matlab
%%      function 'triang'.
%%
%% 5)  pwmout, pwmout_2n and pwmout_3nd are the output of each convertor. There are three here a three level
%%      convertor is considered.
%%
%%%%%%%%%%%%%%%%%%%%%%%%%%%%%%%%%%%%%%%%%%%%%%%%%%%%%%%%%%%%%%%%%%%%%%%%

```

```
function[pwmout,pwmout_2nd,pwmout_3nd,k]=call_PWM(vfund,dt,w,k,VDC,m)
```

```

x=m*vfund;
x1=-m*vfund;

if(k==round(0.02/dt + 1))
k=1;
end
if(x>w(k))
pwm(k)=VDC*1;
else
pwm(k)=0;
end
if(x1>w(k))
pwm2(k)=VDC*1;
else
pwm2(k)=0;
end
pwmout=pwm(k)-pwm2(k);

if(x>w(k+ round((0.02/dt + 1)/3) ))
pwm_2nd(k)=VDC*1;
else
pwm_2nd(k)=0;
end
if(x1>w(k+ round((0.02/dt + 1)/3) ))
pwm2_2nd(k)=VDC*1;
else
pwm2_2nd(k)=0;
end
pwmout_2nd=pwm_2nd(k)-pwm2_2nd(k);

if(x>w(k+ round(2*(0.02/dt + 1)/3) ))
pwm_3nd(k)=VDC*1;
else
pwm_3nd(k)=0;
end
if(x1>w(k+ round(2*(0.02/dt + 1)/3) ))
pwm2_3nd(k)=VDC*1;
else
pwm2_3nd(k)=0;
end
pwmout_3nd=pwm_3nd(k)-pwm2_3nd(k);

```

D. Computer Program Code Listing

```
%%  
%%  
%% File      :      call_getphase.m      %%  
%% Description :      To obtain the phase angle of a sinusoidal signal.      %%  
%%  
%%
```

```
function[mag,ang,Va,Vb,Vc] = call_getphase(V,ws,t,count,dt)
```

```
Va = V(count) ;  
Vb = V(count - round((120*0.02/360)/dt) );  
Vc = V(count - round(2*(120*0.02/360)/dt) );
```

```
%% The signal in the network is negative sinusoidal because of the sign convention adopted for the generator, hence, the -1.57  
%% in the transformation matrix.
```

```
Tran = -2/3 * [ cos(ws*t-1.57) cos(ws*t-2.0944-1.57) cos(ws*t+2.0944-1.57)  
              -sin(ws*t-1.57) -sin(ws*t-2.0944-1.57) -sin(ws*t+2.0944-1.57)  
              1/2 1/2 1/2 ];
```

```
DQ0 = Tran * [Va,Vb,Vc] ;
```

```
d_com = DQ0(1);  
q_com = DQ0(2);
```

```
mag = abs(d_com+q_com*i) ;
```

```
ang = angle(d_com+q_com*i);
```

D. Computer Program Code Listing

```

=====
%%%
%%%
%%% File      :      call_transform.m
%%% Description :      Segregate the instantaneous three-phase quantities into positive and negative d-q sequence
%%%
=====
%%%
%%%%%%%%%%%%%%%%%%%%%%%%%%%%%%%%%%%%%%%%%%%%%%%%%%%%%%%%%%%%%%%%%%%%%%%%%%%%%% Data Required by the call_transform subroutine %%%%%%%%%%%%%%%%%%%%%%%%%%%%%%%%%%%%%%%%%%%%%%%%%%%%%%%%%%%%%%%%%%%%%%%%%%%%%%%
%%%
%%% 1) V is the instantaneous three-phase quantities that need to be segregated.
%%%
%%% 2) count , count2 and act are programming flags used by the author. They carry no mathematical meaning. Set initial
%%% value of count and count2 to 1. Set initial value of act to 1. Count and count2 need to be increased by 1 in the main
%%% program at each time-step.
%%%
%%% 3) V_albe_temp1 and V_albe_temp2 are programming temporary intermittent variables. Set initial value of both to 0.
%%%
%%% 4) Vpd and Vpq are the positive sequence d-q components. Vnd and Vnq are the negative sequence d-q-components
%%%%%%%%%%%%%%%%%%%%%%%%%%%%%%%%%%%%%%%%%%%%%%%%%%%%%%%%%%%%%%%%%%%%%%%%%%%%%%

function[Vpd,Vpq,Vnd,Vnq,count2,act,V_albe_temp1,V_albe_temp2] =
call_transform(V,count,count2,act,dt,t,ws,V_albe_temp1,V_albe_temp2)

Tx = (2/3) * [1 -0.5 -0.5
              0 0.8660 -0.8660 ];

V_albe = Tx * V ; % transforming the instantaneous three-phase quantities into alpha and beta components

%%%%%%%%%%%%%%%%%%%%%%%%%%%%%%%%%%%%%%%%%%%%%%%%%%%%%%%%%%%%%%%%%%%%%%%%%%%%%% Process to delay the alpha and beta components by 90 degrees in order to segregate into positive and negative sequence
%%%%%%%%%%%%%%%%%%%%%%%%%%%%%%%%%%%%%%%%%%%%%%%%%%%%%%%%%%%%%%%%%%%%%%%%%%%%%%

V_albe_temp1(count) = V_albe(1);
V_albe_temp2(count) = V_albe(2);

if(count==(90*0.02/360)/dt)
act=1;
end
if(act==0)
Val_delay=0;
Vbe_delay=0;
end
if(act==1)
Val_delay = V_albe_temp1(count2);
Vbe_delay = V_albe_temp2(count2);
counter=counter+1;
end

%%%%%%%%%%%%%%%%%%%%%%%%%%%%%%%%%%%%%%%%%%%%%%%%%%%%%%%%%%%%%%%%%%%%%%%%%%%%%% Obtain the positive and negative sequence alpha and beta components %%%%%%%%%%%%%%%%%%%%%%%%%%%%%%%%%%%%%%%%%%%%%%%%%%%%%%%%%%%%%%%%%%%%%%%%%%%%%%%

Vpalpha = 1/2 * (V_albe(1) - Vbe_delay) ;
Vpbeta  = 1/2 * (V_albe(2) + Val_delay) ;

Vnalpha = 1/2 * (V_albe(1)+Vbe_delay) ;
Vnbeta  = 1/2 * (V_albe(2)-Val_delay) ;

%%%%%%%%%%%%%%%%%%%%%%%%%%%%%%%%%%%%%%%%%%%%%%%%%%%%%%%%%%%%%%%%%%%%%%%%%%%%%% Transform the positive and negative sequence alpha and beta components to the d-q representation %%%%%%%%%%%%%%%%%%%%%%%%%%%%%%%%%%%%%%%%%%%%%%%%%%%%%%%%%%%%%%%%%%%%%%%%%%%%%%%
%%% The signal in the network is negative sinusoidal because of the sign convention adopted for the generator, hence, the -1.57
in the
%%% transformation matrix

TX_dq = [cos(ws*t+1.5708) sin(ws*t+1.5708)
         -sin(ws*t+1.5708) cos(ws*t+1.5708)];

Vpov_albe = TX_dq * [Vpalpha;Vpbeta] ;

Vpd=Vpov_albe(1); % The positive sequence d-component
Vpq=Vpov_albe(2); % The negtive sequence q-components

```

D. Computer Program Code Listing

```
%%%%%%%%%%%%%%%%%%%%%%%%%%%%%%%%%%%%%%%%%%%%%%%%%%%%%%%%%  
Tx_dq2 = [cos(ws*t+1.5708) -sin(ws*t+1.5708)  
          sin(ws*t+1.5708) cos(ws*t+1.5708)];  
  
Vneg_albe = Tx_dq2 * [ Vnalpha;Vnbeta] ;  
  
Vnd=Vneg_albe(1);           % The negative sequence d-component  
Vnq=Vneg_albe(2);           % The positive sequence q-components
```

D. Computer Program Code Listing

```

%%
%%
%% File      :      call_positivePI.m      %%
%% Description :      Output from the positive PI control block      %%
%%
%%
%%%%%%%%%%%%%%%%%%%%%%%%%%%%%%%%%%%%%%%%%%%%%%%%%%%%%%%%%%%%%%%%%%%%%%%% Data Required by the call_transform subroutine %%%%%%%%%%
%%
%% 1)  Mag is the positive sequence magnitude output from the positive PI control block      %%
%%
%% 2)  Vpd and Vpq are the positive sequence d-q components. Vpdhis and Vpqhis are the positive sequence d-q
%%      component at t = t-dt.      %%
%%
%% 3)  Vref, Ka and Ta are the PI controller parameters. Vref is the desired magnitude of the positive sequence
%%      component.      %%
%%%%%%%%%%%%%%%%%%%%%%%%%%%%%%%%%%%%%%%%%%%%%%%%%%%%%%%%%%%%%%%%%%%%%%%%
function[Mag]=call_positivePI(Mag,Vpd,Vpq,Vpdhis,Vpqhis,dt,Vref,Ka,Ta);

VPIHIS = dt*Ka/Ta * Vref - dt*Ka/(2*Ta) * abs(Vpdhis+i*Vpqhis) + ( 1- dt/(2*Ta)) * Mag ;

Mag = (-dt*Ka/(2*Ta))/(1+dt/(2*Ta))* abs(Vpd+i*Vpq) +VPIHIS/(1+dt/(2*Ta)) ;

Mag = Mag + abs(Vpd+i*Vpq) ;

```

D. Computer Program Code Listing

```

%%=====%%
%%                               %%
%% File       :      call_negativePI.m      %%
%% Description :      Output from the negative PI control block      %%
%%                               %%
%%=====%%

%%%%%%%%%%%%%%%%%%%%%%%%%%%%%%%%%%%%%%%%%%%%%%%%%%%%%%%%%%%%%%%%%%%%%%%%%%%%%% Data Required by the call_transform subroutine %%%%%%%%%%%%%%%%%%%%%%%%%%%%%%%%%%%%%%%%%%%%%%%%%%%%%%%%%%%%%%%%%%%%%%%%%%%%%%%
%%                               %%
%% 1)  Mag is the negative sequence magnitude output from the negative PI control block      %%
%%                               %%
%% 2)  Vnd and Vnq are the positive sequence d-q components. Vndhis and Vnqhis are the positive sequence d-q      %%
%%      component at t = t-dt.      %%
%%                               %%
%% 3)  Vref , Ka and Ta are the PI controller parameters. Vref is the desired magnitude of the negative sequence      %%
%%      component.      %%
%%                               %%
%%%%%%%%%%%%%%%%%%%%%%%%%%%%%%%%%%%%%%%%%%%%%%%%%%%%%%%%%%%%%%%%%%%%%%%%%%%%%%

function[Mag]=call_negativePI(Mag,Vnd,Vnq,Vndhis,Vnqhis,dt,Vref,Ka,Ta);

VNHIS = dt*Ka/Ta * Vref - dt*Ka/(2*Ta) * abs(Vndhis+i*Vnqhis) + ( 1- dt/(2*Ta)) * Mag ;

Mag = (-dt*Ka/(2*Ta))/(1+dt/(2*Ta))* abs(Vnd+i*Vnq) +VNHIS/(1+dt/(2*Ta)) ;

```

D. Computer Program Code Listing

```

%%=====%%
%%                                     %%
%% File      :      Inverse_seq.m      %%
%% Description :      Inverse the phasor d-q sequence components into magnitude and angle of a three-phase %%
%%               quantities              %%
%%=====%%
%%%% Data Required by the Inverse_seq subroutine  %%%%
%%%% 1) MPOV is the magnitude of the positive sequence d-q component, MPOV = abs(Vpd+i*Vpq)  %%%%
%%%% 2) APOV is the angle of the positive sequence d-q component, APOV = angle(Vpd+i*Vpq)  %%%%
%%%% 3) MNEG is the magnitude of the negative sequence d-q component, MNEG = abs(Vnd+i*Vnq)  %%%%
%%%% 4) ANEG is the angle of the positive sequence d-q component, ANEG = angle(Vnd+i*Vnq)  %%%%
%%%% 5) The magnitude of three-phase quantities are used as the modulation index for the STATCOM. Please refer to the %%%%
%%%% STATCOM dynamic control block for reference.  %%%%
%%%%
%%%%
%%%%
function[Mag_Vmod,Ang_Vmod]=Inverse_seq(MPOV,APOV,MNEG,ANEG);

Inverse = [ 1 1 1
            exp(2*2.0944i) exp(2.0944i) 1
            exp(2.0944i) exp(2*2.0944i) 1];
+
Shift_ninety=[1 0 0
              0 1 0
              0 0 1];

POV1 = MPOV*(cos(APOV)+sin(APOV)*i);
NEG1 = MNEG*(cos(ANEG)+sin(ANEG)*i);

Vmod = Inverse*Shift_ninety*[POV1,NEG1,0];

Mag_Vmod=abs(Vmod);
Ang_Vmod=angle(Vmod);
% a vector of three-phase quantities phasor magnitude
% a vector of three-phase quantities phasor angle

```

D. Computer Program Code Listing

```

=====
%%
%%
%% File      :      call_DVR.m
%% Description :      Generate the three-phase DVR output. The call_dvr are similar to the call_statcom file.
%%              :      They share some of the common subroutines.
%%
=====

%%%%%%%%%%%%%%%%%%%%%%%%%%%%%%%%%%%%%%%%%%%%%%%%%%%%%%%%%%%%%%%%%%%%%%%% Data Required by the call_dvr subroutine %%%%%%%%%
%%
%% 1) Vs is the three-phase quantities of the supply side voltage. Vs is a vector, eg Vs = [Vsa;Vsb;Vsc].
%%
%% 2) Vl is the three-phase quantities of load side voltage. Vl is a vector, eg Vl = [Vla;Vlb;Vlc].
%%
%% 3) ma , mb and mc are the modulation index of the three-phase DVR. Set initial value to 1.
%%
%% 3) ka, kb , kc and count are programming flags used by the author to obtain the DVR output. They carry no
%%     mathematical meaning. Set initial value of ka, kb and kc to zero. Set initial value of count to 1.
%%
%% 4) Vdvr is the three phase output of the DVR. Vdvr is a vector, eg Vdvr = [ Vdvra;Vdvrb;Vdvrc].
%%%%%%%%%%%%%%%%%%%%%%%%%%%%%%%%%%%%%%%%%%%%%%%%%%%%%%%%%%%%%%%%%%%%%%%%

%% Vspd and Vspq are the source side positive sequence voltage d-q components. Vsnd and Vsnq are the source side negative
sequence
%% voltage d-q components.

[Vspd,Vspq,Vsnd,Vsnq,count2S,actS,V_albe_temp1S,V_albe_temp2S] =
call_transform(Vs,countS,count2S,actS,dt,t,ws,V_albe_temp1S,V_albe_temp2S);

%% Vlpd and Vlpq are the load side positive sequence voltage d-q components. Vlnq and Vlnq are the load side negative
sequence voltage %% d-q components.

[Vlpd,Vlpq,Vlnq,Vlnq,count2L,actL,V_albe_temp1L,V_albe_temp2L] =
call_transform(Vl,countL,count2L,actL,dt,t,ws,V_albe_temp1L,V_albe_temp2L);

%% Vspdhis is the source side positive sequence d component voltage at t = t- dt. Similarly, for others with 'his' representing the
respective
%% term at t= t-dt.

[Vlspd] = call_PIDVDR(Vlspd,(Vspd+Vlpd),(Vspdhis+Vlpdhis),Vrefpd,Kdvrrpd,Tdvrrpd,dt); % output from the positive
% sequence d component PI
% controller

[Vlspq] = call_PIDVDR(Vlspq,(Vspq+Vlpq),(Vspqhis+Vlpqhis),Vrefpq,Kdvrrpq,Tdvrrpq,dt); % output from the positive
% sequence q component PI
% controller

[Vlsnd] = call_PIDVDR(Vlsnd,(Vsnd+Vlnq),(Vsndhis+Vlnqhis),Vrefnd,Kdvrrnd,Tdvrrnd,dt); % output from the negative
% sequence d component PI
% controller

[Vlsnq] = call_PIDVDR(Vlsnq,(Vsnq+Vlnq),(Vsnqhis+Vlnqhis),Vrefnq,Kdvrrnq,Tdvrrnq,dt); % output from the negative
% sequence q component PI
% controller

%% The angle return Ang_Vmod is taken as the angle for the three-phase modulation signal

[Mag_Vmod,Ang_Vmod] = Inverse_seq(abs(Vlspd+i*Vlspq),angle(Vlspd+i*Vlspq),abs(Vlsnd+i*Vlsnq),angle(Vlsnd+i*Vlsnq));

%% Vdvr is the DVR three phase output voltage Vdvr(1) is phase a, Vdvr(2) is phase b and Vdvr(3) is phase c.

[pwmout,pwmout_2nd,pwmout_3nd,ka]=call_PWMX(-sin(ws*t+Ang_Vmod(1)),dt,0,w,ka,VDC1,ma);
Vdvr(1) = (pwmout + pwmout_2nd + pwmout_3nd)/3 ;

[pwmout,pwmout_2nd,pwmout_3nd,kb]=call_PWMX(-sin(ws*t+Ang_Vmod(2)),dt,0,w,kb,VDC1,mb);
Vdvr(2) = (pwmout + pwmout_2nd + pwmout_3nd)/3 ;

```

D. Computer Program Code Listing

```
[pwmout,pwmout_2nd,pwmout_3nd,kc]=call_PWMX(-sin(ws*t+Ang_Vmod(3)),dt,0,w,kc,VDC1,mc);  
Vdvr(3) = (pwmout + pwmout_2nd + pwmout_3nd)/3 ;
```

D. Computer Program Code Listing

```
%%  
%%  
%% File : call_PIDVR.m %%  
%% Description : Output from the negative PI control block %%  
%%  
%%
```

```
function[Vls] = call_PIDVR(Vls, Vin, Vinhis, Vref, Ka, Ta)
```

```
VLSHIS = dt*Ka/Ta * Vref - dt*Ka/(2*Ta) * Vinhis + (1 - dt/(2*Ta)) * Vls ;
```

```
Vls = (-dt*Ka/(2*Ta))/(1+dt/(2*Ta))* Vin + VLSHIS/(1+dt/(2*Ta)) ;
```

